Thesis for doctoral degree (Ph.D.)

2015

Biomedical Engineering Program

Development of devices and techniques for electroporation and electrical impedance spectroscopy analysis of adherent cells

Tomás García Sánchez

Departament d'Enginyeria Electrònica

Universitat Politècnica de Catalunya

Doctoral program in Biomedical Engineering

Barcelona, March 2015

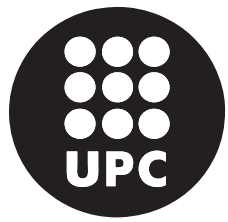

DEVELOPMENT OF DEVICES AND TECHNIQUES FOR ELECTROPORATION AND ELECTRICAL IMPEDANCE SPECTROSCOPY ANALYSIS OF ADHERENT CELLS

Dissertation supervisor : Ramon Bragós Bardia

Electronic and Biomedical Instrumentation Group

Department of Electrical Engineering , UPC
Barcelona, Spain.

A mis padres...

Agradecimientos

Si tuviera que empezar por el principio de esta aventura, llegaría al despacho del profesor Jose Mª Ferrero Corral. Él fue quien un buen día y con una amable sonrisa me animó sin lugar a dudas a encaminar mis pasos a la Ingeniería Biomédica. Gracias allá donde estés. Curiosamente, fue su hijo Chema Ferrero junto con Javier Sainz quienes despertaron mi interés por la Bioelectricidad y posteriormente, hicieron posible el inicio de mi andadura en el laboratorio donde se ha realizado esta tesis, gracias a los dos.

Ya en Barcelona, mis primeros agradecimientos van para Ramon Bragós, mi director de tesis. Gracias por confiar en mí, gracias por tus conocimientos y sobre todo, gracias por haberme dado alas para volar, por estar siempre abierto a escuchar mis propuestas. Sin esa libertad esta tesis no hubiera sido posible. La otra persona directamente responsable de esto es Javier Rosell, gracias también por la confianza depositada en mi, gracias por haberme hecho querer aprender más después de cada conversación papel y boli en mano. A los dos gracias también por vuestra comprensión y apoyo en los momentos menos buenos. Tengo suerte de haber estado rodeado de personas que, como vosotros, promueven las nuevas ideas que hacen avanzar la sociedad.

Esta tesis se ha realizado en la división de Instrumentación y Bioingeniería del Departamento de Ingeniería Electrónica en la Universidad Politécnica de Cataluña. A todos vosotros, gracias. En especial a mis compañeros que, aunque no han estado directamente implicados en la parte científica de esta tesis, han sido parte fundamental en lo personal, gracias por las conversaciones, los cafés,

las risas, etc... Es imposible citaros a todos Hadis, Noelia, Fede, Raul, Ángel, Albert, Victor, ... y a los que ya no estáis Giuseppe, Marco, Ricardo, Aleix, Jose, etc... Especial mención merece Alfonso Méndez, gracias por aguantarnos, por ayudarnos y por enseñarnos.

Gran parte de este trabajo se ha realizado en colaboración con el grupo de Terapia Génica liderado por Anna Mª Gomez-Foix, gracias por haberme introducido en el mundo de la bioquímica y por haberme permitido tomar parte activa en todos los experimentos. Para un ingeniero como yo, no sabéis lo emocionante que ha resultado todo el proceso de aprendizaje de las técnicas experimentales. Gracias a quienes día a día lo han hecho posible, especialmente a Beatriz Sánchez, Maria Guitart y Anna Orozco.

Je dois aussi remercier les parisiens pour l'opportunité d'avoir partagé quelques semaines dans votre laboratoire, il a été un plaisir, merci beaucoup.

Sin duda, tengo que agradecer a mis amigos y toda la gente que me quiere. Ellos han estado a mi lado todo este tiempo y sin saberlo me han ayudado a continuar, a motivarme cuando hacía falta. Gracias por enriquecerme con vuestras ideas, sueños, dudas, divagaciones, cervezas, espero teneros ahí para siempre.

A mi familia, uno de mis pilares fundamentales. Gracias por haberme dado la oportunidad de ser quien soy, de haberme enseñado el valor del esfuerzo y de que los sueños son para perseguirlos. Estos años vuestro ejemplo de lucha, de no rendirse ante las dificultades ha sido fundamental para seguir adelante.

Por último me gustaría hacer una reflexión sobre los investigadores, gracias a todos aquellos científicos anónimos que hacen de su trabajo una pasión. Gracias a vuestra perseverancia, tristemente infravalorada hoy en día, hacéis del mundo un sitio mejor. Espero que seamos capaces de no rendirnos nunca.

"If I have seen further it is by standing on the shoulders of Giants."

Isaac Newton, 1676.

"– Paréceme que vuesa merced ha cursado las escuelas: ¿qué ciencias ha oído?

– La de la caballería andante – respondió don Quijote –, que es tan buena como la de la poesía, y aun dos deditos más.

– No sé qué ciencia sea ésa – replicó don Lorenzo –, y hasta ahora no ha llegado a mi noticia.

– Es una ciencia – replicó don Quijote – que encierra en sí todas o las más ciencias del mundo ....."

Cap. XVIII, II. Don Quijote de la Mancha,

Miguel de Cervantes Saavedra.

Abstract

The present PhD dissertation is focused on the design and implementation of a microelectrode system capable of performing electroporation and electrical impedance measurements to adherent cell monolayers cultured in standard multiwell plates. Along the document, the ability of the proposed device to provoke cell electropermeabilization is first demonstrated. Subsequently, the system is applied in monitoring of the electroporation process by means of fast electrical impedance spectroscopy measurements.

The original concept of the proposed system resides on the momentary placement of the microelectrodes above the cell monolayer avoiding physical contact with the cells by means of microseparators. A modification of the standard printed circuit board (PCB) fabrication technology that helps to improve the current density distribution is developed to manufacture the final microelectrode prototypes. This technology allows producing disposable devices at very low cost.

The performance of the device is tested with different cell lines and using different molecules such as DNA and siRNA. The results confirm its usefulness but show considerable differences between permeabilization and transfection results.

Subsequently, the specific characteristics of the device to perform electrical impedance measurements with a four-electrode method during the electroporation treatment are fully exploited. In this thesis a multisine-based measuring

system capable of acquiring impedance spectra continuously with a time resolution of 1 spectrum/ms is used. In contrast to previous studies, the speed of the measuring system allows to perform full impedance spectroscopy measurements in the time gap between consecutive electroporation pulses and not only before and after the complete electric field application.

The impedance results at low frequency show the ability of the system to detect the fast cell membrane resealing dynamics immediately after each pulse. These fast dynamics are related to the so called short-lived pores and follow a double exponential behavior. Also, an accumulated slow impedance decrease along the complete process is observed related with the long-lived pores. Complementary, the high frequency impedance response shows how the effect of the conductivity variation caused by the diffusion of ions between the intracellular and extracelluar media has also an impact on the impedance measurements.

Different approaches are proposed in the analysis of the measurements of four different cell lines: the direct observation of impedance magnitude and phase, the study of Cole model parameters and finally, the use of an equivalent electrical circuit. The comparative analysis suggest that for the detection of fast cell membrane dynamics, phase of impedance is preferable to its magnitude because it is less disturbed by the collateral conductivity variations. After deep analysis of Cole parameters, an equivalent time constant combining the information of the Cole parameters tau and alpha is proposed as a general analysis parameter for the fast membrane changes. Lastly, the equivalent circuit is useful in order to give or to confirm a physical interpretation to the observed results.

Regarding the slow impedance decrease, it shows a non linear permeabilization rate with pulse number for high electric field intensities, suggesting the existence of a limit for new pore creation with increasing pulse number. It is also demonstrated how the total impedance variation at the end of the treatment can be used as a reliable marker of the success of cell eletropermeabilization with some advantages with respect to traditional chemical methods. The results shown in this thesis demonstrate how fast electrical impedance spectroscopy measurements during an electroporation procedure represent a reliable and alternative method for online monitoring the fast changes produced in the membranes of the sample under treatment.

UNESCO codes: 240602 (Bioelectricity), 240600 (Biophysics), 331110 (Medical instruments), 220202 (Electrical quantities and their measurement).

Contents

Chapter 1

Introduction

Abstract

This introductory chapter aims to give an initial overview of the topics addressed in the present PhD dissertation. The basic problem that focus this research is stated. Also, the specific objectives to accomplish this study are defined. Finally, the framework where this thesis was developed and the outline of the present document are provided as a guide for the reader.

1.1 Introduction

During years, the interaction between electromagnetic fields and cellular structures has been object of research from very different points of view. In particular, *Bioelectricity* has dealt with the interaction of the biological tissues with electric fields ever since the 18th century with the experiments performed by Luigi Galvani in 1780 [1]. The observations made during the first half of the 20th century using electricity to characterize the cell membrane [2–4] represented the definitive step towards the understanding of the basic electrical properties of cells.

For cells under the influence of an electric field, many phenomena can be manifested depending on the characteristics of the field. For weak electric field intensities that are considered to be noninvasive, cells may undergo deformation, rotation or movement caused by electrophoretic and dielectric forces, which are based on the interaction of the cell charges with the electric field and the dielectric polarization of the cell, respectively [5]. These effects are widely exploited in many applications, for instance, with suspended cells, they can be used for cell shorting or for guiding cells in microfluidic systems among others [5]. There are many other effects such as cellular reorientation in the presence of an electric field, tissue repair, cell differentiation, etc. [6, 7].

The interaction of low alternating current (AC) electric fields with biological tissues has been used, not only to manipulate cells, but also as a method to noninvasively characterize them [2]. The measurement of the electrical properties of cells, commonly known as electrical **bioimpedance** (EBI), represents nowadays an alternative method to study different physiological processes in biomedical and biotechnological applications (section 2.2).

On the opposite end, if the intensity of the electric fields is increased, the effect on cells is completely different. These no longer can be considered noninvasive electric fields because they actually produce changes in the membrane. The first observations of this changes revealed the irreversible damage of the cell membrane leading to cell death [8]. However, if the amount of high intensity energy is limited (in duration and amplitude), the cell membrane undergoes reversible structural changes that lead to a transient permeable state of the

membrane which are the basis for two phenomena: **electroporation** (see section 2.1) and electrofusion.

In the present thesis, both ends are joined together by studying electroporation and electrical bioimpedance measurements.

1.2 Problem statement

The two techniques that focus the present research have been applied during years to a wide variety of samples ranging from entire tissues in *in vivo* applications up to cell preparations *in vitro*. In laboratory conditions, the vast majority of eukaryotic cells need to be grown attached to a surface where cells can express all their intrinsic properties as if they were in a tissue. They are called anchorage-dependent cells or most commonly known as **adherent cells**. Along the course of this thesis, the interest is focused on the application of the mentioned techniques to adherent cells *in vitro*. As explained in detail further in the present dissertation (refer to section 2.1.4.1), there are different reasons that justify the interest of performing electroporation to adherent cells.

The main problem for the standard establishment of electroporation of adherent cells is the small number of devices that have been developed for that purpose. Additionally, most of these devices are not designed for their use in combination with standard cultureware and require custom setups, what reduces their applicability. This situation leads to increased costs and provoke a certain degree of refusal and distrust on the final user. In this direction, the low number of biomedical publications regarding electroporation of anchorage-dependent cells in comparison to cells in suspension, supports the fact that electroporation of adherent cells is not a fully established technique in standard laboratory protocols. From this point of view, there is a clear need of developing systems that allow the application of electroporation to anchorage-dependent cells cultured in standard plates.

Additionally, none pre-existing system capable of combining electroporation of adherent cells in standard culture plates and the use of electrical bioimpedance measurements within the same device has been found. The ultimate goal regarding EBI measurements consists in the characterization of the changes

produced in the cell membrane as a consequence of electroporation using this technique. Attending to this problem, previous studies support the viability of these measurements as a suitable method to follow membrane variations. The previous work suggests the need of improving the speed of the measuring techniques based in impedance in order to have a fast method that can capture the dynamical changes that occur during cell membrane electroporation (see section 2.2.5).

1.3 Objectives

Motivated by the ideas exposed in the summary above, **the main purpose** of this PhD thesis is the development and test of a microelectrode system capable of performing electroporation and electrical bioimpedance measurements in adherent cells cultured in standard multiwell culture plates.

Subsequently, once the main goal is achieved. The **second main challenge** in this thesis is to develop new techniques for the electrical characterization of biological samples during electroporation based in the application of fast electrical impedance spectroscopy measurements.

In order to accomplish these two main objectives, different tasks are outlined:

1. Given the lack of previous experience in electroporation of any of the researchers initially involved in this study the first step consisted in becoming familiar with the technique applied to adherent cells. For that purpose experiments were performed with cells grown on a set of commercial microelectrodes trying to reproduce experiments found in the bibliography. These previous results are not shown in the present dissertation but were valuable in order to accumulate experience for the development of the real system.

2. Development and fabrication of a microelectrode assembly using a technology that allows to fulfill the indicated specifications at a low cost. Support the design considerations and possible optimizations by means of theoretical simulations.

3. Test and validation of the device for electroporation with different molecules,

including active compounds such as DNA and also with different cell lines. As a biomedical engineer development of all the biochemical experimental skills that are necessary during the course of experiments and for their interpretation.

4. Build a system capable of successfully implement the use of fast electrical impedance spectroscopy in combination with electroporation.

5. Obtain electrical impedance measurements related with the permeable state of cell membranes during electroporation. Use general or custom models to analyze the results and give possible physiological interpretations to the observations in order to improve the understanding of the dynamics of the phenomenon.

1.4 Thesis framework and outline

The present PhD thesis has been developed in the Electronic and Biomedical Instrumentation group, from the Department of Electronic Engineering at the Universitat Politècnica de Catalunya, Barcelona. This group has been working for more than 30 years in the field of biomedical engineering with special interest in the development of methods and instruments for biomedical applications of electrical impedance tomography and spectroscopy.

This study was initiated in the frame of the research project : VALTEC ACC1Ó 09-1-0061 "Desenvolupament d'un dispositiu d'electroporació per a plaques standard multipouet" founded by CIDEM (Centro de Innovación y desarrollo Empresarial de la Generalitat de Catalunya). This project was developed in conjunction with the Cellular Engineering and Gene Therapy group led by Anna M^{a} Gomez-Foix, from the Department of Biochemistry and Molecular Biology at the Universitat de Barcelona. The goal of this project was the development of a system to perform electroporation in standard multiwell plates.

After the theoretical background both in Electroporation and Bioimpedance expounded in **Chapter 2**, a summary of the main results accomplished during the course of this research project are detailed in Chapter 3 and Chapter 4. In **Chapter 3** the development of the device, from an initial version to an im-

proved prototype, together with some of the main results obtained are shown. The research developed during this first stage derived in a journal paper publication (Appendix A) and a short paper in an international scientific conference (Appendix B). Additionally, there is a PCT patent application in the European Patent Office protecting the intellectual property of the concept.

After the confirmation of the viability of the concept, the next goal was to make tests with different biological samples and active molecules in order to validate the system. Additionally, our research interests made us to go beyond this goal and introduce some improvements in the device in order to extend its use also as a bioimpedance sensor that could be used during electroporation. In **Chapter 4** a summary of the main results obtained for this stage is shown. The most important findings from this chapter are published in a journal paper (Appendix C) and were also communicated in different scientific conferences.

The experiments corresponding with these two chapters (3 and 4) were all performed in the facilities of the Department of Biochemistry and Molecular Biology (Universitat de Barcelona) with the support and supervision of the members of the mentioned collaborator group.

Subsequently, given the recent knowledge developed in our group regarding fast dynamical electrical impedance spectroscopy measurements, the interest was focused on fully exploiting the capability of the designed system to implement these techniques during electroporation. In **Chapter 5** the first results obtained from these fast measurements are shown. For conciseness, a detailed analysis is provided only with a single cell line. The information shown in this chapter has been submitted in December 2014 for publication in the journal Bioelectrochemistry.

Finally, in **Chapter 6**, a general and comparative analysis of the impedance measurements performed in four different cell lines is provided in order to validate our results for a more general situation. The measurements in this chapter were performed with the same system as the one used in Chapter 5. The manuscript including the analysis of these measurements is under preparation for submission to a scientific journal.

In this second stage, after the implementation of the fast measuring methods and some previous tests in Barcelona, we considered very important to

collaborate with other groups with consolidated experience in the field of electroporation. For this reason, these two last chapters are the result of a collaboration with the UMR 8203 Vectorology and Anti-cancerous Therapeutics research unit, from the Integrated Research Cancer Institute in Villejuif, France. All experiments where done during my stay within this group for a total of 7 weeks in October 2013 and May 2014. This work was developed thanks to the Short-Term Scientific Missions grants in the frame of COST Action TD1104 (European network for development of electroporation-based technologies and treatments - EP4Bio2Med).

References

[1] Jaakko Malmivuo and Robert Plonsey. *Bioelectromagnetism: Principles and Applications of Bioelectric and Biomagnetic Fields*. Oxford University Press, USA, 1995.

[2] H. Fricke and S. Morse. The electric resistance and capacity of blood for frequencies between 800 and 4(1/2) million cycles. *J Gen Physiol*, 9(2):153–67, 1925.

[3] Kenneth S. Cole. Permeability and impermeability of cell membranes for ions. *Cold Spring Harbor Symposia on Quantitative Biology*, 8:110–122, 1940.

[4] Antoni Ivorra and Boris Rubinsky. *Historical Review of Irreversible Electroporation in Medicine*, chapter 1, pages 1–21. Series in Biomedical Engineering. Springer Berlin Heidelberg, 2010.

[5] J. Voldman. Electrical forces for microscale cell manipulation. *Annu Rev Biomed Eng*, 8: 425–54, 2006.

[6] C. D. McCaig, A. M. Rajnicek, B. Song, and M. Zhao. Controlling cell behavior electrically: current views and future potential. *Physiol Rev*, 85(3):943–78, 2005.

[7] M. A. Messerli and D. M. Graham. Extracellular electrical fields direct wound healing and regeneration. *Biol Bull*, 221(1):79–92, 2011.

[8] Eberhard Neumann and Kurt Rosenheck. Permeability changes induced by electric impulses in vesicular membranes. *The Journal of Membrane Biology*, 10(1):279–290, 1972.

Chapter 2

Theoretical background

Abstract

In this chapter, the theoretical background that supports the concepts and ideas needed for the development of this thesis is expounded. The first part of the chapter explains the basic concepts about Electroporation, from the fundamentals to the specific application that focus this thesis. In the second part, the basic concepts about Bioimpedance are explained. Some details about the techniques used in this research are given. It is not the aim of this chapter to be a complete literature review about both topics, which are extensively covered in several recent books, but a summary of the basic knowledge necessary to follow the present PhD dissertation.

2.1 Electroporation

2.1.1 Brief historical introduction

The effects related to the application of electric fields to cells and tissues were object of study ever since the beginning of the modern science in the 18th century. However, the first report directly relating the application of high intensity electric field with the breakdown of the plasma membrane was published in 1957 by Stämpfli [1]. A few years later, Sale and Hamilton published three papers explaining the effects of high electric fields on microorganisms [2] and in 1972 Neumann and Rosenheck demonstrated that electric pulses could cause reversible increase in the membrane permeability, which could be used for the uptake of membrane impermeable molecules to cells [3]. This report could be considered as the start trigger that caused other research groups to begin studying the electropermeabilization phenomenon.

Finally, ten years later, in 1982 two important applications of the phenomenon were published. First, Zimmerman demonstrated the fusion of individual cells after the exposure to high electric field pulses [4] and second, in one of the most classical papers nowadays referred in the literature, Neumann et al. were the first to insert genes into cells by means of pulsed electric fields [5]. It was in this report where the term **electroporation** was first proposed. Ever since that moment, and in the last fifty years, the number of applications and the theoretical development of the technique have increased exponentially together with the number of groups that study the technique from diverse points of view [6].

2.1.2 General theory

2.1.2.1 Fundamentals

Membrane of eukaryotic cells represents the interface between the cytoplasm and its surrounding environment and is composed mostly by a double layer of phospholipids, with proteins and other molecules embedded on the structure. Biomembranes act as selectively permeable structures implying that exchange of molecules from the extracellular medium to the cytoplasm and vice versa is

controlled by molecular properties like the size or the charge among others. In general, small hydrophobic molecules can cross phospholipid bilayers by simple diffusion. Water, although it is polar, can also cross cell membrane easily [7]. Other molecules can move across the bilayer with a very slow movement or they cannot cross it at all, this is the case of large uncharged molecules, charged molecules, polar molecules and ions. In these cases it is necessary special transport mechanisms that facilitate or actively perform the transport of these molecules into or out of the cell. For larger macromolecules, endocytosis or exocytosis are the mechanisms used by cells to introduce or secrete substances, respectively.

The introduction of exogenous molecules into the cells is a key tool in the biomedical sciences to study, treat or modify cell function in very different ways. In this direction, the development of new and more efficient delivery methods has been object of study for many research groups over the world [8]. The vast majority of these delivery strategies are based on the chemical modification of the delivered molecules to improve the transport trough the lipid bilayer. In the case of large molecules such as plasmid DNAs, more sophisticated chemical strategies have been developed using cationic liposomes (lipofection)[9], cationic polymers [10], viruses as vectors [11], nanoparticles, etc. In addition to chemical methods, other physical-based attempts are used. Namely, sonoporation which uses high-intensity ultrasounds to create pores in the membrane [12], optical transfection which uses highly focused laser beams, cell squeezing that mechanically compress cell membrane to facilitate the intracellular delivery, electroporation that uses high intensity pulsed electric fields and others [8]. Also the use of nanoparticles in combination with the target molecules are used in the intracellular delivery by biolistic particle delivery systems, magnetofection and others [13, 14]. This thesis is focused in the study and application of electroporation.

Electroporation, also known as electropermeabilization is a phenomenon that occurs during the exposure of biomembranes to short and high instensity electric field pulses. The membrane undergoes structural changes that result in a change in permeability to molecular species [15–18]. If the parameters of the electric field (amplitude, duration, frequency, number of pulses) are adequate, the state of increased permeability is only temporary, meaning that the cell membrane

recovers to the initial pre-pulse conditions (reversible electroporation). On the contrary, if the pulse parameters exceed certain threshold the cell membrane cannot return to the previous conditions resulting in cell death (irreversible electroporation) [19].

2.1.2.2 Theoretical models

Currently, there is an important number of studies that have been performed trying to give a theoretical explanation to electropermeabilization molecular basis. Although different explanations have been proposed to model the phenomenon, none of them has been experimentally confirmed [20, 21]. The most accepted model relates the increase in membrane permeability with the occurrence of hydrophylic pores in the membrane [17, 22–24]. Electropores model states that under the application of an external electric field the amount of energy necessary for the occurrence of a hydrophilic pore decreases, thus increasing the probability in the formation of these pores [22]. The commonly given explanation includes the reorientation of lipid molecules under the presence of the intense electric field creating first hydrophobic pores that expand and finally become hydrophilic pores that are structurally more stable (see Fig. 2.1a). After a determined time, ranging from milliseconds to minutes, pores reseal. Model of electroporation predicts that the diameter of a hydrophilic pore is in the order of several nm and in the moment of maximum membrane conductance the total porated surface is only 0.1 % of the total cell [22]. This theoretical considerations have been confirmed by molecular dynamics simulations of lipid bilayers where a relation between the transmembrane voltage and the probability of pore formation has been demonstrated [25, 26], an example is shown in Fig. 2.1b

Nowadays, the accumulated experimental evidence, the molecular models and the theoretical descriptions are in agreement from a descriptive point of view. However, from a quantitative perspective there are still some discrepancies between models and experimental observations what implies that there are still some mechanisms not fully understood. For this reason the deep understanding of the basic molecular mechanisms responsible for cell electropermeabilization is still an encouraging challenge for many research groups.

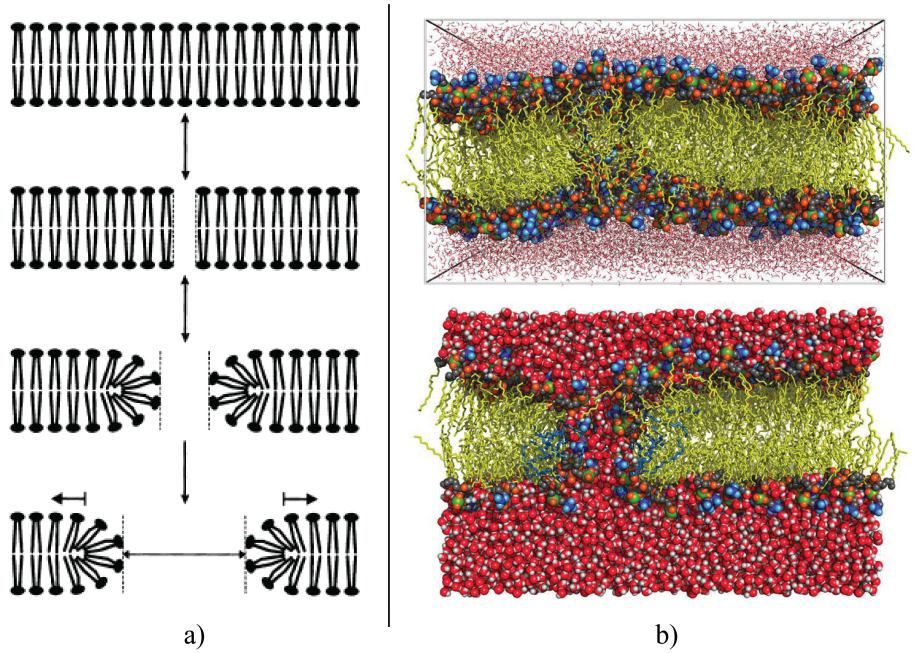

Fig. 2.1 a)Theoretical representation of pore formation. Transition from intact bilayer followed by a hidrophobic pore and finally the creation and expansion of a hydrophilic pore (adapted from [27]). b) Example of molecular simulation showing the formation of hydrophilic pores (extracted from [26]).

2.1.2.3 Physical parameters that influence electroporation

The physical phenomenon in which all theoretical descriptions agree is the mandatory increase of transmembrane voltage under certain threshold to trigger cell permeabilization. Membrane permeabilization is induced when a critical value between 200 mV and 1V is reached [28]. In physiological conditions there is a small voltage difference present in the membrane known as resting transmembrane voltage. It is caused by a concentration gradient of ions, mostly Na^+ and K^+ between intracellular and extracellular compartments and is regulated by passive and active membrane channel proteins. When an external electric field is applied to cells, an induced transmembrane voltage (ITV) is superimposed to the resting potential as a result of redistribution of charges inside the electric field.

The ITV can be calculated analytically for a single cell considering a perfect

non conducting membrane from the steady-state Schwan′s equation [29] defined as:

$$\Delta\Psi_m = f_s \cdot E \cdot R \cdot cos(\vartheta) \tag{2.1}$$

Where R is the radius of the cell, f_s is a factor related with the geometrical properties of cells (1.5 for a perfect spherical cell), E is the electric field intensity applied and ϑ is the angle between the cell membrane and the direction of the electric field. Spherical shape is a reasonable approximation for certain types of cells in particular conditions (in suspension); but many cells differ from this spherical shape considerably. For cells with different shapes other analytical equations have been derived for example for cylindrical, oblate spheroids, etc. [30]. Numerical models have been developed for more complex irregular cell shapes and conformations where it is not possible to find an analytical solution [31–33].

For a general case, it can be derived that electric field intensity is the most important parameter in order to exceed the ITV threshold necessary for electroporation. In other words, it can be stated that there is an electric field strength threshold to initiate membrane permeabilization. Intensity of the electric field controls the induction of pore creation and it also seems to be related with the total area permeabilized [34]. Total duration of electric field exposure, determined both by the duration of each individual pulse (D) and by the number of pulses (N), is related with the amount of molecular transport trough membrane [35, 36], i.e. intensity of permeabilization. There is, however, an intimate relation between the electric field intensity and the time during which the electric is applied [35, 37]. Different combinations of these two parameters are applied to achieve different effects related with membrane poration [38](see Fig. 2.2).

If more than one pulse is applied, the repetition rate also plays a role in the resulting electric field exposure effects. Although some controversial results, generally, low repetition rates (frequency $\leqslant$ 1 Hz) have been shown to be more efficient [39–41]. According to recent studies, this fact could be explained on the basis of the electrosensitization concept proposed in [42]. In accordance to [41], certain level of membrane resealing between consecutive pulses would be beneficial for increased treatment efficacy.

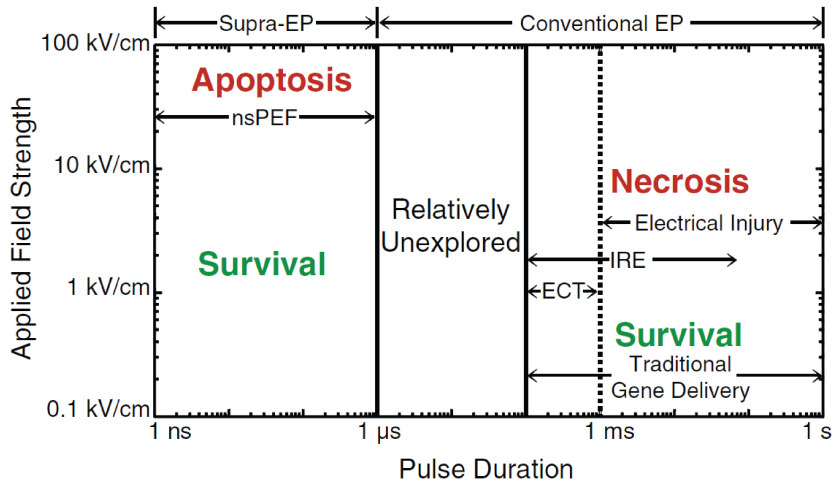

Fig. 2.2 Pulse strength-duration graph showing the regions associated to the main effects and applications due to cell electroporation (extracted from [38]).

The last characteristic of the electric field that has shown an impact on permeabilization rates is the pulse shape. Over the years, traditional pulse generators have used unipolar square wave pulses or exponentially decaying signals obtaining satisfactory results. However, it has been shown that the use of symmetrical bipolar rectangular pulses improves the efficiency of electroporation [34] lowering by around 20 % the voltage needed to achieve the same results that the ones obtained with an equivalent unipolar signal. Additionally, the use of bipolar square pulses has the advantage of reducing the reactions in the electrodes surface preventing the samples from electrolytic contamination [43]. Other pulse characteristics as the rise and fall times and different pulse shapes (triangular, sine waves, modulated signals) have shown no other impact that the one caused by the total amount of time that each signal stays above the threshold of permeabilization [44].

2.1.2.4 Other parameters that influence electroporation

Parameters that define the state of cells during pulse application, their environment and some intrinsic characteristics that differ depending on cell type or specific application have also a great impact on the success of electroporation

treatments.

If we first focus on the influence of cell characteristics, according to equation 6.8, cell size and shape are the two parameters that have an obvious relation with the efficiency of permeabilization regulating the ITV. It is clear that large cells are more sensitive to electric field and depending on the geometrical characteristics of the cell line (parameter f_s) the ITV will also be modified. The selective-size effect represents an advantage for specific treatment of a sample with different cell types such as blood samples [45]. Additionally, the ITV is also affected by cell density and conformation in the sample [33]. Additional cellular characteristics as the cell membrane composition [46], cytoskeleton [47, 48] or cell cycle phase [49, 50] also influence the electroporation results.

Regarding the external conditions that affect membrane electropermeabilization results, many different studies involving factors as temperature, conductivity of external buffer, osmotic pressure or pH have been performed. In the case of temperature, an implicit increase exits as a consequence of Joule heating due to current flow [51, 52]. The temperature rise due to pulses in a wide range of amplitudes and durations can be considered negligible for membrane poration efficacy and cell viability [38]. However, controlled temperature conditions can have a positive impact in the uptake of certain molecules. Specifically, it was demonstrated that higher post-electroporation temperatures increases cell survival and transfection efficiency *in vitro* [53]. Temperature increase can be controlled modifying the composition of the electroporation buffer used in *in vitro* experiments, for example the conductivity. If the conductivity of the buffer is decreased it is observed an increase in cell survival, remaining permeabilization rates almost unaltered [54, 55]. The more likely explanation for this observation is the fact that the conductivity of extracellular medium also modifies the values of ITV and resting potential of cells [55] but there are still some mechanisms not fully understood [56].

Osmotic pressure of electroporation buffer is another factor with influence in permeabilization results. Lowering the osmolarity of pulsing medium (hypoosmotic buffer) transfection, fusion or molecular uptake is enhanced [57–59]. It is believed that the increase of cell size produced by cell swelling together with the water flow to the intracellular space produced by osmotic pressure has a positive impact on the success of treatment. Finally, physiological pH value (pH=7)

yields to optimal viability and transfection rates and significant variations out of this value can cause undesired effects as necrotic tissue areas *in vivo* [60].

2.1.2.5 Dynamics of pore formation and resealing

Another key aspect that has been extensively studied in order to better understand the electroporation phenomenon is the time courses of pore formation and disappearance. The state of the membrane has been studied in the range from μs to hours applying different techniques to describe a process that can be divided in five steps according to [20]:

Due to the limited time resolution of the different monitoring techniques, there is considerably more accumulated information about the stabilization and resealing stages. According to the literature, the recovery process involves different time constants ranging from microseconds to minutes [61–66]. Although

Step	Description	Time scale
Induction	As previously explained, pore formation is initiated immediately when the transmembrane potential surpasses certain critical value.	μs
Expansion	As long as electric field is applied, the number and size of pores increases. During this phase the formation of hydrophilic pores takes place.	ms
Stabilization	After each pulse, only a part of pores remains opened, conforming more stable permeable structures.	ms
Resealing	After treatment, and under reversible electroporation conditions, membrane recovers to its previous non-permeable state.	s
Memory	Some effects derived from pore formation modify the behavior of membrane even when pores have completely resealed.	h

Table 2.1 Electroporation steps according to [20].

different studies do not agree in the values of these time constants, most of them propose a dual recovery process with a fast stage in the range of microseconds followed by a slower mechanisms that can last from milliseconds to minutes [62, 66, 67]. Two populations of pores are believed to be created as a response to pulse application [64, 66, 68, 69], the first population of pores is called short-lived pores [69] and is formed by large pores with a short lifetime, the second population (long-lived pores) is composed by small pores that can last up to hours after pulse application. The vast majority of short-lived structures disappear almost immediately after pulse application ($\leqslant$ 1 ms), it is believed that some of them can shrink to become part of the long-lived pores and others reseal completely in the order of 1 second [66]. The process of membrane resealing is a complex mechanism that is not yet fully understood. The development of improved methods to monitor the changes in the membrane during electroporation is still nowadays a challenge, specially for situations where it is desirable to have real-time information about the success of treatment.

2.1.3 Methods for dynamic monitoring of electroporation

The study of kinetics of creation and evolution of pores has focused the interest of many researchers as an essential approach to understand the deep mechanisms that govern electroporation. If the focus is put in the kinetics of pore formation and resealing, fast dynamical methods are necessary due to the transient behavior of some of the membrane permeable structures within the range of milliseconds [70]. Standard methods that have been applied to study the appearance of pores imply molecular reporters and imaging techniques to measure the molecular transport across the membrane using fluorescent dyes [65, 67, 71, 72]. Other common approach that has been applied to measure the fast membrane response is the use of voltage sensitive dyes in combination with high resolution video microscopy and other techniques [62, 73–75]. These measurements revealed a decrease in transmembrane voltage as a result of pore formation few microseconds after the onset of the electric field. Also electroptical relaxation studies on lipid membranes revealed fast changes in the range of microseconds [76] while molecular transport was detected only few milliseconds after pulsing [67].

Measurements of the electrical properties of membrane during pulse appli-

cation have been extensively used to reveal the temporal evolution of pores. First observations, based on the measurement of electric properties of membrane, reflected the change in membrane conductance few microseconds after the initiation of electric field [3, 77]. Different setups have been used to measure dynamically the electrical properties of small membrane regions by patch-clamp techniques [75, 78, 79], of cell suspensions [80, 81] or tissues[82–84]. Electrical measurements have been usually performed observing the changes in the applied current-voltage waveforms which mainly consist of quasi-dc conductivity changes. Only few studies used alternating current (AC) signals to characterize the impedance of the electroporated samples before and after electroporation [41, 84–86].

Following in section 2.2.5, an extended summary of some previous experiences to dynamically characterize cell membranes during electroporation based on impedance measurements is given.

2.1.4 Applications

As previously explained, electroporation is considered a physical method for molecular delivery and this is, nowadays, the most extended application of the technique. The first experimental protocol for using electroporation described the electro-mediated transfer of genes to mammalian cells [5]. In the recent decades gene electrotransfer has become a standard method in the transfection of a wide variety of eukaryotic cell lines [87] with special interest in some hard to transfect cells lines, endothelial cells, neurons, human embryonic or mesenchymal stem cells, etc. [59, 88]. One of the most challenging goals in today's research is to test and study the function of genes and how to use them in therapeutic applications. Cell-based therapies using genetically modified cells are promising materials in the treatment of several diseases; this is the case of cancer immunotherapy [89], stem cell therapy [90] or tissue regeneration [91].

The first step to perform these studies is to find an efficient and safe method that allows transfer of specific genes into cells. Generally the use of viruses as vectors to transfer genes inside cells is considered one of the most efficient transfection methods. However, its use has been limited by several factors such as immune and inflammatory response [11]. Other chemical transfection

strategies such as calcium phosphate, cationic polymers or liposomes has also limitations such as the high variability on the results and the dependence on the cell type and gene construct. Additionally, there have been reports suggesting that these other strategies may contribute to alterations in gene expression and other phenotypic changes [92]. In contrast, a main distinctive property of the electroporation technique is the fact that it is based only on physical phenomena, thereby avoiding the use of chemical agents.

Mechanisms responsible for gene electrotransfer have been studied in depth by many authors [35, 93, 94], suggesting that several steps are involved: 1) DNA and cell membrane interact leading to the formation of metastable plasmid-membrane complexes, 2) DNA translocates to the cytoplasm in the sites where membrane is permeabilized and 3) DNA travels from the cytoplasm to the nucleus. Additionally, many studies showed that parameters such as cell type, temperature, pulse duration, concentration of ions in the electroporative buffer, osmolarity, etc. altogether have an impact on the efficiency of the procedure [35, 57, 95].

Electroporation has been also used in the transfer of fragments of RNA (siRNA, mRNA) in the study of the immune system among others [96, 97]. Additional to nucleic acids, the transfer of proteins, peptides or antibodies has also shown promising results [98–100]. The use of electroporation in the delivery of different drugs provides an alternative for *in vivo* therapies[101]. Of special interest is the delivery of citotoxic molecules to cancer cells known as electrochemotherapy [102, 103] that has nowadays been included in some protocols of local cancer treatment [104].

In contrast to the above applications that use electroporation in the reversible version, there have been new applications that were proposed more recently that exploit the irreversible electroporation phenomenon. In the field of biomedical applications, irreversible electroporation has been recently proposed and used as a method for nonthermal tissue ablation [105, 106].

Apart from the biomedical applications summarized above, there are other applications that use electroporation in the biotechnology field. Briefly, electroporation is used as a method for microbial deactivation that can be applied for water sterilization as a preservation method in the food industry [107]. Also

it is used as a method to enhance the extraction of different biomolecules from microorganisms or plants [107].

The last important group of applications that cannot be omitted are the ones implying cell electrofusion. Electroporation can result in the fusion of individual cells if their membranes are get into contact [4] and can be applied in the production of antibodies or vaccines [108].

2.1.4.1 Electroporation of adherent cells

As described above, electroporation can be applied both *in vitro* and *in vivo* depending on the application. In this thesis the interest is focused on the use of the technique for treatment of cells *in vitro*, more specifically the treatment of adherent cells. Traditional laboratory electroporation setups consist of plastic cuvettes with two big flat electrodes in opposite sides and are suitable for applying electroporation to cells in suspension [109]. Therefore, in the case of anchorage-dependent cells it is necessary detaching the cells from the substrate by enzymatic treatment. There are many applications where it is not possible to perform cell detachment during the course of an experiment. This is the case, for example, of polarized cells or cellular structures as epithelia, differentiated cell conformations, induced pluripotent stem cells (IPSc), etc. [110]. Also, in the case of cell signaling studies, or gap communication it is not possible to apply electroporation in suspension[111].

Furthermore, detachment procedures prior to cell re-suspension in conventional electroporation cuvettes has shown effects in the normal metabolic functioning of cells and causes alterations in membrane proteins and cytoskeleton [109, 112]. This additional stress to the cells that may affect both the electroporation efficiency and the viability of cells after treatment [113].

Additionally, other factors involved in the efficiency of electroporation, such as surface-to-volume ratio and cytoskeleton, may differ in adherent and suspended cells. Previous studies have demonstrated the influence of cytoskeleton on electroporation results [47, 48], and suggest that the more stable cytoskeleton conformation of cell monolayers has an adverse effect on electroporation results. Furthermore, the different surface area-to-volume ratio (SA:V) may also affect results. In this case, adherent cells have a higher SA:V in comparison with

suspended cells, which should improve electroporation efficiency. According to section 2.1.2.3, cell shape and orientation also play a key role in the efficiency of permeabilization [30, 114]. Cells in suspension have a spheroidal shape and a more homogeneous size, while plated cells have irregular shapes and orientations, what determines which areas of cell membranes are permeabilized [32]. If the aim of *in vitro* experimentation is to have a realistic model of cells in tissues, these differences could play an important role to take into account when results from *in vitro* experiments want to be translated into *in vivo* applications.

Due to all these considerations, many systems have been developed for the application of electroporation pulses to adherent cells attached to a substrate, this specific application is usually known as *in situ* electroporation. A survey of different strategies extracted from [110] is shown in Fig. 2.3. The majority of these different approaches are based on culturing cell monolayers on any modified substrate either porous membranes [112, 115], conductive materials, or arrays of coplanar electrodes [116–119] where the cells are subjected to the electropermeabilization electric field pulses.

Few approaches have applied electroporation to adherent cells growing attached to standard culture materials. In this direction, the basic setups consist of a pair of big electrodes placed at both sides of the cell monolayer [113, 120, 121] or the use a pipette-tip like electrodes [122, 123]. However, most of the described systems are designed to be used within specific applications with custom setups and not in standard culture plates. Additionally, to the best of our knowledge there are no previous setups combining the use of microelectrodes and its application to fully standard culture plates. The main reason for using microelectrodes instead of highly separated big electrodes is our aim for using the same microelectrode assembly also as an electrical impedance sensor of the cells under treatment. Also, the use of microelectrodes implies the advantage of a decrease in the applied voltage what is translated in a reduction of the safety requirements of the equipment.

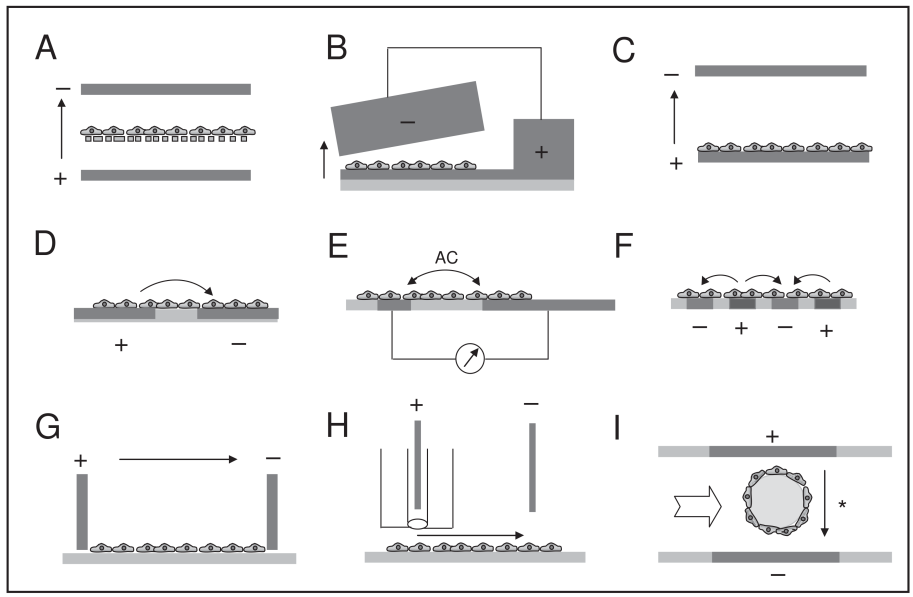

Fig. 2.3 Survey of different strategies for in situ electroporation extracted from [110]. A) Cultivation of cells on porous membranes. B) and C) Cells attached to conductive substrates. D), E) and F) Electroporation with coplanar electrodes. G) Big electrodes are applied above cell monolayer. H) Capillary or pipette tip electrodes are used. I) Cell are grown on beads and electroporated in suspension.

2.2 Electrical bioimpedance measurements

Along the first part of this chapter, the effects produced to the cell membrane as a result of the application of high intensity electric fields resulting in electroporation have been presented. Following, another application derived from the use of electric fields applied to biological materials is explained. In this case, biological materials are exposed to low intensity AC electric fields whose characteristics are designed not to produce any modification on the sample under analysis but to extract their passive electrical properties. This technique is called, in the case of biological samples, Electrical Bioimpedance Measurements (EBI).

2.2.1 Introduction

Historically, measurements of the electrical properties of biological materials began at the end of the XIXth century with the studies developed by G. N. Stewart [124, 125] and few years later by R. Höber in 1910 [126]. Höber measured the electrical impedance of suspensions of erythrocytes up to frequencies of 10 MHz, finding that their impedance decreased with increasing frequency. He concluded that the cells were composed of a poorly conducting membrane surrounding a cytoplasm of relatively low resistivity. Another milestone in the topic was the study conducted in 1925 by Fricke and Morse [127] where, analyzing the dielectric properties of red blood cell suspensions, the authors provided a value for the erythrocyte membrane capacitance as well as its thickness. These studies were the first probes of the ability of electrical bioimpedance as a technique to non-invasively characterize biological samples.

Of special importance is the theoretical work developed by P. Debye [128] and years later by the biophysicist K.S Cole [129, 130] who initiated the development of the theoretical framework and models that prevail until today. Finally, it deserves special mention the work developed by H.P Schwan and coworkers [29, 131–133] who established the basis to perform electrical measurements on biological tissues. Since then, the number of studies on EBI measurements has increased considerably together with the diversification of the applications. For a detailed historical review on the topic and its main applications the reader is

referred to [134–136].

Nowadays, the number of applications of EBI measurements is huge and it is out of the bounds of this chapter to make a review of all of them. The technique is applied both *in vivo* an *in vitro* to analyze different properties of the sample under test. In the clinical field, the main applications are oriented to diagnosis or patient monitoring based on volume changes (blood, air, etc.), calculation of body composition (water, fat, etc.), tissue classification, study of tissue state (cancerous cells, ischemia, etc.), etc. [135, 136]. EBI measurements are also used in standard laboratory applications for cell counting [137], as a detection method in biosensors [138], to estimate cell concentration, to characterize diverse physiological processes, etc.. In Fig. 2.4 the main applications of EBI measurements in the field of biosensing, cell analysis and characterization are summarized.

While all above applications are not directly related to this research, where impedance measurements are applied to study the evolution of cell monolayers during *in vitro* electroporation, there is a big amount of information regarding

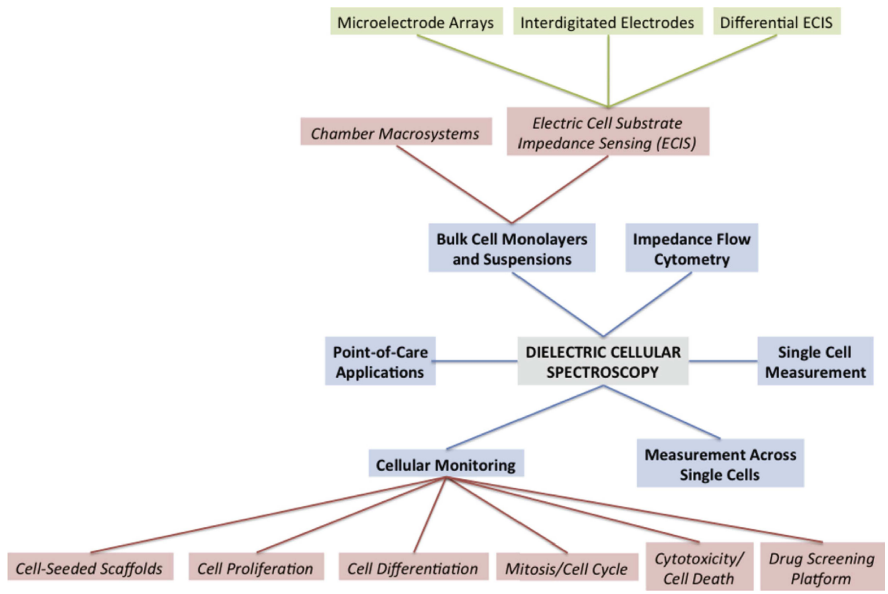

Fig. 2.4 Main applications of EBI measurements in the field of biosensing, cell analysis and characterization extracted from [139].

the characteristics of biological material and its expected behavior that can be obtained from those studies.

Regarding the different approaches used in EBI measurements, the most extended method for extracting the passive electrical properties of biological materials is the Electrical Impedance Spectroscopy (EIS) which consists in the measurement of the electrical impedance response of the object under study at different frequencies [133]. This method is examined in more detail in next sections. Nevertheless, there are other possibilities like Electrical Impedance Tomography (EIT) [140] that is used to obtain parametric images from the inside of 3D objects or Magnetic Induction Spectroscopy [141] which uses magnetic fields instead of electric fields to extract information from the measured sample.

2.2.2 General theory

2.2.2.1 Duality conductor–dielectric

Attending to its electrical properties, any material can be included in two general categories: conductors and dielectrics. In a conductor charges move freely under the influence of an electric field. On the contrary, in a dielectric material charges are fixed and not net movement exists [132]. Thus, in the presence of an electric field, charges in the conductor move to compensate this electric field (conduction current), in the case of dielectrics the effect of the electric field is to provoke a reorientation of charges (displacement current). This last effect is known as polarization. The polarization process is not an immediate phenomenon, on the contrary, it needs a certain amount of time to occur known as the relaxation time τ. Depending on the nature of the material the relaxation time constant can range from pico or nanoseconds to seconds [142].

The duality conductor/dielectric present in many materials is characterized macroscopically by two complementary parameters: conductivity and permittivity. The conductivity σ provides information about the ability of the free charges in the material to move under the influence of an electric field. According to equation 2.2 it is the proportionality factor between the induced electric current density and the electric field. The permittivity ϵ provides an idea of

the ability of the material to store charges and reflects the extent to which charge distributions can be polarized under the influence of the field. Similar to conductivity, ϵ is the proportionality factor between the electric field and the electric displacement vector according to equation 2.3.

$$\vec{J} = \sigma \vec{E} \tag{2.2}$$

$$\vec{D} = \varepsilon \vec{E} = \varepsilon_0 \varepsilon_r \vec{E} \tag{2.3}$$

The conductivity arises from the charges that move freely in biological materials, which mainly consist of hydrated ions present in the intra and extracellular media. In the case of charges that do not move, they are mainly associated with electrical double layers around membrane surfaces (interfacial polarization) or solvated macromolecules, or with polar molecules which (by definition) form a permanent dipole [143]. Specifically, the cell membrane characteristics play a central role in interfacial polarization.

Assuming sinusoidal steady state, and considering losses, permittivity is a complex number according to equation 2.4 whose real part can be identified as the so-called dielectric constant and the imaginary part is known as the dielectric loss that is related to the frequency-dependent conductivity, $\sigma(\omega)$.

$$\varepsilon^*(\omega) = \varepsilon^{'}(\omega) - j\varepsilon^{''}(\omega) \tag{2.4}$$

Finally, the complex permittivity and conductivity are related according to :

$$\sigma^*(\omega) = j\omega\varepsilon^*\varepsilon_0 \tag{2.5}$$

2.2.2.2 Duality relaxation–dispersion

As previously stated, the polarization process is not instantaneous and is characterized by a time constant τ in the time domain. Dielectric dispersion is the

corresponding dependence in the frequency domain (assuming a sinusoidal excitation). Considering a first order response, the Debye's equation characterizing this dependence is given by [128]:

$$\varepsilon^* = \varepsilon_\infty + \frac{\varepsilon_s - \varepsilon_\infty}{1 + j\omega\tau} \tag{2.6}$$

Where ε_∞ corresponds to the permittivity at sufficiently high frequency when the polar or polarizable structures are unable to follow the electric field variation, ε_s is called the 'static' permittivity and is the value at low frequencies where the polarization is completely manifested. A similar expression can be found for complex conductivity. A dispersion consists in the transition from one level to another. The frequency point corresponding to the median value between these two levels is called the characteristic frequency $f_c = 1/2\pi\tau$.

Dielectric properties of biological tissues have been studied over a wide frequency range identifying three major dispersions [136, 144] (see Fig. 2.5).

- α This low frequency dispersion is related to diffusion processes of ionic species and dielectric losses of the material.
- β This dispersion occurs in the range from tens of kHz to tens of MHz and is related to the interfacial polarization of the cell membrane. In this frequency range the cell membrane acts as a barrier for passive transport of ions (capacitive effect) between ionic solutions inside and outside the cell.
- γ Lastly gamma dispersion produced in the range of GHz is due to the polarization of water molecules.

The most important dispersion in biological tissues is the β dispersion as it accounts for the presence of cytoplasmic membranes. This dispersion is usually described by the Maxwell-Wagner interfacial polarization effects. At low frequency, the lipid bilayer constituting the cell membrane has a low ionic permeability and is considered a thin insulating shell surrounded by ionic solutions, on the other hand, at high frequency, the current can flow freely through membrane. This transition from one behavior to the other explains this dispersion. Additional effects as the presence of proteins, intracellular organelles, DNA, etc.

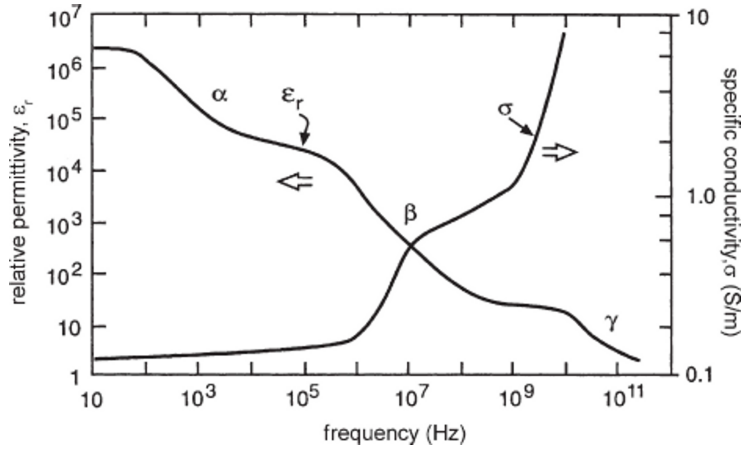

Fig. 2.5 Three major dispersions that biological tissues show in the permittivity and conductivity adapted from [145].

can create small β-dispersions that have also been exploited by some authors [146]. Additionally, in the frequency range where β dispersion is manifested, the adverse or undesired effects of the measuring equipments due to electrode impedance at low frequency and the limitation of the equipment bandwidth are reduced.

2.2.3 Impedance spectroscopy

2.2.3.1 Fundamentals

As it has been exposed above, the dielectric properties of biological tissues are highly dependent on frequency. Thus, it seems clear that for a complete characterization of any living sample, its properties should be studied over a wide frequency range, usually covering the band around the β dispersion. Impedance spectroscopy consists on applying small AC electric field signals of known frequencies to a system and measuring its response. The amplitude and phase difference of the resulting electrical potential (v_0) that develops across the sample with respect to the applied reference signal (i_0) provides the information necessary to obtain the impedance. According to this definition, impedance can be expressed by a phasor or by a complex number as follows:

$$|Z| = \frac{|v_o|}{|i_0|} \qquad and \qquad \angle Z = \theta = \angle i_0 - \angle v_0 \tag{2.7}$$

$$Z = R + jX \qquad j = \sqrt{-1} \tag{2.8}$$

According to the duality conductor–dielectric of biological materials previously explained, the impedance may be expressed in terms of conductance G in parallel with a capacitive reactance X as follows.

$$Z^*(\omega) = \frac{1}{G + j\omega C} \tag{2.9}$$

Considering now a defined section of material with area A and thickness d, the corresponding values relating the real and imaginary parts of the impedance and its passive electric properties are:

$$G = \sigma \frac{A}{d} \tag{2.10}$$

$$C = \varepsilon \frac{A}{d} \tag{2.11}$$

Finally, the complex impedance can be expressed following equation 2.12

$$Z^*(\omega) = \frac{d}{A}\left(\frac{1}{\sigma + j\omega\varepsilon}\right) \tag{2.12}$$

From another point of view, if I[s] and V[s] are considered the Laplace transforms of the sinusoidal AC current and electrical potential respectively, the impedance can be understood as a transfer function of the system under study expressed as:

$$TF(s) \equiv \frac{V[s]}{I[s]} = \frac{v_o}{i_0}\left(cos(\theta) + \frac{s}{\omega} sin(\theta)\right) \tag{2.13}$$

If s=jω, equation 2.13 applies to the frequency domain and is equivalent to equation 2.8.

2.2.3.2 Measuring strategies

The traditional approach to perform EIS measurements consists in the application of a single-frequency sinusoidal electric field signal and by sequentially sweeping the frequency, usually in linear or logarithmic steps, cover the complete band of interest [136]. This is the technique that currently use most of commercial impedance analyzers and usually provides high signal-to-noise ratio (SNR). However, the main drawback of this frequency-domain approach is the long measuring time required for performing a complete spectrum [147].

Depending on the application, the measuring speed should be adapted in order to capture the maximum information from the system under study. For example, in the assessment of certain intrinsic tissue characteristics, the measurement signal can be considered time-invariant as these characteristics do not vary during the measurement interval. In these applications, frequency-domain EIS is regularly used in combination with averaging techniques in order to obtain high quality measurements. However, if the goal is to characterize a dynamical process in real-time this approach fails to provide complete instantaneous information [148]. In this situation, where the measuring speed should be optimal, the other available option is to perform time-domain measurements.

Time-domain EIS measurements are performed making use of signals with a broad spectral content [149]. In this approach, the excitation signal contains simultaneously information at multiple frequencies what considerably reduces the time required to obtain a complete spectrum. The broad bandwidth signals that have been usually applied comprise Dirac and step functions, square waves, pseudo random noise, chirp, multi-sine, etc. [147, 150]. The optimization of these signals in terms of crest factor and energy confinement at certain frequency bands represent the main challenges when using this approach [151]. The processing of the acquired information can be done directly in the time-domain using models, what is usually known as Time Domain Transmissometry (TDT) or Time Domain Reflectrometry (TDR) [142], or can be processed, usually applying the Fourier transform, in the frequency domain. These methods present some limitations as a consequence of the increase in measuring speed related with the accuracy of the measurements, transients, etc. [148].

In the present research EIS measurements are applied to characterize the

impedance variations of cultured cell monolayers during electroporation. Thus, as explained in section 2.1.2.5, a fast method is necessary. From all the time-domain signals proposed, multi-sine excitations have been demonstrated to represent a good option and are used along this thesis as a consequence of the work developed by our group in the last years [151, 152]. Mathematically, a multi-sine signal is composed by the sum of N tones with different frequencies, each one also with its own phase. The time signal expression of a defined multi-sine burst can be expressed as:

$$x(t) = w(t) \sum_{i=1}^{N} (2\pi f_i t + \theta_i) \tag{2.14}$$

where w(t) is a windowing function according to [153]. The optimization of the frequency distribution together with the phases of the different tones can improve the quality of the measurements considerably as explained in [151]. Apart from the signal approach, the EIS measuring strategy is also determined by the equipment used for signal generation and acquisition. Also the electrode arrangement that represents the interface between the equipment and the biological sample plays a key role in the quality of the measurements.

2.2.3.3 Equipment

Regarding the equipment used for EIS measurements in the frequency band corresponding to the β dispersion (i.e. tens of kHz to tens of MHz). The classical options comprise the use of lock-in amplifiers, auto-balanced bridges or the direct measurement of V-I signals. In all cases the non-idealities produced in the system, specially in the electrode-electrolyte interface, make necessary the use of front-end amplifiers for increasing measurement accuracy [154].

The measurement of V-I signals is the most extended approach implemented in specific hardware applications. It is based in the measurement of the potential difference when a reference current is injected in the sample or vice versa. It is also possible to measure both current and voltage in order to have a more accurate reference signal. Considering this last option and depending on the selected method for signal generation (voltage-source (VS) or current-source

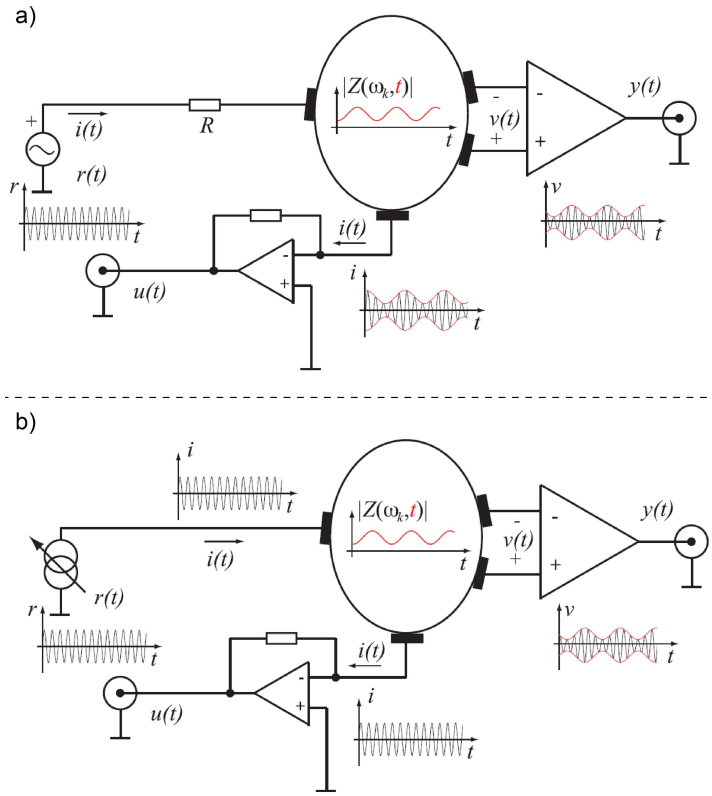

Fig. 2.6 The two different options for the design of the analog front-end. a) Voltage source and b) current source adapted from [155].

(CS) architectures, see Figs. 2.6a and b), the analog front-end is designed to fulfill the requirements of the system.

In Figs. 2.6a and b r(t) is the reference signal that is either directly connected through a resistor R to the sample in the case of the VS front-end, or converted to a current before connection in the case of the CS front-end. The measured voltage v(t) is measured with a differential amplifier and the current is obtained with a current-to voltage converter (transimpedance amplifier). These two approaches have both advantages and drawbacks and, depending on the application, can be more appropriate to use one or the other [155, 156].

As previously explained, the design of the different front-end architectures is highly motivated to reduce the undesired errors that appear due to electrode

polarization. The electrode polarization is caused by the molecular charge redistribution that occurs in the sample-electrode interface. This electrical double layer has a frequency-dependent behavior similar to a combination of a capacitor and a resistor (for the simplest case). Specially, the capacitive effect can disturb the measurements at low frequency if care is not taken to avoid or at least characterize and try to correct this effect.

In the simplest impedance measurement a current is injected into the sample through two electrodes and the resulting voltage drop between these two electrodes is measured. This is the so called **two-electrode method**. Using this electrode arrangement, the measurement includes the effect of the sample-electrode interface in the total impedance. This method can be applied when the impedance of the sample under test is much higher than the electrodes but is not a good option in general biological applications. This justifies the development of the previously explained front-end electronic circuitry where it is possible to separate the connection between the voltage and the current electrodes.

The **four-electrode method**, also called tetrapolar uses a pair of electrodes to inject the current into the sample and another independent pair of electrodes to measure the resulting voltage [157]. Due to the high input impedance of the voltage sensing circuit, the current that flows through this pair of electrodes is negligible and also the influence of their impedance in the measurements. However, this configuration is not able to completely eliminate the effect of the voltage electrodes in the measurements specially at low frequency, where the impedance of the electrodes can be considerably high. This can be caused by common mode voltages that are introduced in the system and cannot be completely rejected by the differential amplifier. There are many other methods proposed to deal with the electrode polarization that disturbs the EIS measurements, the reader is referred to [158, 159] for deeper explanation.

Lastly, in some cases, where it is not possible to use four independent electrodes, **three-electrode method** is used. In this configuration, one of the voltage sensing electrodes is eliminated and one of the current electrodes is used both for current and voltage. If the impedance of this electrode is reduced, for example by maximizing its area, the resulting measurement is nearly free of electrode impedance [160].

2.2.4 Impedance modeling

Once the multifrequency impedance data has been acquired, it is the moment to extract the desired information from the available measurements. This is not always an easy task because, usually, different physiological process can lead to the same effect on the electrical impedance of the sample under study, i.e. impedance measurements lack from specificity. In order to provide a physical interpretation to the impedance results many models have been introduced. Some of them try to correlate each specific process with an independent parameter of the model, others, on the contrary, try to find simplifications that match the measured behavior.

There are two types of models that are usually applied to bioimpedance measurements. On one hand, models can be constructed on the basis of electrical circuital equivalents with lumped components or other not ideal components. On the other hand, mathematical equations have been proposed to mimic the frequency behavior of biological tissues.

Regarding the electrical models, the simplest representation of a cell immersed on an ionic electrolyte contains a resistor, modeling the extracellular medium, in parallel with a capacitor, that models the membrane, and a resistor that model the intracellular conductivity [161]. This equivalent circuit with ideal components corresponds to a simple Debye-type circuit with a single relaxation time constant. However, the broad dispersion of biological tissues over the frequency is not perfectly modeled using this circuit. One possibility is to associate several circuits in cascade, the drawback of this option the increasing complexity of the resulting systems and the lack of physical meaning of the different circuits. The other option is to replace the membrane capacitors by constant phase elements (CPE) which better resemble the frequency-dependent behavior of biological tissues. This elements are introduced to model the distribution of time constants in biological samples [136]. The impedance of this elements is given by equation 2.15 where the exponent α ranges between α=0 (perfect resistor) and α=1 (perfect capacitor). Nonetheless, the physiological interpretation of this parameter is not clear and multiple options have been proposed [136].

$$Z_{CPE}(\omega) = \frac{1}{A(j\omega)^{\alpha}} \tag{2.15}$$

The second option, instead of using electrical equivalent circuits, is the formulation of a mathematical expression that describes the observed frequency behavior of biological tissues. The Cole model, introduced by Kenneth Cole in 1940 [129], is the most extended mathematical model to characterize biological tissues and biochemical materials describing single dispersion phenomena compatible with Fricke's law ([136]. Although in the literature it is usually referred as Cole-Cole impedance model, the actual Cole-Cole model was proposed one year later by Cole brothers [130] to describe the dielectric permittivity. Similar to the CPE element, Cole brothers introduced the concept of a distributed time constant (represented by an exponent α) in order to model the frequency response of biological tissues.

Along chapters 5 and 6 different models will be fully exploited and discussed in the interpretation of the EIS measurements performed during electroporation of adherent cell monolayers.

2.2.5 Measuring impedance during electroporation

As previously explained, the measurement of the changes resulting from membrane electropermeabilization has been object of study from many diverse approaches. In this section the focus is put in the measurement of the electrical properties of membrane during pulse application to reveal the temporal evolution of pores. The vast majority of the studies found in the literature perform these measurements by recording the voltage and current waveforms of the applied electroporation pulses and studying the changes during the pulse (in-pulse) which mainly consist of quasi-dc conductivity changes. In this studies, an abrupt change in the electrical conductivity of cell membrane in response to pulse application has been observed with different setups [76, 79, 80, 84, 162].

Other attempts have used AC signals to study the passive electrical properties of the sample before and after electroporation at single frequencies [68, 85, 163]. Only few studies performed multifrequency measurements (EIS) on electroporated samples [41, 84, 86, 164]. The interest of obtaining information at dif-

ferent frequencies during electroporation relies in the fact that the frequency dependent characteristics of the system and its response would help in the understanding of the effects caused by electric field pulses and their interpretation. For example, Ivorra et al. [84, 165] performed measurements in a tumor tissue model using two frequencies in the interval between pulses (1 kHz and 15.5 kHz at a rate of 500 samples per second) and multifrequency measurements (11 frequencies from 1 kHz to 400 kHz) after pulse application (at a rate of 20 scans per second). All the mentioned approaches only performed full EIS before and after treatment. To the best of our knowledge there are no previous experiences acquiring full spectral impedance information during electroporation.

All the mentioned experiences used traditional EIS approaches based on frequency sweeps to monitor membrane changes. However, this technique is not feasible to monitor the fast dynamical changes in the membrane during pulse application due to the long measuring time needed if compared with the short interpulse period (ususally $\leqslant 1$ s). Other attempts to study the dielectric properties of cells during electroporation and the fast pore dynamics are based in time domain methods such as time domain reflectometry [166] or time domain dielectric spectroscopy [81, 167]. This technique uses rapid voltage pulses with high frequency content and measure the reflected signal applying concepts of transmission line theory [149]. The measured lower frequency bound using this approach is determined by the duration of the voltage pulse applied and the higher frequency is controlled by the rise time of the square pulses.

Other more sofisticated electrical measurements during treatment have also been shown as promising tools to obtain information from biological samples using magnetic resonance electrical impedance tomography [168] and electrical impedance tomography [82, 169].

References

[1] R. Stampfli. A new method for measuring membrane potentials with external electrodes. *Experientia*, 10(12):508–9, 1954.

[2] A. J. H. Sale and W. A. Hamilton. Effects of high electric fields on microorganisms: I. killing of bacteria and yeasts. *Biochimica et Biophysica Acta (BBA) - General Subjects*, 148(3):781–788, 1967.

[3] Eberhard Neumann and Kurt Rosenheck. Permeability changes induced by electric impulses in vesicular membranes. *The Journal of Membrane Biology*, 10(1):279–290, 1972.

[4] U. Zimmermann. Electric field-mediated fusion and related electrical phenomena. *Biochimica et Biophysica Acta (BBA) - Reviews on Biomembranes*, 694(3):227–277, 1982.

[5] E. Neumann, M. Schaefer-Ridder, Y. Wang, and P. H. Hofschneider. Gene transfer into mouse lyoma cells by electroporation in high electric fields. *EMBO J*, 1(7):841–5, 1982.

[6] Damijan Miklavčič. Network for development of electroporation-based technologies and treatments: Cost td1104. *The Journal of Membrane Biology*, 245(10):591–598, 2012.

[7] B. S. Brown. *Biological Membranes*. Biochemical Society, London, UK, 1996.

[8] Xiang Gao, Keun-Sik Kim, and Dexi Liu. Nonviral gene delivery: What we know and what is next. *The AAPS Journal*, 9(1):E92–E104, 2007.

[9] P L Felgner, T R Gadek, M Holm, R Roman, H W Chan, M Wenz, J P Northrop, G M Ringold, and M Danielsen. Lipofection: a highly efficient, lipid-mediated dna-transfection procedure. *Proceedings of the National Academy of Sciences*, 84(21):7413–7417, 1987.

[10] RL Walzem, MA Hickman, JB German, and RJ Hansen. Transfection of avian lmh-2a hepatoma cells with cationic lipids. *Poultry Science*, 76(6):882–886, 1997.

[11] Q. Liu and D. A. Muruve. Molecular basis of the inflammatory response to adenovirus vectors. *Gene Ther*, 10(11):935–40, 2003.

[12] H. Pan, Y. Zhou, F. Sieling, J. Shi, J. Cui, and C. Deng. Sonoporation of cells for drug and gene delivery. *Conf Proc IEEE Eng Med Biol Soc*, 5:3531–4, 2004.

[13] Sha Jin and Kaiming Ye. Nanoparticle-mediated drug delivery and gene therapy. *Biotechnology Progress*, 23(1):32–41, 2007.

[14] O. Mykhaylyk, Y. S. Antequera, D. Vlaskou, and C. Plank. Generation of magnetic nonviral gene transfer agents and magnetofection in vitro. *Nat Protoc*, 2(10):2391–411, 2007.

[15] T. Y. Tsong. Electroporation of cell membranes. *Biophys J*, 60(2):297–306, 1991.

[16] S. Y. Ho and G. S. Mittal. Electroporation of cell membranes: A review. *Critical Reviews in Biotechnology*, 16(4):349–362, 1996.

[17] James C. Weaver and Yu A. Chizmadzhev. Theory of electroporation: A review. *Bioelectrochemistry and Bioenergetics*, 41(2):135–160, 1996.

[18] J. Teissié, N. Eynard, B. Gabriel, and M. P. Rols. Electropermeabilization of cell membranes. *Advanced Drug Delivery Reviews*, 35(1):3–19, 1999.

[19] Avigail Ben-Or and Boris Rubinsky. *Experimental Studies on Irreversible Electroporation of Cells*, chapter 3, pages 63–83. Series in Biomedical Engineering. Springer Berlin Heidelberg, 2010.

[20] J. Teissie, M. Golzio, and M. P. Rols. Mechanisms of cell membrane electropermeabilization: A minireview of our present (lack of ?) knowledge. *Biochimica et Biophysica Acta (BBA) - General Subjects*, 1724(3):270–280, 2005.

[21] C. Chen, S. W. Smye, M. P. Robinson, and J. A. Evans. Membrane electroporation theories: a review. *Medical and Biological Engineering and Computing*, 44(1):5–14, 2006.

[22] J. C. Weaver. Electroporation of cells and tissues. *Plasma Science, IEEE Transactions on*, 28(1):24–33, 2000.

[23] Kyle C. Smith, John C. Neu, and Wanda Krassowska. Model of creation and evolution of stable electropores for dna delivery. *Biophysical Journal*, 86(5):2813–2826, 2004.

[24] Wanda Krassowska and Petar D. Filev. Modeling electroporation in a single cell. *Biophysical Journal*, 92(2):404–417, 2007.

[25] Mounir Tarek. Membrane electroporation: A molecular dynamics simulation. *Biophysical Journal*, 88(6):4045–4053, 2005.

[26] Rainer A. Böckmann, Bert L. de Groot, Sergej Kakorin, Eberhard Neumann, and Helmut Grubmüller. Kinetics, statistics, and energetics of lipid membrane electroporation studied by molecular dynamics simulations. *Biophysical Journal*, 95(4):1837–1850, 2008.

[27] T. Kotnik, P. Kramar, G. Pucihar, D. Miklavcic, and M. Tarek. Cell membrane electroporation- part 1: The phenomenon. *Electrical Insulation Magazine, IEEE*, 28 (5):14–23, 2012.

[28] J. Teissié and M. P. Rols. An experimental evaluation of the critical potential difference inducing cell membrane electropermeabilization. *Biophysical Journal*, 65(1):409–413, 1993.

[29] H. P. Schwan. Electrical properties of tissue and cell suspensions. *Adv Biol Med Phys*, 5:147–209, 1957.

[30] Tadej Kotnik, Gorazd Pucihar, and Damijan Miklavcic. Induced transmembrane voltage and its correlation with electroporation-mediated molecular transport. *Journal of Membrane Biology*, 236(1):3–13, 2010.

[31] G. Pucihar, T. Kotnik, B. Valic, and D. Miklavcic. Numerical determination of transmembrane voltage induced on irregularly shaped cells. *Ann Biomed Eng*, 34(4):642–52, 2006.

[32] G. Pucihar, D. Miklavcic, and T. Kotnik. A time-dependent numerical model of transmembrane voltage inducement and electroporation of irregularly shaped cells. *IEEE Trans Biomed Eng*, 56(5):1491–501, 2009.

[33] M. Pavlin, N. Pavselj, and D. Miklavcic. Dependence of induced transmembrane potential on cell density, arrangement, and cell position inside a cell system. *IEEE Trans Biomed Eng*, 49(6):605–12, 2002.

[34] Tadej Kotnik, Lluis M. Mir, Karel Flisar, Marko Puc, and Damijan Miklavcic. Cell membrane electropermeabilization by symmetrical bipolar rectangular pulses. *Bioelectrochemistry*, 54(1):83–90, 2001.

[35] H. Wolf, M. P. Rols, E. Boldt, E. Neumann, and J. Teissie. Control by pulse parameters of electric field-mediated gene transfer in mammalian cells. *Biophysical Journal*, 66(2, Part 1):524–531, 1994.

[36] Marie-Pierre Rols Teissie and Justin. Electropermeabilization of mammalian cells to macromolecules: Control by pulse duration. *Biophysical Journal*, 75:1415–1423, 1998.

[37] M. R. Prausnitz, B. S. Lau, C. D. Milano, S. Conner, R. Langer, and J. C. Weaver. A quantitative study of electroporation showing a plateau in net molecular transport. *Biophys J*, 65(1):414–22, 1993.

[38] James C. Weaver, Kyle C. Smith, Axel T. Esser, Reuben S. Son, and T. R. Gowrishankar. A brief overview of electroporation pulse strength-duration space: A region where additional intracellular effects are expected. *Bioelectrochemistry*, 87(0):236–243, 2012.

[39] A. M. Lebar, G. C. Troiano, L. Tung, and D. Miklavcic. Inter-pulse interval between rectangular voltage pulses affects electroporation threshold of artificial lipid bilayers. *NanoBioscience, IEEE Transactions on*, 1(3):116–120, 2002.

[40] G. Pucihar, L. M. Mir, and D. Miklavcic. The effect of pulse repetition frequency on the uptake into electropermeabilized cells in vitro with possible applications in electrochemotherapy. *Bioelectrochemistry*, 57(2):167–172, 2002.

[41] A. Silve, A. Guimera Brunet, B. Al-Sakere, A. Ivorra, and L. M. Mir. Comparison of the effects of the repetition rate between microsecond and nanosecond pulses: Electropermeabilization-induced electro-desensitization? *Biochimica et Biophysica Acta (BBA) - General Subjects*, 1840(7):2139–2151, 2014.

[42] O. N. Pakhomova, B. W. Gregory, V. A. Khorokhorina, A. M. Bowman, S. Xiao, and A. G. Pakhomov. Electroporation-induced electrosensitization. *PLoS One*, 6(2):e17100, 2011.

[43] T. Kotnik, D. Miklavcic, and L. M. Mir. Cell membrane electropermeabilization by symmetrical bipolar rectangular pulses. part ii. reduced electrolytic contamination. *Bioelectrochemistry*, 54(1):91–5, 2001.

[44] T. Kotnik, G. Pucihar, M. Reberšek, D. Miklavčič, and L. M. Mir. Role of pulse shape in cell membrane electropermeabilization. *Biochimica et Biophysica Acta (BBA) - Biomembranes*, 1614(2):193–200, 2003.

[45] S. Sixou and J. Teissié. Specific electropermeabilization of leucocytes in a blood sample and application to large volumes of cells. *Biochimica et Biophysica Acta (BBA) - Biomembranes*, 1028(2):154–160, 1990.

[46] Sophie Raffy and Justin Teissié. Control of lipid membrane stability by cholesterol content. *Biophysical Journal*, 76(4):2072–2080, 1999.

[47] Marie-Pierre Rols and Justin Teissié. Experimental evidence for the involvement of the cytoskeleton in mammalian cell electropermeabilization. *Biochimica et Biophysica Acta (BBA) - Biomembranes*, 1111(1):45–50, 1992.

[48] Chryso Kanthou, Simona Kranjc, Gregor Sersa, Gill Tozer, Anze Zupanic, and Maja Cemazar. The endothelial cytoskeleton as a target of electroporation-based therapies. *Molecular Cancer Therapeutics*, 5(12):3145–3152, 2006.

[49] A. Delgado-Canedo, D. G. Santos, J. A. Chies, K. Kvitko, and N. B. Nardi. Optimization of an electroporation protocol using the k562 cell line as a model: role of cell cycle phase and cytoplasmic dnases. *Cytotechnology*, 51(3):141–8, 2006.

[50] Muriel Golzio, Justin Teissié, and Marie-Pierre Rols. Cell synchronization effect on mammalian cell permeabilization and gene delivery by electric field. *Biochimica et Biophysica Acta (BBA) - Biomembranes*, 1563(1–2):23–28, 2002.

[51] Rafael V. Davalos and Boris Rubinsky. Temperature considerations during irreversible electroporation. *International Journal of Heat and Mass Transfer*, 51(23–24):5617–5622, 2008.

[52] I. Lackovic, R. Magjarevic, and D. Miklavcic. Three-dimensional finite-element analysis of joule heating in electrochemotherapy and in vivo gene electrotransfer. *Dielectrics and Electrical Insulation, IEEE Transactions on*, 16(5):1338–1347, 2009.

[53] Marie-Pierre Rols, Christine Delteil, Guillaume Serin, and Justin Teissié. Temperature effects on electrotransfection of mammalian cells. *Nucleic acids research*, 22(3):540, 1994.

[54] C S Djuzenova, U Zimmermann, H Frank, V L Sukhorukov, E Richter, and G Fuhr. *Effect of medium conductivity and composition on the uptake of propidium iodide into electropermeabilized myeloma cells*, volume 1284. 1996.

[55] Gorazd Pucihar, Tadej Kotnik, Masa Kanduser, and Damijan Miklavcic. The influence of medium conductivity on electropermeabilization and survival of cells in vitro. *Bioelectrochemistry*, 54(2):107–115, 2001.

[56] Jianbo Li, Wenchang Tan, Miao Yu, and Hao Lin. The effect of extracellular conductivity on electroporation-mediated molecular delivery. *Biochimica et Biophysica Acta (BBA) - Biomembranes*, 1828(2):461–470, 2013.

[57] Muriel Golzio, Marie-Pierre Mora, Catherine Raynaud, Christine Delteil, Justin TeissiÈ, and Marie-Pierre Rols. Control by osmotic pressure of voltage-induced permeabilization and gene transfer in mammalian cells. *Biophysical Journal*, 74(6):3015–3022, 1998.

[58] C. Barrau, J. Teissié, and B. Gabriel. Osmotically induced membrane tension facilitates the triggering of living cell electropermeabilization. *Bioelectrochemistry*, 63(1–2):327–332, 2004.

[59] A. Liew, F. M. Andre, L. L. Lesueur, M. A. De Menorval, T. O'Brien, and L. M. Mir. Robust, efficient, and practical electrogene transfer method for human mesenchymal stem cells using square electric pulses. *Hum Gene Ther Methods*, 24(5):289–97, 2013.

[60] P. Turjanski, N. Olaiz, F. Maglietti, S. Michinski, C. Suarez, F. V. Molina, and G. Marshall. The role of ph fronts in reversible electroporation. *PLoS One*, 6(4):e17303, 2011.

[61] L. V. Chernomordik, S. I. Sukharev, S. V. Popov, V. F. Pastushenko, A. V. Sokirko, I. G. Abidor, and Y. A. Chizmadzhev. The electrical breakdown of cell and lipid membranes: the similarity of phenomenologies. *Biochimica et Biophysica Acta (BBA) - Biomembranes*, 902(3):360–373, 1987.

[62] M. Hibino, H. Itoh, and K. Kinosita Jr. Time courses of cell electroporation as revealed by submicrosecond imaging of transmembrane potential. *Biophysical Journal*, 64(6): 1789–1800, 1993.

[63] Kazuhiko Kinosita and Tian Yow Tsong. Formation and resealing of pores of controlled sizes in human erythrocyte membrane. *Nature*, 268(5619):438–441, 1977.

[64] G. Saulis. Kinetics of pore disappearance in a cell after electroporation. *Biomed Sci Instrum*, 35:409–14, 1999.

[65] Martin Bier, Stephanie M. Hammer, Daniel J. Canaday, and Raphael C. Lee. Kinetics of sealing for transient electropores in isolated mammalian skeletal muscle cells. *Bioelectromagnetics*, 20(3):194–201, 1999.

[66] D. A. Zaharoff, J. W. Henshaw, B. Mossop, and F. Yuan. Mechanistic analysis of electroporation-induced cellular uptake of macromolecules. *Exp Biol Med (Maywood)*, 233(1):94–105, 2008.

[67] Gorazd Pucihar, Tadej Kotnik, Damijan Miklavčič, and Justin Teissié. Kinetics of transmembrane transport of small molecules into electropermeabilized cells. *Biophysical Journal*, 95(6):2837–2848, 2008.

[68] P. M. Ghosh, C. R. Keese, and I. Giaever. Monitoring electropermeabilization in the plasma membrane of adherent mammalian cells. *Biophysical Journal*, 64(5):1602–1609, 1993.

[69] Mojca Pavlin and Damijan Miklavcic. Theoretical and experimental analysis of conductivity, ion diffusion and molecular transport during cell electroporation - relation between short-lived and long-lived pores. *Bioelectrochemistry*, 74(1):38–46, 2008.

[70] Ralf W. Glaser, Sergei L. Leikin, Leonid V. Chernomordik, Vasili F. Pastushenko, and Artjom I. Sokirko. Reversible electrical breakdown of lipid bilayers: formation and evolution of pores. *Biochimica et Biophysica Acta (BBA) - Biomembranes*, 940(2): 275–287, 1988.

[71] S. M. Kennedy, Z. Ji, J. C. Hedstrom, J. H. Booske, and S. C. Hagness. Quantification of electroporative uptake kinetics and electric field heterogeneity effects in cells. *Biophys J*, 94(12):5018–27, 2008.

[72] M. N. Teruel and T. Meyer. Electroporation-induced formation of individual calcium entry sites in the cell body and processes of adherent cells. *Biophysical Journal*, 73(4): 1785–1796, 1997.

[73] Kazuhiko Kinosita Jr, Masahiro Hibino, Hiroyasu Itoh, Masaya Shigemori, Ken'ichi Hirano, Yutaka Kirino, and Tsuyoshi Hayakawa. *Events of Membrane Electroporation Visualized on a Time Scale from Microsecond to Seconds*, pages 29–46. Academic Press, San Diego, 1992.

[74] W. Frey, J. A. White, R. O. Price, P. F. Blackmore, R. P. Joshi, R. Nuccitelli, S. J. Beebe, K. H. Schoenbach, and J. F. Kolb. Plasma membrane voltage changes during nanosecond pulsed electric field exposure. *Biophys J*, 90(10):3608–15, 2006.

[75] Lars H. Wegner, Wolfgang Frey, and Sina Schönwälder. A critical evaluation of whole cell patch clamp studies on electroporation using the voltage sensitive dye annine-6. *Bioelectrochemistry*, 92(0):42–46, 2013.

[76] T. Griese, S. Kakorin, and E. Neumann. Conductometric and electrooptic relaxation spectrometry of lipid vesicle electroporation at high fields. *Physical Chemistry Chemical Physics*, 4(7):1217–1227, 2002.

[77] Kazuhiko Kinosita Jr and Tian Yow Tsong. Voltage-induced conductance in human erythrocyte membranes. *Biochimica et Biophysica Acta (BBA) - Biomembranes*, 554 (2):479–497, 1979.

[78] R. J. O'Neill and L. Tung. Cell-attached patch clamp study of the electropermeabilization of amphibian cardiac cells. *Biophysical Journal*, 59(5):1028–1039, 1991.

[79] K. Kitamura, B. Judkewitz, M. Kano, W. Denk, and M. Hausser. Targeted patch-clamp recordings and single-cell electroporation of unlabeled neurons in vivo. *Nat Methods*, 5 (1):61–7, 2008.

[80] Mojca Pavlin and Damijan Miklavcic. Effective conductivity of a suspension of permeabilized cells: A theoretical analysis. *Biophysical Journal*, 85(2):719–729, 2003.

[81] A. L. Garner, Chen Nianyong, Yang Jing, J. Kolb, R. J. Swanson, K. C. Loftin, S. J. Beebe, R. P. Joshi, and K. H. Schoenbach. Time domain dielectric spectroscopy measurements of hl-60 cell suspensions after microsecond and nanosecond electrical pulses. *Plasma Science, IEEE Transactions on*, 32(5):2073–2084, 2004.

[82] R. V. Davalos, D. M. Otten, L. M. Mir, and B. Rubinsky. Electrical impedance tomography for imaging tissue electroporation. *IEEE Trans Biomed Eng*, 51(5):761–7, 2004.

[83] U. Pliquett, R. Elez, A. Piiper, and E. Neumann. Electroporation of subcutaneous mouse tumors by rectangular and trapezium high voltage pulses. *Bioelectrochemistry*, 62(1):83–93, 2004.

[84] A. Ivorra, B. Al-Sakere, B. Rubinsky, and L. M. Mir. In vivo electrical conductivity measurements during and after tumor electroporation: conductivity changes reflect the treatment outcome. *Phys Med Biol*, 54(19):5949–63, 2009.

[85] Judith A. Stolwijk, Christoph Hartmann, Poonam Balani, Silke Albermann, Charles R. Keese, Ivar Giaever, and Joachim Wegener. Impedance analysis of adherent cells after in situ electroporation: Non-invasive monitoring during intracellular manipulations. *Biosensors and Bioelectronics*, In Press, Corrected Proof, 2011.

[86] E. Pasqualotto, A. Ferrario, M. Scaramuzza, A. De Toni, and M. Maschietto. Monitoring electropermeabilization of adherent mammalian cells through electrochemical impedance spectroscopy. *Procedia Chemistry*, 6(0):79–88, 2012.

[87] Urska Cegovnik and Srdjan Novakovic. Setting optimal parameters for in vitro electrotransfection of b16f1, sa1, lpb, sck, l929 and cho cells using predefined exponentially decaying electric pulses. *Bioelectrochemistry*, 62(1):73–82, 2004.

[88] E. T. Jordan, M. Collins, J. Terefe, L. Ugozzoli, and T. Rubio. Optimizing electroporation conditions in primary and other difficult-to-transfect cells. *J Biomol Tech*, 19(5): 328–34, 2008.

[89] Joseph N. Blattman and Philip D. Greenberg. Cancer immunotherapy: A treatment for the masses. *Science*, 305(5681):200–205, 2004.

[90] S. Kumar, D. Chanda, and S. Ponnazhagan. Therapeutic potential of genetically modified mesenchymal stem cells. *Gene Ther*, 15(10):711–5, 2008.

[91] S. T. Andreadis. Gene-modified tissue-engineered skin: the next generation of skin substitutes. *Adv Biochem Eng Biotechnol*, 103:241–74, 2007.

[92] Yuriy Fedorov, Alan King, Emily Anderson, Jon Karpilow, Diane Ilsley, William Marshall, and Anastasia Khvorova. Different delivery methods-different expression profiles. *Nat Meth*, 2(4):241–241, 2005.

[93] S. I. Sukharev, V. A. Klenchin, S. M. Serov, L. V. Chernomordik, and A. Chizmadzhev Yu. Electroporation and electrophoretic dna transfer into cells. the effect of dna interaction with electropores. *Biophys J*, 63(5):1320–7, 1992.

[94] Maša Kandušer and Damijan Miklavčič. *Electroporation in Biological Cell and Tissue: An Overview*, chapter 1, pages 1–37. Food Engineering Series. Springer New York, 2009.

[95] Saša Haberl, Damijan Miklavčič, and Mojca Pavlin. Effect of mg ions on efficiency of gene electrotransfer and on cell electropermeabilization. *Bioelectrochemistry*, 79(2): 265–271, 2010.

[96] J. Jantsch, N. Turza, M. Volke, K. U. Eckardt, M. Hensel, A. Steinkasserer, C. Willam, and A. T. Prechtel. Small interfering rna (sirna) delivery into murine bone marrow-derived dendritic cells by electroporation. *J Immunol Methods*, 337(1):71–7, 2008.

[97] O. Met, J. Eriksen, and I. M. Svane. Studies on mrna electroporation of immature and mature dendritic cells: effects on their immunogenic potential. *Mol Biotechnol*, 40(2): 151–60, 2008.

[98] M. P. Rols, C. Delteil, M. Golzio, P. Dumond, S. Cros, and J. Teissie. In vivo electrically mediated protein and gene transfer in murine melanoma. *Nat Biotechnol*, 16(2):168–71, 1998.

[99] S. Kwee, H. V. Nielsen, and J. E. Celis. Electropermeabilization of human cultured cells grown in monolayers : Incorporation of monoclonal antibodies. *Journal of Electroanalytical Chemistry*, 298(1):65–80, 1990.

[100] Claudio Schönenberger, Anette Schütz, Alfredo Franco-Obregón, and Marcy Zenobi-Wong. Efficient electroporation of peptides into adherent cells: investigation of the role of mechano-growth factor in chondrocyte culture. *Biotechnology Letters*, 33(5):883–888, 2011.

[101] Lluis M. Mir. Therapeutic perspectives of in vivo cell electropermeabilization. *Bioelectrochemistry*, 53(1):1–10, 2001.

[102] L. M. Mir, S. Orlowski, Jr. Belehradek, J., and C. Paoletti. Electrochemotherapy potentiation of antitumour effect of bleomycin by local electric pulses. *Eur J Cancer*, 27(1):68–72, 1991.

[103] G. Sersa, B. Stabuc, M. Cemazar, D. Miklavcic, and Z. Rudolf. Electrochemotherapy with cisplatin: clinical experience in malignant melanoma patients. *Clin Cancer Res*, 6 (3):863–7, 2000.

[104] D. Miklavčič, G. Serša, E. Brecelj, J. Gehl, D. Soden, G. Bianchi, P. Ruggieri, C. R. Rossi, L. G. Campana, and T. Jarm. Electrochemotherapy: technological advancements for efficient electroporation-based treatment of internal tumors. *Medical & Biological Engineering & Computing*, 50(12):1213–1225, 2012.

[105] R. Davalos, L. Mir, and B. Rubinsky. Tissue ablation with irreversible electroporation. *Annals of Biomedical Engineering*, 33(2):223–231, 2005.

[106] B. Rubinsky, G. Onik, and P. Mikus. Irreversible electroporation: a new ablation modality–clinical implications. *Technol Cancer Res Treat*, 6(1):37–48, 2007.

[107] S. Haberl, D. Miklavcic, G. Sersa, W. Frey, and B. Rubinsky. Cell membrane electroporation-part 2: the applications. *Electrical Insulation Magazine, IEEE*, 29(1): 29–37, 2013.

[108] Hiroshi Tanaka, Keiji Shimizu, Takashi Hayashi, and Suyu Shu. Therapeutic immune response induced by electrofusion of dendritic and tumor cells. *Cellular Immunology*, 220(1):1–12, 2002.

[109] L. Raptis and K. L. Firth. Electrode assemblies used for electroporation of cultured cells. *Methods Mol Biol*, 423:61–76, 2008.

[110] Judith A. Stolwijk. *Electric Manipulation and Impedance Analysis of Adherent Cells on Gold-Film Electrodes*. PhD thesis, 2011.

[111] L. Raptis, A. Vultur, H. L. Brownell, E. Tomai, A. Anagnostopoulou, R. Arulanandam, J. Cao, and K. L. Firth. Electroporation of adherent cells in situ for the study of signal transduction and gap junctional communication. *Methods Mol Biol*, 423:173–89, 2008.

[112] Kilian J. Müller, Mirko Horbaschek, Kurt Lucas, Ulrich Zimmermann, and Vladimir L. Sukhorukov. Electrotransfection of anchorage-dependent mammalian cells. *Experimental Cell Research*, 288(2):344–353, 2003.

[113] Qiang Zheng and Donald C. Chang. High-efficiency gene transfection by in situ electroporation of cultured cells. *Biochimica et Biophysica Acta (BBA) - Gene Structure and Expression*, 1088(1):104–110, 1991.

[114] M. Rebersek, C. Faurie, M. Kanduser, S. Corovic, J. Teissie, M. P. Rols, and D. Miklavcic. Electroporator with automatic change of electric field direction improves gene electrotransfer in-vitro. *Biomed Eng Online*, 6:25, 2007.

[115] Takeshi Ishibashi, Kimiyasu Takoh, Hirokazu Kaji, Takashi Abe, and Matsuhiko Nishizawa. A porous membrane-based culture substrate for localized in situ electroporation of adherent mammalian cells. *Sensors and Actuators B: Chemical*, 128(1): 5–11, 2007.

[116] Yu-Cheng Lin, Min Li, Chun-Sheng Fan, and Li-Wha Wu. A microchip for electroporation of primary endothelial cells. *Sensors and Actuators A: Physical*, 108(1-3):12–19, 2003.

[117] K. S. Huang, Y. C. Lin, C. C. Su, and C. S. Fang. Enhancement of an electroporation system for gene delivery using electrophoresis with a planar electrode. *Lab Chip*, 7(1): 86–92, 2007.

[118] Wei Zewen, Huang Huang, Liang Zicai, and Li Zhihong. A high performance electroporation chip integrating multi-well plate and annular interdigital microelectrodes. In *Micro Electro Mechanical Systems (MEMS), 2010 IEEE 23rd International Conference on*, pages 951–954, Zewen.

[119] Huang Huang, Zewen Wei, Yuanyu Huang, Deyao Zhao, Lianghong Zheng, Tianjing Cai, Mengxi Wu, Wei Wang, Xianfeng Ding, Zhuan Zhou, Quan Du, Zhihong Li, and Zicai Liang. An efficient and high-throughput electroporation microchip applicable for sirna delivery. *Lab on a Chip*, 11(1):163–172, 2011.

[120] Ami A. Deora, Fernando Diaz, Ryan Schreiner, and Enrique Rodriguez-Boulan. Efficient electroporation of dna and protein into confluent and differentiated epithelial cells in culture. *Traffic*, 8(10):1304–1312, 2007.

[121] Elke De Vuyst, Marijke De Bock, Elke Decrock, Marijke Van Moorhem, Christian Naus, Cyriel Mabilde, and Luc Leybaert. In situ bipolar electroporation for localized cell loading with reporter dyes and investigating gap junctional coupling. *Biophysical Journal*, 94(2):469–479, 2008.

[122] J. A. Kim, K. Cho, M. S. Shin, W. G. Lee, N. Jung, C. Chung, and J. K. Chang. A novel electroporation method using a capillary and wire-type electrode. *Biosens Bioelectron*, 23(9):1353–60, 2008.

[123] Jessica Olofsson, Mikael Levin, Anette Stromberg, Stephen G. Weber, Frida Ryttsen, and Owe Orwar. Scanning electroporation of selected areas of adherent cell cultures. *Analytical Chemistry*, 79(12):4410–4418, 2007.

[124] G. N. Stewart. Researches on the circulation time in organs and on the influences which affect it: Parts i.-iii. *J Physiol*, 15(1-2):1–89, 1893.

[125] G. N. Stewart. The charges produced by the growth of bacteria in the molecular concentration and electrical conductivity of culture media. *J Exp Med*, 4(2):235–43, 1899.

[126] R. Höber. Eine methode die elektrische leitfaehigkeit im innern von zellen zu messen. *Arch. Ges. Physiol.*, (133):237–259, 1910.

[127] Hugo Fricke. The electric capacity of suspensions with special reference to blood. *The Journal of General Physiology*, 9(2):137–152, 1925.

[128] P. Debye. *Polar Molecules*. New York, 1929.

[129] Kenneth S. Cole. Permeability and impermeability of cell membranes for ions. *Cold Spring Harbor Symposia on Quantitative Biology*, 8:110–122, 1940.

[130] Kenneth S. Cole and Robert H. Cole. Dispersion and absorption in dielectrics i. alternating current characteristics. *The Journal of Chemical Physics*, 9(4):341–351, 1941.

[131] H. P. Schwan. Electrode polarization impedance adn measurements in biological materials. *Annals of the New York Academy of Sciences*, 148(1):191–209, 1968.

[132] K. R. Foster and H. P. Schwan. Dielectric properties of tissues and biological materials: a critical review. *Crit Rev Biomed Eng*, 17(1):25–104, 1989.

[133] K.R. Foster and H.P. Schwan. *Dielectric properties of tissues - A review*, pages 25–102. CRC Press, Boca Raton, Fla., 2nd ed. edition, 1995.

[134] E. T. McAdams and J. Jossinet. Tissue impedance: a historical overview. *Physiological Measurement*, 16(3A):A1, 1995.

[135] Jean-Pierre Morucci, Max E. Valentinuzzi, Bernard Riguard, Carmelo J. Felice, Nicolas Chaveau, and Pierre-Marie Marsili. *Bioelectrical Impedance Techniques in Medicine*, volume 24 (Issues 4-6) of *Critical Reviews in Biomedical Engineering*. Bergell House, Inc., New York, 1996.

[136] S. Grimnes Martinsen and O. G. *Bioimpedance and Bioelectricity Basics*. Academic Press, San Diego, CA, 2000.

[137] Tao Sun and Hywel Morgan. Single-cell microfluidic impedance cytometry: a review. *Microfluidics and Nanofluidics*, 8(4):423–443, 2010.

[138] Britta Lindholm-Sethson, Josefina Nyström, Martin Malmsten, Lovisa Ringstad, Andrew Nelson, and Paul Geladi. Electrochemical impedance spectroscopy in label-free biosensor applications: multivariate data analysis for an objective interpretation. *Analytical and Bioanalytical Chemistry*, 398(6):2341–2349, 2010.

[139] Khalil Heileman, Jamal Daoud, and Maryam Tabrizian. Dielectric spectroscopy as a viable biosensing tool for cell and tissue characterization and analysis. *Biosensors and Bioelectronics*, 49(0):348–359, 2013.

[140] R.H. Bayford. Bioimpedance tomography (electrical impedance tomography). *Annual Review of Biomedical Engineering*, 8(1):63–91, 2006.

[141] H. Scharfetter, R. Casanas, and J. Rosell. Biological tissue characterization by magnetic induction spectroscopy (mis): requirements and limitations. *Biomedical Engineering, IEEE Transactions on*, 50(7):870–880, 2003.

[142] OG Martinsen, S Grimnes, and HP Schwan. *Interface phenomena and dielectric properties of biological tissue*, volume 20, chapter 20, page 2643–2653. 2002.

[143] R. Pethig and D. B. Kell. The passive electrical properties of biological systems: their significance in physiology, biophysics and biotechnology. *Physics in Medicine and Biology*, 32(8):933, 1987.

[144] H. P. Schwan. Electrical properties of tissues and cell suspensions: mechanisms and models. In *Engineering in Medicine and Biology Society, 1994. Engineering Advances: New Opportunities for Biomedical Engineers. Proceedings of the 16th Annual International Conference of the IEEE*, pages A70–A71 vol.1.

[145] Mimoza Ibrani, Luan Ahma, and Enver Hamiti. *The Age-Dependence of Microwave Dielectric Parameters of Biological Tissues*. Microwave Materials Characterization. 2012.

[146] R. D. Stoy, K. R. Foster, and H. P. Schwan. Dielectric properties of mammalian tissues from 0.1 to 100 mhz; a summary of recent data. *Physics in Medicine and Biology*, 27 (4):501, 1982.

[147] B. Sanchez, G. Vandersteen, R. Bragos, and J. Schoukens. Basics of broadband impedance spectroscopy measurements using periodic excitations. *Measurement Science and Technology*, 23(10):105501, 2012.

[148] U. Pliquett. Time-domain based impedance measurement: strengths and drawbacks. *Journal of Physics: Conference Series*, 434(1):012092, 2013.

[149] Y. Feldman, Irina Ermolina, and Y. Hayashi. Time domain dielectric spectroscopy study of biological systems. *Dielectrics and Electrical Insulation, IEEE Transactions on*, 10(5):728–753, 2003.

[150] M. Min, U. Pliquett, T. Nacke, A. Barthel, P. Annus, and R. Land. Broadband excitation for short-time impedance spectroscopy. *Physiol Meas*, 29(6):S185–92, 2008.

[151] B. Sanchez, G. Vandersteen, R. Bragos, and J. Schoukens. Optimal multisine excitation design for broadband electrical impedance spectroscopy. *Measurement Science and Technology*, 22(11):115601, 2011.

[152] B. Sanchez, E. Louarroudi, E. Jorge, J. Cinca, R. Bragos, and R. Pintelon. A new measuring and identification approach for time-varying bioimpedance using multisine electrical impedance spectroscopy. *Physiological Measurement*, 34(3):339, 2013.

[153] F. J. Harris. On the use of windows for harmonic analysis with the discrete fourier transform. *Proceedings of the IEEE*, 66(1):51–83, 1978.

[154] David Yélamos, Óscar Casas, Ramon Bragós, and Javier Rosell. Improvement of a front end for bioimpedance spectroscopy. *Annals of the New York Academy of Sciences*, 873 (1):306–312, 1999.

[155] B. Sanchez, E. Louarroudi, R. Bragos, and R. Pintelon. Harmonic impedance spectra identification from time-varying bioimpedance: theory and validation. *Physiological Measurement*, 34(10):1217, 2013.

[156] Mohamadou Youssoufa, Oh Tong In, Wi Hun, Sohal Harsh, Farooq Adnan, Woo Eung Je, and McEwan Alistair Lee. Performance evaluation of wideband bio-impedance spectroscopy using constant voltage source and constant current source. *Measurement Science and Technology*, 23(10):105703, 2012.

[157] Herman P. Schwan and Clifford D. Ferris. Four-electrode null techniques for impedance measurement with high resolution. *Review of Scientific Instruments*, 39(4):481–485, 1968.

[158] Ishai Paul Ben, S. Talary Mark, Caduff Andreas, Levy Evgeniya, and Feldman Yuri. Electrode polarization in dielectric measurements: a review. *Measurement Science and Technology*, 24(10):102001, 2013.

[159] F. Bordi, C. Cametti, and T. Gili. Reduction of the contribution of electrode polarization effects in the radiowave dielectric measurements of highly conductive biological cell suspensions. *Bioelectrochemistry*, 54(1):53–61, 2001.

[160] Y. Salazar, R. Bragos, O. Casas, J. Cinca, and J. Rosell. Transmural versus nontransmural in situ electrical impedance spectrum for healthy, ischemic, and healed myocardium. *Biomedical Engineering, IEEE Transactions on*, 51(8):1421–1427, 2004.

[161] H. Fricke and S. Morse. The electric resistance and capacity of blood for frequencies between 800 and 4(1/2) million cycles. *J Gen Physiol*, 9(2):153–67, 1925.

[162] Henning Krassen, Uwe Pliquett, and Eberhard Neumann. Nonlinear current–voltage relationship of the plasma membrane of single cho cells. *Bioelectrochemistry*, 70(1): 71–77, 2007.

[163] Uwe Pliquett, R. Langer, and James C. Weaver. Changes in the passive electrical properties of human stratum corneum due to electroporation. *Biochimica et Biophysica Acta (BBA) - Biomembranes*, 1239(2):111–121, 1995.

[164] Uwe Pliquett and MarkR Prausnitz. *Electrical Impedance Spectroscopy for Rapid and Noninvasive Analysis of Skin Electroporation*, volume 37 of *Methods in Molecular Medicine*, chapter 30, pages 377–406. Humana Press, 2000.

[165] A. Ivorra and B. Rubinsky. In vivo electrical impedance measurements during and after electroporation of rat liver. *Bioelectrochemistry*, 70(2):287–95, 2007.

[166] U. F. Pliquett and K. H. Schoenbach. Changes in electrical impedance of biological matter due to the application of ultrashort high voltage pulses. *Dielectrics and Electrical Insulation, IEEE Transactions on*, 16(5):1273–1279, 2009.

[167] J. Zhuang and J. F. Kolb. Time domain dielectric spectroscopy of nanosecond pulsed electric field induced changes in dielectric properties of pig whole blood. *Bioelectrochemistry*, 2014.

[168] M. Kranjc, F. Bajd, I. Serša, and D. Miklavčič. Magnetic resonance electrical impedance tomography for measuring electrical conductivity during electroporation. *Physiological Measurement*, 35(6):985, 2014.

[169] Y. Granot, A. Ivorra, E. Maor, and B. Rubinsky. In vivo imaging of irreversible electroporation by means of electrical impedance tomography. *Phys Med Biol*, 54(16):4927–43, 2009.

Chapter 3

Design and implementation of a microelectrode assembly for non contact *in situ* electroporation of adherent cells

Abstract

This chapter focuses on the design and implementation of the initial prototypes of microelectrodes developed during this thesis. The objective of this work was to develop a system capable of performing *in situ* electroporation on adherent cells growing in standard multi-well plates with minimal invasiveness of the operation. The novelty of the design resides, on one hand, in the position of the microelectrode with respect to the cell monolayer, and on the other, in the fabrication technology used. Standard printed circuit board (PCB) technology is used allowing interelectrode distances in the order of tens of microns what dramatically reduces the voltages applied to the samples. Simulations are performed to study and compare the electric field distribution in both prototypes. Permeabilization tests assayed with a fluorescent FITC-dextran are shown for different cell lines. The information explained along this chapter resulted in two publications (see Appendices A and B).

3.1 Introduction

As described in chapter 2, traditional *in vitro* equipment perform electroporation in cuvettes where cells are suspended in order to apply electric field pulses [1]; however, the majority of mammalian cell lines used in biomedical research are adherent cells. As previously explained, some grounds exist for the suitability of *in situ* electroporation of adherent cells. With the term *in situ* the reader should understand the fact that electroporation is applied directly to adherent cell monolayers preventing any modification of the state and conformation of cell monolayers.

As stated in 2.1.4.1, cell detachment previous to electric pulse application is eliminated, thus preserving the intact cellular characteristics of the sample, reducing the cell stress and the invasiveness of the procedure. Additionally, *in situ* electroporation allows treatment of differentiated cells [2], which better resemble in-vivo cell phenotype. Is precisely in-vivo tissue electroporation, which is nowadays applied in the clinical treatment of different diseases [3–6], the perfect example where cells are not in suspension during the application of electric fields and supports the fact that electroporation of adherent cells describes a better model to study different aspects that could be translated in the improvement of the response to therapeutic treatments.

Most of the previous systems that apply electroporation *in situ* to adherent cell cultures consist of microfabricated electrode structures deposited into planar substrates where cell monolayers are grown [7–9], refer to section 2.1.4.1 for a summary of these and other *in situ* electroporation setups. One of the main advantages of using microelectrode assemblies consists in dramatic reduction in inter-electrode distances when compared with suspension setups. This reduction in the distance between anode and cathode means that lower voltages are applied in order to reach the same electric field intensities, thus leading to simpler and cheaper pulse generators as well as to a reduction in safety issues.

Moreover, the application of microelectrodes structures in the field of cellular biology used as sensors is perfectly well known. The reduction in the dimensions of the electrodes to values comparable to the cell size allows developing local and more accurate and precise measurements. In this direction, the device presented

herein is also conceived to be used as a sensor for electrical impedance recordings of the state of cell monolayer. However this characteristic will be fully explained and exploited in following chapters.

The drawback of the current microelectrode arrays used for *in vitro* electroporation, is the cost of the fabrication techniques that are used. As previously stated, if cells are grown on top of the microelectrodes, then, thin film fabrication technologies are necessary what implies, apart from the high costs, the impossibility to use standard culture ware. Along this chapter, a standard fabrication method which allows to dramatically reduce the device costs is used to implement a microelectrode structure. Additionally, the device presented this chapter has been conceived to be used in standard multi-well culture plates. To the best of our knowledge, there are no previous devices combining the advantages of using microelectrodes structures with the possibility of application to standard culture plates.

3.2 Rationale of the device

The conception of the device is based in the two main requirements exposed above: the use of a microelectrodes structure applicable both for electroporation and electrical impedance measurements of a cell monolayer and the integration of the device to be used in standard multi-well culture plates.

As previously shown, all devices using planar microelectrodes setups require adherent cells to be grown on the surface of them. Nevertheless, the modification of the growing surface to include the patterned microelectrodes implies the use of non-standard culture ware. The use of non-standard surfaces implies, in some cases, some trust issues in the final biomedical user. Additionally, regarding the effectiveness of the treatment, as pointed out in a previous study [10], cell attachment to the microelectrodes during electroporation creates a high permeability region mostly located around the area of contact between cells and electrodes. However, some molecules cannot precipitate to the bottom surface difficulting their pass across the membrane.

In order to fulfill these design specifications, the only alternative consisted on a system capable of momentarily placing the microelectrodes at a short distance

above the cell monolayer during the application of the electric field pulses and removing them afterward. For this purpose, it was necessary the integration of microseparators as elements, on one hand, to ensure the precise placement of the microelectrodes completely parallel and at a fixed distance to the cell monolayer, and on the other hand, to avoid direct contact between the cell monolayer and the electrodes. The use of these elements minimizes the invasiveness of the operation, being the cells treated identically as in other routine chemical manipulations performed in a standard culture plate. In Fig. 3.1a a schematic representation of the top positioning principle is depicted in Fig. 3.1b a detailed view of the microseparators patterned on the microelectrodes is shown.

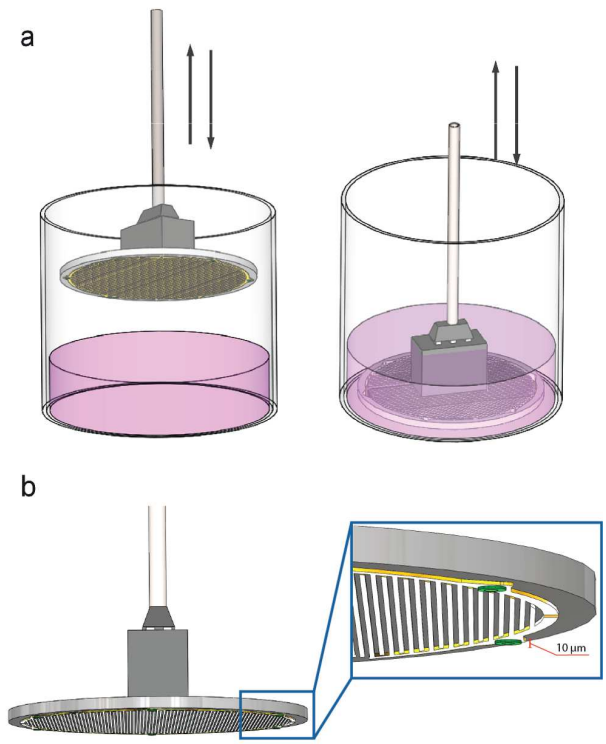

Fig. 3.1 Schematic representation of the device. (a) Principle of operation showing how electrodes are placed parallel to the bottom surface of the multi-well plates. (b) Detailed view of the micro-separations used to avoid contact between electrodes and cells.

3.3 Materials and Methods

3.3.1 Electrode assembly

Regarding the specific requirements of the system we can define the following design specifications.

- Circular geometry of the substrate in order to fit and cover to whole surface of the multi well culture plates.
- Dimensions (width and spacing of the microelectrodes) in the order of tens of microns in order to use low voltages for electroporation.
- Fabrication of a disposable device what involves the need of using a low cost fabrication technology.
- Connections cannot be placed in the same plane of the substrate where the microelectrodes are patterned due to the top positioning principle. This restriction suggests the use of a bilayer design.
- Non cytotoxic materials should be used in order to avoid undesired effects as cell death or other interferences during the course of an experiment.

3.3.1.1 Geometry

The electrode geometry design is based on an interdigitated structure consisting in six independent lines forming three active arrays of electrodes on a circular substrate. Each electrode in the array connected alternately to +V or -V terminals of the pulse generator for electroporation (see Fig. 3.2). By increasing the spacing between electrodes, the maximum of the electric field is displaced in the vertical direction. Nevertheless, for a constant electric field, increasing the gap between electrodes involves also increasing the voltage applied. In the present case, we are interested in maximizing the electric field in the region separated from the electrode surface where cells actually grow. The choice of the dimensions is optimized to maximize the electric field while maintaining low voltages. According to the minimal resolution of the fabrication technology used (50 μm), some different designs were tested using different electrode width

(W) and spacing (S). Namely, W_1=50 μm and W_2=75 μm and three different spacings S_1=75 μm, S_2=100 μm and 150 μm. In Fig. 3.3 a picture of the different designs is shown. Based on the quality of the final fabricated design, the minimal width was fixed to 75 μm (lower dimensions lead to errors and short circuits). Finally, the choice of the spacing between adjacent lines was done based on the fact that the higher the space between lines, the more separated the electric field lines from the electrodes surface. This was supported by some basic electric field simulations performed (data not shown). The final spacing used was 150 μm.

The conception of this topology, which contains six independent sets of microelectrodes, also enables to perform electrical bioimpedance measurements in 2-wire or 4-wire configurations. This characteristic is not exploited in the present work and will be treated in deep detail in next chapters.

3.3.1.2 Fabrication technology

A - Initital Prototype

In the present device we propose to make use of standard printed circuit board (PCB) Class 7 bilayer technology according to high density integration (HDI) IPC regulation to manufacture our microelectrode assembly (Lab Circuits S.A. 08460 Barcelona, Spain). In the past few years, PCB technology has reached a resolution of tens of micrometers and some studies have been conducted to demonstrate the biocompatibility of a wide variety of materials used in PCB manufacturing processes in order to include this technology as a feasible option in the construction of lab-on-a-chip devices [11]. Additionally, this technology fulfills other specific requirements for the present case as the significant reduction in manufacturing costs. If one of our goals is to help electroporation to be introduced as a standard laboratory technique, it is desirable to supply low cost disposable devices. The requirement regarding the placement of the connections is also easily overcome with the standard PCB bilayer technology that allow to place the connector in the opposite face of the structure using metalized laser microvias to connect both sides, thus giving an easy top connectivity to the electrode assembly.

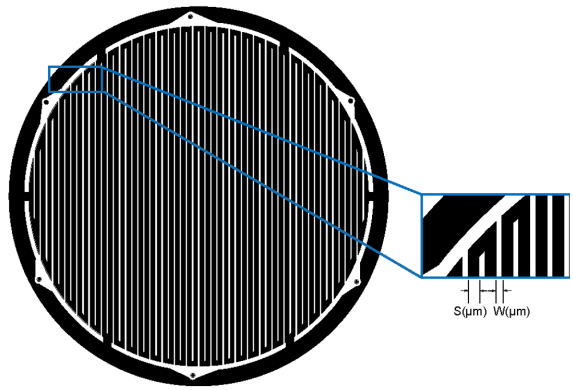

Fig. 3.2 Interdigitated topology of the electrode assembly.

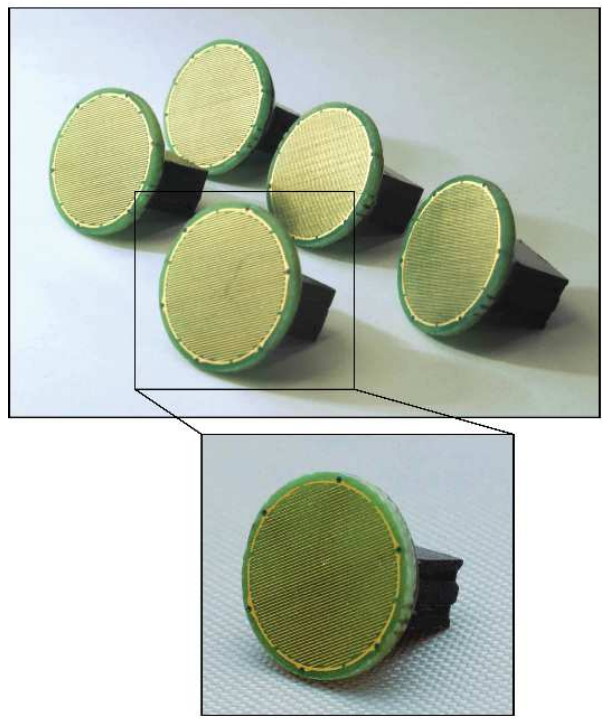

Fig. 3.3 Picture of the different designs fabricated varying the width and spacing between lines and a detailed view of one of them.

The microelectrodes where fabricated using 15 mm diameter discs made of a FR4-135Tg substrate with 1 mm thickness and a thin copper foil (20 μm) as the conductive layer. The chosen diameter is compatible with the dimensions of standard 24 multiwell plates. Once the electrodes were patterned on copper following the standard fabrication procedures, a final Nickel (Ni)/Gold (Au) plating was deposited using Electroless Nickel Immersion Gold (ENIG) technique in order to avoid the toxicity of the copper (Cu). The final result consists on a Cu/Ni/Au three-layered structure with thickness of 20 μm, 0.7 μm and 0.01 μm respectively.

Following the idea of *in situ* application to cell monolayers, small micro-separations were created to avoid direct contact between the electrodes and the monolayer what could cause mechanical stress or damages to the cells. These separations were constructed using a final layer of photosensible epoxy PSR-4000 GP01EU (Taiko Ink Mfg. Co.) with thickness of 10 μm. Once the structure was covered with the epoxy resin, six circular micro-separators were patterned on the surface of the electrodes equally distributed along the perimeter of the discs. Thickness of cell monolayers is usually between 3 μm and 8 μm in most of cell lines attached to a surface [12, 13] consequently 10 μm is enough to avoid direct contact with the electrodes.

B - Improved prototype

After the first experiments and results with the prototype described above, we encountered some deficiencies and limitations. The main observation relates with the high electric currents necessary to trigger the electroporation of cells. We observed that the excessive increase in the applied current resulted in the appearance of undesired electrolytic reactions and gas bubble formation with increasing duration of electric field pulses. These effects were definitively unacceptable for the good operation of the system.

Analyzing our system, in comparison with other microelectrode devices, we found that due to the high thickness of the copper conductor foil (20 μm) if compared with those of thin-film technologies, electric current density mainly concentrates in the lateral spacing between electrodes. Furthermore if we take into account the relative distance between cells and electrodes, electric fields applied should be much greater than usual leading to the observed electrolytic

reactions that would irreversibly damage cell monolayer. In order to eliminate this effect, we decided to fill the lateral gap volume between adjacent electrodes with a non-conductive material. With this strategy, current flow in this area is avoided. Thus, the region where the electric field is forced to a maximum is vertically separated away from the inter-electrode area, and it is this region to which the cell monolayer adheres (see Fig. 3.4).

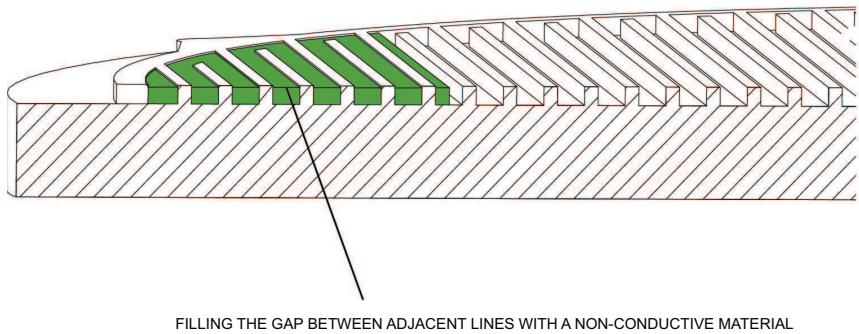

Fig. 3.4 Schematic representation of the concept applied to improve the current density in the area of interest.

The fabrication process consists on a modification of the one described previously. First, microelectrodes are patterned in copper similarly to the process used for the first prototype; namely, photomask UV light exposure of photoresist pre-coated boards, and development of photoresist and chemical etching of unwanted copper areas. The process is modified at this point when the structure is covered again with a photosensible epoxy PSR-4000 GP01EU (Taiko Ink Mfg. Co.) in order to fill the lateral gap between electrodes with a non-conductive material. After curing, microabrasion is performed to remove the epoxy excess from the surface of microelectrodes until copper areas are exposed again. Subsequently, the process continues as in the first prototype with ENIG coating and patterning of microseparators. Schematic explanation of the complete fabrication process is shown in Fig. 3.5.

In addition to the previous characteristics, from an economical point of view, the standard PCB fabrication technology used involves a drastic reduction in

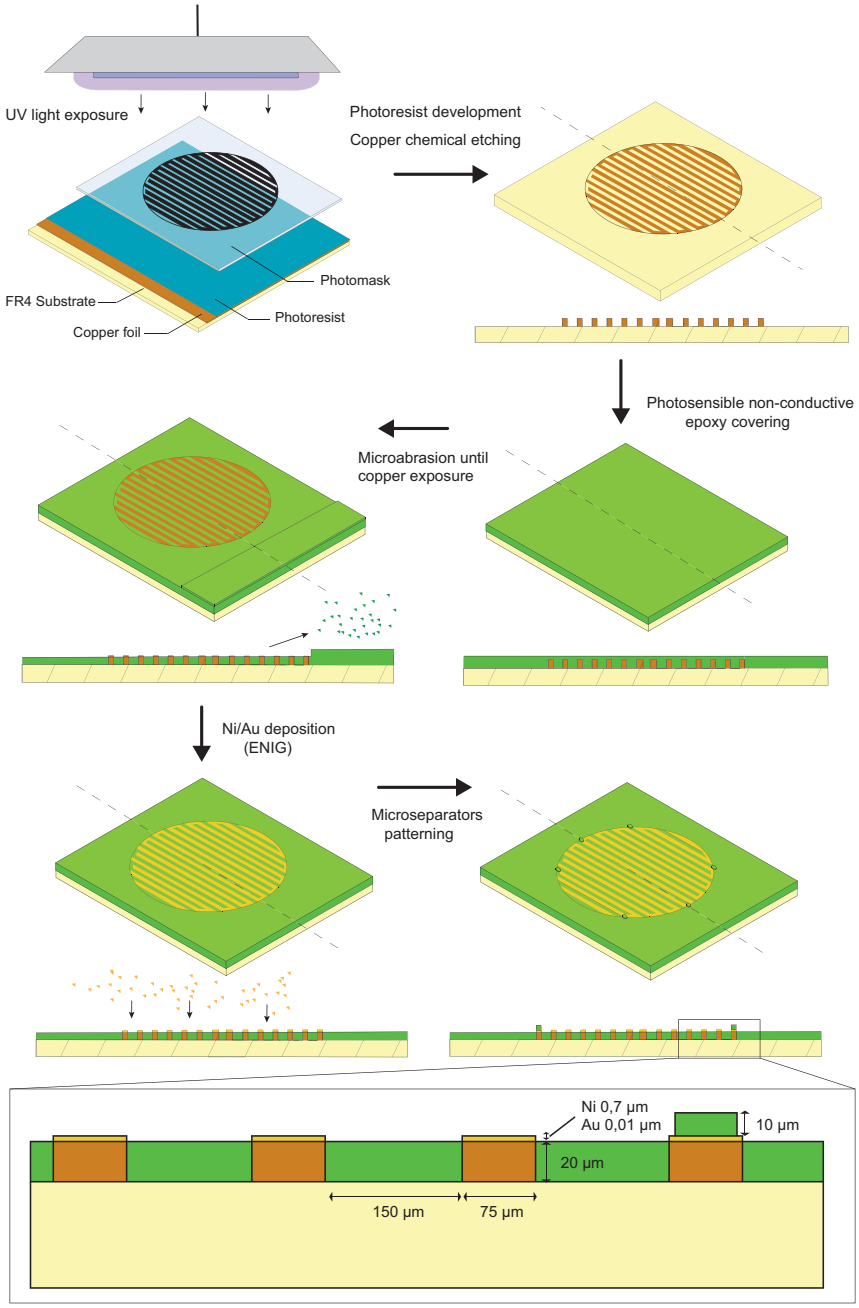

Fig. 3.5 Schematic representation of the complete modified PCB fabrication process of the microelectrode assembly.

costs, thereby allowing the production of low-cost disposable devices. Although the fabrication costs depend on the fabrication scale, when compared with thin-film technologies the reduction in cost may be of the order of 10-50 times. In addition, electrode degradation and cross contamination between experiments are avoided by using disposable equipment. Other additional costs involving cleaning and sterilization are also eliminated.

3.3.1.3 Simulations

In order to evaluate the distribution and uniformity of the electric field created by the electrode assembly, finite element simulations were performed during the development process using commercial software COMSOL Multiphysics 3.5 using the AC/DC module.

First, the electric field for the initial prototype was studied. A 2D simplification of the structure reproducing the exact dimensions of the electrodes was simulated. The conductivity used for the different parts is σ=0,004 S/m for the FR4 substrate, σ=5,998 10^7 S/m for copper electrodes and σ=0.16 S/m for poration media. Boundary conditions in the electrodes were set to fixed current ports or ground alternatively.

In Fig. 3.6**a** the current density distribution is shown. In order to have an idea of the electric field distribution in the region, separated from the electrodes, where cells should be growing as a monolayer, cross sectional plots are represented. Fig. 3.6**b** depicts the electric field values along a horizontal line separated 15 μm from the electrodes. From this plot it can be stated that cells under the center of the electrodes will not be electroporated because the electric field intensity in these areas will not be high enough. On the other hand, the effect in the areas where the electric field is over the threshold will be very uniform, only 4% of variation as indicated in the plot. In Fig. 3.6**c** the electric field values along a vertical line are plotted. As shown in the figure, there is an electric field reduction in vertical direction with a maximum decrease of 10% between the highest and the lowest points of the line. In the light of these simulations, we concluded that the vast majority of the current applied was lost in the lateral volume between electrodes. As already explained in section 3.3.1.2, we determined that an improved design was necessary.

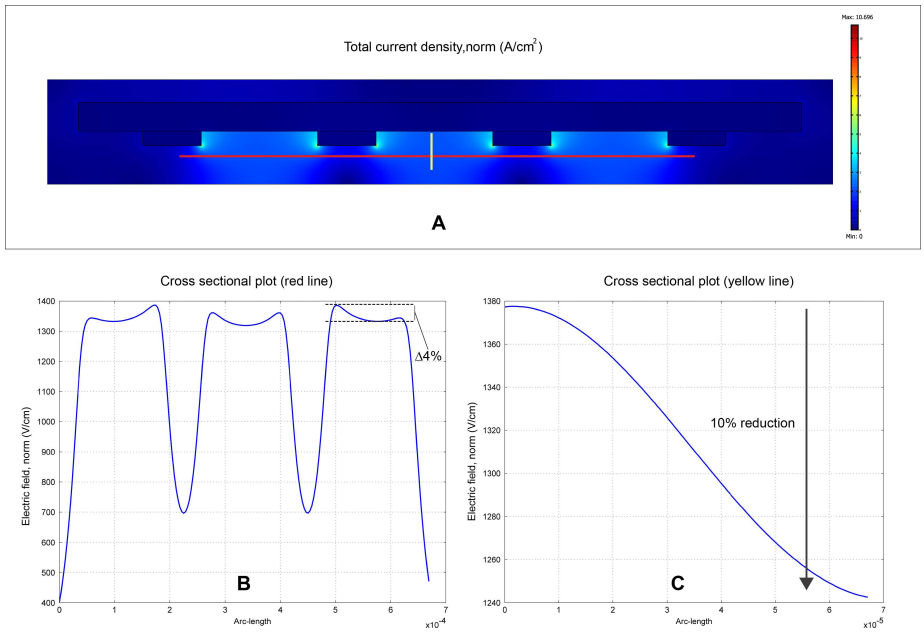

Fig. 3.6 Electric field simulations run on COMSOL Multiphysics 3.5. **A)** Total current density in (A/cm^2) is plotted in the 2D simplification simulated. **B)** Cross sectional plot of the electric field distribution along an horizontal line 15 μm apart from the surface of the electrodes (red line in A). **C)** Cross sectional plot of the electric field distribution along a vertical line (yellow line in A

As a following step, we made some simulations in order to evaluate the increase in current density caused by the modification of the initial design. The simulation parameters are similar to those used previously but including in this case a new subdomain between electrodes representing the non-conductive material added in this prototype. The conductivity of the region was set to σ=0.004 S/m.

In Fig. 3.7 a comparison between the new and the previous design is depicted. In this case the current density is represented in an arrow plot together with the electric field. Results from the simulations demonstrate the resulting increase in the electric field intensity in the area of interest by around twofold in the case where the spacing is filled with a non-conductive material and when the same electric current is injected. This results reinforce the suitability of the modification proposed for the improved prototype.

In addition, we plotted electric field cross-section values for the simulation

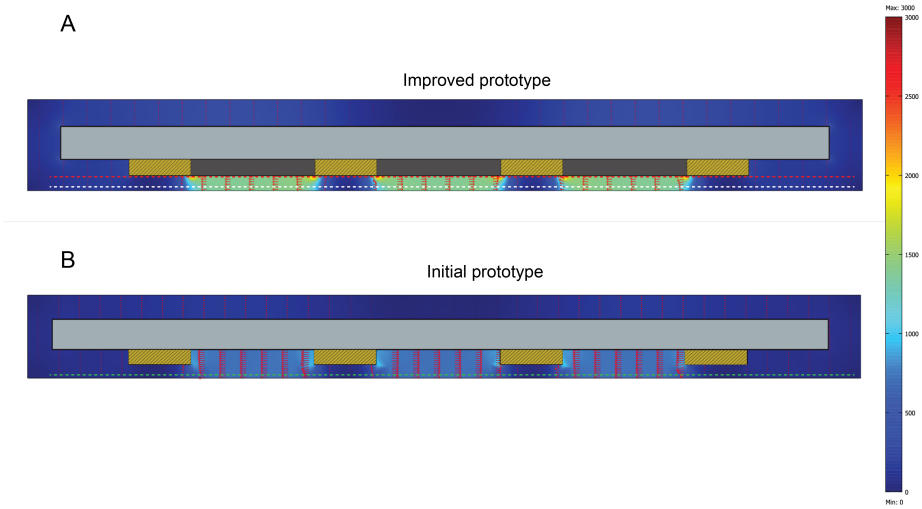

Fig. 3.7 Electric field simulations on COMSOL Multiphysics 3.5. Comparison between the two prototypes fabricated. Electric field intensity is plotted in colors. Arrow plot shown the current density.

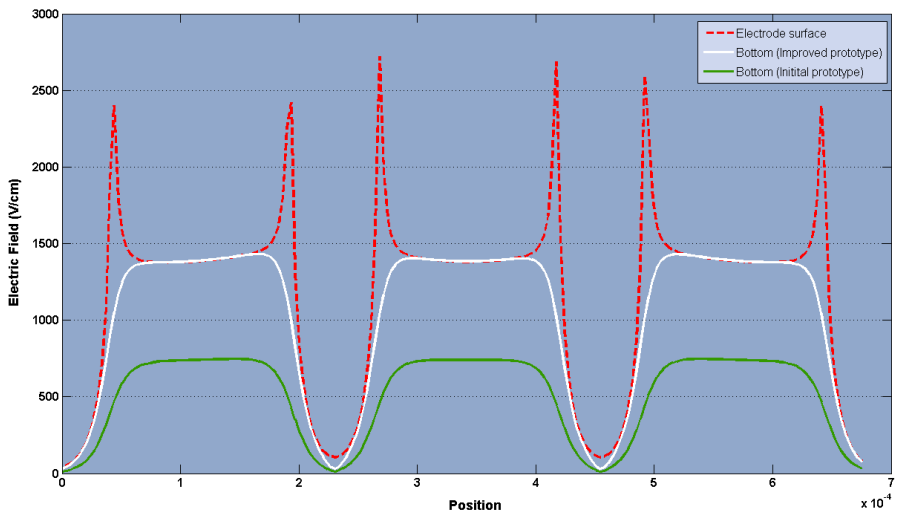

Fig. 3.8 Electric field line plots. Comparison between the electric field in the surface of electrodes and 15 μm away for the two prototypes fabricated

in Fig. 3.7. Electric fields created along three lines are shown. One of them in the surface of the electrodes (dotted red line) and the other two (dotted white and green lines) 15 μm away from the surface of electrodes (see Fig. 3.8).

From these simulations it can also be concluded that the use of micro-separations has the advantage of applying more uniform electric fields. These plots help to demonstrate that considerably irregular electric fields are presented in the surface area of the electrodes what could irreversibly damage cell membranes near these areas. As already stated by other authors, more uniform electric fields are created short distance away from the electrodes surface [8, 14] supporting the advantage of the device in contrast with systems were cells are grown in the surface of the microelectrodes.

3.3.2 Additional equipment

A - Automatic positioning system

Regarding the aim of standard laboratory use, an automatic system was designed to perform experiments in 24 multiwell plates inside of a sterile cabinet automatically. For experiments, the electrode assembly is automatically positioned using a self-constructed positioner. This system is based on a self-constructed x-y positioning table where the multiwell is placed and a z linear displacement positioner where electrodes are mounted. The device makes use of stepper motors controlled by Labview 2009 (National Instruments) software. In addition, using this automatic system, the displacement speed of the electrode can be controlled. An excessive speed could produce a harmful fluid pressure to cells. For that reason, in all the experiments we used a controlled movement to settle the electrode on the bottom of the well plates ensuring that the fluid displacement does not harm the monolayer. Also the force applied against the surface is always the same.

B - Electric field pulse delivery

Electric field pulse delivery was performed making use of a biphasic stimulator developed in our laboratory and first conceived for long-term contraction of cultured muscle cells [15]. The stimulator generates bipolar pulses acting as a fixed current source or a voltage source with intensities **(A)** ranging from 1 mA

up to 800 mA or voltages from 0 to 50 Vp, minimal duration **(D)** of each part of the bipolar signal is 100 μs and the minimal period **(T)** is 1 ms. There is an additional parameter **(Tt)** that allows to set the time separation between positive and negative part of the pulse (min value 100 µs), see Fig. 3.9. The device is fully programmable by RS-232 connection to a PC. As previously studied by other authors, the use of bipolar pulses enhances the transfection efficiency [16, 17] and reduces electrolytic gas bubble formation in metal electrodes [18].

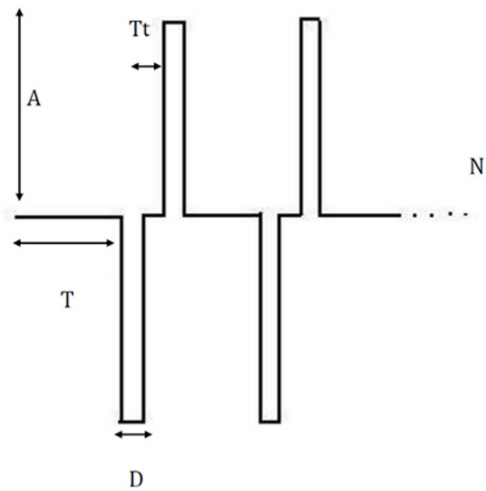

Fig. 3.9 Biphasic waveform parameters

From the initial analysis we made, maybe biased by our background of electrical engineers, voltage needs to be adjusted if a fixed current is applied, and vice-versa, because voltage is usually interpreted as the voltage measured in the same electrodes that apply the current, which usually is the only pair of electrodes in the system. This voltage waveform is affected by the medium impedance and, mainly, by the electrode interface impedance, which is nonlinear. The voltage waveform in the medium, however, and given the purely resistive behavior of saline solutions, corresponds to the product of the current waveform by a cell constant and the medium resistivity. We have checked this in previous projects by using four electrode set-ups, that is, injecting the current by a pair of electrodes and measuring the resulting voltage in the medium with a different pair of electrodes connected to a high input impedance differential am-

plifier, partially described in [19]. That way, the current through the measuring electrodes is negligible, and the measured voltage waveform is not affected by the electrode impedance but only by the medium resistivity and by the current waveform. Performing these measurements we are able to see the actual voltage waveform only in the medium and not affected by electrode/electrolyte interfacial phenomena. With this setup, in the case of applying a constant current square pulse, a constant voltage square pulse was measured. We have not checked this again with the electrode set-up described herein due to the small distances between adjacent current injection microelectrodes, and the impossibility of placing voltage sensing electrode between them but the electrical basis is the same than in the previously tested set-ups.

All these reasons lead us to use the biphasic stimulator acting as a current controlled source. Although electroporation is usually applied with fixed voltage sources, we believe that current controlled sources ensure that cell membrane is polarized by the same current over the complete electroporation treatment. Other advantages over voltage controlled approaches are described in detail in [20]. Due to the application of a defined constant current, in order to have an estimate of the voltage to distance ratio, it was necessary to measure the voltage drop, in this case between the same current injection microelectrodes as described in section 3.3.4. For calculations, we considered the voltage values measured during the first pulse applied.

3.3.3 Cells and chemicals

For the experiments described in this chapter, C2C12 mouse myogenic cell line and HEK 293 human embryonic kidney cell line were used. Cells were cultured as a monolayer in Dulbecco's Modified Eagle Medium (DMEM) supplemented with 10% fetal bovine serum and added with penicillin, streptomycin and fungizone.

Regarding the buffer used during the application of electric field pulses we decided to use a low conductivity electroporation buffer (LCEB). Low conductive media are regularly used in electroporation experiments. In our case we decided to use this type of buffer in order to reduce the possible heating of extracellular medium and also to avoid electrolytic reactions. As observed by

[21], LCEBs do not affect significantly the permeabilization results but improve the survival rates of cells after treatment. In our case the LCEB consisted of 10 mM Na_2HPO_4 pH (7.4), 1 mM $MgCl_2$ and 250 mM sucrose. Conductivity of 1.6 mS/cm. Measurements were made using Conductimeter GLP32, Crison, (Barcelona-Spain) after calibrating the equipment with two different conductivity patterns.

In order to assess the permeabilization results we decided to use a molecular fluorescent reporter. The use of this type of markers allows visualizing the results short after the application of the electric field and give direct information about of the extent of membrane permeabilization. The advantage of these molecules is that results are not masked depending on secondary cellular mechanisms that are necessary in other situations. For the experiments we decided to use fluorescein isothiocyanate-dextran (FITC-dextran). FITC-dextrans are used as a fluorescent probe to study cell processes such as cell permeability, phagocytosis and endocytosis and to study mechanisms of biomolecular delivery. These markers can be purchased commercially in different molecular weights and may be used to study the size selectivity of the pores formed in the membrane. In our case we used FD20S (Sigma-Aldrich, Madrid, Spain) average molecular weight 20 kDa. When stated, FD20S was added to the LCEB at a final concentration of 2.5 mg/ml.

When stated, viability was analyzed on the same treated cells 24 hours after the electroporation procedure. Cells remaining adhered after 24 hours were considered viable. Quick panoptic staining kit (Qumica clnica aplicada S.A., Amposta, Spain) was used to mark all the cells and then they were examined under a Leica DMI 4000B inverted microscope for fluorescence. Cells were automatically counted using free software ImageJ (MacBiophotonics).

3.3.4 Electroporation procedure

Both C2C12 and HEK293 cell lines were plated in 24-multi-well plates at a cell concentration of $5x10^4$/well and $7x10^4$/well, respectively. The plates were cultured at 37ºC in a humidified 5% CO2 incubator for approximately 24 h, to reach 50-60% confluence.

Before the application of electric pulses, the electrode assembly was sterilized

with a 70% ethanol solution and then rinsed with sterile distilled water and finally immersed in LCEB before use.

For the first set of experiments performed with the initial prototype, cells were rinsed with phosphate buffered saline (PBS) and then 150 μl of LCEB were added to each well. Immediately, the multi-well plate was placed in the automatic electroporation system and electric field pulses were applied. Eight biphasic pulses, with duration (D) of 100 μs, time separation between positive and negative part of the pulse (Tt) of 100 µs and frequency repetition of 1 Hz were applied with different current intensities (A). The electric field values were calculated as voltage to distance ratios (E=V/d) measuring the voltage drop with an oscilloscope put in parallel with the biphasic stimulator divided by the distance between adjacent electrodes (75 μm). These values correspond to an approximation of the electric field on the surface of the electrodes, but it should be taken into consideration that electric field affecting cell membranes is lowered about 10% because the relative distance between electrodes and cells. In control cells, no electric pulses were applied but the electrode was positioned above the cell monolayer for an equivalent period of time. After the electroporation procedure cells were incubated for an additional 30 minute period in the incubator. After this period, the electroporation buffer was removed and cells were rinsed twice with PBS and replaced with fresh culture medium and left for 2 hours in the incubator for complete resealing. Then, cells were examined under a Leica DMI 4000B inverted microscope for fluorescence, to detect FD20S, which has an excitation wavelength 485 nm and emission at 510 nm. Images were taken with a digital camera Leica DFC 300x. Results for these first experiments are shown in next section.

Following the construction of the improved prototype, we performed a new set of experiments including some modifications in the protocol with respect to the one described above. We increased the amount of buffer added during the application of pulses to 250 μl per well. The electroporation conditions were fixed to four biphasic pulses, with 100 μs separation between positive and negative part of the pulse, frequency repetition of 1 Hz and duration of 1 ms. We also reduced the time elapsed between the application of pulses and the removal of electroporation buffer to 10 minutes before the 2 hours resting time in the incubator for complete resealing. The rest of the procedure remained unaltered.

3.4 Results and Discussion

The objective of this study was to design, fabricate ant test the use of the proposed electrode assembly for *in situ* electropermeabilization of adherent cells growing in standard multi-well plates with minimal invasiveness of the operation. The design and fabrication have been already described in the previous section. As a result of the optimization process and supported by simulations, a modified procedure based on standard PCB technology has been developed where the gap between adjacent lines is filled with a non-conductive material in order to improve electric field intensity in the area of interest. Along this section the experiments done to assess the suitability of the presented systems to perform electroporation to cell monolayers are shown.

For this purpose, adherent cell monolayers were subjected to electroporation with our system and its performance was assessed by the intracellular delivery of the fluorescent FITC-dextran FD20S, which has a molecular radius of 3.2 nm [22]. Previous to the results shown herein, we first performed a high number of tests, in which duration, amplitude and number of pulses were varied, to find the optimal electric field parameters that caused effective reversible electroporation. Once we found the suitable range of parameters for these experiments, we finally decided to fix the duration and to apply different electric field intensities in order to test the performance of the system. Along this chapter a summary of the most relevant results is shown.

In this section, the results obtained with the initial prototype are described first. These results correspond with the initial stage of development of the device and are intended to give an idea of the viability of the concept. Subsequently, the fabrication method was modified as previously described. The results after this modification of the prototype are shown in second place.

B - Initial prototype

Among the conditions tested during the optimization stage for the first prototype, we determined that with the electric currents required to cause permeabilization of cells a fixed short-duration of 100 µs was optimal to avoid bubble gas formation caused by electrolysis of water. Increasing the duration of pulses

lead to the formation of electrolytic reactions with the current intensities required. In addition, we observed that due to the small distance between cells and electrodes, cell monolayer detached when bubbles appeared caused by both pH changes and mechanical stress of bubbles themselves. In consequence, in the following experiments, we varied the amplitude of pulses at this fixed 100 μs duration.

In Fig. 3.10, we show an electric field-dependent fluorescent label of C2C12 myoblasts. Very few fluorescent cells were observed after application of electric field of 1.2 kV/cm (Fig. 3.10**a**). Data also reveal that permeabilization yield increased with increasing electric field amplitude and reached a maximum when the electric field in the electrodes surface was 2.2 kV/cm. Fig. 3.10**e** shows the quantification of the results as percentage of fluorescent cells calculated with respect to the total number of cells 2 hours after the application of the treatment. Thus, these results indicate the uptake of FD20S into adhered C2C12 electroporated cells with up to 50% of efficiency for the best case.

In Fig. 3.11 the effect of treatment of cell line HEK 293 with four different electric field amplitudes 1.2, 1.6, 2 and 2.2 kV/cm is shown. The micrographs also show, as expected, an increase in the number of fluorescent cells as a function of electric field intensity. On the other hand, in electroporated HEK 293 (see Fig. 3.11**c** and Fig. 3.11**d**) we observed the presence of giant cells, what suggests that cell fusion occurred with the highest electric fields applied.

As also known for those skilled in the field, the application of high electric field pulses can induce fusion of a wide variety of cells under certain conditions. One of the main conditions to achieve cell electrofusion is the establishment of membrane-membrane contact between cells. In our case, adherence of cells to the culture plate facilitated cell contact for fusion. Other methods classically force cell-cell contact by dielectrophoresis, chemicals or centrifugation. The observation of cell fusion in HEK 293 cells but not in C2C12 cells, may be due to the fact that the extent of cell electrofusion in vitro and in vivo is cell line dependent and involves cell type-specific membrane properties and/or secretion of proteases [23]. In contrast, the conditions for electropermeabilization of both adherent cell lines in our study resulted to be very similar. Likewise, relatively little difference in electropermeabilization of plated CHO and B16F1 cells was reported, whereas significant differences were observed between the two cell lines

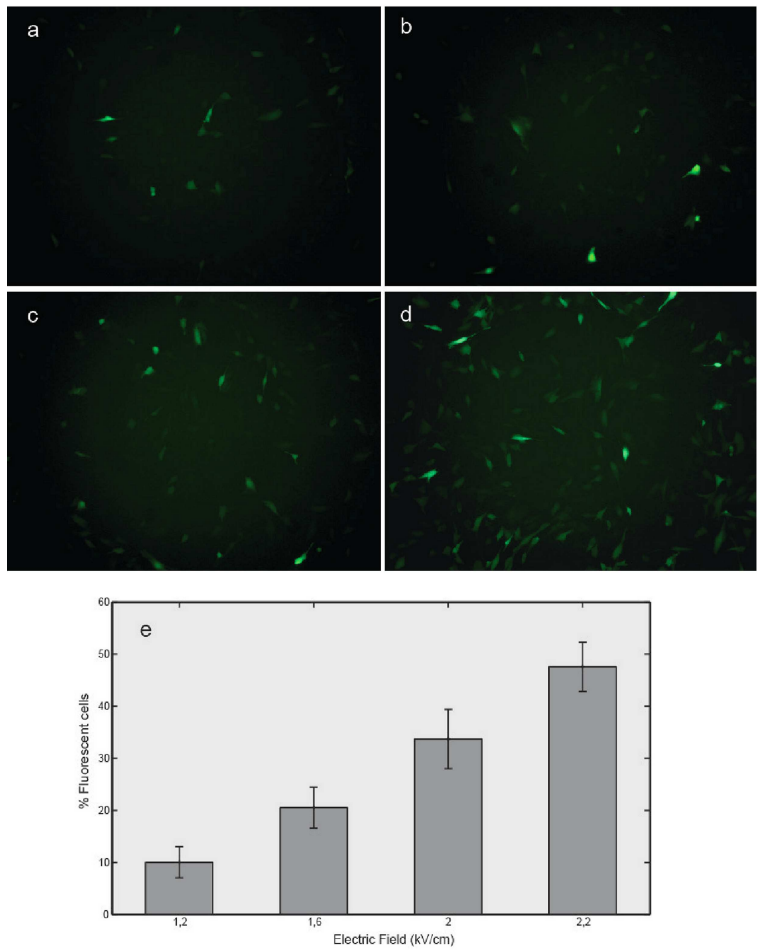

Fig. 3.10 Micrograph of C2C12 cells after electroporation. Cells were electroporated in the presence of FD20S at different electric field intensities: (a)1.2 kV/cm, (b) 1.6 kV/cm, (c)2 kV/cm and (d) 2.2 kV/cm. After cell electroporation and recovery, images of cell monolayers were taken at 10x magnification. A representative image is shown. Lower insert is the quantitative analysis of the results calculated as the percentage of fluorescent cells. Results are expressed in means ± SD of at least five measurements.

in a suspension [24].

These first results confirmed the principle of operation of the device and also revealed valuable knowledge subsequently applied in the optimization of both the electrode assembly and the experimental protocols. Results after the modification of the initial prototype are shown below only for C2C12 cell line.

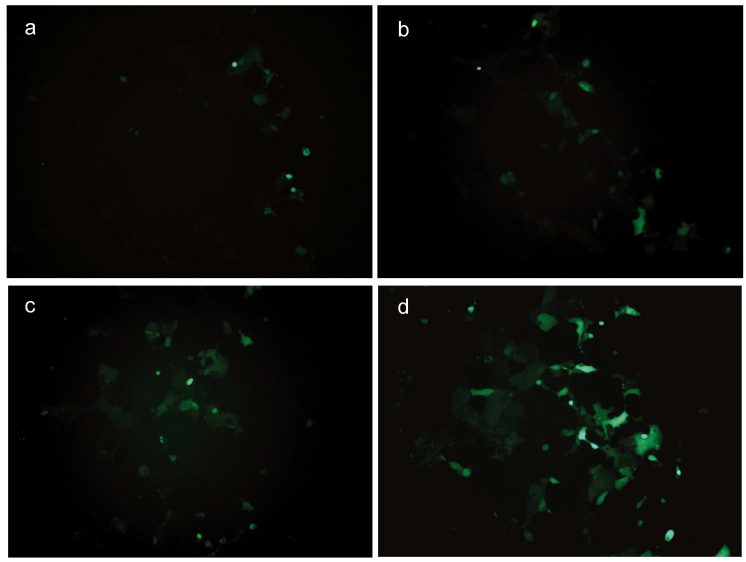

Fig. 3.11 Micrograph of HEK 293 cells after electroporation. Cells were electroporated in the presence of FD20S at different voltages: (a) 1.2 kV/cm, (b) 1.6 kV/cm, (c) 2 kV/cm and (d) 2.2 kV/cm. After cell electroporation and recovery, as described in Materials and Methods, images of cell monolayers were taken at 10x magnification. A representative image is shown.

B - Improved prototype

Similar to the previous case, we first run a set of experiments for optimization. In this case we observed that the reduction in the electric currents applied made possible to use longer durations for the electric field pulses. For that reason, in this set of experiments we fixed the duration to 1 ms and reduced the number of pulses applied to four. We decided to test the system with this longer duration due to the fact that in the next stage our objective would be to use plasmid DNA. According to the theory exposed in chapter 2, longer durations are used with increasing size of the molecule to be inserted by electroporation.

Fig. 3.12a shows the extent of permeabilization as a function of electric field intensity. Percentage of fluorescent cells was calculated dividing the number of marked cells by the total number of cells for each individual well plate. Experiments were duplicated in two different days under the same conditions and each condition repeated three times within each day.

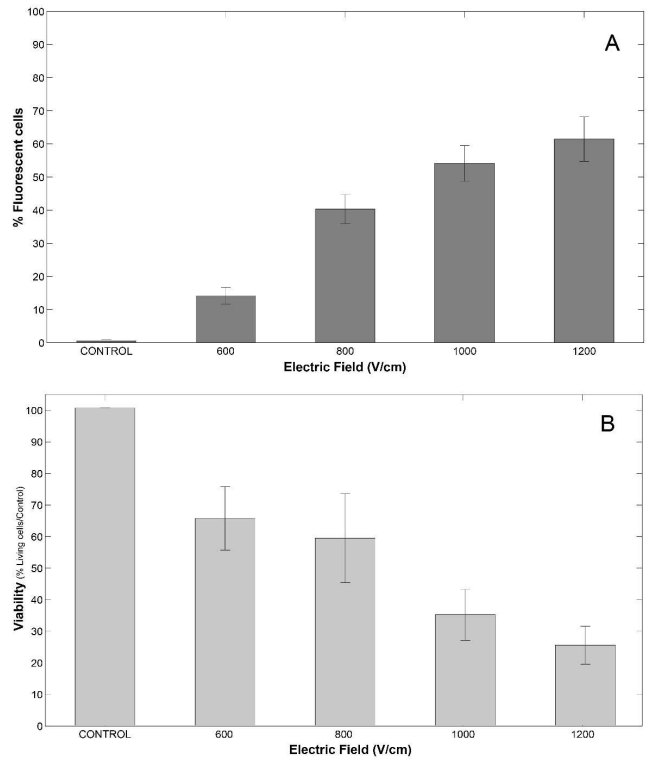

Fig. 3.12 A) Percentage of fluorescent cells for different electric fields as the number of cells marked with FD20S with respect to the total number of cells in each individual well. B) Viability results for the same electric fields in (A) 24 hours after application of treatment. Percentage was calculated as the number of attached cells divided by number of cells in control.

As expected, an increase in the electric field intensity applied led to an increase in the percentage of electroporated cells. For the best case 60% of cells on average were permeabilized. Fig. **b** shows the number of viable cells after 24 hours of the electroporation procedure. The percentage of viability was calculated dividing the number of attached cells for each condition by the number of cells in control. Also as expected, viability decreased when electric fields were increased. For the lowest condition about 65% of cells remained viable after 24 hours.

The present results indicate effective electroporation of adhered C2C12 cell line as stated by the uptake of FD20S into the cells cytoplasm using the im-

proved prototype presented above. Additionally, the modification of the initial design resulted in a considerable decrease in the electric current injected to obtain reversible permeabilization what also resulted in the possibility of increasing the duration of pulses avoiding electrolytic reactions.

The electrode assembly was applied in the successful electroporation of adherent cell monolayers with minimal invasiveness of the device. The treatment was applied directly to standard multiwell plates where cells had been initially grown avoiding additional stress to the cell culture by trypsinization or other post treatment steps. Although the reduction in manipulation of adherent cells should be translated in an increased viability comparing with other systems, our results still show excessive cell death. Even for the lowest electric field, viability is poor if compared with the extent of permeabilization for that condition. On the contrary, good results were observed in control cells where the microelectrode assembly was placed but no electric pulses were applied suggesting that indeed no mechanical damage or cytotoxicity were caused to the cell monolayer.

3.5 Conclusions

In this study we tested a new electrode assembly design, based on the principle of *in situ* electroporation of adherent cell monolayers growing in standard multi-well plates. First we demonstrated the ability of the design for performing electroporation in cultured cell monolayers. We achieved effective electroporation using this set of microelectrodes with the advantage of making use of low voltages due to the small distances between adjacent lines. We also validated the concept of the use of micro-separations between the electrodes and the bottom surface of the growing plates providing a significant advantage: avoiding contact with the cell monolayer, thus causing minimal stress to the cell culture. Furthermore, *in situ* treatment of cells simplified the process and saved several harvesting and processing steps, usually necessary in traditional systems, what may contribute to improve the yield of the process.

First, the initial device was successful in introducing FD20S into two different cell lines. The success in the electroporation of C2C12 cell line, usually resistant to chemical gene transfer methods suggests that it may be valuable to

deliver other macromolecules such as drugs, DNA or antibodies. Additionally, as collateral effect, we observed cell electrofusion in HEK 293 cell line, thus making this device also useful to induce cell fusion.

Subsequent to some observations made in the initial design, some modifications in the fabrication process of the electrode assembly were proposed. The aim of this new prototype was to improve the electric current distribution and to concentrate the electric current flux in the region of interest, thus reducing the total electric current injected by the pulse generator. A second set of experiments was performed with this improved prototype using C2C12 cell line. We also demonstrated the successful performance of the new design and the advantages with the respect to the initial prototype in terms of current reduction and consequently enabling the increase of pulse duration if required. All the results shown herein are just a summary of the multiple experiments performed for the optimization of both devices.

When compared to the available commercial electroporation equipment, this device has the advantages of simpler cell culturing and preparation processes mainly due to the use of standard culturing plates. Additionally, the cheap technology used in the fabrication of the electrodes and the low voltages needed implies a significant reduction in costs both of the electrodes and the pulse generator. Once the initial concept has been demonstrated to be feasible, the system should be tested for the introduction of active molecules such as DNA plasmids, siRNAs, proteins or others, and the number of cell lines should be extended.

References

[1] L. Raptis and K. L. Firth. Electrode assemblies used for electroporation of cultured cells. *Methods Mol Biol*, 423:61–76, 2008.

[2] Marco Sandri, Elena Bortoloso, Alessandra Nori, and Pompeo Volpe. Electrotransfer in differentiated myotubes: a novel, efficient procedure for functional gene transfer. *Experimental Cell Research*, 286(1):87–95, 2003.

[3] Lluis M. Mir. Therapeutic perspectives of in vivo cell electropermeabilization. *Bioelectrochemistry*, 53(1):1–10, 2001.

[4] A. M. Bodles-Brakhop, R. Heller, and R. Draghia-Akli. Electroporation for the delivery of dna-based vaccines and immunotherapeutics: current clinical developments. *Mol Ther*, 17(4):585–92, 2009.

[5] Louise Wichmann Matthiessen, Richard Ling Chalmers, David Christopher George Sainsbury, Sivakumar Veeramani, Gareth Kessell, Alison Claire Humphreys, Jane Elisabeth Bond, Tobian Muir, and Julie Gehl. Management of cutaneous metastases using electrochemotherapy. *Acta Oncologica*, 50(5):621–629, 2011.

[6] D. Miklavčič, G. Serša, E. Brecelj, J. Gehl, D. Soden, G. Bianchi, P. Ruggieri, C. R. Rossi, L. G. Campana, and T. Jarm. Electrochemotherapy: technological advancements for efficient electroporation-based treatment of internal tumors. *Medical & Biological Engineering & Computing*, 50(12):1213–1225, 2012.

[7] Huiqi He, Donald C. Chang, and Yi-Kuen Lee. Using a micro electroporation chip to determine the optimal physical parameters in the uptake of biomolecules in hela cells. *Bioelectrochemistry*, 70(2):363–368, 2007.

[8] Yu-Cheng Lin, Min Li, Chun-Sheng Fan, and Li-Wha Wu. A microchip for electroporation of primary endothelial cells. *Sensors and Actuators A: Physical*, 108(1-3):12–19, 2003.

[9] Huang Huang, Zewen Wei, Yuanyu Huang, Deyao Zhao, Lianghong Zheng, Tianjing Cai, Mengxi Wu, Wei Wang, Xianfeng Ding, Zhuan Zhou, Quan Du, Zhihong Li, and Zicai Liang. An efficient and high-throughput electroporation microchip applicable for sirna delivery. *Lab on a Chip*, 11(1):163–172, 2011.

[10] Huiqi He, Donald C. Chang, and Yi-Kuen Lee. Micro pulsed radio-frequency electroporation chips. *Bioelectrochemistry*, 68(1):89–97, 2006.

[11] Manuela Mazzuferi, Roberta Bovolenta, Massimo Bocchi, Tanja Braun, Joerg Bauer, Erik Jung, Bruno Iafelice, Roberto Guerrieri, Federica Destro, Monica Borgatti, Nicoletta Bianchi, Michele Simonato, and Roberto Gambari. The biocompatibility of materials used in printed circuit board technologies with respect to primary neuronal and k562 cells. *Biomaterials*, 31(6):1045–1054, 2009.

[12] M. Durante, G. Gialanella, G. F. Grossi, and M. Pugliese. Thickness measurements on living cell monolayers by nuclear methods. *Nuclear Instruments and Methods in Physics Research Section B: Beam Interactions with Materials and Atoms*, 73(4):543–549, 1993.

[13] D. Bettega, P. Calzolari, S. M. Doglia, B. Dulio, L. Tallone, and A. M. Villa. Technical report: Cell thickness measurements by confocal fluorescence microscopy on c3h10t1/2 and v79 cells. *Int J Radiat Biol*, 74(3):397–403, 1998.

[14] Wang Lisen, L. Flanagan, and A. P. Lee. Side-wall vertical electrodes for lateral field microfluidic applications. *Microelectromechanical Systems, Journal of*, 16(2):454–461, 2007.

[15] M. Marotta, R. Bragos, and A. M. Gomez-Foix. Design and performance of an electrical stimulator for long-term contraction of cultured muscle cells. *Biotechniques*, 36(1):68–73, 2004.

[16] Elke De Vuyst, Marijke De Bock, Elke Decrock, Marijke Van Moorhem, Christian Naus, Cyriel Mabilde, and Luc Leybaert. In situ bipolar electroporation for localized cell loading with reporter dyes and investigating gap junctional coupling. *Biophysical Journal*, 94 (2):469–479, 2008.

[17] Ephrem Tekle, R. Dean Astumiant, and P. Boon Chock. Electroporation by using bipolar oscillating electric field: An improved method for dna transfection of nih 3t3 cells. *Proc Natl Acad Sci U S A*, 88:4230–4234, 1991.

[18] R. Ziv, Y. Steinhardt, G. Pelled, D. Gazit, and B. Rubinsky. Micro-electroporation of mesenchymal stem cells with alternating electrical current pulses. *Biomed Microdevices*, 11(1):95–101, 2009.

[19] A. Llucià-Valldeperas, B. Sanchez, C. Soler-Botija, C. Gálvez-Montón, C. Prat-Vidal, S. Roura, J. Rosell-Ferrer, R. Bragos, and A. Bayes-Genis. Electrical stimulation of cardiac adipose tissue-derived progenitor cells modulates cell phenotype and genetic machinery. *Journal of Tissue Engineering and Regenerative Medicine*, pages n/a–n/a, 2013.

[20] Daniel R. Merrill, Marom Bikson, and John G. R. Jefferys. Electrical stimulation of excitable tissue: design of efficacious and safe protocols. *Journal of Neuroscience Methods*, 141(2):171–198, 2005.

[21] Gorazd Pucihar, Tadej Kotnik, Masa Kanduser, and Damijan Miklavcic. The influence of medium conductivity on electropermeabilization and survival of cells in vitro. *Bioelectrochemistry*, 54(2):107–115, 2001.

[22] Jayakrishna Ambati, Christina S. Canakis, Joan W. Miller, Evangelos S. Gragoudas, Aurelie Edwards, David J. Weissgold, Ivana Kim, Fransois C. Delori, and Anthony P. Adamis. Diffusion of high molecular weight compounds through sclera. *Investigative Ophthalmology and Visual Science*, 41(5):1181–1185, 2000.

[23] S. Salomskaite-Davalgiene, K. Cepurniene, S. Satkauskas, M. S. Venslauskas, and L. M. Mir. Extent of cell electrofusion in vitro and in vivo is cell line dependent. *Anticancer Res*, 29(8):3125–30, 2009.

[24] Igor Marjanovič, Saša Haberl, Damijan Miklavčič, Maša Kandušer, and Mojca Pavlin. Analysis and comparison of electrical pulse parameters for gene electrotransfer of two different cell lines. *The Journal of Membrane Biology*, 236(1):97–105, 2010.

Chapter 4

A new spiral microelectrode assembly for electroporation and impedance measurements of adherent cell monolayers

Abstract

In this chapter, a new spiral microelectrode topology following the same concept than in the previous chapter, is presented. The new structure is optimized for improved electric field distribution and specially conceived to perform electrical impedance spectroscopy measurements of the state of cell monolayers during electroporation. The system is tested in four cell lines (CHO, HEK293, 3T3-L1 and FTO2B) with a fluorescent dye (FITC 20 kDa). Subsequently gene electrotransfer is assayed with plasmid DNA encoding GFP. Additionally, siRNA α-GFP transfection is tested only in GFP gene-expressing CHO cells. Molecule delivery results show considerable differences between permeabilization (FITC 20 kDa) and gene transfer rates as well as cell line dependence on gene expression. Successful siRNA electro-mediated delivery is shown for CHO cells. Impedance measurements are shown for CHO and 3T3-L1 cells and relate impedance and electroporation. The results shown in this chapter derived in journal paper publication (see Appendix C).

4.1 Introduction

As explained in detail in 2.1.4, one of the main applications of electroporation is the introduction of genetic material into cells. Due to the previously highlighted advantages with respect to other alternative methods, gene electrotransfer has attracted the interest of many researchers and its use is nowadays an established protocol in many laboratories. Nevertheless, gene electrotransfer *in vitro* is usually applied to cells in suspension, however, as stated in the previous chapter, the application of electroporation to adhered cells has significant advantages in many studies. This is the case, for instance, of transfection of differentiated muscle cells which are, similarly to the majority of postmitotic cells, refractory to standard protocols for gene transfer [1]. In addition, the transfection of stem cells during differentiation is commonly used in many studies [2] and the possibility of enabling *in situ* gene transfer of these cells is also valuable.

Along this chapter, a new microelectrode topology following the same concept of performing electropermeabilization *in situ* to cells growing in standard culture plates is presented. The goal of this study is to test the suitability of the device to be applied in the electric field-mediated gene transfer of adherent cell monolayers in standard conditions. The presented device is tested in the electroporation-mediated uptake of various molecules in four different cell lines (CHO, HEK293, 3T3-L1 and FTO2B). As a initial step to test the system for cell permeabilization, fluorescent dye (FITC 20 kDa) is used. Once the parameters for successful electroporation are found, the system is applied in the gene electrotransfer treatment of the four cell lines with a plasmid DNA encoding GFP. Finally, siRNA α-GFP electrotransfection is tested only in GFP gene-expressing CHO cells.

One important improvement of the new spiral topology, comparing to the previous design, is the more uniform electric current distribution over the treated surface. However, the main feature of the new microelectrode design is the optimized topology to perform electrical impedance measurements of the cell monolayer under treatment using a four-electrode method. Similar to the assemblies presented in the previous chapter, the use of patterned microseparators allows to perform these measurements without direct contact between the mi-

croelectrodes and the cells. The non-contact concept together with the fact that EIS is a label-free technique, enable to acquire information from the cell monolayer under the electrodes prior, during or after electroporation using a minimally invasive method. As explained in 2, measurements of the electrical properties of membrane during pulse application have been used to detect the changes produced in the cell membrane. In this regard, electrical impedance spectroscopy (EIS) is a feasible tool for online label-free monitoring of the electroporation process [3, 4].

Due to the expertise of the research group in the field of EIS measurements on biological tissues, the technique is now applied to study cell electropermeabilization with the aim of contributing in the improvement of the available methods to monitor the state of cell membranes during treatment. The starting point is that monitoring the evolution of the complete impedance spectrum has the advantage of providing additional information about the different events that may occur during electroporation. In this chapter, we test the suitability of the new design to perform EIS during the interval between pulses in order to study how parameters such as electric field amplitude or pulse number affect the state of cell membranes.

4.2 Materials and Methods

4.2.1 Microelectrode assembly

In accordance with the concept of performing electroporation to adherent cell monolayers cultured in standard multiwell plates already exposed in the previous chapter, a new topology of microelectrodes is presented. The electrode assembly consists of six equally spaced lines coiled in parallel to form six spirals around the center of a circular disc. The same technique described in section 3.3.1.2B (improved prototype) is used to fabricate this topology. Also the same positioning principle above the cell monolayer is used with this new assembly (Fig.4.1A). The actual active area of this microelectrode assembly, i.e. the area covered by electrodes, is 70 % of the total surface of a 24 multiwell culture plate.

The six spiral lines that make up the new structure have almost equal length; this property implies that the volume of medium between adjacent lines is also the same. An uncoiled version of the structure corresponds to six straight parallel lines with equal length. During application of electroporation pulses, each of these six lines is connected alternatively to positive or negative terminals of the pulse generator. The equivalent circuit of the new structure represented is composed of the parallel association of five identical resistances (see Fig 4.1C). This characteristic leads to a uniform electric current distribution along all these lines if a fixed current (see section 3.3.2) is imposed on the terminals of the pulse generator. This improved electric field distribution compared to the previous setup is the first advantage of the new microelectrode assembly presented.

The other key distinctive feature of the new microelectrode structure is that it is specially conceived to perform electrical impedance measurements on the cell monolayer during electroporation procedure with a four-electrode configuration. The interest of measuring the impedance variations during pulse application relays on the need of developing non-invasive, label-free techniques capable of monitoring the pore formation and resealing during electroporation. These can be useful for the real-time control and optimization of the experimental conditions for each specific treatment [5]. Tetrapolar measuring strategies have been demonstrated to be more suitable for living cell measurements [6] in comparison to classical two wire methods as explained in 2.2.3.3. In Fig. 4.1B a schematic

representation of connections is shown both for electroporation and impedance measurements. In this case we use a modified arrangement of a four-electrode measuring configuration by duplicating potential measurement terminals High

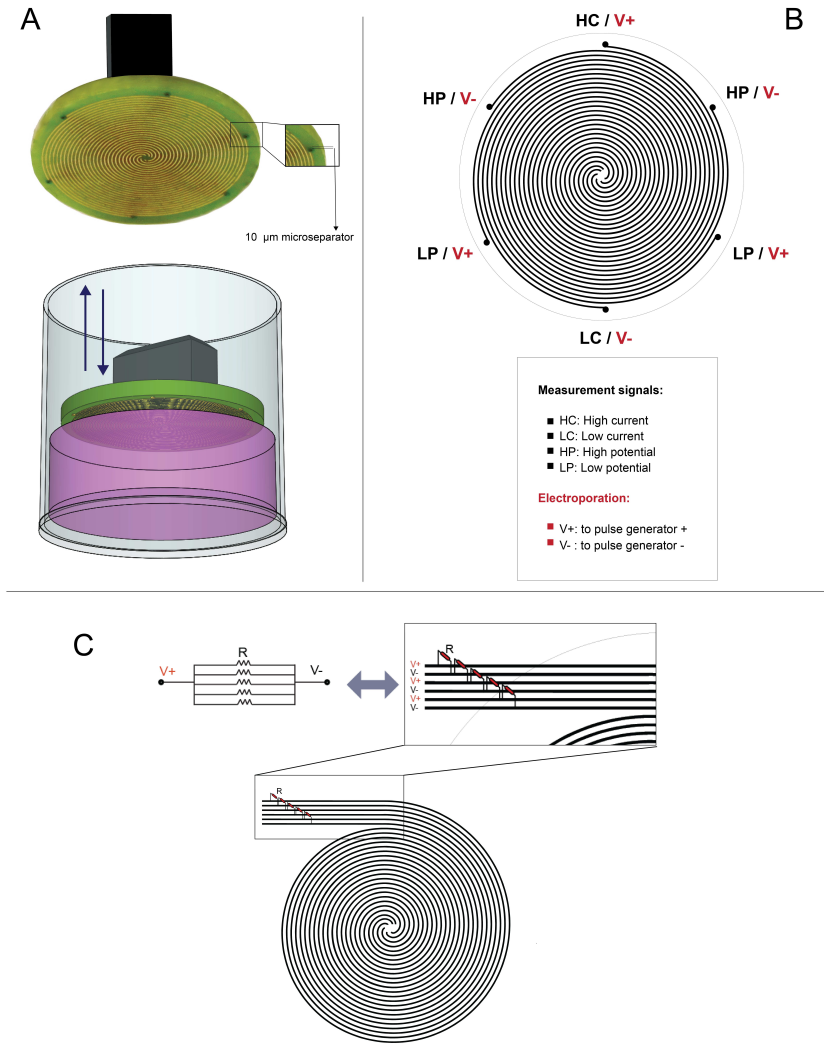

Fig. 4.1 A) Photograph of the real microelectrode assembly showing the spiral geometry, details of the 10 µm microseparators and a schematic representation of the application concept. B) Schematic representation of the spiral topology with details on the different connection configurations. C) Equivalent parallel association of the six lines conforming the spiral topology.

Potential (HP) and Low Potential (LP). This modification, together with the use of the spiral geometry, allows to perform impedance measurements over the whole area of cells covered by the microelectrode assembly during electroporation. This characteristic supplies averaged information on the whole sample under treatment and not only local changes.

4.2.2 Sensitivity study

Sensitivity parameter, referred to electrical impedance, provides information about the contribution of each infinitesimal volume of the sample under test to the total measured impedance. It is considered for simplification that the electrical properties throughout the sample are uniform [7, 8]. Calculations of sensitivity field distribution are very useful to characterize each specific geometry of electrodes and provide valuable information of the possible errors affecting the measured values.

Sensitivity is usually calculated by means of finite elements simulations. In the present case we made use of commercial software COMSOL Multiphysics v4.2. Sensitivity parameter was evaluated following a two-steps study within the AC/DC module as described below:

1. **Step 1:** Compute the current density vector J_1 created when a current **I** is injected between the HC and LC terminal electrodes.

2. **Step 2:** Compute the current density vector J_2 created when a current **I** is injected between the HP and LP terminal electrodes.

Once we obtained these values sensitivity was calculated as:

$$\boldsymbol{S} = \frac{\boldsymbol{J_1 \cdot J_2}}{\boldsymbol{I^2}} \tag{4.1}$$

The vector dot product of these two variables can result in positive, negative or null values depending on the magnitude and angle. A positive value of the sensitivity is interpreted as a region where an increase in the conductivity is

translated in a decrease in the impedance measured. On the opposite, negative value regions contribute inversely, i.e. an increase in the conductivity results in an increase in the impedance measured.

In Fig. 4.2 the simplified geometry simulated corresponding to a part of a 2D sectional cut of the spiral is depicted. In the detailed view of the simulated structure, the materials used for simulation are indicated. On the bottom, a zoom of the surface plot for the obtained sensitivity distribution is shown. The numerical values of the simulation should not be taken into consideration as they

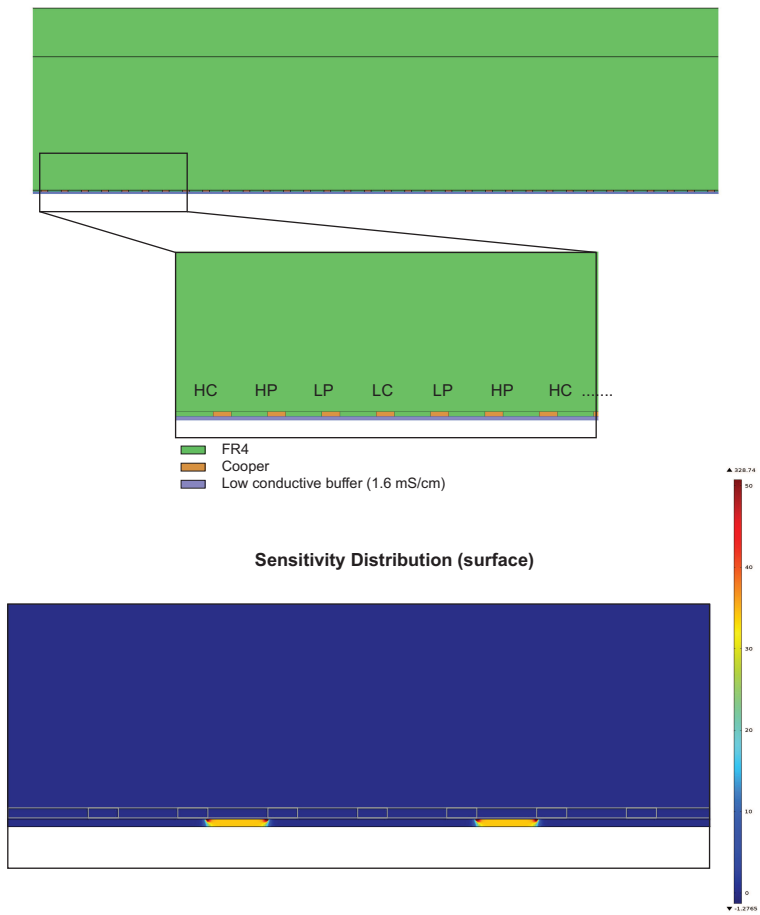

Fig. 4.2 Geometry used in the sensitivity simulations (upper insert). Zoom of the resulting surface plot showing the sensitivity distribution (lower insert).

are not intended to be realistic given the fact that it is a 2D simplification. The information of the resulting distribution should be extracted from the color scale where the reader can have an idea on how the sensitivity varies in the geometry.

In Fig. 4.3 sensitivity values are plotted along a line separated 10 μm from the electrodes surface. From this plot it can be concluded that sensitivity is significantly higher in the areas located between voltage detection electrodes (HP and LP). In the zoom view it can be observed that negative values are generated between voltage and current injection electrodes although the absolute value of these negative sensitivity areas is considerably lower than the positive values.

This sensitivity study supports the idea that the new microelectrode arrangement is suitable for extracting correct impedance information from the sample

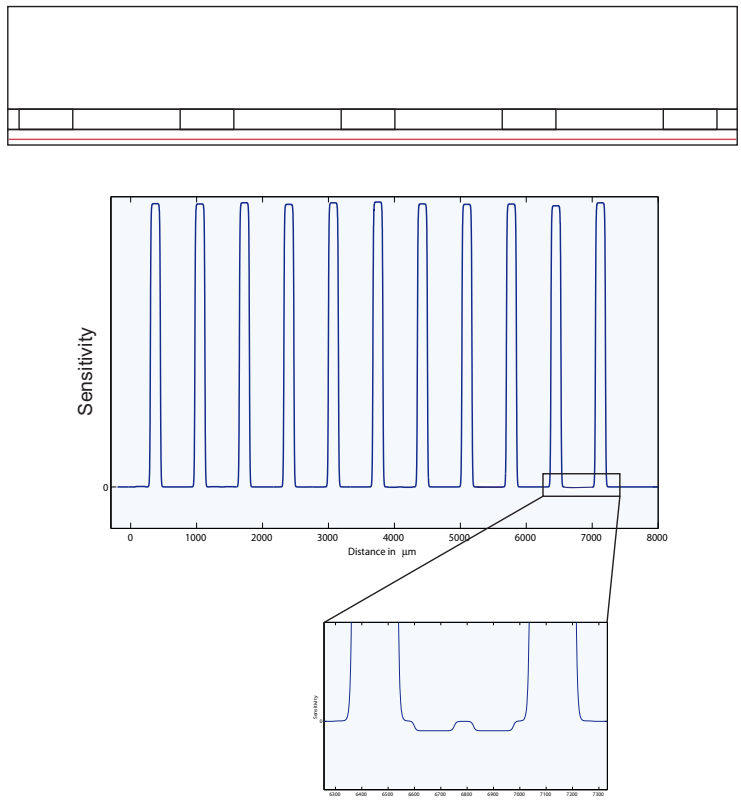

Fig. 4.3 Calculated sensitivity distribution along a line 10 μm away from the surface of the electrodes (red line in the upper insert).

under test with negligible errors due to negative sensitivity areas. According to the simplification performed in the simulation, we can conclude that the region with a high positive sensitivity, meaning the area from which the impedance variations will have a great impact in the total measured impedance, in comparison with the total area simulated, corresponds to 33% of the total surface.

4.2.3 Electric Field Simulations

In order to evaluate the electric field created by the electrode assembly, finite element simulations are performed with commercial software COMSOL Multiphysics 4.2a using the AC/DC module. A geometrically exact 3D model of the structure is simulated by setting boundary conditions alternatively as a ground or fixed voltage terminal (30 V) for each consecutive line. Conductivity of the simulated electroporation buffer is set to 1.6 mS/cm. In Fig. 4.4, the electric field intensity in V/cm is plotted in a parallel plane 8 μm away from the surface of the microelectrodes showing the overall distribution of electric field in the structure. Due to the cylindrical symmetry of the spiral structure, the electric field created has a wide distribution of directions. This fact, together with the distribution of shapes and orientations of a cell monolayer, can lead us to the assumption that an averaged uniform effect is created in the electroporated monolayer. As previously remarked, this implies an important advantage of the new design.

In order to show the local electric field, a 2D simplification of a cross section of the structure is also simulated similarly to the 3D case (Fig. 4.5). Also a plot of the electric field along a line separated 8 μm of the surface of the electrodes is shown. As observed, high electric field uniformity is achieved in the 150 μm space between lines (5,5% of variation). In the 2D simulation we can also have an estimate of the reduction in the electric field intensity from the surface of electrodes to the local electric field seen by cell membranes. This reduction is approximately 6.5% in the middle of the gap between electrodes.

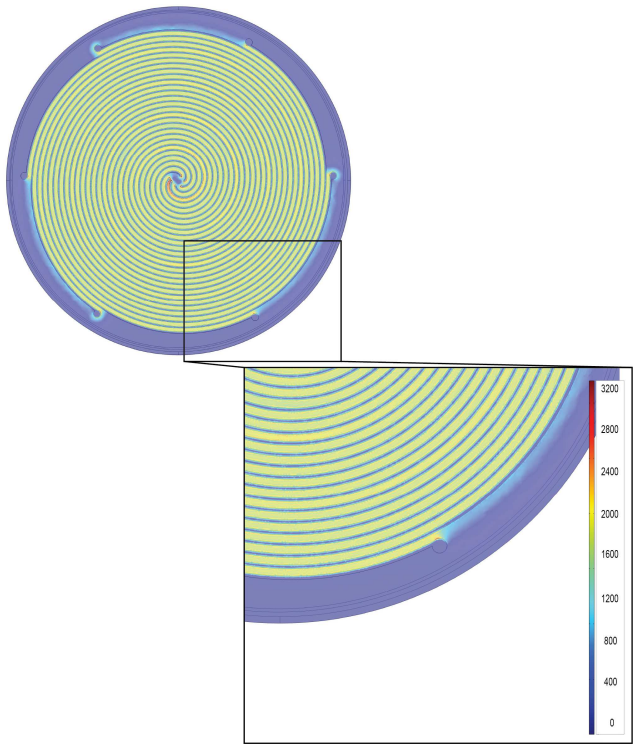

Fig. 4.4 COMSOL simulation of a 3D exact model, electric field intensity (V/cm) is plotted in a parallel plane 8 µm away from the surface of the electrodes. Zoom on a part of the electrode is shown.

4.2.4 Electrical impedance spectroscopy measurements

Given the fact that the same microelectrode structure can be used both for electroporation and measurements, this system enables to obtain impedance information during pulse application. Specifically, in this study it is possible to perform EIS measurements during the interpulse interval of an electroporation treatment. This is valuable to study the evolution of the membrane poration pulse after pulse and not only before and after treatment.

To perform the electrical bioimpedance spectroscopy measurements we use a (periodic) multisine excitation as the reference signal based on the recent findings of the research group where this thesis has been developed [9]. The

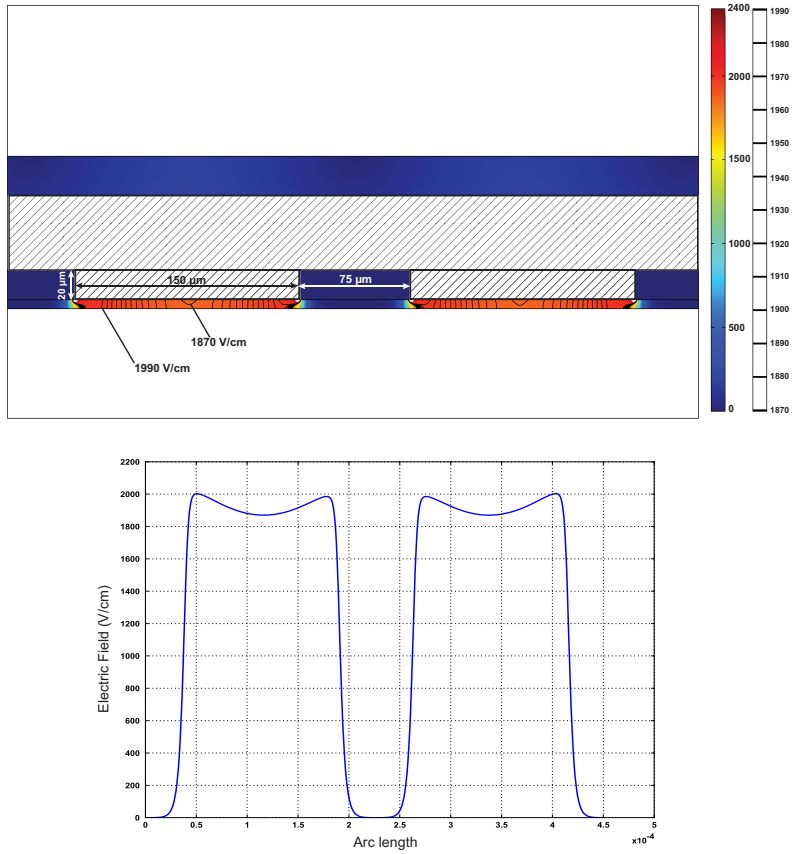

Fig. 4.5 Upper part: 2D simplification of a cross section of the geometry showing electric field intensity (V/cm) in colour, electric field contour lines. Lower part: a plot of the electric field values along a line separated 8 µm of the surface of the electrodes.

multisine burst includes 21 frequencies bilaterally quasi-logarithmically (BQL) distributed from 5 kHz to 1.313 MHz. As explained in 2.2.3.2 the time-domain signals can be optimized for a better performance of the measuring system. In the present case, the BQL distribution is designed on the basis of three key points: i) to concentrate a higher number of frequencies around the impedance relaxation of the biological sample under test, ii) to minimize the intermodulation products at the selected frequencies increasing the Signal to Noise Ratio (SNR) at those frequencies and iii) to minimize the injected energy to the system. In order to minimize the Crest Factor (CF) of the signal, the optimal phase

angles are obtained with a genetic algorithm in Matlab. The obtained CF for the present signal is 2,7 [10]. The total measuring time for each multisine burst is 2 ms (generation and acquisition) and the total number of spectra acquired immediately after each pulse is 20 for averaging.

The measurement system is built in a NI PXIe-1062Q chassis from National Instruments. The system includes an embedded dualcore controller PXIe-8130. The reference signal is generated with the NI PXIe-5122 arbitrary waveform generator (200 MS/s, 16-bit), voltage and current response are acquired, filtered with anti-Alias filters (1,5 MHz) and digitized at 20MHz sample rate with a two-channel high-speed digitizer card PXIe-5122 (100 MS/s, 14-bit). A custom built analog front-end is used to interface the microelectrodes and the measurement hardware. Namely, the measuring reference signal is injected to the sample through a precision resistor (1 kOhm). The voltage sensing terminals are buffered with two high input impedance wideband operational amplifiers (AD8066), and the difference between them is then amplified with a differential line receiver (MAX4145). Current is measured after conversion to voltage through a transimpedance amplifier based on operational amplifier AD8066. The front-end stage has a bandwidth greater than 20 MHz with a CMRR above 60 dB up to 10 MHz. Additionally, the NI PXI-2530 high-density multiconfiguration multiplexer/matrix is used for commutation between electroporation and measurement connections after each pulse. Finally, the pulse generator described in section 3.3.2 is also programmed and syncronized with the measurement equipment, all together controlled by a software developed in LabView.

4.2.5 Cell culture

The FTO2B rat hepatoma and the HEK 293 human embryonic kidney cell lines are cultured as a monolayer in Dulbecco's modified Eagle medium (DMEM) supplemented with 10 % fetal bovine serum (FBS) and 1 % penicillin, streptomycin and fungizone (PSF). The Chinese hamster ovary (CHO) cell line is cultured in DMEM/Ham's F12 with glutamine medium (PAA: The Cell Culture Company) supplemented with 10 % FBS and 1 % PSF. The Mouse 3T3-L1 pre-adipocytes are cultured in DMEM supplemented with 10 % FBS, 1 % PSF and 25 mM Hepes.

All cell lines are plated in 24-multiwell plates at different cell concentrations.

The CHO and FTO2B cell lines are plated at 7 x 10^4 cells/well, the HEK 293 cell line at 9 x 10^4 cells/well, and finally the 3T3-L1 cell line at 4.5 x 10^4 cells/well. Plates are cultured at 37 °C in a humidified 5 % CO_4incubator for approximately 24 h to reach 50–60 % confluence.

4.2.6 Chemicals, gene constructs and recombinant adenoviruses

Two different low-conductivity electroporation buffers are used in the experiments. A low-conductivity electroporation buffer I (LCEB-I) is used with CHO and FTO2B cell lines. The LCEB-I consisted of 10 mM Na_2HPO_4 (pH 7.4), 1 mM $MgCl_2$ and 250 mM sucrose [11]. Conductivity was 1.6 mS/cm. The second buffer is a low-conductivity electroporation buffer II (LCEB-II) and its composition is: 300 mM sorbitol, 4.2 mM KH2PO_4, 10.8 mM K_2HPO_4, 1 mM $MgCl_2$, and 2 mM HEPES, pH 7.20 [12]. The LCEB-II is used with HEK 293 and 3T3-L1 cell lines. Conductivity is 4.35 mS/cm.

The conductivity of the electroporation buffers is measured experimentally using a conductimeter GLP32 (Crison, Barcelona-Spain) after calibration with two different conductivity patterns following the instructions provided by the manufacturer.

For experiments using fluorescein isothiocyanate (FITC)-dextran average molecular weight 20000 Da (FD20S) with approximate Stokes' radii of 33 Å, 2.5 mg/ml FD20S (Sigma-Aldrich, Madrid, Spain) is added to the LCEB-I or LCEB-II buffers. Plasmid electrotransfection experiments are performed by adding pEGFP-N1 [13] at 10 μg/ml to the corresponding buffer. This amount of DNA has low toxicity in accordance with data reported by other authors [14]. For the polycation transfection experiments, pEGFP-N1 is transfected at a final concentration of 0.5 μg/ml using Genejuice (Merck Millipore) following the manufacturer's guidelines. Finally, for siRNA knockdown experiments, CHO cells are transduced, 24 h after seeding, with an adenovirus expressing the enhanced green fluorescent protein (EGFP) under the control of the CMV promoter at a multiplicity of infection (MOI) of 1 for 2 h. siRNA α-GFP (Ambion, Life Technologies) is added to LCEB-I at a final concentration of 2 μg/ml 30 min after transduction.

4.2.7 Experimental Procedure

The electrode assembly is sterilized with a 70 % ethanol solution, rinsed with sterile distilled water and finally immersed in the corresponding electroporation buffer before use. 200 μl of LCEB-I or LCEB-II supplemented with FD20S, pEGFP-N1 or siRNA α-GFP are added to each well 5 min before the application of electric pulses. Multiwell plates are immediately placed in the automatic positioning system responsible for sequentially placing the electrode assembly above the cell monolayer of each individual well. The configuration is conducted through a software interface front panel where experimental conditions can be configured. The electric field pulse delivery is performed by a biphasic stimulator configured as a fixed current source. Eight biphasic pulses, with a duration of 1 ms, time separation between the positive and negative parts of the pulse of 100 μs and frequency repetition of 1 Hz are applied with different current intensities to generate voltage-to-distance ratios 0.8, 1, 1.2, 1.6, 1.8 and 2 kV/cm on the surface of the microelectrodes. These values are calculated as the voltage drop measured in the first pulse applied with a digital oscilloscope (TDS3024B; Tektronix) connected in parallel with the terminals of the biphasic stimulator divided by the distance between adjacent microelectrodes (150 μm). It is important to point out that the actual electric field intensity affecting cell membranes is lowered due to the distance between electrodes and cells (see section 4.2.3). No electric pulses are applied in the control cells, although the electrode is positioned above the cell monolayer for an equivalent period of time. All experiments are performed at room temperature (20 $\pm$ 2 °C).

In FD20S experiments, after the electroporation procedure, cells are incubated for a 30-min period in the incubator for cell recovery. After this period, the electroporation buffer is removed and the cells are rinsed twice with PBS; the cells are then incubated with a fresh culture medium for 2 h to allow complete membrane resealing before assessing the results. The cells are then examined under a Leica (Wetzlar, Germany) DMI 4000B inverted microscope for fluorescence to detect FD20S, which has an excitation wavelength of 485 nm and emission at 510 nm. Images are taken with a digital camera (Leica DFC 300x, 10x magnification).

In plasmid DNA or siRNA electroporation experiments, 1 ml of corresponding fresh culture medium is added to the 200 μl of LCEB 10 min after further

incubation of the electroporation and cells for 24 h before gene expression is studied.

For EIS measurements, the cells are cultured as previously described. Before pulse application, cells are incubated for 5 minutes with LCE I or II (depending on the cell line) at room temperature for stabilization; the microelectrode assembly is also positioned above the cell monolayer for 1 minute before initiating the measurements. Impedance spectra are measured immediately before the first electric field pulse and also between consecutive pulses. Eight electric field pulses are applied with 1ms duration, 1 Hz frequency repetition, and voltage to distance ratio of 200, 600, 1000 and 1400 V/cm.

4.2.8 Cell viability assay

Independent experiments are performed to assess cell viability using the corresponding electroporation buffer without any additional molecule being added (FDS20 or pEGFP-N). Adherent cells that remain attached after 24 hours of electroporation treatment are considered viable. Briefly, 200 μl of LCEB I or II, depending on the cell line, are added to each well containing the adherent cells, and electroporation is performed in conditions equivalent to those in the corresponding plasmid transfection experiment. 200 μl/well of 4% formaldehyde are added twenty-four hours after the electroporation treatment. Following a 10 min incubation period at room temperature, the fixative solution is removed and the cells are rinsed twice with phosphate-buffered saline (PBS). Fixation is performed due to spontaneous cell detachment that occurs during subsequent cell staining and washing. Afterwards, cells are stained with Hoechst 1 μg/ml for 10 min in agitation. The cells are then washed with PBS for 10 min in agitation, and finally culture media are completely aspirated. Once dried, the cells are examined under a Leica (Wetzlar, Germany) DMI 4000B inverted microscope for fluorescence.

Cell viability is determined by counting the adherent cells stained with Hoechst that remain on the plate; and the percentage of viable cells is calculated with respect to the cells present in controls in which no electric pulses are applied. ImageJ automatic nucleus counter within the particle analysis plugin is used to process the images.

4.2.9 Flow cytometry

Flow cytometry is used to provide a rapid, sensitive and accurate assessment of fluorescent cells, thereby obviating cell counting under a microscope. The technique has the advantage of objectively and automatically measuring fluorescent cells, thus eliminating cell debris and aggregates from the final median values.

Cells in 24-multiwell plates are trypsinized for about 5 min. Thereafter trypsinization is stopped with medium containing FBS. To achieve the necessary number of cells to be detected by flow cytometry, the cells present in three wells are pooled for each condition. Cells in suspension are centrifuged at 1500 rpm for 5 min and pellets are resuspended in 0.5 ml of the corresponding culture medium. Experiments are carried out using a Cytomics FC500 MPL flow cytometer (Beckman Coulter, Inc, Fullerton, CA). Excitation of the sample is performed using a 488 nm air-cooled argon-ion laser at 15 mW power. The instrument is set up with the standard configuration: forward scatter (FS), side scatter (SS), and green (525 nm) fluorescence for GFP. Fluorescence is collected in logarithmic scale. Optical alignment is checked using 10 nm fluorescent beads (Flow-Checkfluorospheres, Beckman Coulter). The cell population is selected by gating in a FS vs. SS dot plot, excluding aggregates and cell debris. Results are presented as % of green fluorescent cells versus the total number of cells.

4.2.10 RNA extraction, reverse transcription, and real-time PCR

In order to perform siRNA experiments, total RNA is extracted from CHO cells cultured in 24-multiwell plates using the RNeasy minikit (Qiagen, Valencia, CA, USA), and cell extracts are homogenized using a Polytron (Kynematica Polytron, Westbury, NY). The cells present in four wells are pooled for each condition. Total RNA (0.5 μg) is retro-transcribed (RT) with TaqMan reverse transcription reagents from Applied Biosystems (Branchburg, NY, USA) using random hexamers. Real-time PCR is performed using the ROCHE sequence detection system with the TaqMan universal PCR master mix and probes (Applied Biosystems) for EGFP gene. The 18S rRNA gene is used as the endogenous control to normalize the threshold cycle (CT). Fold change is estimated by the $2^{-\Delta\Delta CT}$ method [15].

4.3 Results and Discussion

4.3.1 Cell permeabilization

The main objective of this chapter was to present the new electrode assembly and to test its usefulness for the electroporation-mediated introduction of different molecules to cell monolayers. Also to test the suitability for performing EIS measurements of the cell monolayer during electroporation.

The first step is to test its performance for cell permeabilization using a fluorescent dye with a small molecular size if compared with that of a standard plasmid DNA. Particularly, we use FITC-dextran, average molecular weight 20000 Da (FD20S). The use of this type of fluorescent probe is able to provide direct information about the extent of membrane permeabilization, i.e. "pores" created during electroporation, and it is useful for acquiring a preliminary idea of the ability of cell permeabilization of the system. Active molecules such as plasmid DNA, for example, require additional and complex cellular mechanisms to be activated in order to assess the effectiveness of the treatment [16] and long optimization procedures are usually needed to increase the transfection rates. For this reason, the efficiency of permeabilization and the electrotransfection results are not directly related, as already shown by previous authors [17]. Nevertheless, we believe that some prior information on the system performance to be useful before testing the system on plasmid DNA electrotransfer.

Fig. 4.6 shows representative micrographs of FD20s uptake in each of the four cell lines used in subsequent electrotransfection experiments for the best condition. A range of different electric field intensities is tested, while the other electric field parameters remained fixed as described in Materials and Methods, section 4.2.7. We consider the best conditions to be the combination of electric field parameters leading to a significant extent of permeabilization preserving acceptable levels of cell viability. CHO cells are subjected to 1600 V/cm; HEK293 to 1600 V/cm, FTO2B to 1800 V/cm, and 3T3L1 to 1400 V/cm. The remaining constant parameters are 8 pulses, 1 ms duration and 1 Hz frequency repetition. These results confirm the suitability of the device for performing electroporation of diverse adherent cell monolayers grown in standard multi-well culture plates.

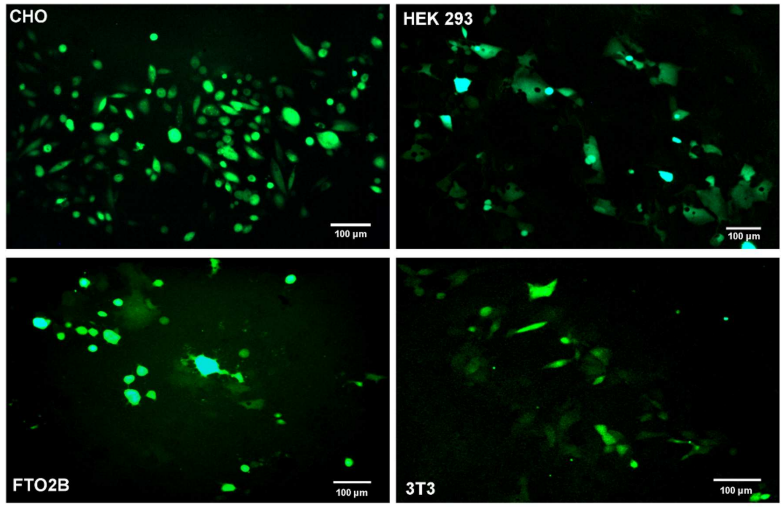

Fig. 4.6 Representative micrographs for the best condition of FD20s uptake in electropermeabilized tested cell lines. CHO cells are subjected to 1600 V/cm voltage to distance ratio; HEK293 to 1600 V/cm, FTO2B to 1800 V/cm, and 3T3L1 to 1400 V/cm. The remaining constant parameters were 8 pulses, 1 ms duration and 1 Hz frequency repetition. 10x magnification.

4.3.2 Plasmid electrotransfer and cell viability

Experiments are next conducted using plasmid pEGFP-N1 to be transferred by electroporation. The parameters used in these experiments are similar to the ones chosen for permeabilization tests, none additional optimization is performed to increase transfection rates as the goal of this part of the study is to show the ability of the system to be used in the electroporation-mediated introduction of active molecules to cell monolayers such as plasmid DNA's. In order to obtain the suitable conditions for optimal transfection rates not only pulse parameters should be optimized but also incubation times, temperature, confluence of monolayers, concentration of plasmid, etc..

In parallel with electrotransfection experiments, viability assays reproducing the same conditions are also performed. Additionally, as a standard method for comparison, polycation mediated transfection is assayed in all of the four cell lines with the same plasmid pEGFP-N1. As indicated in section 4.2.1 the active area of electrodes is 70 % of the total growing surface in each culture plate. For this reason, and in order to draw a realistic comparison between

the polycation transfection method affecting 100 % of cells and electroporation, results obtained with the chemical method are normalized by a factor of 0.7.

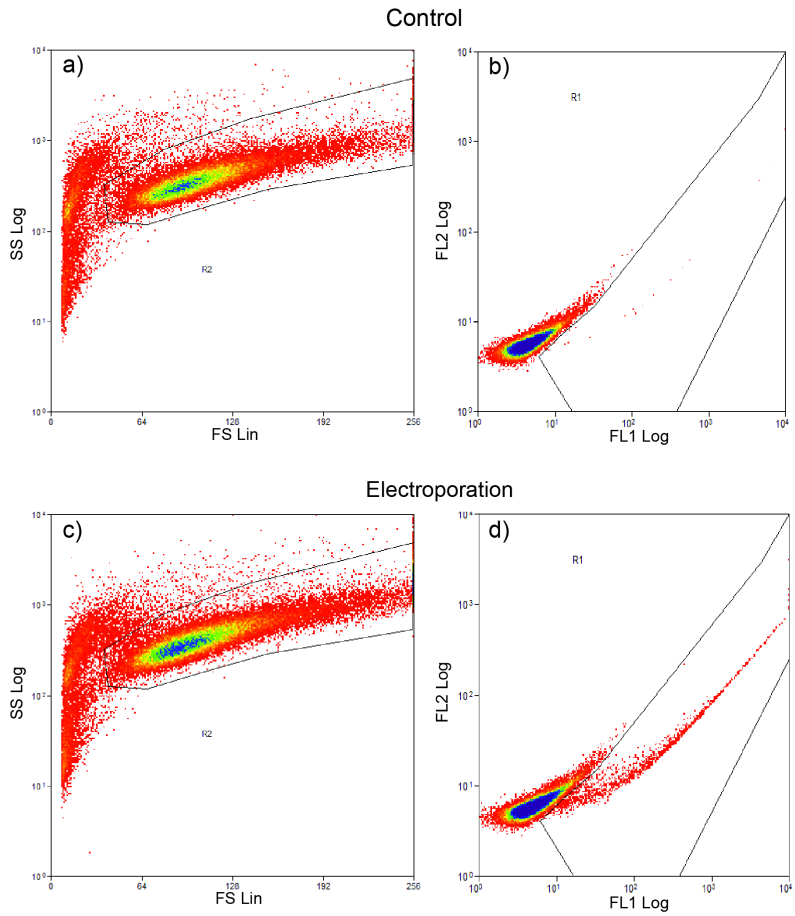

Fig. 4.7 Flow cytometry dot plots for an electroporated sample and a negative control. Left: FS vs. SS plot for gating the cell population to analyze. Right: FL1 vs FL2 plot gating the cells showing green fluorescence.

Both cell transfection and viability are assessed twenty-four hours after completion of the experiments. EGFP gene expression is assessed by using flow cytometry, while data are presented as percentages of the cells showing green fluorescence with respect to the total cell population remaining viable after 24 h. Fig. 4.7 depicts an example of flow cytometry results analized (control VS treated cells). The cell population is selected by gating in a FS vs. SS dot plot,

excluding aggregates and cell debris.Subsequently, the gated population is plotted in a FL1 vs FL2 plot. FL1 corresponding with EGFP fluorescence and FL2 related with the autofluorescence of cells. % of transfection is obtained setting a gate for this second plot. Results in Fig. 4.8 show, for each analyzed cell line, EGFP expression levels corresponding to four different electric field intensities within the range tested, and also for polycation-based transfection. Cell viability is assessed by analyzing the percentage of cells stained with Hoechst for each condition against controls where no electric pulses are applied. The corresponding viability for each electric field level is also shown in Fig. 4.8.

For the interpretation of the results, we categorize cells into two groups. The first group is composed of CHO and HEK 293 cells that can be considered as easy to transfect cell lines. CHO cells in suspension have been extensively used in previous electrotransfection studies, showing consistently good results [18, 19]. Nevertheless, when electroporation is applied directly to plated CHO cells, efficiency outputs are considerably reduced [11]. In our case, for the highest electric field tested, up to 10 % of gene transfection efficiency in CHO cells is observed, which is higher than that obtained with the standard polycationic chemical method used (around 7 %). Cell viability above 50 % is preserved even for the highest electric field tested. The HEK 293 cell line is also known for its feasibility for DNA plasmid transfection with varied chemical agents. A maximum of 16.5 % of plasmid transfection efficiency is obtained, concomitant to cell viability around 80 %, when the highest electric field shown is applied. Results with higher electric fields are not shown because cell fusion is extensively observed in this cell line. The reason for the observed fusion lies in the fact that in this cell line cells grow creating contacts between them even for low confluence cell density. In HEK 293 cells, polycationic transfection shows better results than electrotransfection, achieving up to 26 % of transfection efficiency.

In the second group, consisting of hard to transfect cell lines, we include 3T3 and FTO2B cells, both of which are usually transfected using viral vectors due to their inability to successfully respond to other transfection methods [20, 21]. In accordance with this notion, no detectable gene expression using polycationic transfection is achieved in either of these two cells lines. Nevertheless, positive results are obtained with the use of elecroporation. Almost 3 % of cells express EGFP in the 3T3-L1 cell line, while more than 6 % do so in the case of FTO2B

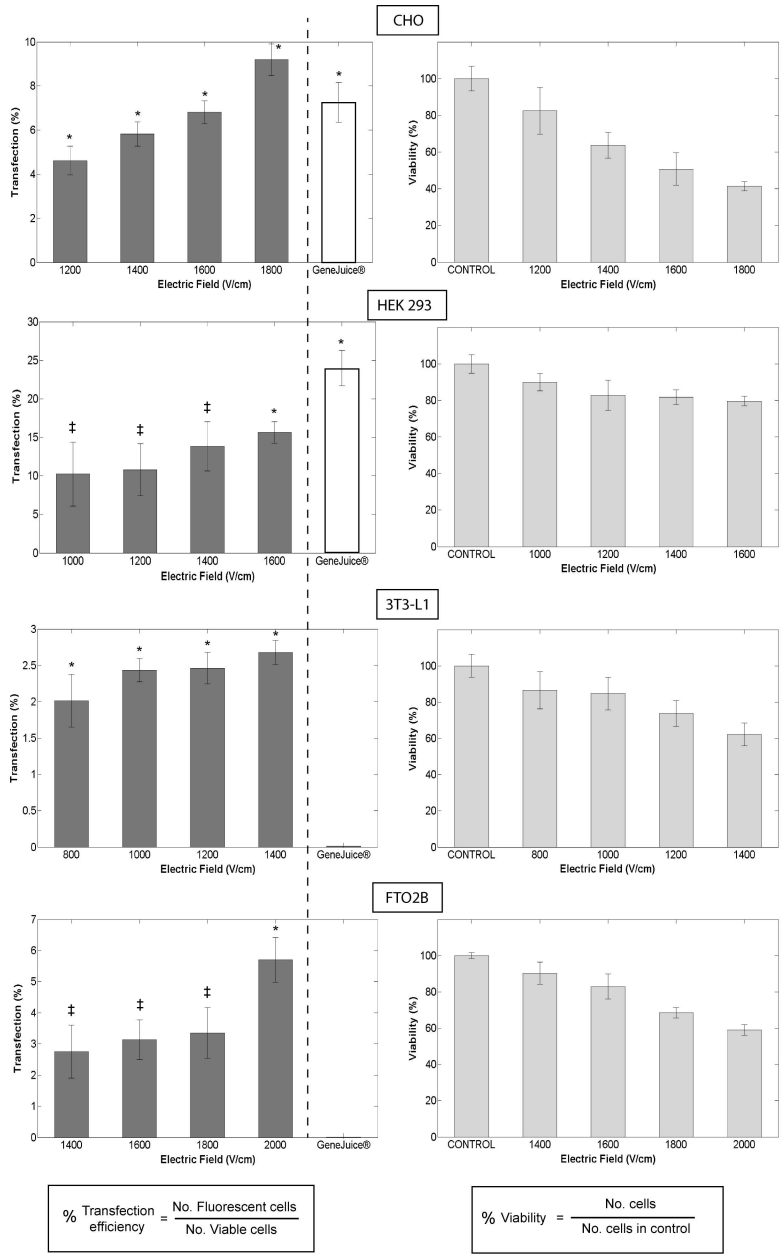

Fig. 4.8 Left:Transfection efficiency, electroporation treatment (dark bars), polycation transfection (white bars). Rigth: Cell viability results for the same electric fields of electrotransfection experiments. Results from a minimum of 3 different experiments are pooled together and are presented as means ± SD. Please note that the scale in transfection results are different for each cell line. Significance of differences of unpaired Student's t test for transfection efficiency of each electric field condition versus control (no electroporation) and also for polycation transfection versus control (no treatment): $*p<0.001$, ‡ $p<0.05$.

cells. In both cases, cell viability remains above 60 % for the highest electric field condition tested. These results indicate how in situ electroporation of adherent cell monolayers may provide an option where other transfection methods show only limited effectiveness.

Our overall gene expression results using electrotransfection could be considered low when compared with other electroporation strategies. First, the reader should take into account, as previously pointed, the fact that none optimization was performed. In this study, based on previous experiences, we fix all parameters except electric field intensity. However, it is necessary to point out that the influence of other parameters may be decisive for improving transfection rates, as shown recently in [22, 23].

Additionally, and specifically for the given setup, some factors should be taken into account in order to explain these findings. The first consideration is the state of adherence of cells at the moment of pulse application. As already mentioned, some studies demonstrate that gene electrotransfection efficiency is lower in plated cells when compared with cells in suspension exposed to equivalent treatments [11]. This observation may be explained by the different distribution in sizes and shapes of adherent cells and how it affects the induced transmembrane voltage (ITV), while differences in the cellular cytoskeleton may also account for reduced performance.

Given the fact that in our system, the space between the electrodes and the cell monolayer at the moment of pulse application is very small (10 μm), the geometry of the system may also provide some explanation. In this small space, the volume of electroporation buffer supplemented with pEGFP-N1 is also small, so the number of molecules of plasmid available in the vicinity of cell membranes is relatively low. In addition, diverse studies have demonstrated that an essential step for a successful transfection is DNA/membrane interaction during application of pulses, followed by translocation of plasmid after the electric field ceases [16, 24]. The substantial differences observed between FD20S experiments, where high permeabilization rates are obtained, and plasmid electrotransfection, can be partly explained by the restricted effectiveness of these processes. Nevertheless, the electrode assembly is positioned above the cell monolayer immediately before the application of pulses and removed immediately after. For this reason, neither the interaction of DNA molecules with

cell membranes before pulses, which improves the efficiency of transfection [25], nor the post pulse molecular kinetics should be highly influenced by the system. The observations made support the fact that the main mechanism responsible for DNA insertion during electroporation is the electrophoretic force produced by electric field pulses [26]. According to [18] the role of electrophoretic DNA movement is not necessarily determinant on the transfection efficiency of plated cells if the concentration of plasmid is optimal. Although the concentration used in the experiments described herein agrees with the optimal concentration proposed in that paper (10 μg/ml), the reduction in volume for the present case could imply an increase in the optimal concentration value necessary for this geometry.

4.3.3 siRNA electrotransfer

siRNA has become an important technology for manipulating cellular phenotypes, understanding gene functions and discovering novel therapeutic targets [27, 28]. However, owing to their size and high negative charge, siRNA cell delivery remains problematic [29].

In the light of these delivery problems, we decided to test the utility of the device in the transfection of EGFP-targeting siRNA. Prior to the siRNA experiments, a dose-response test with an adenovirus vector expressing EGFP was performed at different MOI (0.25, 0.5, 1, 2.5, 5) in CHO cells. Using flow cytometry, we found that the MOI of 1 was the best transduction condition, in which 39.9 % of CHO cells were positively fluorescent with respect to the total viable cells as assessed by scatter-gated fluorescence analysis. MOIs higher than 2.5 led to a saturation of the transduction effect with values ranging from 74 % to 87 %. siRNA experiments were then performed in previously transduced CHO cells using an adenovirus vector expressing EGFP. Shortly after transduction, cells were incubated with siRNA α-GFP and electroporated according to the same protocol used in the previous experiments of plasmid DNA transfection. RNA extraction and quantitative gene expression analyses using real-time PCR were performed twenty-four hours after treatment. Fig. 4.9 shows relative EGFP gene expression for two different electric field conditions against a control where no electric field was applied but siRNA was added. A group of control

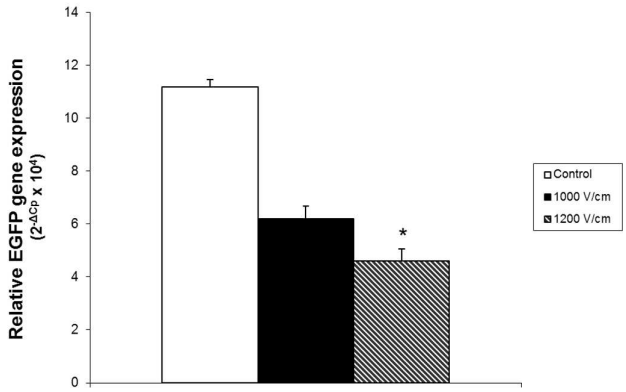

Fig. 4.9 EGFP mRNA levels after siRNA electrotransfection in CHO cells. Cells transduced with an adenovirus expressing EGFP are electroporated with two different electric field intensities in the presence of EGFP-targeted siRNAs; no electric field is applied to control cells. Data are the means ± SD of at least four different samples. Significance of differences in cells treated with 1200 V/cm versus control: $*p < 0.05$.

cells in which electric field was applied but siRNA was not added, was also assayed. No differences were observed between either type of control (data not shown). After transfection with EGFP-targeted siRNA, EGFP mRNA levels were reduced by 1.8-fold for 1000 V/cm electric field intensity and 2.7-fold for 1200 V/cm when compared to control cells. The present data are therefore consistent with the idea that electrotransfection can be a useful siRNA delivery system.

4.3.4 Electroporation Impedance monitoring

The results of electrical impedance spectroscopy measurements during the electroporation procedure are shown in Fig. 4.10 for CHO cells and Fig. 4.11 for the 3T3-L1 cell line, respectively. For the different electric field intensities tested, the normalized impedance module spectra evolution can be observed in the upper part of both figures. Normalization is performed in terms of initial measurements corresponding to the pre-pulse state of cell monolayers. Arrow lines show the direction of the temporal evolution from initial state (pre-electroporation state), and subsequently pulse after pulse until the final state (8 pulses applied). Before experiments with cell monolayers, the system was tested with an elec-

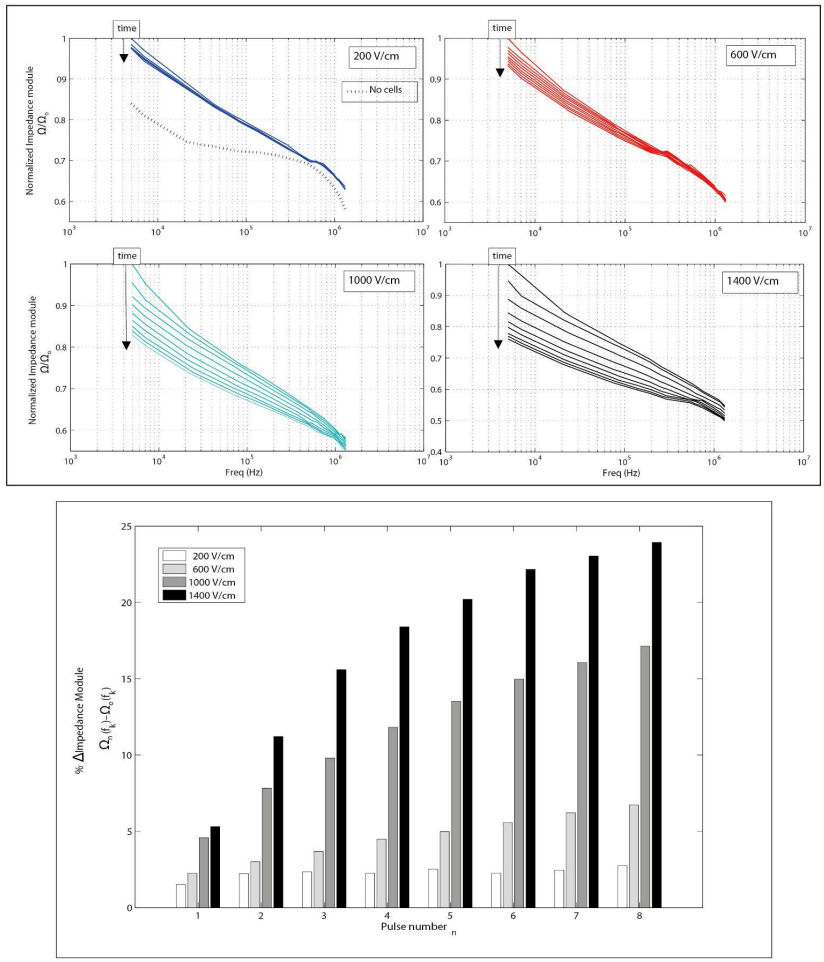

Fig. 4.10 Impedance spectroscopy measurements in the CHO cell line. Top: Normalized impedance module spectra evolution during electroporation for different voltage to distance ratios. Arrow lines show the direction of the temporal evolution from the initial state until the final state. Bottom: Percentage of impedance module change for a frequency $f_k = 5$ kHz after each pulse with respect to the pre-electroporation values.

troporation buffer only, with the purpose of ensuring that results obtained were a direct reflection of the cellular response. The maximum impedance change for these measurements in the absence of cells, including that for the highest electric field tested, was below 2 % (data not shown).

A dose-response relationship between the electric field intensity applied and

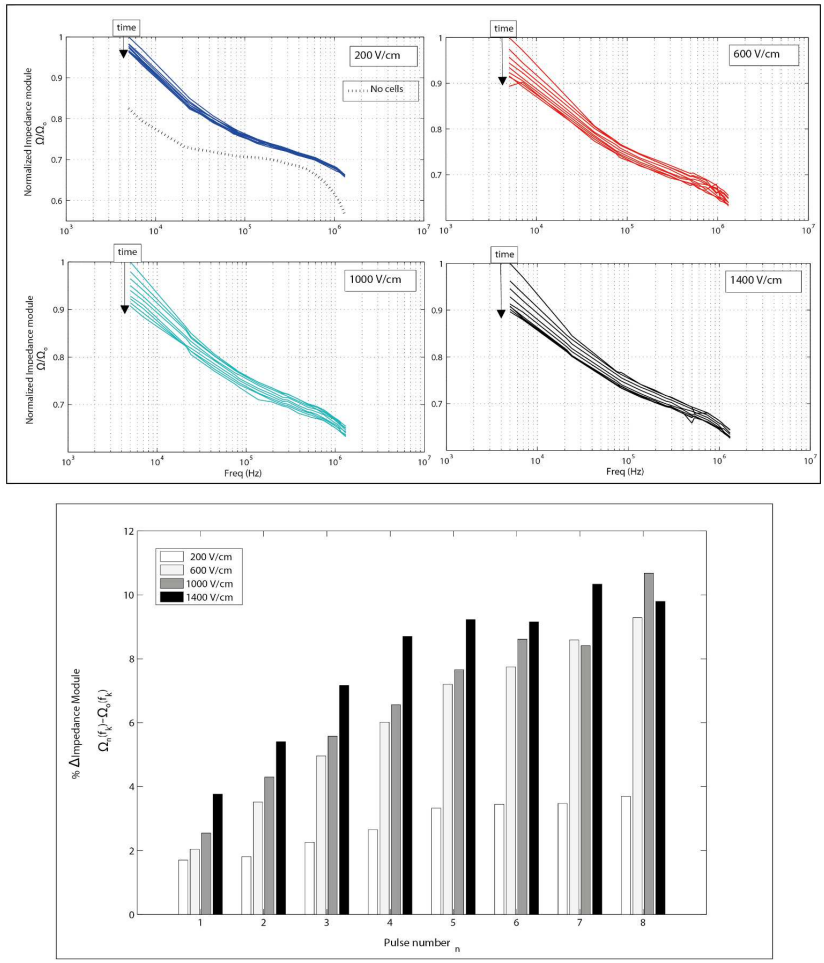

Fig. 4.11 Impedance spectroscopy measurements in the 3T3-L1 cell line. Top: Normalized impedance module spectra evolution during electroporation for different voltage to distance ratios. Arrow lines show the direction of the temporal evolution from the initial state until the final state. Bottom: Percentage of impedance module change for a frequency $f_k = 5$ kHz after each pulse with respect to the pre-electroporation values.

the relative impedance change measured can be clearly observed. This is in accordance with the fact that a higher permeabilized area of cell membrane is achieved with higher electric fields. One may also observe that impedance module change is significantly higher at low frequencies, as was expected according to bioimpedance basic theory [30] and also in agreement with predictions made by theoretical models [31]. As explained in 2.2 low frequency impedance of

living structures is increased by the presence of cell membranes behaving as insulators, as frequency increases, impedance decreases describing a dispersion [32]. When these membranes are permeabilized, low frequency signals are able to find new current paths, thus decreasing impedance in the range of low frequencies. This was also predicted by theoretical models. At high frequency, current flows freely across the membranes and no significant change due to electroporation should be observed. This observations will be discussed in detail in next chapters.

Although impedance change is higher at low frequencies, our explanation for the observed decrease in impedance at high frequency is that two basic events affecting the impedance recordings are occurring at the same time; first, membrane poration, and second, a change in conductivity of the extracellular medium caused by ion exchange. In the present setup, where the conductivity of the extracellular buffer is several times lower than the intracellular medium, the unbalanced concentration of ions may lead to leakage of these ions across the pores by passive diffusion (Pavlin and Miklavcic, 2008). This may account for the different magnitude of the relative change observed at low and high frequency, and supports the idea that with the acquisition of complete impedance spectra, different effects can be separated.

The lower part of Figs. 4.10 and 4.11 shows the percentage of variation of normalized impedance module with respect to the initial state for the lowest frequency of 5 kHz after the application of each biphasic pulse. The impedance variation increases with the increase in electric field intensity in both cell lines. For the lowest electric field condition, one may observe that a voltage to distance ratio of 200 V/cm is clearly under the electroporation threshold for CHO cells, and no significant impedance changes are observed even with pulse repetition. For the 3T3-L1 cells, the change in the lowest condition is also very small. In regard to the remaining conditions, the increase in pulse number is also reflected in an increase of the impedance variation. Nevertheless, the rate of change is not linear with pulse number. A stabilization in the impedance variation may be observed, indicative of an asymptotic behavior and revealing the fact that a saturation effect is produced. In the case of CHO cells, this non-linear evolution is clearly shown for 1000 and 1400 V/cm, while in the case of 3T3-L1 cells it is observed in all conditions unless the lowest intensity. In addition, in CHO

cells, the % of impedance variation clearly differs between the four electric field intensities along the complete procedure. On the contrary, for 3T3-L1 the differences between the three highest conditions decrease pulse after pulse until there are not significant at the end of the procedure. This can be explained because membrane poration saturates before the end of the procedure in 3T3-L1 cell line in accordance with the asymptotic behavior previously described.

These changes may be related with the accumulative creation of stable pores in the cell membrane that are not able to reseal in the interval between pulses, which according to (Pavlin and Miklavcic, 2008) are known as long-lived pores. When the membrane reaches a level of poration, the induction of a transmembrane voltage over the threshold becomes more difficult, which may account for the saturation effect observed.

The measurements shown in this section correspond to our first study of the feasibility of the new electrode assembly to monitor impedance changes during electroporation with the same set of microelectrodes used to apply electric field pulses, with the particularity that these measurements are performed *in situ* and with no contact with cells. From the results shown above, it is demonstrated that this system is suitable both for performing electroporation and monitoring the electroporation process. Next chapters will be focused in the detailed study of the impedance variations of various cell lines during electroporation. In order to extract information about the dynamics of pore formation, a reduction in the measuring time of each spectrum will allow us to significantly increase the number of spectra acquired between pulses .

4.4 Conclusions

Our aim with this study was to continue the development of a system capable of performing electroporation *in situ* of adherent cells growing in standard multi-well tissue culture plates with the added value of enabling bioimpedance measurements during the procedure. A new electrode assembly based on spiral geometry has been tested in four different adherent cell lines. Permeabilization experiments using a fluorescent dye were performed as an initial step. Secondly, plasmid electrotransfer was assayed, and finally siRNA delivery was tested in

one of the cell lines. Additionally, EIS measurements in two cell lines have been shown.

Our results indicate the high effectiveness of the system in membrane permeabilization of each of the cell lines tested using FD20S, while low-yielding but still successful results are obtained when plasmid encoding EGFP is used. In addition, we found cell line dependence on gene electrotransfection rates. We also show a reduction of EGFP gene expression after electrotransfection of siRNA α-GFP into CHO cells. We reveal the advantages of this new spiral electrode design for improving the uniformity of the electroporation treatment, and also for conducting four electrode electrical impedance measurements during membrane poration with the same set of microelectrodes. This is demonstrated by the observed decrease in the impedance module as a response to the electric field application, suggesting the creation of new paths for electric current in the cell membranes.

As revealed in some other studies, transfection yields obtained in adherent cells are lower than those in suspended cells. Nevertheless, in many cases it is still desirable to perform electroporation to plated cells, because it is mandatory to preserve other cellular properties typical of cell monolayers. Further effort should be focused on addressing the key differences leading to different transfection rates and on finding a compromise between electroporation in suspension or in plated cells. In order to increase the transfection rates obtained further optimization should include not only working within a range of different electric field intensities, but also testing other electric field parameters (pulse duration, frequency, number of pulses, polarity, etc.), different buffer compositions, cell densities and so on. Nonetheless, this work demonstrates the applicability of our system in a standard laboratory scenario as a new approach of applying electroporation using a low cost disposable device.

Regarding the monitoring of the electroporation process by means of EIS measurements, in the present chapter only a brief viability study has been conducted. Once the concept has been validated, the goal is the optimization of the measuring system to increase the time resolution in order to acquire information about the dynamical phenomena that occur in the cell membranes during electroporation. This will be shown in the following part of this thesis.

References

[1] Marco Sandri, Elena Bortoloso, Alessandra Nori, and Pompeo Volpe. Electrotransfer in differentiated myotubes: a novel, efficient procedure for functional gene transfer. *Experimental Cell Research*, 286(1):87–95, 2003.

[2] F. Yates and G. Q. Daley. Progress and prospects: gene transfer into embryonic stem cells. *Gene Therapy*, 13(20):1431–1439, 2006.

[3] R. V. Davalos, D. M. Otten, L. M. Mir, and B. Rubinsky. Electrical impedance tomography for imaging tissue electroporation. *IEEE Trans Biomed Eng*, 51(5):761–7, 2004.

[4] E. Pasqualotto, A. Ferrario, M. Scaramuzza, A. De Toni, and M. Maschietto. Monitoring electropermeabilization of adherent mammalian cells through electrochemical impedance spectroscopy. *Procedia Chemistry*, 6(0):79–88, 2012.

[5] J. Wegener, C. R. Keese, and I. Giaever. Recovery of adherent cells after in situ electroporation monitored electrically. *Biotechniques*, 33(2):348, 350, 352 passim, 2002.

[6] E. Sarró, M. Lecina, A. Fontova, C. Solà, F. Gòdia, J. J. Cairó, and R. Bragós. Electrical impedance spectroscopy measurements using a four-electrode configuration improve online monitoring of cell concentration in adherent animal cell cultures. *Biosensors and Bioelectronics*, 31(1):257–263, 2012.

[7] David B. Geselowitz. An application of electrocardiographic lead theory to impedance plethysmography. *Biomedical Engineering, IEEE Transactions on*, BME-18(1):38–41, 1971.

[8] Grimnes Sverre and G. Martinsen Ørjan. Sources of error in tetrapolar impedance measurements on biomaterials and other ionic conductors. *Journal of Physics D: Applied Physics*, 40(1):9, 2007.

[9] B. Sanchez, G. Vandersteen, R. Bragos, and J. Schoukens. Optimal multisine excitation design for broadband electrical impedance spectroscopy. *Measurement Science and Technology*, 22(11):115601, 2011.

[10] B. Sanchez and R. Bragos. *Fast Electrical Impedance Spectroscopy for Moving Tissue Characterization Using Bilateral QuasiLogarithmic Multisine Bursts Signals*, volume 22 of *IFMBE Proceedings*, chapter 259, pages 1084–1087. Springer Berlin Heidelberg, 2009.

[11] Igor Marjanovič, Saša Haberl, Damijan Miklavčič, Maša Kandušer, and Mojca Pavlin. Analysis and comparison of electrical pulse parameters for gene electrotransfer of two different cell lines. *The Journal of Membrane Biology*, 236(1):97–105, 2010.

[12] Elke De Vuyst, Marijke De Bock, Elke Decrock, Marijke Van Moorhem, Christian Naus, Cyriel Mabilde, and Luc Leybaert. In situ bipolar electroporation for localized cell loading with reporter dyes and investigating gap junctional coupling. *Biophysical Journal*, 94 (2):469–479, 2008.

[13] Cèlia García-Martínez, Mario Marotta, Rodrigo Moore-Carrasco, Maria Guitart, Marta Camps, Silvia Busquets, Eulàlia Montell, and Anna M. Gómez-Foix. Impact on fatty acid metabolism and differential localization of fatp1 and fat/cd36 proteins delivered in cultured human muscle cells. *American Journal of Physiology - Cell Physiology*, 288(6): C1264–C1272, 2005.

[14] Toshibumi Shimokawa, Ko Okumura, and Chisei Ra. Dna induces apoptosis in electroporated human promonocytic cell line u937. *Biochemical and Biophysical Research Communications*, 270(1):94–99, 2000.

[15] Kenneth J. Livak and Thomas D. Schmittgen. Analysis of relative gene expression data using real-time quantitative pcr and the $2^{\Delta\Delta ct}$ method. *Methods*, 25(4):402–408, 2001.

[16] Muriel Golzio, Justin Teissié, and Marie-Pierre Rols. Direct visualization at the single-cell level of electrically mediated gene delivery. *Proceedings of the National Academy of Sciences*, 99(3):1292–1297, 2002.

[17] Marie-Pierre Rols, Christine Delteil, Muriel Golzio, and Justin Teissié. Control by atp and adp of voltage-induced mammalian-cell-membrane permeabilization, gene transfer and resulting expression. *European Journal of Biochemistry*, 254(2):382–388, 1998.

[18] Masa Kanduser, Damijan Miklavcic, and Mojca Pavlin. Mechanisms involved in gene electrotransfer using high- and low-voltage pulses – an in vitro study. *Bioelectrochemistry*, 74(2):265–271, 2009.

[19] Karolina Cepurniene, Paulius Ruzgys, Rimantas Treinys, Ingrida Satkauskiene, and Saulius Satkauskas. Influence of plasmid concentration on dna electrotransfer in vitro using high-voltage and low-voltage pulses. *The Journal of Membrane Biology*, 236(1): 81–85, 2010.

[20] RL Walzem, MA Hickman, JB German, and RJ Hansen. Transfection of avian lmh-2a hepatoma cells with cationic lipids. *Poultry Science*, 76(6):882–886, 1997.

[21] David J. Orlicky and Jerome Schaack†. Adenovirus transduction of 3t3-l1 cells. *Journal of Lipid Research*, 42(3):460–466, 2001.

[22] Saša Haberl, Maša Kandušer, Karel Flisar, Duša Hodžić, Vladimir Boštjan Bregar, Damijan Miklavčič, Jean-Michel Escoffre, Marie-Pierre Rols, and Mojca Pavlin. Effect of different parameters used for in vitro gene electrotransfer on gene expression efficiency, cell viability and visualization of plasmid dna at the membrane level. *The Journal of Gene Medicine*, 15(5):169–181, 2013.

[23] A. Liew, F. M. Andre, L. L. Lesueur, M. A. De Menorval, T. O'Brien, and L. M. Mir. Robust, efficient, and practical electrogene transfer method for human mesenchymal stem cells using square electric pulses. *Hum Gene Ther Methods*, 24(5):289–97, 2013.

[24] Cécile Faurie, Matej Rebersek, Muriel Golzio, Masa Kanduser, Jean-Michel Escoffre, Mojca Pavlin, Justin Teissie, Damijan Miklavcic, and Marie-Pierre Rols. Electro-mediated gene transfer and expression are controlled by the life-time of dna/membrane complex formation. *The Journal of Gene Medicine*, 12(1):117–125, 2010.

[25] T. D. Xie and T. Y. Tsong. Study of mechanisms of electric field-induced dna transfection. v. effects of dna topology on surface binding, cell uptake, expression, and integration into host chromosomes of dna in the mammalian cell. *Biophysical Journal*, 65(4):1684–1689, 1993.

[26] S. I. Sukharev, V. A. Klenchin, S. M. Serov, L. V. Chernomordik, and A. Chizmadzhev Yu. Electroporation and electrophoretic dna transfer into cells. the effect of dna interaction with electropores. *Biophys J*, 63(5):1320–7, 1992.

[27] David Bumcrot, Muthiah Manoharan, Victor Koteliansky, and Dinah Sah. Rnai therapeutics: a potential new class of pharmaceutical drugs. *Nat Chem Biol*, 2(12):711–719, 2006.

[28] A. de Fougerolles, H. P. Vornlocher, J. Maraganore, and J. Lieberman. Interfering with disease: a progress report on sirna-based therapeutics. *Nat Rev Drug Discov*, 6(6): 443–53, 2007.

[29] Huang Huang, Zewen Wei, Yuanyu Huang, Deyao Zhao, Lianghong Zheng, Tianjing Cai, Mengxi Wu, Wei Wang, Xianfeng Ding, Zhuan Zhou, Quan Du, Zhihong Li, and Zicai Liang. An efficient and high-throughput electroporation microchip applicable for sirna delivery. *Lab on a Chip*, 11(1):163–172, 2011.

[30] Antoni Ivorra. *Tissue Electroporation as a Bioelectric Phenomenon: Basic Concepts*, chapter 2, pages 23–61. Series in Biomedical Engineering. Springer Berlin Heidelberg, 2010.

[31] Thiruvallur R. Gowrishankar and James C. Weaver. An approach to electrical modeling of single and multiple cells. *Proceedings of the National Academy of Sciences*, 100(6): 3203–3208, 2003.

[32] K.R. Foster and H.P. Schwan. *Dielectric properties of tissues - A review*, pages 25–102. CRC Press, Boca Raton, Fla., 2nd ed. edition, 1995.

Chapter 5

Interpulse multifrequency electrical impedance measurements during electroporation of adherent differentiated myotubes

Abstract

In this chapter the advantages of the microelectrodes presented in Chapter 4 to perform EIS measurements on adherent cells during electroporation are fully exploited. The time resolution of the proposed measuring system (1 spectrum/ms) enables to acquire 860 spectra during the window between pulses of a classical electroporation treatment (8 pulses, 100 μs, 1 Hz). The experiments are performed in monolayers of differentiated myotubes. The information acquired, analyzed with the Cole model, reveals two different membrane dynamics in agreement with the existence of two populations of pores. The time constants of the short-lived pores dynamics show differences depending on the electric field intensity. Thanks to the EIS information, the system is able to also measure the collateral conductivity variations due to ion diffusion during electroporation. Finally, in order to reinforce the physical interpretation of the results, an electrical equivalent model is proposed. These results have been submitted in December 2014 for publication to the journal *Biolelectrochemistry*.

5.1 Introduction

The accumulated experimental evidence about electroporation have lead to the deep understanding of the effects of different parameters on the efficacy of the treatments. However, as previously explained, from a molecular point of view, there is no a definitive explanation of the underlying mechanisms that govern the structural changes in the membrane during electroporation (refer to 2.1.2.2). Also, has previously pointed out in section 2.1.3, different approaches have been proposed to study the fast dynamical behavior of cell membranes during electroporation. Some of changes occur within the range of milliseconds [1], consequently a measuring system with at least a time resolution in the order of milliseconds is necessary.

In the present study, a multisine-based approach is used to measure the membrane changes due to cell electropermeabilization. As a consequence of the work recently developed in the group in the direction of dynamic impedance monitoring [2], this measuring approach is able to perform complete impedance spectra within 1 millisecond. After the integration of this method with the system described in chapter 4, the setup presented along this chapter is able to follow impedance spectra of cells in the interval of time between consecutive pulses with a resolution of 1 spectrum/1 ms. For the best of our knowledge, this is the first time that EIS is performed with such a fast method during cell electroporation.

Other attempts to study the fast pore dynamics based in other time domain methods such as time domain reflectometry [3] or time domain dielectric spectroscopy [4, 5] have been previously shown. However, these techniques use rapid voltage pulses with high frequency content and measure the reflected signal applying concepts of transmission line theory [6].

In the present study, measurements are performed in monolayers of differentiated myotubes. As explained before, the microelectrode assembly used is specifically conceived to apply electroporation to adherent cells *in situ* and to perform EIS measurements on the whole area covered by cells with a modified 4-electrode arrangement. The interest of using differentiated cells *in vitro* is based on the fact that they describe more realistic models to study different

aspects that could be translated into the clinical applications. For example, in the case of muscle tissue it has been shown the potential interest of using electroporation as a tool for electrogenetherapy *in vivo* [7] and how a real time control system would be desirable for safe and efficient gene transfer [8].

Measurements are adjusted to Cole impedance model and the time constants for pore resealing are extracted and analyzed. The different effects observed in the impedance variation during pulse application are discussed and an additional circuital model is used in order to give a complete data analysis. The goal of this study is to test the proposed microelectrode assembly in conjunction with the multisine-based approach to characterize the fast changes produced in the cell membrane during pulse application with a high time resolution.

5.2 Materials and Methods

5.2.1 Measurement setup

5.2.1.1 Reference signal

The multisine excitation used in this work has the same characteristics than the one previously described in chapter 4. Summarizing, the multisine burst consists of 21 frequencies following a Bilateral Quasi-Logarithmic (BQL) distribution from 5 kHz to 1,313 MHz. The duration of each multisine burst is 1 ms.

5.2.1.2 Hardware

The same hardware architecture than the one described in previous chapter is used for these experiments (refer to section 4.2.4 for detailed information). However, in the previous chapter the system was not able to continuously acquire impedance information during the interval between consecutive pulses. Consequently, the previous system was not suitable to follow in real-time the fast dynamical impedance variations pulse after pulse. To overcome this limitations, a new controlling LabView-based software was developed. In the new version, data streaming is performed to avoid memory overflow on the on board acquisition card due to the big amount of data generated, this row data is saved in binary format for subsequent post-processing in Matlab. This way the number of measurements between consecutive pulses could be considerably increased. Additionally, in order to start the measurements with the minimum delay after each pulse as possible and always at the same instant of time, sincronization was necessary. In the new system commutation between electroporation or measurement connections is synchronously performed thanks to a hardware-based trigger signal generated by the pulse generator at the beginning of each pulse. All these improvements make that during a typical electroporation treatment consisting of 8 - 100 μs pulses with a repetition rate of 1 Hz (interpulse period 1 s), the optimized system is able to continuously acquire 860 spectra (860 ms) between consecutive pulses. In Fig. 5.1a a block diagram of the complete system is depicted.

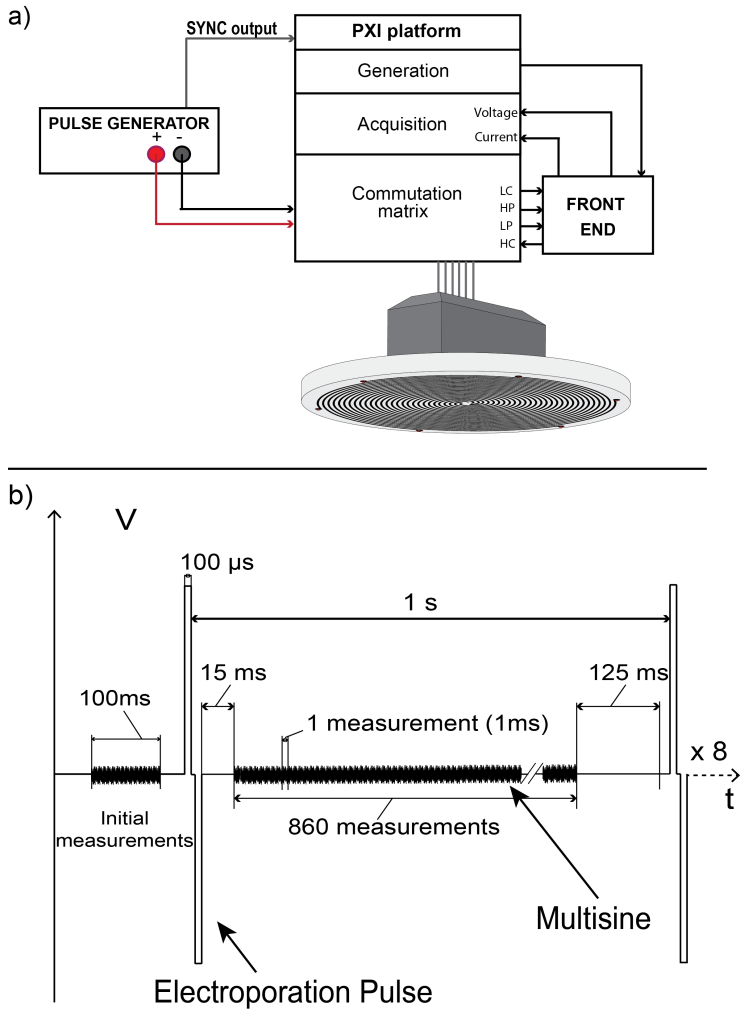

Fig. 5.1 Schematic representation of the measurement setup. a) Measurement system block diagram. b) Electroporation and measurement signal sequence.

The sequence of electroporation/measurements begins with 100 continuous initial pre-electroporation measurements (100 ms). Subsequently the micro-electrodes are automatically connected to the pulse delivery equipment and the pulse generation is initiated. When the trigger signal from the pulse generator is detected by the PXI-2530 system, the connections are switched to the measuring system after a fixed delay of 15 ms. Subsequently, 860 multisine bursts

are continuously generated and acquired. Immediately, connections are again switched to the pulse generator and the system waits for the next pulse (125 ms). The sequence is repeated until completing the 8 pulses of the electroporation treatment. In Fig. 5.1b the sequence of electroporation and measurement signals is detailed.

5.2.1.3 Data pre-processing

The bioimpedance is estimated by measuring and processing an integer number of periods of the sample current and voltage response. The impedance calculation is based on the division of the output-input Fast Fourier Transform (FFT) coefficients at the excited frequencies [9]. The FFT is calculated for a temporal window corresponding to the duration of each multisine burst (1 ms). Once the impedance is calculated, noise reduction is performed with a moving average filter (length n=10) independently for each 860 ms continuous measurement segment.

The effects of the system frequency response produced by the microelectrodes, cables, amplifiers, etc., are compensated using a three-reference calibration method [10]. The references are obtained measuring saline solutions with different conductivities using the same setup.

5.2.2 Microelectrodes

The microelectrodes used in this study correspond with the spiral assembly presented in the previous chapter. The microelectrode is positioned momentarily above the cell monolayer during electroporation/measurements procedure avoiding direct contact with cells thanks to the microseparators as previously described. The special four-electrode measurement arrangement consisting of duplicating the potential measurement terminals allows to use the whole area covered by the microelectrodes as the measuring area. As explained, the interest of using a four-electrode configuration is to reduce the effects of the electrode polarization caused by the electrode-electrolyte interface [11] and improve the ability of the system to detect changes related to the cells [12, 13].

5.2.3 Cells and chemicals

C2C12 myoblasts are seeded into 24 muti-well plates at a initial density of 15×10^3 cells/well with 1 ml of growth medium comprising Dulbecco's Modified Eagle's Medium (DMEM; High Glucose, GlutaMAX Supplement, pyruvate. Life technologies, Saint Aubin, France) supplemented with 10% fetal bovine serum (FBS) and 1% penicillin-streptomycin. Cells are kept in an incubator at 37° under a 5% CO_2 atmosphere for 36-48 h until the confluence is about 80-90%. Subsequently cells are rinsed once with PBS and once with DMEM and medium is switched to 500 μl of differentiation medium consisting of DMEM supplemented with 2% FBS (Gibco, Carlsbad, CA, USA). After 5 days of differentiation, cells are used for experiments.

A low-conductivity electroporation (LCE) buffer consisting of 250 mM sucrose, 10 mM Tris and 1 mM $MgCl_2$ (pH 7, osmolarity 287 mmol/kg, conductivity 0,1 S/m) is used during the electroporation pulse delivery and impedance measurements.

Finally, as a permeabilization reporter, fluorescent nucleic acids stain Yo-Pro-1 Iodide (λ_{ex}=491 nm, λ_{em}=509 nm, Life technologies, Saint Aubin, France) was added to the permeabilization buffer at a final concentration of 1 μM.

5.2.4 Experimental procedure

For experiments, cells are removed from incubator and washed once with LCE buffer. Subsequently, 200 μl LCE + Yo-Pro (1 μM) are added. From here, the complete experiment is performed in a controlled temperature chamber at 37°. Cells are left during 10 min for stabilization. After this period, the microelectrode assembly is positioned manually above the cell monolayer by means of a custom built applicator. Immediately after that, the LabView software which controls the whole system initiates the electroporation-measurements sequence described above. Once the sequence is finished, the microelectrodes are carefully removed and cells are left during 15 additional minutes for resealing. Afterward, cells are washed twice with PBS and replaced with fresh culture medium before inspection under inverted microscope Zeiss Axio Observer Z1 (Carl Zeiss, Jena, Germany) to detect Yo-Pro fluorescence.

5.3 Results and Discussion

In this section the most relevant findings resulting from the measurements are showed and discussed. First, an illustrative example of measurements performed in a cell monolayer and in a cell free culture plate are compared in order to study the ability of the system to detect changes in the cells as a result of electropermeabilization. Once assessed, a mathematical compensation is proposed to reduce the effects of the system on the measurements. Subsequently data modeling is used to extract complete information from the measurements. First, the Cole model is used and a deep analysis on some of its parameters is presented for different electric field conditions. Finally, an equivalent electrical circuit is used to improve the understanding of the different effects observed in the measurements and confirm some previous assumptions done during the analysis.

5.3.1 Cell monolayer vs. cell free measurements: illustrative example

5.3.1.1 Comparison

During the course of experiments, negative controls were performed in the absence of cells reproducing the same conditions as in the case of measurements with cells. These tests were performed in order to study the impact on the measurements of undesired effects, mainly electrode polarization impedance (EPI) changes, temperature variations, etc.. In Fig. 5.2 the evolution of the real and imaginary part during the course of a single experiment is depicted for the same electric field (1200 V/cm, E=V/d with V=18 V and d=150 μm) applied to a cell monolayer and to a cell free culture plate, both containing the same low-conductive buffer. Five different frequencies corresponding to the lower band of the total of 21 frequencies of each spectrum acquired are shown. The reason to make the comparison at low frequency is because the impact of both cell membrane permeabilization and electrode polarization impedance (EPI) changes is maximum at this frequency band [14, 15].

The different behavior in both cases is clearly noticeable from the observation

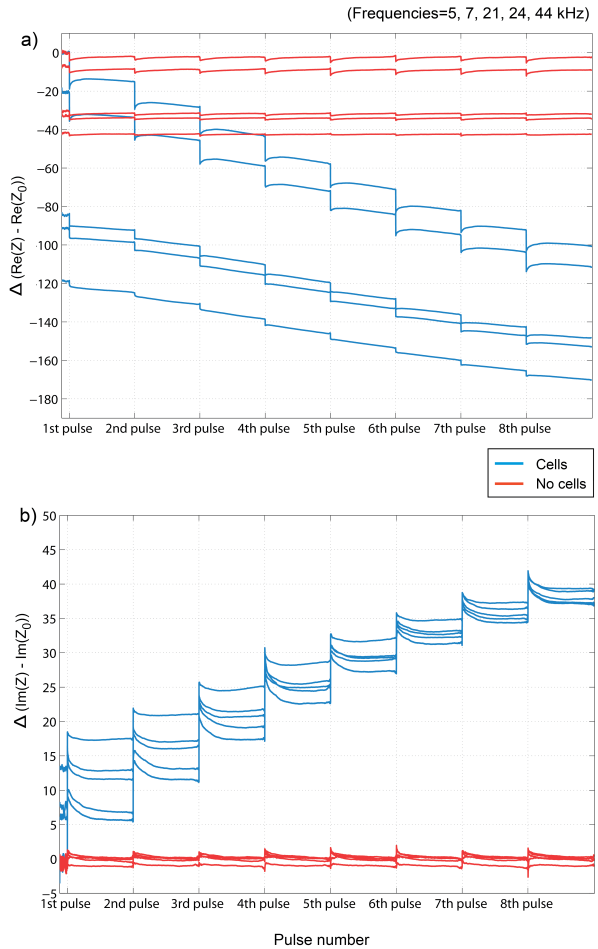

Fig. 5.2 Comparison of interpulse impedance evolution (a) real and b) imaginary part) for an electric field of 1200 V/cm (E=V/d, with V=18 V and d=150 μm) applied to a myotubes monolayer (cells) and to a cell free culture plate (No cells) with the same extracellular buffer. The evolution at frequencies of 5, 7, 21, 24 and 44 kHz is presented normalized with respect to the impedance measured at f= 5 kHz for time t=0 (Z_0). The reader should be aware that although measurements pulse after pulse are plotted continuously there is a delay between the end of an interpulse measurement and the beginning of the next one (see section 5.2).

of the variations in the real and imaginary part as showed in the figure. This demonstrates that the measuring setup is sensitive to detect the impedance changes produced in the cells during electroporation and that these predominate over other effects in the measurements. Following, a detailed explanation for the impedance change observed in the measurements without cells is given.

From all possible undesired effects affecting our system that can justify the small changes observed in the absence of cells, EPI transient variations in response to the application of high electric field pulses, are the most likely explanation. Given that the same microelectrodes are shared both for applying the electroporation pulses and for recording impedance, the exponential transient behavior observed in the absence of cells, can correspond to the temporal disruption of the electrode-electrolyte interface double layer in response to a high current density passing through the electrodes as observed by previous studies [15–17]. When certain voltage is applied to the interface between metal electrodes and electrolytic buffer, the system is displaced from its equilibrium. Immediately after the voltage/current step, the charges redistribute in order to reach equilibrium again. An exponential behavior can be observed as the consequence of double layer capacitance discharge [18].

The perturbation of this effect on the measurements is minimized by introducing the two different strategies previously described in section 5.2; i) the application of bipolar EP pulses should minimize the reactions occurring in the electrode-electrolyte interface as a consequence of reducing the net charge transfer during pulse application [19]. However for the pulse durations used herein this cannot completely eliminate them; ii) four-electrode measuring strategies reduce the effect of electrode polarization by minimizing the current driven by the voltage sensing electrodes [11]. However, this technique can fail to completely eliminate the effect of the EPI due to the electrode impedance mismatch [20] among others.

5.3.1.2 Compensation

Although as explained above the effect of the pulses in the measurements is very small in comparison to the changes detected in the presence of cells, it is still desirable to perform some kind of compensation in order to have more accurate information of the impedance evolution during cell membrane electroporation.

First, we can make the assumption that the EPI behaves identically in response to the application of pulses of a fixed electric field intensity either in the absence or presence of cells. This is true while there is no direct contact between

cells and electrodes that could modify the current density through electrodes and thus the behavior of the EPI. Second, according to the basic equivalent circuits used to model the electrode-electrolyte interface, the EPI is represented in series with the sample under test [15, 21, 22], thus we can consider the EPI variation as an additive effect in the total impedance (see Fig. 5.3). Based on these assumptions, we can state that the temporal evolution of measured impedance in the presence of cells is the sum of two terms: a small contribution of the EPI, and the predominant change caused by the cells themselves. Thus, although the effect of EPI is very small in comparison to the response obtained with cells, it is possible to subtract the normalized temporal evolution of the measurements without cells to have a better measure of the behavior of the cells alone. As the response of the EPI is frequency dependent, the temporal evolution of impedance data for each individual frequency is corrected with the corresponding temporal evolution of cell free measurements. All following measurements shown in this work are compensated for this effect.

The above explanation deals with the compensation of a temporal effect in the impedance evolution. The reader should not confuse this compensation with the regular techniques applied to correct the contribution of electrode polarization in the impedance spectrum. Usually these techniques are applied in non-dynamic measurements of biological tissues such as methods based on algorithms (single exponent method, impedance fitting, etc.) or hardware-based methods (electrode distance variation, substitution, frequency variation, four electrode technique, etc.) [15, 23].

5.3.2 Data modeling

One of the main advantages of acquiring complete spectral information instead of single frequency measurements from the system under study is the possibility of using models to better understand and predict the behavior of these systems. This represents one of the main reasons that motivates the use of EIS measurements to characterize electroporation in this thesis. In the present work we use two models to study the evolution of impedance during electroporation of a cell monolayer. First we use the widely known Cole model for its simplicity, subsequently we introduce a more complex equivalent circuit (see Fig. 5.3).

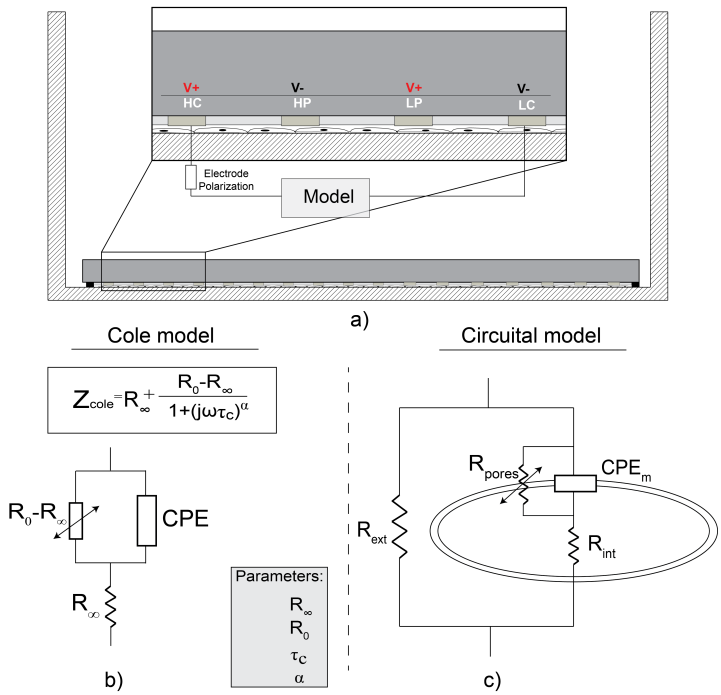

Fig. 5.3 Schematic representation of the cell-electrode system. a) Schematic view of the geometry is presented, notice that the Electrode Polarization Impedance (EPI) is represented in series with the cell model (refer to section 5.3.1.2). b) and c) Cole model and the equivalent circuit proposed are summarized.

The Cole model, is the most extended model to characterize biological tissues and biochemical materials describing single dispersion phenomena. This mathematical model is fully described by four parameters: R_0 represents the resistances at very low frequency, R_∞ accounts for the resistance at very high frequency, α is the exponent in the model (that can be interpreted as a measure of the deviation from an ideal resistor (α=0) or capacitor (α=1) in the equivalent circuit) and τ_c is the characteristic relaxation time constant of the circuit.

The electrical model proposed in this study is shown in Fig. 5.3c. It corresponds to the simple version of a 2R-1C circuit augmented by a resistor in parallel with the membrane capacitance proposed by Fricke and Morse [24] to simulate the conducting state of the membrane. The only difference is that in the presented circuit, the capacitance is replaced by a CPE (CPE_m) which

better resembles the frequency-dependent behavior of the membrane capacitor. Similar models have been used by previous authors to study the electrical properties of cells during electroporation [25–29].

5.3.3 The Cole model

In an unaltered cell monolayer, current at very low frequencies is blocked by the presence of cell membranes, implying that R_0 corresponds mostly to the extracellular resistance. At high frequency, current flows freely across the membrane what involves that R_∞ accounts for the parallel association of both intracellular and extracellular resistances. When the cell membrane is permeabilized as a consequence of electroporation, the previous situation is no longer valid. In an electroporated sample, current at low frequencies can find new paths through membrane. In this conditions, R_0 should be significantly modified by the dynamics of pore formation while R_∞ should not be so sensitive to the creation of pores in the membrane. Indirectly, the conductivity changes in the extracellular and intracellular resistances derived from ion leakage through membrane pores should affect the values of both R_0 and R_∞.

After data calibration as described in section 5.2.1.3 measurements were plotted in a Wessel diagram to confirm that they describe a single dispersion arc compatible with Cole model as observed in Fig. 5.4a (dots). After confirmation, all data sets (100 + 8x860) were adjusted to the model with a MATLAB routine. In Fig. 5.4a the data corresponding to the initial (pre-electroporation) state of a single experiment and the adjusted model are shown. Fig. 5.4b shows the evolution of the Cole arcs during complete electroporation treatment of the same sample (E=1200 V/cm,8 pulses, 1 Hz). The temporal evolution of Cole model parameters R_0 and R_∞ during pulse application for the same data is shown in Fig. 5.4c and d.

The observation of R_0 evolution reveals two different dynamic processes. First, a fast recovery of the impedance values immediately after pulse application is noticed (**short-term evolution**). Secondly, an accumulated impedance decay throughout time with slower behavior is superimposed (**long-term evolution**). This two different processes are in accordance to the existence of two type of permeable structures with different dynamics (short-lived and long-lived pores). On the contrary, the evolution of R_∞ only reveals one maintained de-

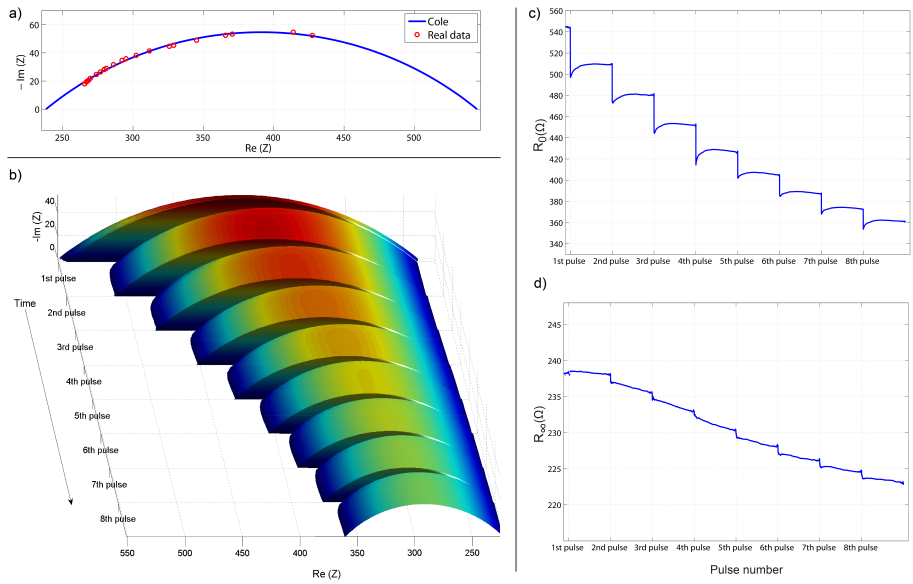

Fig. 5.4 Example of adjusted calibrated data to the Cole model; a) Initial pre-electroporation state, dots represent the real data while the line corresponds to the adjusted model; b) plot of the temporal evolution of the adjusted Cole arcs for a single experiment applying E=1200 V/cm,8 pulses, 1 Hz. Evolution of parameters R_0 and R_∞ for the same example are shown in c) and d)

cay in the impedance similar to the long-term evolution of R_0. Given that the appearance of pores in the membrane involves a great variation of the resistive current paths through membrane, represented mainly by R_0 and R_∞, for conciseness, only the detailed analysis for R_0 and R_∞ is given below. The extended analysis of the other two Cole parameters α and τ_c is omitted in this study and will be shown in next chapter.

5.3.3.1 Short-term analysis

First, we focus on the transient impedance recovery observed in R_0 and termed as short-term evolution. In order to make an independent analysis of this process, it is necessary to separate it from the long-term decay superimposed in the behavior of R_0. Fig. 5.5a shows an illustrative example of the obtained long-term evolution (dashed lines) for each electric field condition. The resulting long term component is then subtracted from the original data to obtain the corrected short-term information. In Fig. 5.5b the corrected mean value

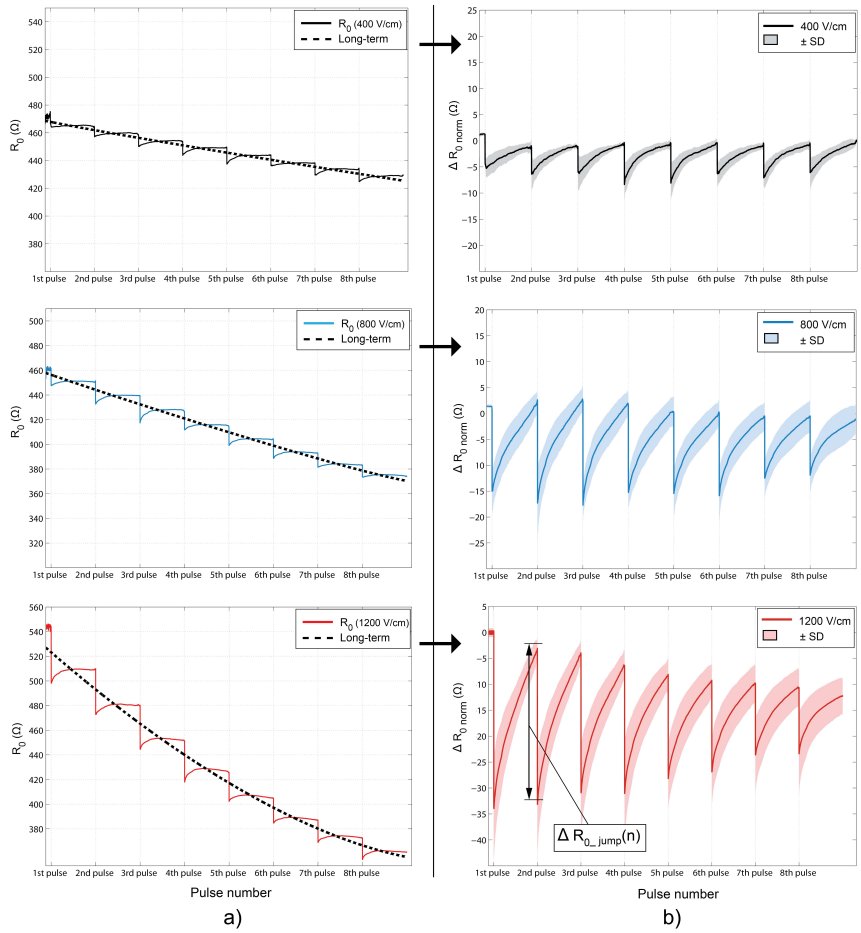

Fig. 5.5 Analysis of parameter R_0. a) An illustrative example of the fitted long-term impedance decay for each electric field condition is shown. b) The corrected short-term dynamics after subtracting the long-term decay is shown, mean values (± SD) are extracted from at least three repetitions for each electric field pooled together.

(± SD) of the short-term dynamics for at least three repetitions of each electric field is shown. The analysis of the fast impedance recovery after each pulse can now be studied independently.

The short-term evolution observed in R_0 is in accordance with the resealing of the short-lived pores that are formed in the plasma membrane immediately after the initiation of the electric field and start to reseal immediately after the electric field ceases. In accordance to 2.1.2.5, two populations of pores

are believed to be created as a response to pulse application [30–33], the first population (short-lived pores) is formed by large pores with a short lifetime, the second population (long-lived pores) is composed by small pores that can last up to hours after pulse application. Most of short-lived pores disappear with life times $\leqslant 1$ ms, however some of them can become part of the long-lived pores and others completely disappear in around 1 second [32]. Additionally, according to a model proposed in [34], this short-term variation would be related to the conducting state of the membrane while the long-term evolution that is analyzed in next section would be due to the state of permeability maintained in the membrane on a bigger time scale. The present short-term analysis is focused on the changes produced in the membrane up to one second after pulse and provide information about the dynamics of the first population of pores described above.

In order to have a quantitative measure of the time constants for this dynamic evolution, the 8 fragments of measurements corresponding to each inter-pulse window are individually studied. The corrected short-term information reveals a double exponential behavior according to equation 6.8. Fig. 5.6 illustrates an example of the fitted double exponentials for the different electric field intensities. The term **fast** (τ_1) is used to describe the first part of the function, where there is a rapid variation of the function. The second part shows a more gradual increase referred as **slow** (τ_2). The individual data sets are processed in MATLAB to obtain the values of the time constants τ_1 and τ_2.

$$f(t) = Ae^{-t/\tau_1}{}_{(Fast)} + Be^{-t/\tau_2}{}_{(Slow)} \tag{5.1}$$

Subsequently, the evolution over the process of the obtained time constants pulse after pulse is studied. The results for both τ_1 and τ_2 are shown in Fig. 5.7a and b.

According to these results, the transient changes in the low frequency impedance parameter R_0 show that the resealing of short-lived pores is governed by a two-stage process. First, a fast recovery step where a big amount of pores disappear within the range of some hundreds of milliseconds. The time constant (τ_1) for this stage shows no evolution during the course of the 8 electroporation pulses. This indicates that the first resealing mechanism responsible for

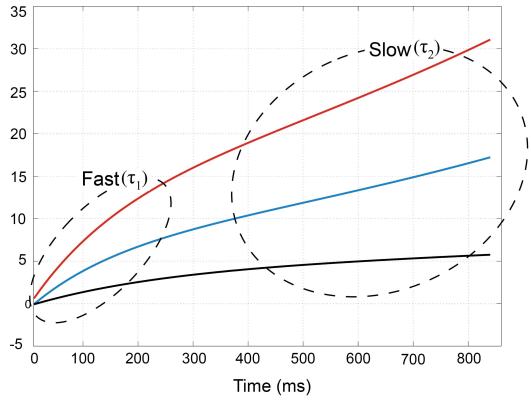

Fig. 5.6 Double exponential short-term analysis. Example of the calculated double exponentials for the three different electric fields indicating the fast and slow terms of the function.

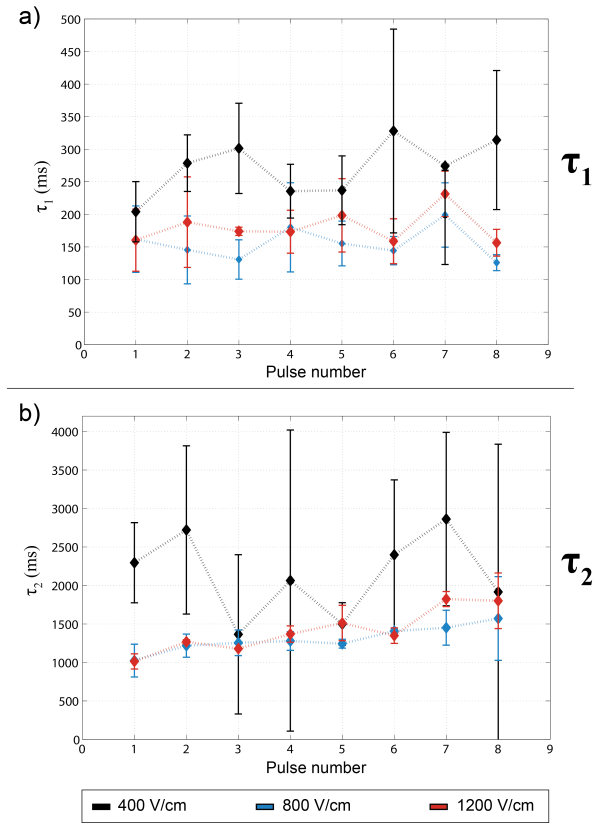

Fig. 5.7 a) Evolution with pulse number of the mean time constant τ_1 for each electric field, error bars correspond to ± sd. b) Evolution with pulse number of the mean time constant τ_2 for each electric field, error bars correspond to ± SD

the closing of these pores is stable over time. This fact allows to calculate the mean value of τ_1 as the average of the values obtained for the 8 inter-pulse fragments of each experiment (Fig. 5.8). The mean calculated time constants differ considerably between the lowest electric field (400 V/cm) where the value is around twofold bigger than the values obtained for the other two electric field intensities. As confirmed by fluorescent dye uptake, the case of 400 V/cm corresponds to the lower bound of permeabilization while in the case of 800 V/cm and 1200 V/cm cells are extensively permeabilized. In Fig. 5.9 a representative micrograph for each electric field condition is shown. This could explain the differences observed. Electric fields near to the threshold of permeabilization could not be enough to trigger the creation of large short-lived pores and only few small pores with slower behavior appear and fully reseal. Furthermore, the incomplete closure of short-lived pores as a result of a certain level of irreversibility in the case of 800 V/cm and 1200 V/cm, can also be a faster process than the complete membrane repair produced with 400 V/cm.

Time Constant	**400 V/cm**	**800 V/cm**	**1200 V/cm**
Fast (τ_1)	271.6 ± 43 ms	155.3 ± 24.6 ms	180.1 ± 25.4 ms
	***		
	**		
		ns	
Slow (τ_2)	2.14 ± 0.53 s	1.3 ± 0.16 s	1.41 ± 0.28 s
	**		
	*		
		ns	
*** *p<0.0001*	** *p<0.001*	* *p<0.005*	ns: *non-significant statiscical difference*

Fig. 5.8 Mean values (± SD) of the time constants for the double exponential functions corresponding to the short-term analysis of parameter R_0. The term fast describes the initial rapid variation of the function and slow relates to the following gradual increase. Values from at least three repetitions are pooled together. Significance of differences of unpaired Student's t-test, p values are indicated in the figure footnotes.

In the second stage pores close gradually with a slower time constant (τ_2). Again there is a significant difference between the behavior of the lowest electric

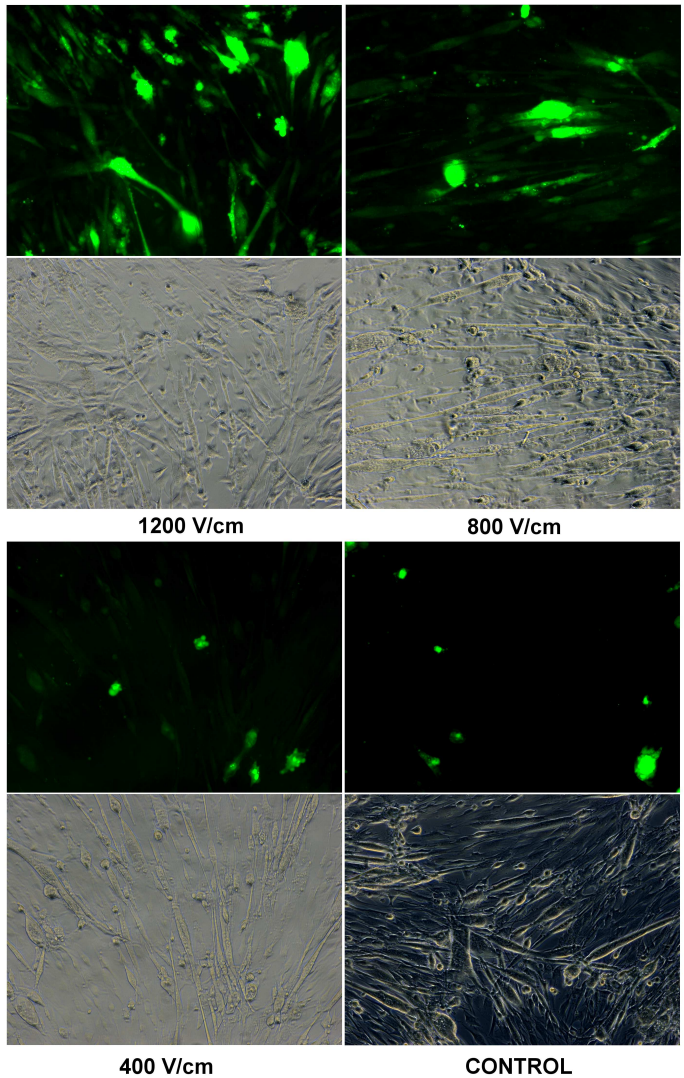

Fig. 5.9 Representative micrographs (phase contrast and fluorescent images) for each electric field condition. Results show permeabilization dependence with field intensity.

field and the other two. An increase in the value of τ_2 over time is observed for 800 and 1200 V/cm while 400 V/cm shows no evolution. The time constant increases from around 1 s at the beginning of the treatment to more than 1.5 s at the end. The extension in the duration of this stabilization stage with increasing pulse number can be the consequence of a gradual loss in the resealing ability of

cell membranes due to the accumulated effect of the pulse repetition. This can be explained on the basis that for 800 V/cm 1200 V/cm irreversible damage is produced in the cell membrane as previously stated. If the mean values of τ_2 are calculated similar to τ_1 the results again differ significantly between 400 V/cm and the other two conditions (Fig. 5.8). The calculated values are in accordance with observations made previously by other authors that also measured durations of around one second for the total lifetime of these pores [32, 35–38]. According to these measurements, in a traditional electroporation protocol, where the delay between pulses is usually one second, the majority of short-lived pores reseal before the next pulse is applied, but when potential irreversible membrane defects are produced, the stabilization of membrane needs longer durations.

Fig. 5.10 depicts the evolution of the impedance drop immediately after the pulse calculated as the difference between the value at the end of one inter-pulse measurement and the value at the beginning of the next one (see 5.5b, lower insert). It clearly shows electric field dependence increasing the impedance drop with higher electric fields. This supports the fact that the number (or the size) of short-lived pores increases with field magnitude. Additionally, the decreasing value over time for 800 and 1200 V/cm can be explained by the reduction in the number of new pores created. This can be attributed to the fact that once the membrane is permeabilized, it is more difficult to reach again the transmembrane voltage threshold for electroporation, thus reducing the ability of pore formation pulse after pulse. In the case of 800 V/cm and 1200 V/cm this is caused by the fact that the membrane do not recover completely before a new pulse is applied what can be the consequence of irreversible membrane destabilization.

5.3.3.2 Long-term analysis

The accumulated impedance decay corresponding to the long-term evolution observed in R_0 and R_∞ is analyzed next. Fig. 5.11 shows the percentage of variation with respect to the initial pre-electroporation state of cell monolayers during the complete 8 pulses electroporation treatment. The data is obtained from fitting parameters R_0 and R_∞ to double exponential functions (refer to

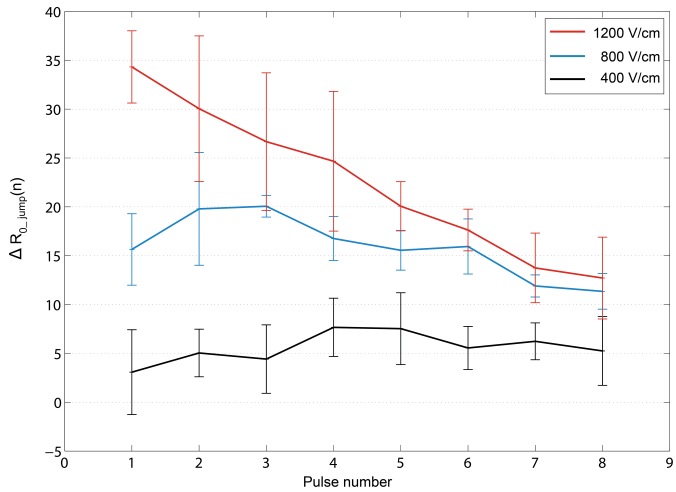

Fig. 5.10 Evolution of the impedance drop immediately after each pulse for the different electric fields. Mean ± SD of at least three repetitions.

Fig. 5.5a dashed lines for an example of the results obtained with R_0, a similar procedure is applied to R_∞).

Comparing the evolution of both parameters, it is noticeable that the relative % variation clearly differs between the low and high frequency resistances. In the case of the highest electric field (1200 V/cm), for example, parameter R_0 reduces to ≈70% while R_∞ decreases to ≈93%. Furthermore, electric field dependence is also clearly observed in both parameters being the relative change bigger with increasing electric fields.

The differences in the relative % of variation observed between R_0 and R_∞ are explained on the basis that two events affecting the impedance recordings are occurring at the same time; first, the creation of pores in the membrane and second, the change in conductivity of the extracellular and intracellular media caused by ion diffusion. As explained before, in an electroporated cell, R_0 is sensitive to the changes produced in the membrane because a fraction of the low frequency measuring signals can now flow through it. On the contrary, at high frequency, membrane does not act as a barrier for current flow either before or after electroporation, thus R_∞ should remain constant. Nevertheless, a change of the intracellular and/or extracellular conductivities should influence

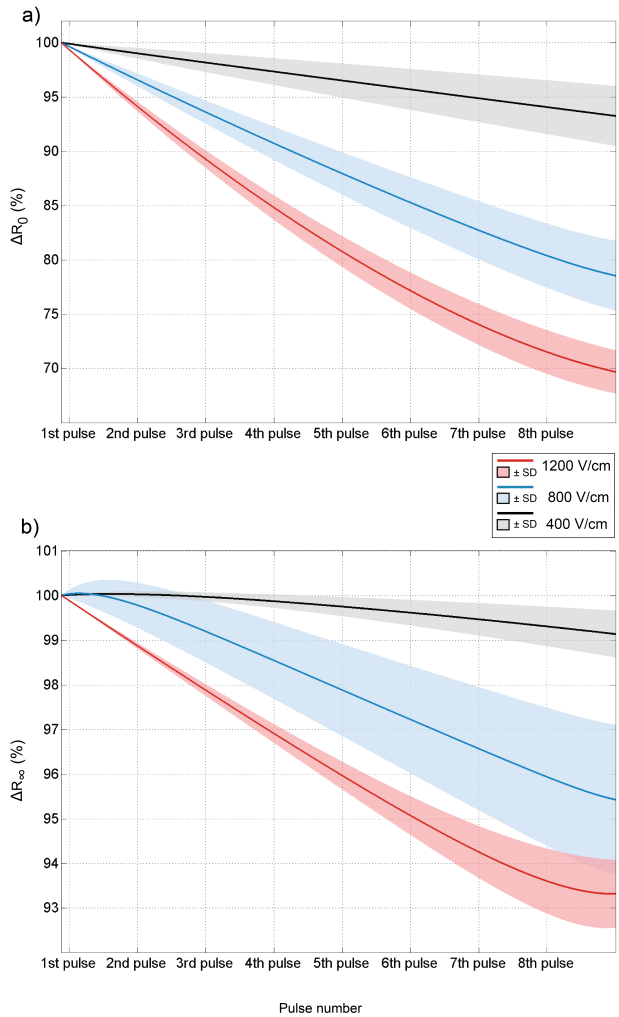

Fig. 5.11 Adjusted exponential for the long term decay of parameters R_0 (a) and R_∞ (b) represented as the % variation from initial pre-electroporation state. Shadow area corresponds to the standard deviation from at least three repetitions.

both parameters.

As demonstrated by previous authors, a conductivity increase in the extracellular media with kinetics in the range of several seconds is detected above the threshold of electroporation [39]. This conductivity variation is explained by the leakage of ions across the disturbed membrane by passive diffusion. Regarding

the behavior of R_∞ and considering that it is determined by the parallel association of the intracellular and extracellular resistances, it is necessary, in order to explain the total decay observed, to make the assumption that the changes in the extracellular conductivity have a bigger impact on the registered impedance. If both the increase in the extracellular conductivity and the decrease of the intracellular conductivity would have the same effect, there should be no significant variation in R_∞. This assumption can be considered true as long as measurements are performed in a low-conductive buffer with conductivity several times lower than the intracellular space. Additionally, it is reasonable to infer that the changes in the volume corresponding to the extracellular space have a higher impact on the measured impedance due to spatial distribution of the components in the system. There is a layer of extracellular medium between the electrodes and the cells (see Fig. 5.3). Therefore, the variation of R_∞ is then explained by the release of ions from the cell to the extracellular medium attending to a diffusion mechanism in the range of several seconds.

In the case of R_0, apart from the change in conductivity explained above, the long-term impedance decay accumulated is the result of the creation of more stable pores in the membrane that do not reseal in the time scale considered. These pores are described usually as long-lived pores and are believed to be the ultimate responsible for the success, in terms of macromolecules uptake, of any electroporation treatment. From Fig. 5.11a it can be observed that R_0 follows an asymptotic behavior suggesting that the number of stable pores does not linearly increase with pulse number and there maybe a limit for new pores formation. This is in accordance to the fact that from a certain level, increasing the number of pulses does not improve the effectiveness of the electroporation treatment [40, 41].

The Cole model has been used in the analysis because it is a standard, widespread and simple method and it has been shown how the information contained in R_0 can be used for analyzing membrane variations in response to pulse application. However, the drawback of such a simple mathematical model is the fact that it does not include a specific parameter that accounts for membrane poration uniquely. As discussed above, the parameters R_0 and R_∞ are contributed by the intracellular and extracellular conductivity variations and also by the membrane resistance changes. For this reason, it is not possible to

fully analyze those effects independently and some assumptions have been done in the analysis of Cole parameters. In the following section, a more complex equivalent circuit is proposed and used in order to demonstrate that some of the previous assumptions are correct.

5.3.4 Augmented electrical equivalent circuit

The proposed electrical equivalent circuit used in this section consists of a simple approximation of a single 2R-1C dispersion modified by the presence of an additional parallel resistance and the replacement of the capacitance by a CPE. The parameters R_{ext} and R_{int} correspond to the extracellular and intracellular resistances respectively and the additional resistance R_{pores} simulates the opening and closing of membrane pores (see Fig. 5.3c). The goal of using an equivalent electrical model is to be able to observe the behavior of the different parts of the system separately and based on their physical meaning, to have a correct interpretation of the measurements. This information is then used to confirm if the previous assumptions made with Cole parameters are correct.

The analysis of the electrical equivalent is only shown for an illustrative example, valid to demonstrate the adequacy of the model and its interpretation. Data corresponds to a single experiment applying 1200 V/cm, the same analysis was made for the rest of conditions showing a similar behavior. First, the values for the initial pre-electroporation state are found manually to set the initial conditions to the fitting algorithm. Subsequently, circuit parameters are obtained automatically for each spectrum. The algorithm is based on the solution of a least squares minimization problem using a method that allow to set bounds to the variables inspired in the Zfit algorithm in Matlab [42]. During the course of the fitting procedure, it was noticed that there was more than one possible set of parameters solving the system. For this reason some restrictions are imposed to the algorithm in accordance to the expected evolution of the parameters. Namely, it is imposed a lower bound for R_{int} corresponding to its initial pre-electroporation value. Considering the release of ions from the cytoplasm, it is unlikely the decrease of R_{int} during the experiment. Additionally, the α exponent is also forced not to increase, this condition is imposed by interpreting that lower values of α mean that the CPE tends to the behavior of

an ideal resistor what seems reasonable after membrane poration.

In order to confirm that both models are compatible, the equivalent R_0 and R_∞ for the proposed circuit are calculated following the equations:

$$R_0 = R_{ext}//(R_{int} + R_{pores}) \tag{5.2}$$

$$R_\infty = R_{ext}//R_{int} \tag{5.3}$$

Fig. 5.12a shows the initial fitted model and the corresponding measured data. In Figs. 5.12b and c parameters R_0 and R_∞ from the two models are plotted together for the same set of measurements. It is clearly noticeable that the calculated parameters from the equivalent circuit lead to similar behavior than those from Cole model confirming the equivalence of both models.

Fig. 5.12d, e and f show the evolution of parameters R_{pores}, R_{ext} and R_{int} respectively. The evolution of R_{pores} is in agreement with the proposed dual dynamic process which occurs in the membrane during the course of pulse application as discussed in previous section. This confirms that the variations observed in the parameter R_0 of the Cole model are mainly modulated by the changes due to membrane poration and validate the analysis made in the previous section. In the case of R_{ext} (Fig. 5.12d), the extracted parameter shows a maintained slow decrease over time, while R_{int} shows a negligible increase and can be considered constant. This is in agreement with the assumption that R_∞ from the Cole model is mainly influenced by the increase on the conductivity of the extracellular medium produced by the diffusion of ions and that the effect of R_{int} is negligible in the present setup. This is because the extracellular conductivity is several-fold lower than the intracellular conductivity, thus the ion leakage has a higher impact on R_{ext}. The previous observations validate the assumptions made during the analysis of the Cole model parameters where R_0 reflects the membrane changes and R_{infty} the variation in the composition of the extracellular medium.

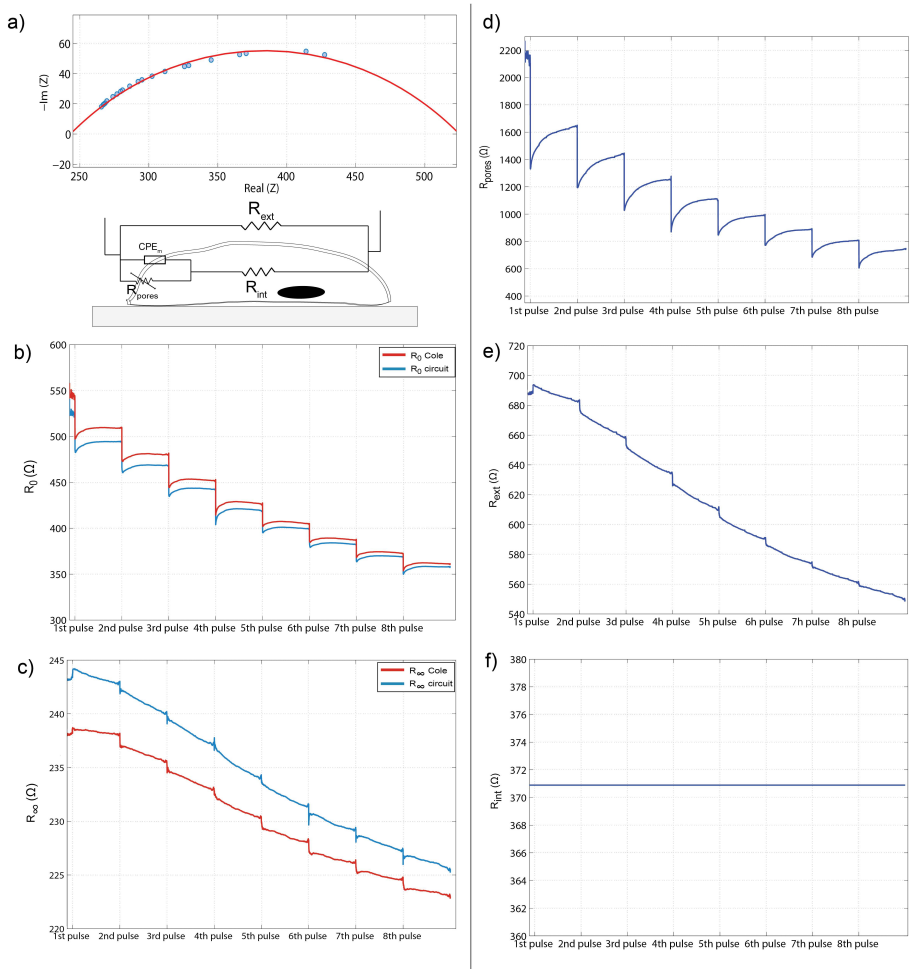

Fig. 5.12 Adjusted equivalent circuit. a) Data and fitted arc for the initial pre-electroporation state of a single experiment applying 1200 V/cm. b) and c) Comparison of the calculated R_0 and R_∞ for the equivalent circuit and the obtained for the Cole model. d), e) and f) Evolution of parameters R_{pores}, R_{ext} and R_{int} of the equivalent circuit, respectively.

5.4 Conclusions

In this study a fast EIS technique based on multisine excitation is used to measure impedance variations of differentiated myotubes monolayers during electroporation. The system enables, for the first time, to perform continuous multifrequency measurements with a time resolution of 1 spectrum/ms during the interpulse time window between consecutive pulses of a regular electroporation treatment (8 pulses, 100 μs, 1 Hz). Additionally, the characteristics of the microelectrode assembly used allows performing the experiments directly *in situ* with cells cultured in standard 24 multi-well plates.

In order to get the most from the multifrequency information obtained, data sets are adjusted to Cole impedance model. The analysis of parameter R_0 shows two different dynamics. One corresponding to the kinetics of short-lived pores that start to reseal immediately after pulse application. This fast resealing process agrees with a double exponential function with two time constants. A fast time constant in the order of hundreds of milliseconds and a slow time constant in the order of 1 second. The observed behavior differs between the lowest electric field tested, which corresponds with the threshold for permeabilization, and the other two conditions, where cells are extensively permeabilized. This supports the idea that near to the threshold of permeabilization some mechanisms responsible for structural changes in the membrane during electroporation either are not triggered, or are fully reversible, or can be considered negligible. The second slow variation observed in R_0 is attributed to the accumulation of more stable pores in the membrane pulse after pulse. The increase in membrane permeability due to these pores is not linear with pulse number and shows an asymptotic behavior suggesting a limit for permeabilization with pulse number.

The analysis of R_∞ shows a slow decrease reflecting changes in the system that cannot be only a direct reflect of the changes in the cell membrane because at high frequency the measuring signals are much less affected by the presence of membranes. These collateral effects are caused by the increase in the conductivity of the extracellular space produced by the diffusion of ions through membrane pores.

In order to confirm the analysis made using Cole model parameters and given

that some effects could be simultaneously influencing these parameters, measurements are subsequently adjusted to an electrical equivalent circuit. The independent observation of the circuit elements and its direct physical interpretation is useful to confirm the assumptions made with Cole model parameters. The results support that the double dynamics observed in R_0 are compatible with the changes produced in the membrane due to the formation of pores. Furthermore, the constant behavior obtained in R_{int} demonstrates that the results are compatible with the hypothesis that the intracellular conductivity, which theoretically should increase during the process, has a negligible impact on the obtained results in comparison with the changes produced in the extracellular composition.

The information obtained from the present multifrequency measurements supports the fact that when acquiring complete spectra instead of single frequency measurements, more information about the system can be extracted. The present results demonstrate how fast EIS measurements during an electroporation procedure represent a reliable and alternative method for online monitoring the changes produced in the sample under treatment. This conclusion also has a great interest in *in vivo* applications where the control of the tissue permeabilization during pulse delivery is critical to achieve the desired effect [8, 43, 44].

References

[1] Ralf W. Glaser, Sergei L. Leikin, Leonid V. Chernomordik, Vasili F. Pastushenko, and Artjom I. Sokirko. Reversible electrical breakdown of lipid bilayers: formation and evolution of pores. *Biochimica et Biophysica Acta (BBA) - Biomembranes*, 940(2):275–287, 1988.

[2] B. Sanchez, E. Louarroudi, E. Jorge, J. Cinca, R. Bragos, and R. Pintelon. A new measuring and identification approach for time-varying bioimpedance using multisine electrical impedance spectroscopy. *Physiological Measurement*, 34(3):339, 2013.

[3] U. F. Pliquett and K. H. Schoenbach. Changes in electrical impedance of biological matter due to the application of ultrashort high voltage pulses. *Dielectrics and Electrical Insulation, IEEE Transactions on*, 16(5):1273–1279, 2009.

[4] A. L. Garner, Chen Nianyong, Yang Jing, J. Kolb, R. J. Swanson, K. C. Loftin, S. J. Beebe, R. P. Joshi, and K. H. Schoenbach. Time domain dielectric spectroscopy measurements of hl-60 cell suspensions after microsecond and nanosecond electrical pulses. *Plasma Science, IEEE Transactions on*, 32(5):2073–2084, 2004.

[5] J. Zhuang and J. F. Kolb. Time domain dielectric spectroscopy of nanosecond pulsed electric field induced changes in dielectric properties of pig whole blood. *Bioelectrochemistry*, 2014.

[6] Y. Feldman, Irina Ermolina, and Y. Hayashi. Time domain dielectric spectroscopy study of biological systems. *Dielectrics and Electrical Insulation, IEEE Transactions on*, 10 (5):728–753, 2003.

[7] E. Fattori, N. La Monica, G. Ciliberto, and C. Toniatti. Electro-gene-transfer: a new approach for muscle gene delivery. *Somat Cell Mol Genet*, 27(1-6):75–83, 2002.

[8] D. Cukjati, D. Batiuskaite, F. Andre, D. Miklavcic, and L. M. Mir. Real time electroporation control for accurate and safe in vivo non-viral gene therapy. *Bioelectrochemistry*, 70(2):501–7, 2007.

[9] B. Sanchez, E. Louarroudi, R. Bragos, and R. Pintelon. Harmonic impedance spectra identification from time-varying bioimpedance: theory and validation. *Physiological Measurement*, 34(10):1217, 2013.

[10] J. Z. Bao, C. C. Davis, and Robert E. Schmukler. Impedance spectroscopy of human erythrocytes: system calibration, and nonlinear modeling. *Biomedical Engineering, IEEE Transactions on*, 40(4):364–378, 1993.

[11] Herman P. Schwan and Clifford D. Ferris. Four-electrode null techniques for impedance measurement with high resolution. *Review of Scientific Instruments*, 39(4):481–485, 1968.

[12] Chang Zu-yao, G. A. M. Pop, and G. C. M. Meijer. A comparison of two- and four-electrode techniques to characterize blood impedance for the frequency range of 100 hz to 100 mhz. *Biomedical Engineering, IEEE Transactions on*, 55(3):1247–1249, 2008.

[13] E. Sarró, M. Lecina, A. Fontova, C. Solà, F. Gòdia, J. J. Cairó, and R. Bragós. Electrical impedance spectroscopy measurements using a four-electrode configuration improve online monitoring of cell concentration in adherent animal cell cultures. *Biosensors and Bioelectronics*, 31(1):257–263, 2012.

[14] H. P. Schwan. Electrode polarization impedance adn measurements in biological materials. *Annals of the New York Academy of Sciences*, 148(1):191–209, 1968.

[15] Ishai Paul Ben, S. Talary Mark, Caduff Andreas, Levy Evgeniya, and Feldman Yuri. Electrode polarization in dielectric measurements: a review. *Measurement Science and Technology*, 24(10):102001, 2013.

[16] E. T. McAdams and J. Jossinet. Nonlinear transient response of electrode—electrolyte interfaces. *Medical and Biological Engineering and Computing*, 38(4):427–432, 2000.

[17] E. A. Brown, J. D. Ross, R. A. Blum, Nam Yoonkey, B. C. Wheeler, and S. P. DeWeerth. Stimulus-artifact elimination in a multi-electrode system. *Biomedical Circuits and Systems, IEEE Transactions on*, 2(1):10–21, 2008.

[18] Byoung-Yong Chang and Su-Moon Park. Integrated description of electrode/electrolyte interfaces based on equivalent circuits and its verification using impedance measurements. *Analytical Chemistry*, 78(4):1052–1060, 2005.

[19] Daniel R. Merrill, Marom Bikson, and John G. R. Jefferys. Electrical stimulation of excitable tissue: design of efficacious and safe protocols. *Journal of Neuroscience Methods*, 141(2):171–198, 2005.

[20] I. Petrova Galidia. Influence of electrode impedance changes on the common-mode rejection ratio in bioimpedance measurements. *Physiological Measurement*, 20(4):N11, 1999.

[21] L. A. Geddes. Historical evolution of circuit models for the electrode-electrolyte interface. *Annals of Biomedical Engineering*, 25(1):1–14, 1997.

[22] H. Kalvoy, G. K. Johnsen, O. G. Martinsen, and S. Grimnes. New method for separation of electrode polarization impedance from measured tissue impedance. *Open Biomed Eng J*, 5:8–13, 2011.

[23] F. Bordi, C. Cametti, and T. Gili. Reduction of the contribution of electrode polarization effects in the radiowave dielectric measurements of highly conductive biological cell suspensions. *Bioelectrochemistry*, 54(1):53–61, 2001.

[24] H. Fricke and S. Morse. The electric resistance and capacity of blood for frequencies between 800 and 4(1/2) million cycles. *J Gen Physiol*, 9(2):153–67, 1925.

[25] Antoni Ivorra. *Tissue Electroporation as a Bioelectric Phenomenon: Basic Concepts*, chapter 2, pages 23–61. Series in Biomedical Engineering. Springer Berlin Heidelberg, 2010.

[26] A. Silve, A. Guimera Brunet, B. Al-Sakere, A. Ivorra, and L. M. Mir. Comparison of the effects of the repetition rate between microsecond and nanosecond pulses: Electropermeabilization-induced electro-desensitization? *Biochimica et Biophysica Acta (BBA) - General Subjects*, 1840(7):2139–2151, 2014.

[27] H. Shagoshtasbi and Lee Yi-Kuen. A new equivalent circuit model for micro electroporation systems. In *Nano/Micro Engineered and Molecular Systems (NEMS), 2011 IEEE International Conference on*, pages 662–665, 2011.

[28] Yong Huang and Boris Rubinsky. Micro-electroporation: Improving the efficiency and understanding of electrical permeabilization of cells. *Biomedical Microdevices*, 2(2):145–150, 1999.

[29] L. F. Cima and L. M. Mir. Macroscopic characterization of cell electroporation in biological tissue based on electrical measurements. *Applied Physics Letters*, 85(19):4520–4522, 2004.

[30] G. Saulis. Kinetics of pore disappearance in a cell after electroporation. *Biomed Sci Instrum*, 35:409–14, 1999.

[31] P. M. Ghosh, C. R. Keese, and I. Giaever. Monitoring electropermeabilization in the plasma membrane of adherent mammalian cells. *Biophysical Journal*, 64(5):1602–1609, 1993.

[32] D. A. Zaharoff, J. W. Henshaw, B. Mossop, and F. Yuan. Mechanistic analysis of electroporation-induced cellular uptake of macromolecules. *Exp Biol Med (Maywood)*, 233(1):94–105, 2008.

[33] Mojca Pavlin and Damijan Miklavcic. Theoretical and experimental analysis of conductivity, ion diffusion and molecular transport during cell electroporation - relation between short-lived and long-lived pores. *Bioelectrochemistry*, 74(1):38–46, 2008.

[34] M. Leguèbe, A. Silve, L. M. Mir, and C. Poignard. Conducting and permeable states of cell membrane submitted to high voltage pulses: Mathematical and numerical studies validated by the experiments. *Journal of Theoretical Biology*, 360(0):83–94, 2014.

[35] Judith A. Stolwijk, Christoph Hartmann, Poonam Balani, Silke Albermann, Charles R. Keese, Ivar Giaever, and Joachim Wegener. Impedance analysis of adherent cells after in situ electroporation: Non-invasive monitoring during intracellular manipulations. *Biosensors and Bioelectronics*, In Press, Corrected Proof, 2011.

[36] M. Pavlin, M. Kanduser, M. Rebersek, G. Pucihar, F. X. Hart, R. Magjarevic, and D. Miklavcic. Effect of cell electroporation on the conductivity of a cell suspension. *Biophys J*, 88(6):4378–90, 2005.

[37] Huiqi He, Donald C. Chang, and Yi-Kuen Lee. Nonlinear current response of micro electroporation and resealing dynamics for human cancer cells. *Bioelectrochemistry*, 72 (2):161–168, 2008.

[38] Michelle Khine, Cristian Ionescu-Zanetti, Andrew Blatz, Lee-Ping Wang, and Luke P. Lee. Single-cell electroporation arrays with real-time monitoring and feedback control. *Lab on a Chip*, 7(4):457–462, 2007.

[39] Mojca Pavlin, Vilko Leben, and Damijan Miklavčič. Electroporation in dense cell suspension—theoretical and experimental analysis of ion diffusion and cell permeabilization. *Biochimica et Biophysica Acta (BBA) - General Subjects*, 1770(1):12–23, 2007.

[40] H. Wolf, M. P. Rols, E. Boldt, E. Neumann, and J. Teissie. Control by pulse parameters of electric field-mediated gene transfer in mammalian cells. *Biophysical Journal*, 66(2, Part 1):524–531, 1994.

[41] J. Teissie, M. Golzio, and M. P. Rols. Mechanisms of cell membrane electropermeabilization: A minireview of our present (lack of ?) knowledge. *Biochimica et Biophysica Acta (BBA) - General Subjects*, 1724(3):270–280, 2005.

[42] Jean-Luc Dellis. Zfit : http://www.mathworks.com/matlabcentral/fileexchange/19460-zfit, 2010.

[43] Julie Gehl Mir and Lluis M. Determination of optimal parameters for in vivo gene transfer by electroporation, using a rapid in vivo test for cell permeabilization. *Biochemical and Biophysical Research Communications*, 261:377–380, 1999.

[44] Y. Granot, A. Ivorra, E. Maor, and B. Rubinsky. In vivo imaging of irreversible electroporation by means of electrical impedance tomography. *Phys Med Biol*, 54(16):4927–43, 2009.

Chapter 6

Electrical bioimpedance spectroscopy study of various cell lines during *in vitro* electroporation: comparative analysis

Abstract

In this chapter the electrical impedance response of four different cell lines during electroporation is analyzed and compared using the same experimental setup that the one presented in the previous chapter. The aim of this study is to test the suitability of the system when applied in a more general situation. First, it is shown how the system is useful for characterizing the cell monolayers before electroporation. Along the analysis, different methods are proposed to study the impedance evolution of the different cell lines during electroporation. It is shown that, in all cases, the system is able to detect impedance changes related to pore dynamics and that some parameters are more suitable to be used in the analysis of a general situation. Additionally, the information of the accumulated impedance change at the end of the treatment is compared to the permeabilization rates obtained with a chemical method. The results confirm how impedance measurements are a suitable method in order to monitor electropermeabilization in real-time.

6.1 Introduction

The development of reliable techniques for monitoring the course of electroporation has been object of study during years. Along the course of this thesis, the aim is to contribute in the improvement of the electrical methods for this purpose. The increasing use of electroporation for treating localized tumors in cancer patients [1] motivates the development of reliable tools to control in real-time the procedure. Nevertheless, electroporation is currently performed without a **real-time** control regarding the extent and degree of permeabilization and usually some tests are performed prior to treatment as proposed in [2]. As shown, the measurement of electric properties of the sample under treatment during electroporation represents an optimal option given the possibility of acquiring immediate information from the system. One of the first studies to use a real-time control applied to non-viral gene therapy used the pulse current to voltage ratio has a predictor of the extent of permeabilization and used this information to adjust the electric field applied [3]. By the same time, other authors also applied a feedback control system to deliver the appropriate electric field to single cells [4]. Other electrical measurements during treatment have also been shown as promising tools to obtain information from biological samples using magnetic resonance electrical impedance tomography [5] and electrical impedance tomography [6, 7].

In the present study, electrical impedance spectroscopy measurements of four different cell lines (C2C12 myoblasts, C2C12 differentiated mytoubes, DC3F and HeLa cells) cultured as monolayers in standard multi-well plates are analyzed during electroporation. The same experimental setup presented in the previous chapter, which is able to perform electroporation and impedance spectroscopy measurements in the interval between consecutive pulses with a high temporal resolution, is used. The measuring system enables to obtain information about the kinetics of pore formation and resealing both in the short and long term. The comparison of the impedance response of the different cell lines can bring important information about the general performance of the system and is useful in order to confirm its ability to measure the effects of electroporation in various situations.

In order to analyze the full spectral impedance information acquired, differ-

ent methods are proposed. This comparative analysis is performed with the aim of discerning which parameters can provide better information in a general situation. First, the magnitude and phase angle of impedance are shown at different individual frequencies. Subsequently, in order to take advantage of the complete spectral information, data modeling is applied to measurements. The parameters of the widely known Cole model are deeply analyzed and discussed. Additionally, an alternative modification of Cole model is also discussed. Finally, measurements are adjusted to a complete circuital model whose components are correlated with different processes occurred during electroporation. The goal of this study is also to give some insights in the possibilities that full spectral information can have in comparison with single frequency measurements. However, the vast amount of information generated during the experiments is still under study and it would be unrealistic trying to give a complete and definitive analysis.

6.2 Materials and Methods

The materials and methods used for this study correspond exactly to the ones presented in the previous chapter, refer to section 5.2 for a full detailed description. Only the information related to the cell culture procedure used for the new cell lines included in this study is detailed below.

Additionally, it should be pointed out in this section that the same compensation procedure explained in 5.3.1.2, which is used to reduce the effects appeared in the electrodes by subtracting frequency by frequency the small variations recorded in the absence of cells for each electric field, is also applied to the present measurements.

6.2.1 Cell culture

C2C12 mouse myoblasts and HeLa human cervix carcinoma cells are seeded into 24 muti-well plates at a initial density of 40×10^3 cells/well and 50×10^3 respectively, with 1 ml of growth medium comprising Dulbecco's Modified Eagle's Medium (DMEM; High Glucose, GlutaMAX Supplement, pyruvate. Gibco, Carlsbad, CA, USA) supplemented with 10% fetal bovine serum (FBS) and 1% penicillin-streptomycin.

In the case of DC3F chinese hamster fibroblasts, cells are seeded at a initial density of 350×10^3 cells/well with 1 ml of growth medium (in this case Minimal Esential Medium (MEM; GlutaMAX. Gibco, Carlsbad, CA, USA) supplemented with 10% fetal bovine serum (FBS) and 1% penicillin-streptomycin. All cells are kept in an incubator at 37° under a 5% CO_2 atmosphere for 24 h until full confluence.

Finally, C2C12 differentiated myotubes are obtained following the procedure explained in the previous chapter.

6.3 Results and Discussion

In this section the main findings extracted from the electrical impedance spectroscopy measurements performed during the electroporation treatment of the four cell lines used (C2C12 myotubes, DC3F, C2C12 myoblasts and HeLa) are shown. First, the measurements corresponding to the initial pre-eletroporation state of monolayers are shown and discussed. Subsequently, the measurements performed in the interpulse interval between consecutive pulses are shown for an illustrative example corresponding to the highest electric field assayed in each cell line. These illustrative examples are discussed from three different perspectives:i) first, the magnitude and phase angle impedance response is shown, ii) second, the Cole model parameters extracted from the same set of measurements are discussed, iii) and finally, an electrical equivalent circuit is used to model the measurements.

Further in this section, the analysis is divided in two parts in order to study: in a first part the fast impedance variations detected short after pulse application, and then, the long-term accumulated impedance decrease is analyzed.

6.3.1 Pre-electroporation impedance measurements

The present results show the measurements performed in each cell line prior to electroporation pulse application. As explained before, electrical impedance spectroscopy measurements can be used to detect differences between different samples both *in vitro* and *in vivo*, or between healthy and abnormal states of the same sample, also it can give an estimator about cell concentration, etc. In this section, the goal is to test the ability of the system to extract characteristics of the cell lines under study. Information about the cell monolayers before electroporation is useful to assess the conditions of the sample under treatment. Additionally, the information extracted from these measurements could be useful for the subsequent analysis during electroporation.

In Fig. 6.1 a representative micrograph of each cell line is shown. It can be observed at a glance that there exist significant differences in dimensions

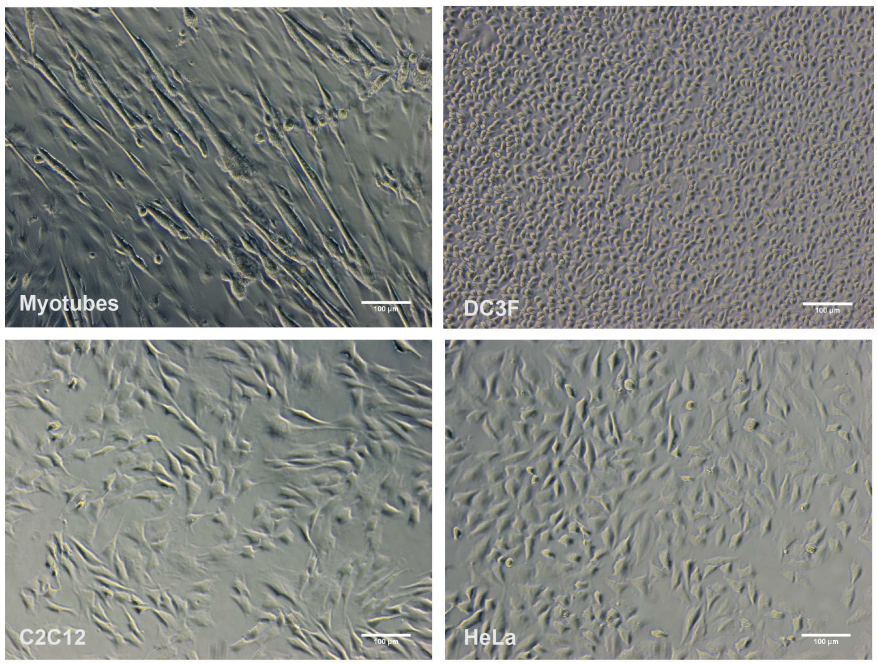

Fig. 6.1 Representative phase contrast micrographs of the cell lines included in the study. 10x magnification.

and organization between them. While myotubes show considerable elongated shapes with marked differences between their long and short axis and a very inhomogeneous conformation, DC3F cells are on the contrary very homogeneous. C2C12 and HeLa cells are in the intermediate situation between the other two.

First, the initial measurements are fitted to the Cole model. In the frequency band ranging from some kHz to some MHz corresponding to the β dispersion, biological tissues usually show one single relaxation phenomenon following Cole equation 6.1. However, in some cases the structural inhomogeneity of tissues, secondary cellular processes such as cell to cell gap junctions or intracellular organelles, among others, result in a the appearance of a second sub-relaxation. In these cases it is usual to adjust the impedance data to an association of two or more Cole arcs functions. In the case of a series association of two elements the impedance follows equation 6.2.

$$Z_{single} = R_{\infty} + \frac{R_0 - R_{\infty}}{1 + (j\omega \frac{f}{f_c})^{\alpha}} \tag{6.1}$$

$$Z_{double} = R_{\infty_1} + R_{\infty_2} + \frac{R_{0_1} - R_{\infty_1}}{1 + (j\omega \frac{f}{f_{c_1}})^{\alpha_1}} + \frac{R_{0_2} - R_{\infty_2}}{1 + (j\omega \frac{f}{f_{c_2}})^{\alpha_2}} \tag{6.2}$$

From the parameters of this mathematical model (R_0, R_∞, α and f_c), it has been shown that α and the characteristic frequency (f_c) are directly related with the intrinsic properties of the biological sample under study [8–11]. Specifically, it has been suggested that the characteristic frequency is intimately related to cell size and shape [10]. In order to make a comparison between the different cell lines, the dimensions of cells (major (D1) and minor (D2) axes of cells) are first obtained manually using the image processing software ImageJ (MacBiophotonics). From this two dimensions, the average cell size, defined as the mean value of the major axis and the minor axis, is calculated. Subsequently, impedance for each cell line is fitted to a single Cole arc. In Fig. 6.2 the central relaxation frequency (f_c) is plotted against cell size. As expected [12], it can be observed a good correlation between the cell size and the characteristic frequency showing an inversely proportional relation.

The detailed observation of the data from the cell lines with non homogeneous sizes (Myotubes, C2C12 and HeLa), reveals that the measurements could be fitted to a double arc instead of a single arc system. The differences between long and short axis of these cell lines can explian the appearance of two relaxations, each corresponding to one predominant dimension of the cell monolayer.

In Fig. 6.3 each dimension (D1 and D2) is plotted against the corresponding characteristic frequency (f_{c1} and f_{c2}) of a double Cole arc. The results show again an inverse relation between cell size and characteristic frequency. In the case of myotubes it would be reasonable to think that the cell size measurements maybe inaccurate due to the big differences between individual cells. This can explain the relatively high f_c in the case of myotubes if compared to the other cell lines and suggest that the results shown here represent just an approximation.

According to these measurements, the present setup is able to detect dif-

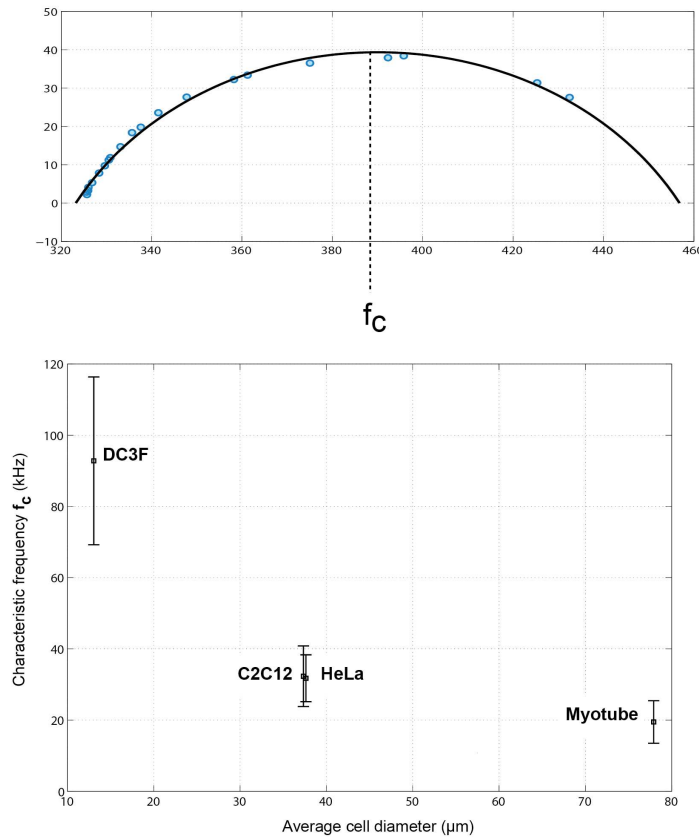

Fig. 6.2 Characteristic relaxation frequency f_c, obtained from fitting the pre-electroporation measurements to a single arc Cole model, plotted against the average cell size, calculated as the mean of the major (D1) and minor (D2) axes of cells.Results from at least three repetitions pooled together are shown.

ferences between cell lines. In the proposed analysis, these differences are attributed to the cell size and organization of the cell monolayer. For this reason the system is not able to show any differences in the impedance spectrum of C2C12 and HeLa cells that are really similar in sizes and cell monolayer organization. Clear differences are shown between C2C12 myoblasts and myotubes what demonstrates that the system is able to detect differentiation. The suitability of the present system as a tool for continuously monitoring the differentiation process with a minimally invasive system should be studied in depth but lies beyond the scope this thesis.

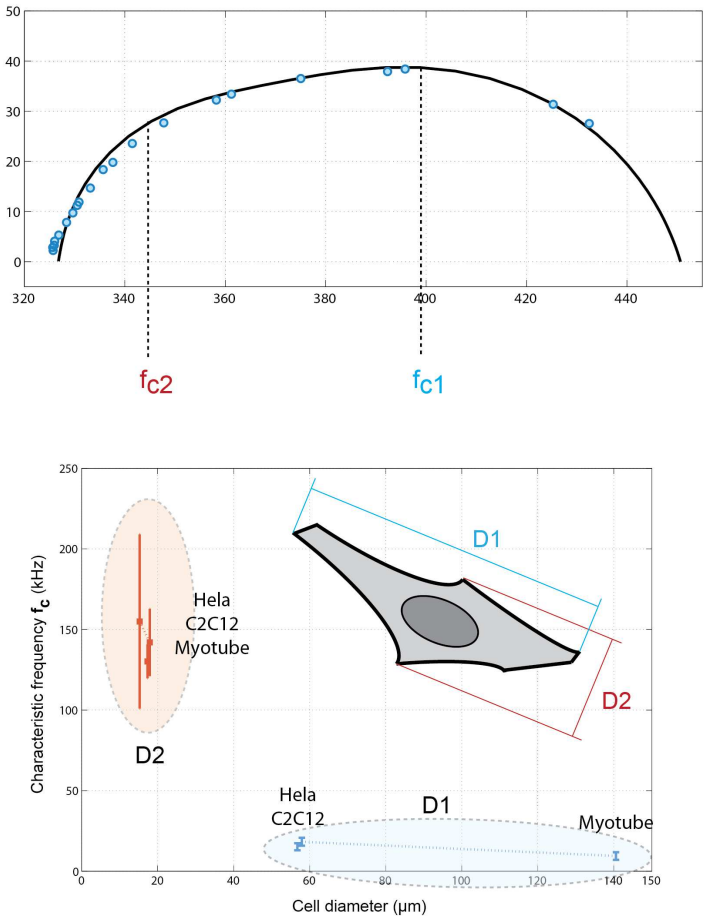

Fig. 6.3 Characteristic relaxation frequencies f_{c1} and f_{c2}, obtained from fitting the pre-electroporation measurements to a double arc Cole model, plotted against the cell size axis D1 and D2 respectively. Results from at least three repetitions pooled together are shown.

It has been shown how the measurements can be fitted to a single Cole arc, however when the cell monolayer shows a certain degree of inhomogeneity it is possible to use a double arc function. In both cases, the characteristic frequency of the Cole model, which corresponds to the maximum of the imaginary part can be used as a comparative parameter. In addition, these initial measurements have shown that it is possible to have information of the pre-electroporation state of the cell monolayer under treatment in a non-invasive way, what could be interesting in subsequent steps of the experimental procedure.

6.3.2 Measurements during electroporation treatment: illustrative examples

Along the first part of this section it is intended to show an illustrative example of the results obtained from the measurements performed during electroporation. The measurements correspond to the electric field condition when the maximum permeabilization was observed for each cell line without noticeable massive cell death. This field intensities were chosen performing previous permeabilization tests applying a range of different intensities. Specifically, these intensities (calculated as E=V/d) are 1200 V/cm for Myotubes and 1400 V/cm for the rest of cell lines. As previously detailed in 5.2, 850 spectra are recorded in each time lapse between consecutive pulses. The aim of this section is to study if the detailed observation and comparison of the impedance response of different cell lines can bring additional information and is useful to validate the system as well as to select which parameters of the analysis can provide more and better information.

6.3.2.1 Magnitude and phase

As a first step to better understand the present results it is helpful to observe the individual magnitude and phase response of the different cell lines. In Figs 6.4 and 6.5 the impedance response over the complete electroporation procedure is shown. The creation and disappearance of pores in the membrane should have a higher impact in the response at low frequencies. In this frequency band, the porated membrane no longer behaves as an insulator because the membrane is partially shunted by a trans-membrane resistor. At higher frequencies the impact becomes less and less pronounced. In an ideal situation, with no other colateral effects apart from membrane permeabilization, the impedance at high enough frequencies should not be affected by membrane poration. For this reason, from the 21 measured frequencies within each multisine burst, only the first six corresponding to 5, 7, 21, 24, 44 and 75 kHz are plotted for conciseness.

The magnitude response is first discussed. Following a similar analysis than that of the previous chapter, two different dynamics are expected. First, a fast recovery of impedance immediately after pulse application corresponding to

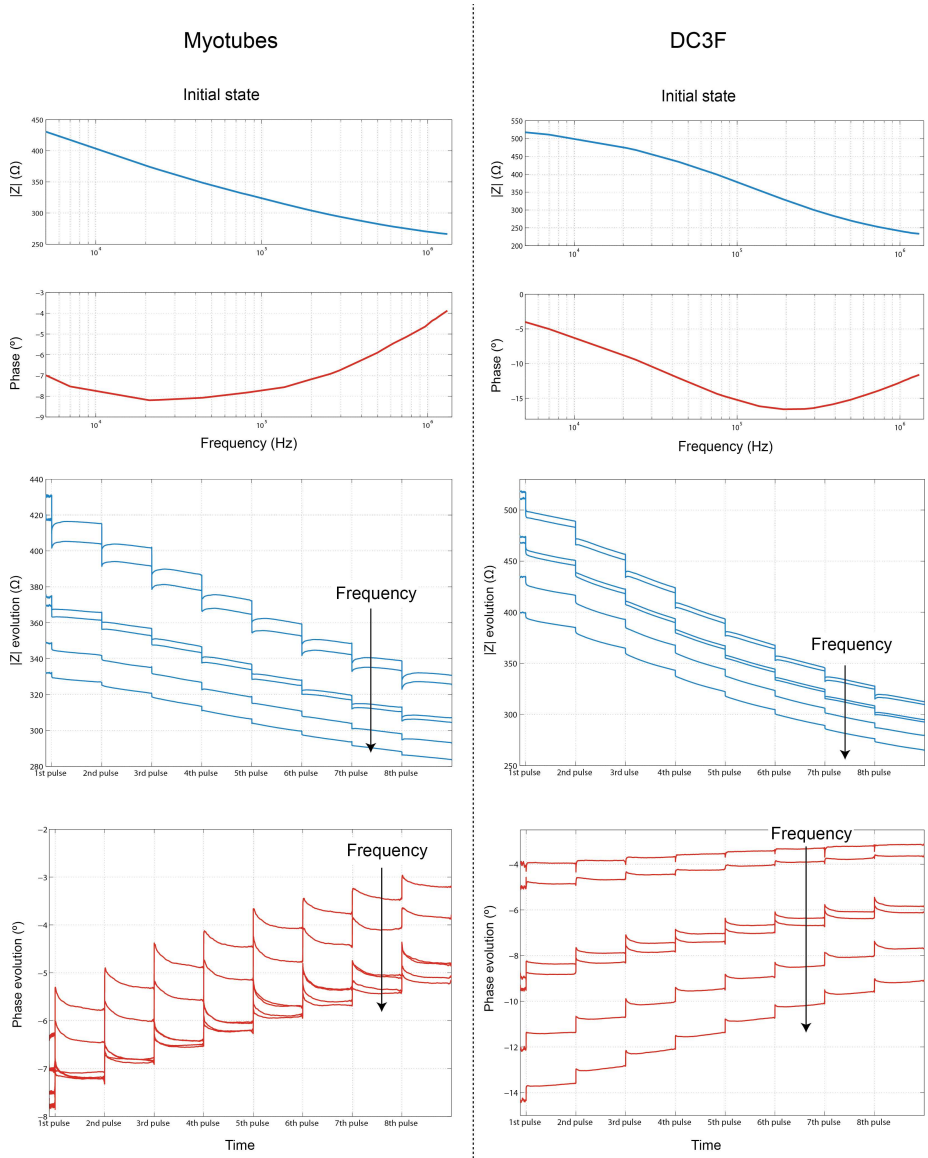

Fig. 6.4 Bode plot of the initial pre-electroporation state of myotubes and DC3F cells (upper inserts). Evolution of the impedance magnitude and phase angle during the application of 8 electroporation pulses. Illustrative examples for myotubes (E=1200 V/cm, left) and DC3F cells (E=1400 V/cm, right). Only data corresponding to 5, 7, 21, 24, 44 and 75 kHz are shown. The arrows in the figures indicate increasing frequency. The reader should be aware that although measurements pulse after pulse are plotted continuously there is a delay between the end of an interpulse measurement and the beginning of the next one (see section 5.2).

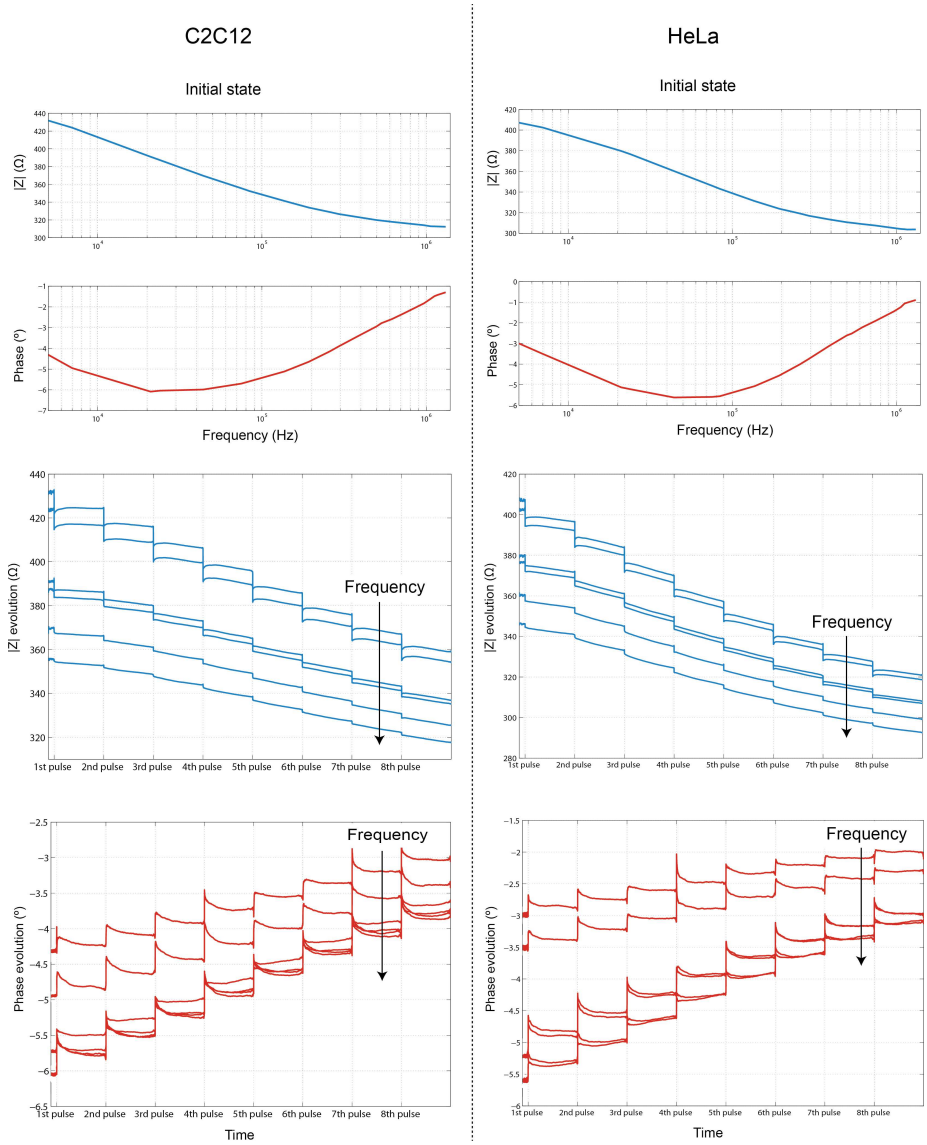

Fig. 6.5 Bode plot of the initial pre-electroporation state of C2C12 and HeLa cells (upper inserts). Evolution of the impedance magnitude and phase angle during the application of 8 electroporation pulses. Illustrative examples for C2C12 (E=1400 V/cm, left) and HeLa cells (E=1400 V/cm, right). Only data corresponding to 5, 7, 21, 24, 44 and 75 kHz are shown. The arrows in the figures indicate increasing frequency. The reader should be aware that although measurements pulse after pulse are plotted continuously there is a delay between the end of an interpulse measurement and the beginning of the next one (see section 5.2).

short-term membrane resealing. Secondly, an accumulated impedance reduction with slower dynamical behavior.

Focusing first on the magnitude decrease that is accumulated pulse after pulse along the complete treatment, it can be observed that the behavior is similar for all cases. Magnitude follows an exponential decrease implying that with increasing pulse number the reduction in magnitude is successively smaller. As previously discussed, this observation is compatible with two different processes superimposed: the creation of more stable pores that do not reseal during pulse application and the increase of conductivity due to leakage of ions, mostly K^+, from the cell cytoplasm into the extracellular volume.

Focusing next on the fast recovery process, it can be observed from Fig. 6.4 that the behavior differs depending on the cell line analyzed. In the case of myotubes, a fast recovery of the magnitude immediately after each pulse is clearly noticeable at the lowest frequencies. However, in the case of DC3F cells this recovering process is not evident and seems to be masked by a slow impedance decay accumulated along the complete measuring time. Only at the end of the procedure, after pulses number 7 and 8, a slight recovery can be observed in the magnitude of DC3F. The situation in Fig. 6.5 is intermediate, it is still possible to observe a recovery of impedance magnitude after each pulse but it is small comparing to the recovery observed in myotubes.

The observations made in the different cell lines suggest that depending on the analyzed case, the fast magnitude recovery resulting from short-term membrane resealing could be mixed with a second process consisting in a monotonous decrease of the impedance magnitude what makes impossible to differentiate them. This process agrees with the diffusion of ions through membrane pores and explains why the recovery of impedance magnitude is better detected at the end of the treatment. When the amount of ions that leak decreases due to the reduction in concentration gradients, the effect of the conductivity change is smaller and does not mask the membrane resealing.

The reason to explain the differences observed between cell lines could relay on the different dimensions of cells. The thickness of monolayers varies depending on cell line and thus the geometrical characteristics of the measurement setup (cell constant). In Fig. 6.6 a brief explanation of this concept is depicted.

The distance L1, between mytoubes and measurement microelectrodes is considerable shorter than the distance L2 for the case of DC3F cells. Considering that for a fixed electrode arrangement, the impedance sensitivity parameter depends on the distance from the electrodes [13–15] being higher for proximal layers to the microelectrodes than for deeper layers, this could explained the differences observed. From another point of view, the % of the total volume under the microelectrodes that is occupied by cells and extracellular medium is considerably different in both cases what could also influence the results. An electrode set-up with shorter separators or other strategies such as growing cells on a thin film matrix could be implemented to reduce this effect.

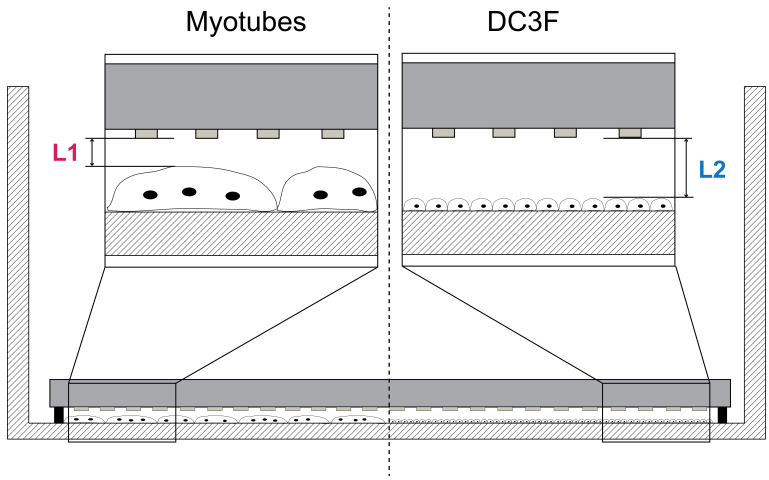

Fig. 6.6 Schematic representation (not to scale) depicting the possible impact of the cell line thickness on the measurements. The distances (L1 and L2) between microelectrodes and the sample under test differs depending on the cell line. Also, the measured percentage of extracellular volume changes between cell lines.

If the phase angle evolution is now studied, it can be observed that measurements show a fast dynamic change pulse after pulse for all cases. This observation suggests that the effect of conductivity change in the extracellular bulk electrolyte has considerably less impact in the phase angle of impedance than in its magnitude. This can be partially explained attending to the calculation of the phase angle of the impedance according to equation 6.3. This equation implies a quotient between imaginary and real parts of the system. On one hand, the imaginary part should be less sensitive to a conductivity change

but still not completely immune. This way, if both quantities are divided, the common contribution of the conductivity variation should be considerably reduced in the final result.

$$\theta(Z) = \arctan \frac{Im(Z)}{Re(Z)} \tag{6.3}$$

The only difference that can be noticed between cell lines is the frequency that exhibits the maximum variation. This is clearly shown in Fig. 6.4 where in the case of myotubes the maximum change occurs at the lowest frequency and in the case of DC3F cells the point of maximum variation is displaced to higher frequencies. For C2C12 and HeLa cells the maximum variation is placed in between the previous ones. This is related to the results previously discussed in Fig. 6.2. The phase variation is higher in frequencies around the maximum of the imaginary part (f_c).

Phase angle measurements are generally suitable in those applications where the geometry of the system is not constant because they are less susceptible to variations in the cell constant of the system. Phase measurements have been used by many authors as a marker to estimate different parameters in clinical applications [16–19]. In the present setup the distance between cells and microelectrodes varies with cell line, what is translated in a change in the cell constant as previously stated. The similarities observed in the behavior of phase angle for the different cell lines reinforces the fact that phase is more immune to geometry variations and represents a more appropriate parameter for comparison.

6.3.2.2 Cole model parameters

Complete information about the measured system can be studied in a simple way by adjusting impedance data to a model. As previously explained, data modeling is an advantageous method to use full spectral information in a single analysis. In the present section, the impedance response shown above for each cell line is fitted to the widely known Cole model. As exposed in previous

chapters, this mathematical description of impedance is characterized for its simplicity and has been extensively applied in the field of bioimpedance measurements. However, physical interpretation of model parameters is far from being completely understood what represents a limitation in many cases.

In the present study the aim of using Cole equation, and subsequently analyzing the evolution of its parameters, is to find out which provides better information to characterize each of the different processes taking place during the electroporation phenomenon. In Figs. 6.7 to 6.10 the evolution of the fitted Cole arcs and their corresponding parameters is shown for each cell line.

According to the analysis made in the previous chapter, R_0 should be significantly modified by the dynamics of pore formation in response to the creation of new current paths at low frequency. Additionally, a change in conductivity should also have an impact in R_0. On the contrary, R_∞ should not vary due to membrane poration but should be modified also by changes in the conductivity of the extracellular buffer.

Comparing the behavior of parameter R_0 with the low frequency magnitude response shown in the previous section, it can be noticed, as expected, that they perfectly match. This implies, as discussed in the case of impedance magnitude, that the fast dynamics of short-term pore resealing that should be observed in R_0 can be masked and not be distinguishable depending on cell line. For instance, in the same manner that fast resealing is observable in the magnitude response of myotubes, so it also appears in parameter R_0 of Fig. 6.7. However, in the case of DC3F cells it is not possible to distinguish the fast dynamic recovery from the superimposed slow decay similarly to the observations made in its magnitude response.

In the same way, R_∞ follows the same behavior observed in the magnitude response at the highest measurement frequencies (data not shown). As previously stated, the modification of this parameter is directly related to conductivity variations mostly in the extracellular volume. The comparison of the different cell lines shows that this parameter behaves very similar in all cases what makes sense with the fact that at high frequency cell membrane is "transparent" to the measuring signals. This way, the modification in the distance between cells and microelectrodes, that is believed to be responsible for the differences observed

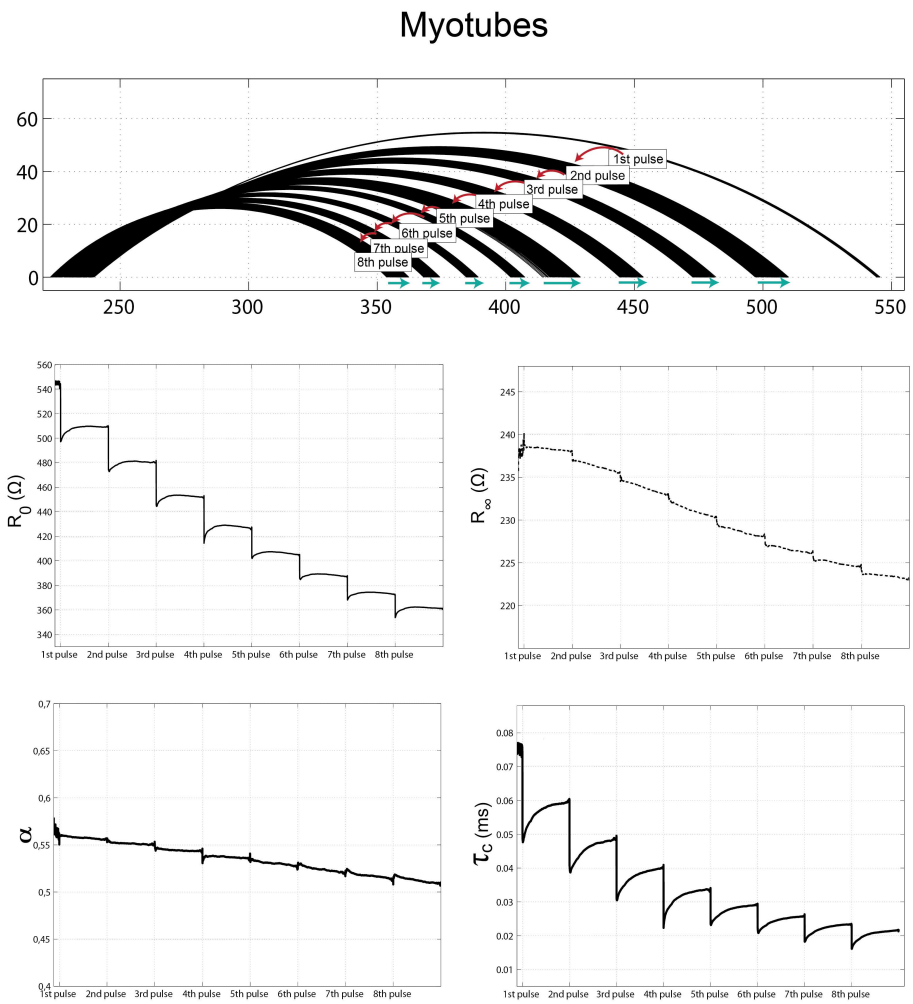

Fig. 6.7 Evolution of the fitted Cole arcs pulse after pulse during a complete electroporation treatment (upper insert). The red arrows show the tendency pulse after pulse, the green arrows indicate the direction of the arcs immediately after each pulse. The evolution of R_0, R_∞, α and τ_c ($1/f_c$) is shown for monolayer of myotubes treated with 1200 V/cm.

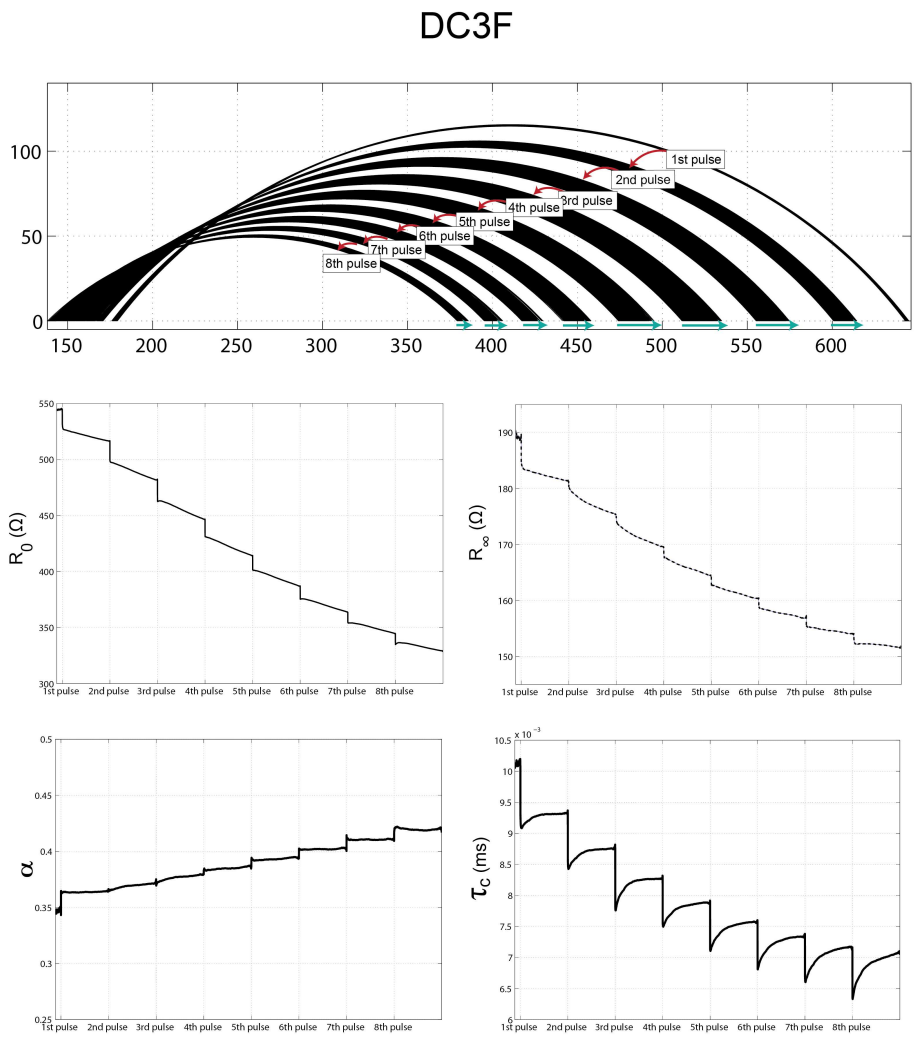

Fig. 6.8 Evolution of the fitted Cole arcs pulse after pulse during a complete electroporation treatment (upper insert). The red arrows show the tendency pulse after pulse, the green arrows indicate the direction of the arcs immediately after each pulse. The evolution of R_0, R_∞, α and τ_c ($1/f_c$) is shown for monolayer of DC3F cells treated with 1400 V/cm.

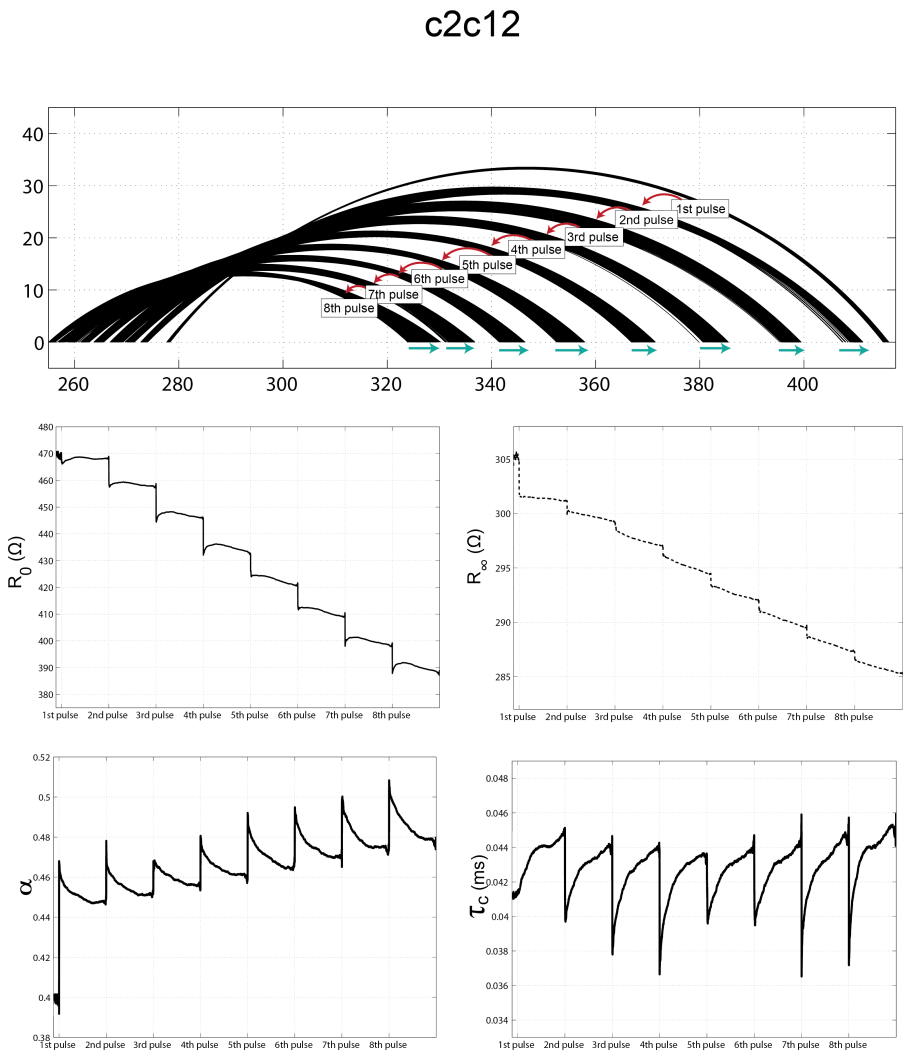

Fig. 6.9 Evolution of the fitted Cole arcs pulse after pulse during a complete electroporation treatment (upper insert). The red arrows show the tendency pulse after pulse, the green arrows indicate the direction of the arcs immediately after each pulse. The evolution of R_0, R_∞, α and τ_c ($1/f_c$) is shown for monolayer of C2C12 cells treated with 1400 V/cm.

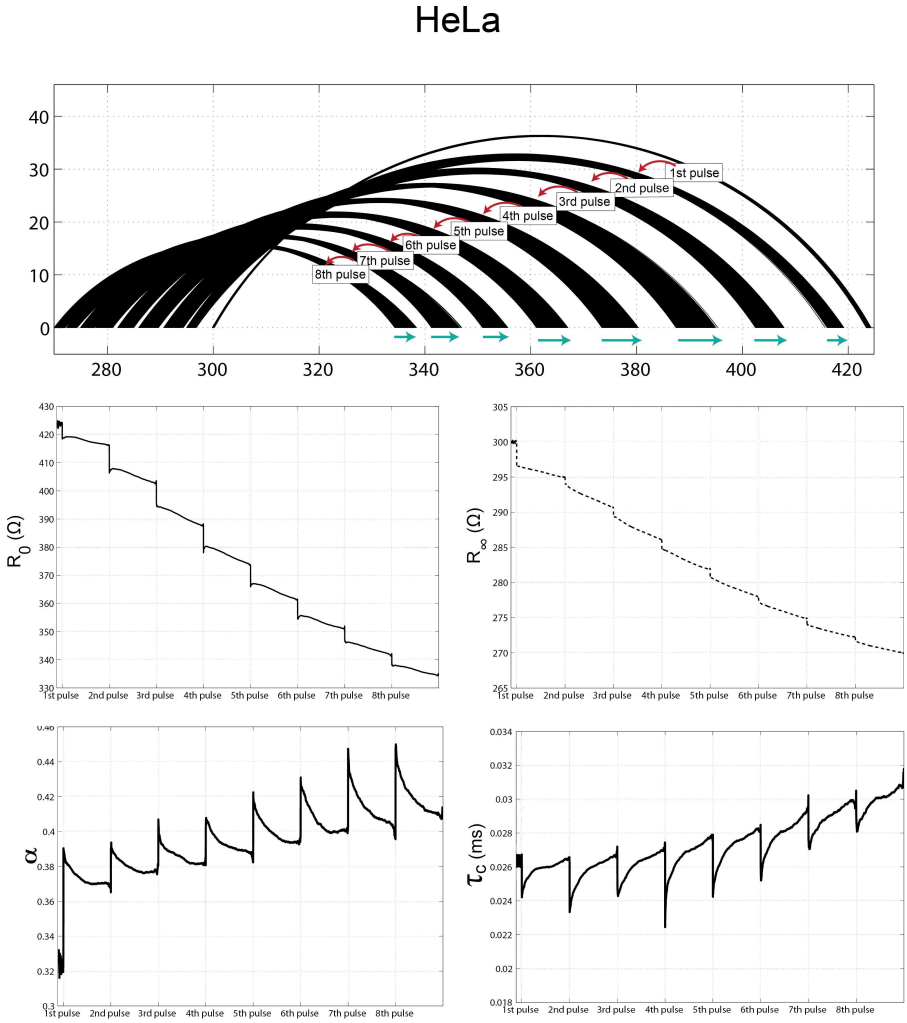

Fig. 6.10 Evolution of the fitted Cole arcs pulse after pulse during a complete electroporation treatment (upper insert). The red arrows show the tendency pulse after pulse, the green arrows indicate the direction of the arcs immediately after each pulse. The evolution of R_0, R_∞, α and τ_c ($1/f_c$) is shown for monolayer of HeLa cells treated with 1400 V/cm.

in the magnitude response for the different cell lines at low frequencies, is not important for the measured impedance at high frequency.

Theoretically, the Cole model can be represented with an equivalent circuit with three hypothetical elements: R_∞, ΔR (=R_0-R_∞) and a constant phase element (CPE) (see Fig. 6.12). Biological materials rarely show a single time constant Debye response (τ=RC) [15] thus the CPE following equation 6.4, is introduced in the Cole equation to model a certain distribution of time constants whose broadness is controlled by the parameter α. Lower α indicates a broader distribution of time constants.

$$Z_{CPE} = \frac{1}{(Kj\omega\tau)^\alpha} \tag{6.4}$$

The comparison of the evolution of the time constant (τ_c) and the exponent α for the different cell lines reveals some differences. In the case of myotubes and DC3F cells, the time constant shows a very similar behavior with a fast dynamic change combined with a slow accumulated decay. In the case of C2C12 and HeLa cells, the behavior of τ_c shows only a fast recovery after each pulse with negligible accumulated evolution. In all cases it is clear that the time constant decreases immediately after each pulse and it has a fast recovery shortly after the pulse. The main difference observed between cell lines is the long-term evolution of the parameter.

The evolution of α for the first two cell lines shows negligible rapid variation and the accumulated slow decay is very small. Exponent α for the other two cell lines shows a well defined fast variation after each pulse together with an increasing tendency over time.

The previous observations suggest that the information contained in τ_c and α is complementary depending on the cell line. One possibility to explain this is because maybe the fitting algorithm to Cole equation could have multiple solutions and does not uniquely assign a change in the impedance to a defined parameter. Attending to equation 6.5 it appears reasonable to think that these two parameters cannot be analyzed independently as they both influence the

time constant in the equivalent pseudo RC association of the Cole model.

$$\tau_{c_{Cole}} = [(R_0 - R_\infty)K]^{\frac{1}{\alpha}} \tag{6.5}$$

In Fig. 6.11 the term $(\tau_c)^\alpha$ is calculated and depicted for each cell line. It can be observed that the combination of both parameters results in a similar behavior for all cell lines. Only in the case of DC3F cells, the fast recovery appears to be somehow masked by the exponent α, if it is compared with the evolution of the corresponding τ_c alone shown in Fig. 6.8.

According to these results the equivalent time constant $(\tau_c)^\alpha$ represents a suitable parameter to study the short-term recovering of cell membrane associated with the closing of the short-lived pores immediately after each electroporation pulse. τ_c^α has the advantage of providing information about the relation between the equivalent resistance/capacitance network of the cell membrane at the same time.

For the interpretation of the combined information contained in $(\tau_c)^\alpha$, it maybe useful to attend to the interpretation of each parameter separately. On the one hand, the relaxation frequency alone (f_c) has been previously used as

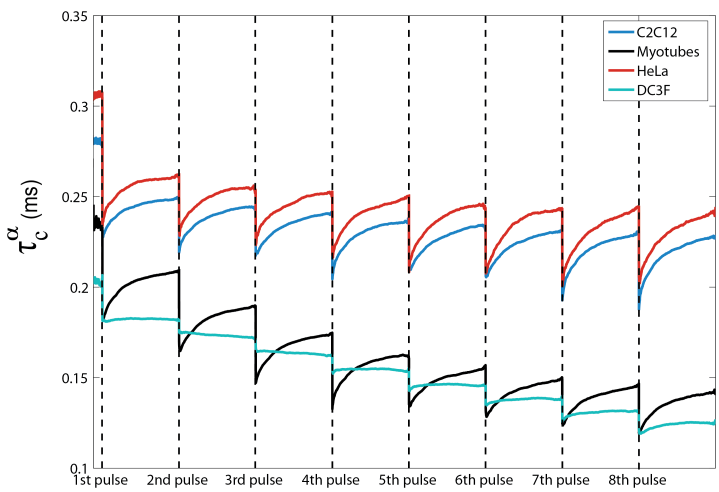

Fig. 6.11 Evolution of the association of Cole parameters τ_c^α for the same data shown in Figs. 6.7 to 6.10.

an indicator to differentiate between normal and cancerous tissue [11]. The given explanation in this study dealt with the differences in polarizability of healthy and abnormal cells. In the case of electroporation, this interpretation is perfectly compatible. It is reasonable to think that the creation of pores changes the ability to store charges in the cell membrane and thus its ability to be polarized. On the other hand, the interpretation of α is more complex, it has been suggested that it is related with the heterogeneity of the sample under study, due to unbalances in the intra/extracellular volumes, different shapes and sizes, presence of organelles, structural alterations, etc. [9, 15]. All interpretations agree that it is a measure of the dispersion of time constants. In the present case it can be seen as a complementary parameter of the mean time constant values of τ_c.

Lastly, the observed variation in the time constant τ_c deserves an additional explanation. During the search for a plausible reason for the changes detected in this parameter, it was found a paper that deserves special comments. The article written by Sverre Grimnes and Orjan G. Martinsen [20] proposes an alternative model to Cole equation for cases when it is observed a variation of the equivalent time constant. The proposed model, depicted in Fig. 6.12, adds an independent conductance G_{var} in parallel with the CPE. In opposition, the Cole model implies that the conductance in parallel with the CPE is not an independent parameter but a part of the Cole dispersion mechanism. Further theoretical explanation about this can be found in [15]. According to the authors, this modified model implies that the variations in the time constant (τ_{zm}) can be the consequence of changes in the parallel independent conductance G_{var}. In the Cole model it is shown that variations in the time constant cannot be due to variations in the parallel conductance ΔG. In the same study they demonstrate the suitability of the new model in the example of skin, where the sweat ducts are modeled as the parallel independent conductance.

In the present case, according to the physical mechanism of electroporation, the creation of membrane pores can be understood as the appearance of a shunting conductance in parallel to the membrane. The uncertainty in this situation is if it can be considered as an independent mechanism with no effects on the CPE as it is proposed in the modified model. In order to study the suitability of this model to the present measurements, the new model is applied

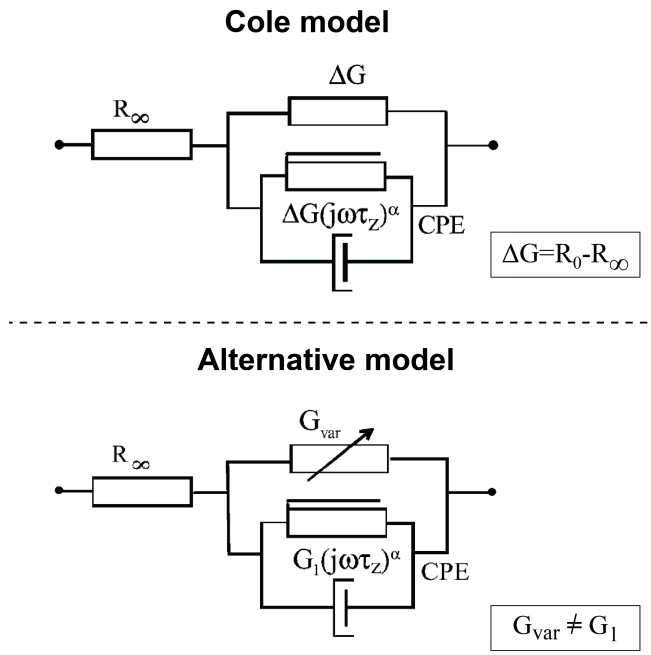

Fig. 6.12 Equivalent circuits corresponding to the Cole model and to the alternative model proposed in [20].

as an example in the case of myotubes and DC3F cells. The conductance G_1 is obtained following the inverse analysis proposed in the cited paper according to equation 6.6 with a nominal time constant τ_Z of 1 second. G_{var} is obtained from the forward analysis according to equation 6.7.

$$G_1 = G_{var} \frac{1}{(\tau_z \omega_{zm})^{\alpha}} \tag{6.6}$$

$$G_{var} = \frac{1}{R_0 - R_{\infty}} \tag{6.7}$$

In Fig. 6.13 the calculated parameters G_1 and G_{var} are plotted. According to these results, it is difficult to observe a clearly differentiated behavior between both of them. This means that the changes produced on the measured sample are influencing both the CPE and the parallel conductance what brings to the

conclusion that they do not respond to independent processes. This implies that the modified model does not represent any improvement with respect to the classical Cole model for the present case. However, the idea of modeling pore creation with an additional resistance in parallel to the membrane CPE is applied in next section using a complete equivalent electrical model.

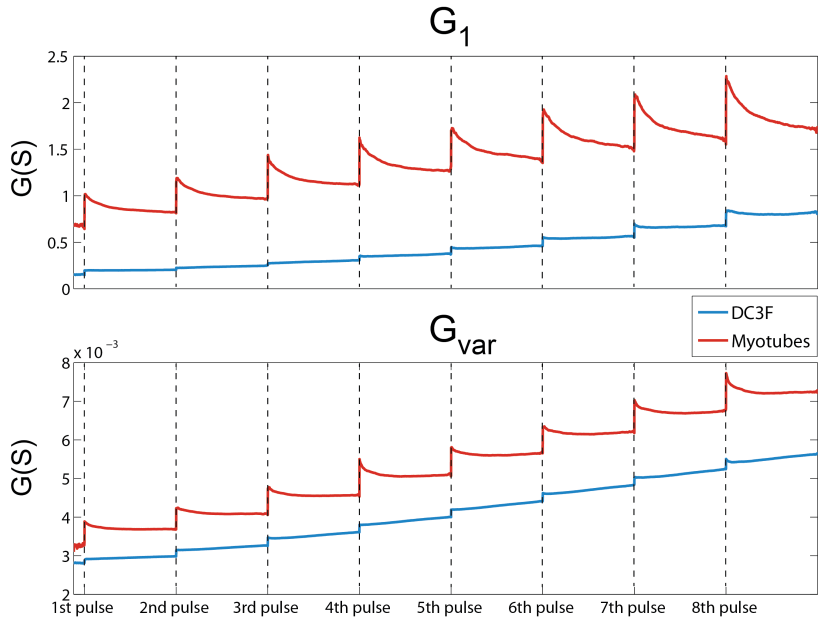

Fig. 6.13 Analysis of the parameters G_1 and G_{var} for the model proposed in [20] for the measurement examples of myotubes and DC3F cells.

6.3.2.3 Equivalent electrical circuit

The last modeling alternative used in the analysis of the present measurements is based on an electrical circuit model. The proposed electrical equivalent shown in Fig. 6.14 corresponds to the one previously used in chapter 5 section 5.3.4. Briefly, the parameters R_{ext} and R_{int} correspond to the extracellular and intracellular resistances respectively. The cell membrane is modeled as a CPE in parallel to an additional resistance R_{pores} that simulates the opening and

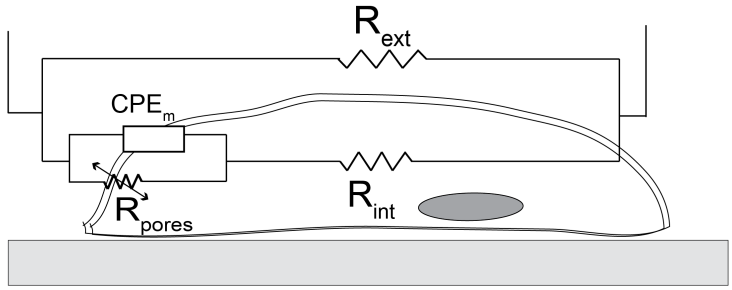

Fig. 6.14 Electrical equivalent circuit used to model the measurements. R_{ext} and R_{int} correspond to the extracellular and intracellular resistances respectively. The cell membrane is modeled as a CPE in parallel to an additional resistance R_{pores}.

closing of membrane pores.

The measurements for each cell line are fitted to the model with a Matlab routine. First, the values for the initial pre-electroporation state are found manually to set the initial conditions to the fitting algorithm. As there is more than one possible set of parameters solving the system, some restrictions are imposed. In the present analysis it is imposed that R_{int} cannot decrease during the course of electroporation what would be in opposition to the expected release of ions from the cytoplasm. After several tests it is observed the need for an additional restriction in R_{ext}. The expected variation of this parameter is a slow continuous process due to diffusion of ions. To model the evolution of this parameter, the long-term behavior observed in R_0 from the Cole is used. The decaying trend in R_0 is extracted, normalized and applied to R_{ext}.

In Fig. 6.15 the evolution the resulting fitted parameter R_{pores} is plotted for each cell line. It can be noticed the similarity in the behavior of this parallel resistance in all cases. According to the previous discussion in the sections above, the evolution of R_{pores} agrees with the expected dual dynamic process (short-term + long-term).

These results demonstrate how attributing to R_{ext} a variation in accordance to a conductivity change in the extracellular buffer, and restricting the behavior of R_{int} to be incremental, it is possible to observe the evolution of membrane pores not mixed with any other collateral effect. These observations support all

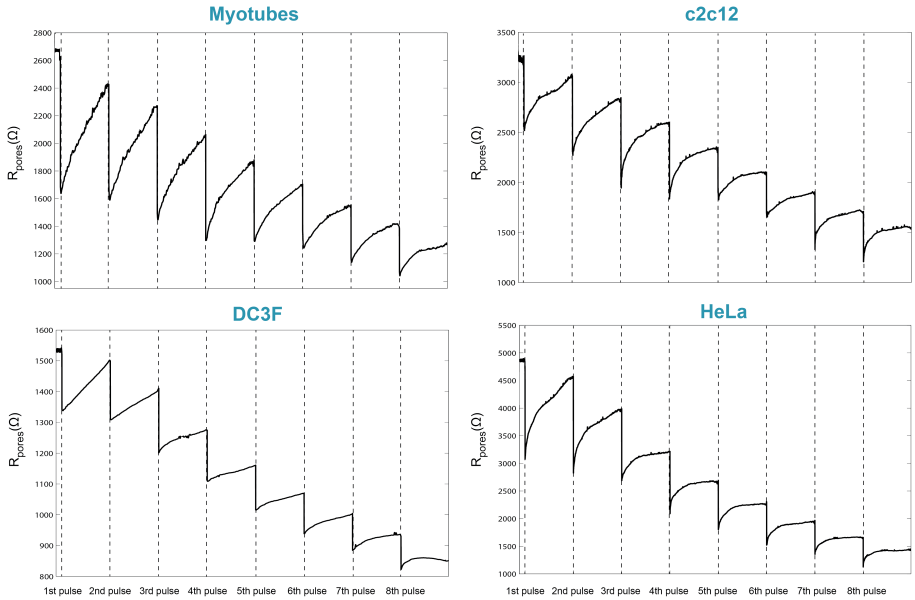

Fig. 6.15 Evolution of equivalent circuit parameter R_{pores} for the four cell lines analyzed. Data corresponding to the same example shown in the previous sections.

the previous discussion about the masking effect of a conductivity variation in the measured membrane events.

The advantage of this equivalent circuit is the possibility of associating a physical meaning to each parameter and separately studying the effect of each one of them. Comparing the different cell lines, the agreement in the observed behavior suggests that this model can be a suitable option for modeling the electroporation phenomenon independently of the cell line analyzed. Unfortunately, the fitting algorithms in this case are considerably more time consuming that the strategies used in Cole parameter extraction what leads to be not a good choice for real-time scenarios. Additionally, there is a need of imposing conditions to the fitting algorithm what is not necessary in the Cole model.

Following, a comparative study of the different discussed parameters is performed with the aim of extracting which is the most adequate for the study of the fast membrane dynamics.

6.3.3 Fast membrane variations: comparative analysis and parameter selection

To this point, the different approaches for the analysis of the impedance measurements during electroporation have been presented. It has been shown that the information of membrane dynamics can be contained in different parameters depending on the approach. Summarizing:

Magnitude and phase

According to section 6.3.2.1 it has been shown that the information about the fast resealing process pulse after pulse can be detected in the **phase angle** at low frequency for all cell lines. On the contrary, depending on the cell line, this information is masked in the magnitude response by an accumulated impedance decrease related with the exchange of ions. It is demonstrated that the conductivity changes in the extracellular bulk electrolyte has considerably less impact in the phase angle that in the magnitude response, what makes it suitable for studying fast membrane resealing. The only difference observed between cell lines is the frequency where the phase variations are maximum. This implies that, for each cell line, the frequency should be chosen previous to the analysis.

Cole model

The classical impedance model applied to the present measurements show considerable variability in the behavior of parameters depending on cell line. R_0 and R_∞ show similar behavior than that of low and high frequency magnitude response respectively. This makes R_0 not immune to conductivity variations and thus not suitable for short-term dynamics study. The analysis of the other two Cole parameters τ_c and α reveals fast dynamic variations in both of them. However the information is expressed in different manner depending on the cell line. The association of these two parameters as an equivalent time constant τ_c^α shows similar behavior in all cases and seems to be the best and more uniform parameter to study fast resealing of cell membrane during pulses independently of cell line.

Equivalent circuit

Lastly, an electrical circuit is used to model the different contributions to the system. This model allows to independently analyze and simulate the behavior of different components. The preconditioning for parameter R_{ext} is obtained from the slow trend observed in Cole parameter R_0. With the restrictions explained above, the resistance $\mathbf{R}_{pores}$ follows a double kinetic evolution in accordance with the creation of two types of pores (short-lived and long-lived pores). This model is useful to confirm the assumptions made in the previous analysis and to find a physical interpretation for the different phenomena observed. However, it does not represent a good option for extracting immediate information about the course of the electroporation procedure because it needs some previous restrictions and the fitting algorithms are not optimal in terms of computational costs.

In accordance to the previous chapter, the transient changes corresponding to the resealing of short-lived pores are governed by a two-stage process modeled by a double exponential function. A first step where massive pores closing occurs within the range of some hundreds of milliseconds, and a second step with a slower resealing rate in the order of one second. In order to compare the different approaches, the dynamic behavior of the different parameters is fitted to double exponential functions (equation 6.8). First, the long term tendency is subtracted from the complete data sets to obtain the corrected short-term information that is subsequently fitted in Matlab.

$$f(t) = Ae^{-t/\tau_1} + Be^{-t/\tau_2} \tag{6.8}$$

In Fig. 6.16 the mean values of the time constant τ_1 extracted for each parameter are shown for each cell line. The values correspond to the measurements of at least three repetitions for the highest electric field assayed (1200 V/cm in the case of myotubes, 1400 V/cm in the rest). The time constant (τ_1) shows no evolution during the course of the 8 electroporation pulses for any of the analyzed parameters (data not shown) what enables to extract the mean value of a complete treatment.

Analyzing the results obtained for the fast time constant τ_1, it can be noticed the high similarity in the values obtained with the different methods. In the

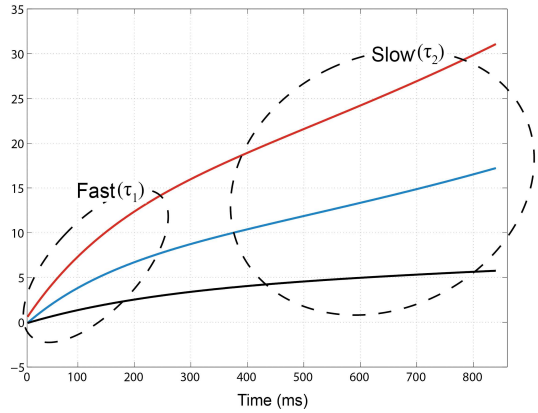

Method	Time Constant	Myotubes	DC3F	C2C12	HeLa
Phase angle					
	τ_1	168.8 ± 22 ms (f=5 kHz)	171.7 ± 18 ms (f=21 kHz)	171.7 ± 25 ms (f=21 kHz)	155.7 ± 22 ms (f=24 kHz)
τ_c^{α} **(Cole)**					
	τ_1	175.4 ± 12 ms	187.8 ± 14 ms	182.9 ± 23 ms	165.6 ± 11 ms
R_{pores}					
	τ_1	185 ± 15 ms	198.4 ± 70 ms	151.4 ± 27 ms	125.9 ± 8 ms

Fig. 6.16 Values obtained for the fast time constant τ_1 after fitting the corrected information in each parameter to a double exponential function. Mean values ± SD are calculated from at least three repetitions for the highest electric field assayed (1200 V/cm in the case of myotubes, 1400 V/cm in the rest). In the case of phase angle the particular frequency chosen for the analysis is 5 kHz for myotubes, 21 kHz for c2c12 and Hela and 24 kHz for DC3F cells.

case of the parameter R_{pores} it can be observed that values are slightly smaller but still in the same order of magnitude. Interpreting the dynamics of the fast time constant with the resealing of the first population of short-lived pores as discussed in previous chapter, it can be concluded from the observed results that the mechanisms for this stage of membrane resealing are similar in all the cell lines analyzed. As previously stated, τ_1 shows no evolution pulse after pulse what means that the mechanisms responsible for this fast membrane repair are not affected over time.

In the case of τ_2 an increasing evolution is observed for the values extracted from the analysis made with the phase angle and with the parameter R_{pores}, on the contrary τ_c^{α} shows no marked evolution. For this reason the mean values cannot be calculated as in the case of τ_1. As an example, the evolution of τ_2 for the circuital parameter R_{pores} is shown in Fig. 6.17. The increase of τ_2 with increasing pulse number can the interpreted as a gradual loss in the resealing ability of cell membranes due to the accumulated effect of pulse repetition. This makes the information contained in this parameter of special interest to detect the level when cells begin to be unable to reseal and thus useful to differentiate between reversible or irreversible electroporation. This observation would need deeper study in the future but could represent an irreversibility marker for real time monitoring of tissues during *in vivo* irreversible electroporation ablation.

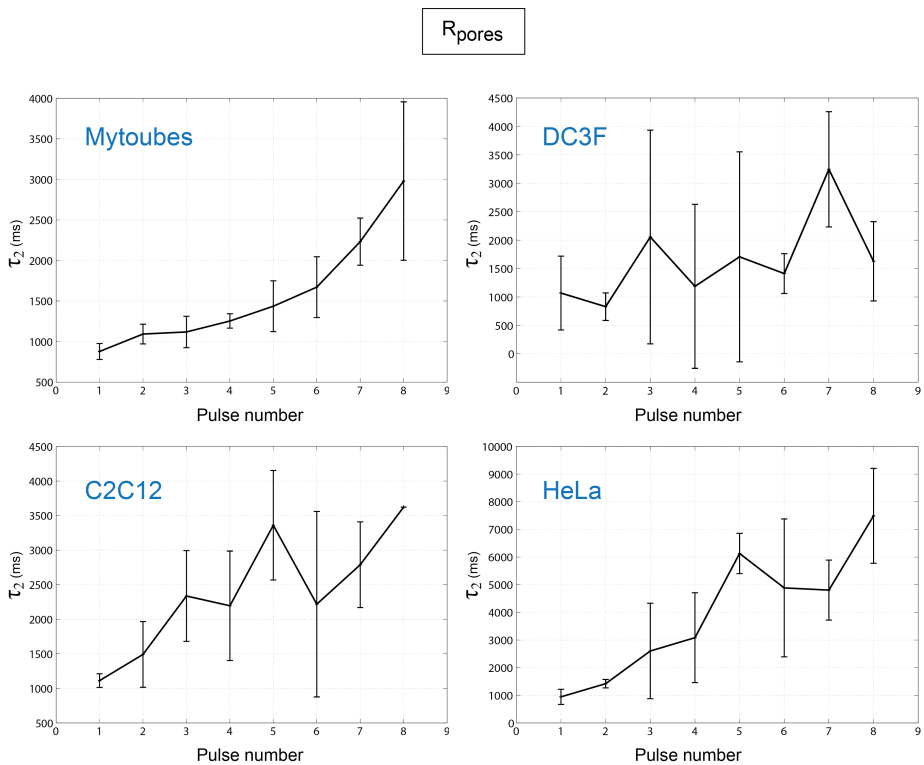

Fig. 6.17 Evolution of time constant τ_2 pulse after pulse calculated for parameter R_{pores}. Mean values ± SD are calculated from at least three repetitions for the highest electric field assayed (1200 V/cm in the case of myotubes, 1400 V/cm in the rest).

Summarizing, the comparative analysis of τ_1 and τ_2 for the three methods proposed has been shown. First, the observation of the mean values of τ_1 (between 125-200 ms) obtained from the different methods brings very similar results what implies that nothing can be said to decide which method represents a better option. Additionally, for the tested experimental conditions, τ_1 shows no significant changes over time what makes it useless to extract information about the evolution of the treatment. However, taking into account the results from the previous chapter, where the values of this time constant differed with the electric field intensity, it could be interesting to use this information in order to adjust the intensity of the applied pulses.

Following, the analysis of the slow time constant (τ_2) brings different results depending on the method. It shows an increasing variation pulse after pulse for the values obtained both from the analysis of the phase angle and from the equivalent circuit parameter R_{pores}. However, the combined information of $(\tau_c)^\alpha$ from the Cole model remains stable over time. Although this was not demonstrated in the present study, the observed increasing values of τ_2 could be related with the gradual loss of the resealing ability of membrane and thus could provide useful information to detect the initiation of irreversible electroporation.

Comparing the different methods applied to the analysis of the fast membrane dynamics, phase angle behaves very similarly in all cell lines what represents an advantage if the aim is to extract a global parameter suitable for any treated sample. However, the analysis of phase angle needs a previous decision on which frequency is analyzed because depending on the cell line the maximum changes are shifted to a different frequency. The decision of the chosen frequency could be extracted from the information of the pre-electroporation impedance measurements (section 6.3.1). In the case of Cole parameter extraction no previous information is needed at all but it is difficult to correctly interpret the results. Finally, the equivalent circuit needs some assumptions that are extracted from the later analysis of measurements after treatment and thus is not a suitable method to apply on line during treatment but a good method to confirm the results obtained with the other methods.

6.3.4 Long-term membrane variations

6.3.4.1 Complete evolution

In this section, the accumulated impedance decay observed is analyzed during the application of the complete electroporation treatment. This accumulated decrease over time is explained by two different processes affecting impedance simultaneously: first the progressive increase in membrane permeability as a consequence of the accumulation of long-lived pores that do not close during electroporation treatment and second, a change in conductivity due to diffusion of ions. As explained before, impedance at low frequency can be affected by the two processes while at high frequency, conductivity variations should be the main responsible for the variations observed. If the aim is to extract information about the extent of membrane permeabilization by means of electrical impedance, it can be useful to combine the information of low and high frequency in order to partly compensate the variations that are not due to membrane poration.

The long-term impedance decrease is observed both in magnitude and phase angle of impedance for all cell lines (see Figs. 6.4 and 6.5). As expected, the amplitude of this variation depends on the frequency analyzed; for lower frequencies the change detected is bigger than for higher frequencies. In Fig. 6.18 an example of this dependency is shown for the magnitude of C2C12 cells.

As expected, this effect is also perfectly reflected in parameters R_0 and R_∞ (refer to Figs. 6.7 to 6.10) being the amplitude of variation of R_0 (low frequency) much higher than the change in R_∞ (high frequency).

In order to have an estimate of the total impedance change during the complete process, the long-term trend is extracted from the low and high frequency magnitude responses for at least three repetitions of each electric field intensity assayed in all cell lines. An example in the case of c2c12 cells (1400 V/cm) is shown in Fig. 6.18 (blue and red lines correspond to low and high frequency respectively). Subsequently, the quotient between these two quantities is normalized to show data in percentage of total change with respect to the initial pre-electroporation state. The same equivalent analysis could be performed using R_0 and R_∞ (data not shown).

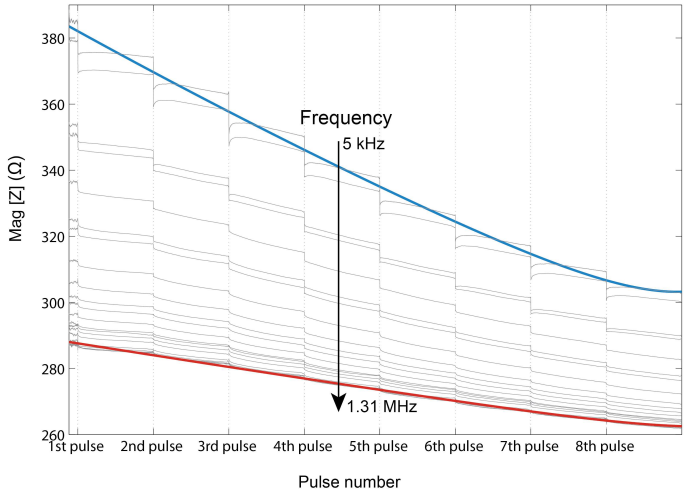

Fig. 6.18 Long-term impedance magnitude variation for the lowest frequency (5 kHz, blue) and for the highest frequency (1.31 MHz, red).Example for and electric field of 1400 V/cm applied to C2C12 myoblasts.

In Figs. 6.19 and 6.20 the resulting mean long-term variation is shown for all cell lines and electric field intensities tested. In all cases, it can be clearly noticed an electric field dependence increasing the % of variation with increasing electric field intensity. Additionally, it is noticed that the behavior over time is different for the highest electric conditions. It is observed that instead of a linear decrease of impedance with pulse number, there is an asymptotic evolution, meaning that the rate of decrease is reduced pulse after pulse. As previously discussed, this observation can be the consequence that when a certain level of permeabilization is reached the effectiveness of pulse application decreases.

As recently proposed in [21], the reduction in the rate of stable pore formation may be a consequence of cell electro-desensitization. This concept can be applied in the present situation because it suggests that the application of an electric field has less effect when the cell membrane is highly perturbed that when the membrane is more organized. In the mentioned paper, the authors relate this observation with the time that membrane has to reseal between consecutive pulses but can also be explained on the basis of the number pulses applied because it also modifies the state of accumulated membrane perturbation.

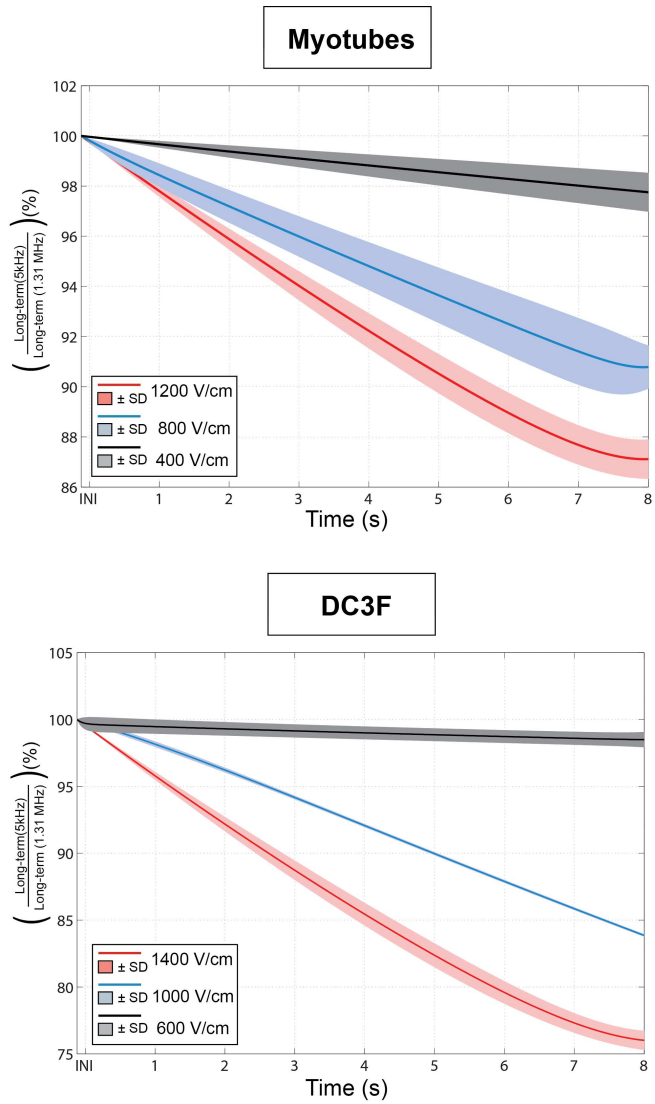

Fig. 6.19 Long-term impedance variation calculated from the quotient between low and high frequency impedance magnitude. Data is shown as the percentage of total change with respect to the initial pre-electroporation state. Data shown for at least three repetitions pooled together for each electric field intensity assayed in the case of myotubes and DC3F cells.

6.3.4.2 Long-term evolution & Permeabilization rates

In section 6.3.3 it was shown how the observation of the slow time constant τ_2 could be used as a marker to detect the loose of resealing ability of cells

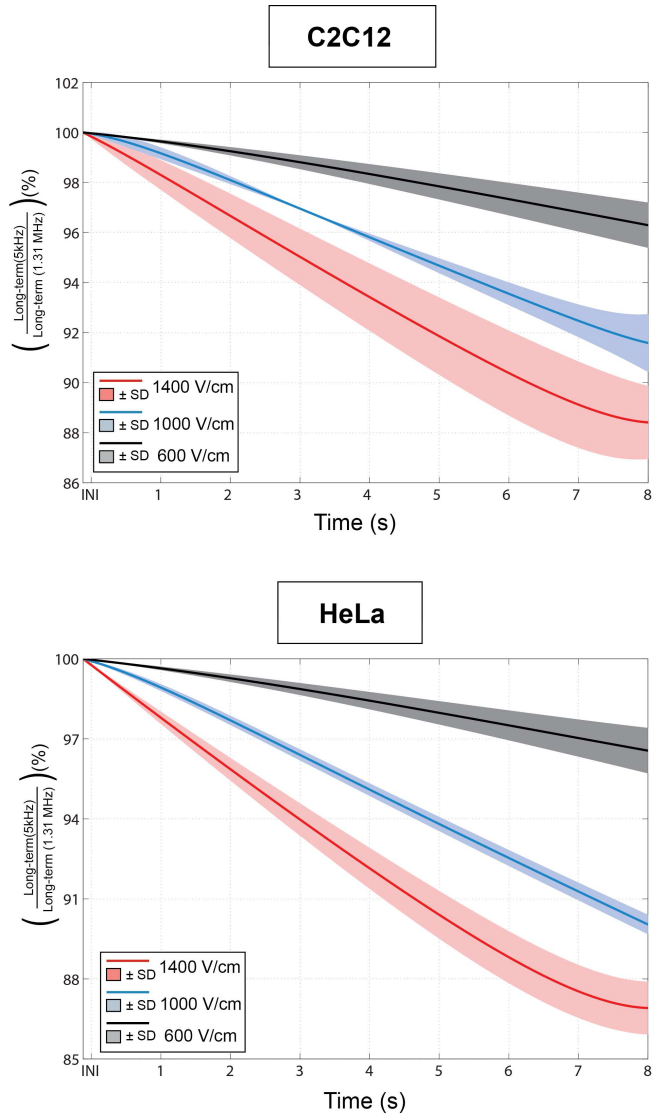

Fig. 6.20 Long-term impedance variation calculated from the quotient between low and high frequency impedance magnitude. Data is shown as the percentage of total change with respect to the initial pre-electroporation state. Data shown for at least three repetitions pooled together for each electric field intensity assayed in the case of c2c12 myoblasts and HeLa cells.

what could be used to detect the threshold of irreversible electroporation. The detection of this limit in real time would be useful to find the optimal conditions

either for reversible or irreversible treatments. In this part, the aim is to study if the information extracted from the long-term impedance variation could be useful as an indicator of the success of the treatment. As demonstrated in previous studies, the vast majority of molecular transport (cell uptake) occurs through the long-lasting membrane structures (long-lived pores) [22–24]. For this reason, the measure of the variation in the long-term impedance, which provides information about the creation of these pores, should be correlated with the amount of molecular species that reach cell cytoplasm.

As described in 5.2, the success of cell permeabilization was measured using the fluorescent reporter Yo-Pro-1 Iodide. Fig. 6.21 shows, as an example, a micrograph of each cell line after treatment. It is noticeable that in the case of DC3F cells, due to the small size of this cell line and maybe also due to the absence of intercelular communication, it is possible to observe black areas (non permeabilized) corresponding to the region under the microelectrodes where the electric field is near to zero. In order to quantify the extent of permeabilization, at least three different fields of each sample were registered under fluorescent microscope and subsequently analyzed with the free image processing software ImageJ (MacBiophotonics)[25]. This analysis was not performed in myotubes due to the complexity of the monolayer (multinucleated cells) and the inability of identifying single cells automatically. In Fig. 6.22 the quantification procedure using the automatic cell nucleus counting plug-in is shown for an example of DC3F cells treated with 1400 V/cm.

Following, the total % of impedance variation extracted from the value at the end of the treatment (t=8 s) in Figs. 6.19 and 6.20 is compared with the obtained permeabilization rates. In Fig. 6.23 both values are plotted together (permeabilization rates are normalized in order to show both quantities on a similar scale).

The results in Fig. 6.23 show a clear correlation between impedance and permeabilization rates for the three cell lines analyzed. For the lowest electric field condition the results clearly differ from the other two both for permeabilization rates and impedance variation. However, in the case of the two highest electric fields the differences between them are not obvious. In order to have a measure of the significance of differences, an unpaired Student's t-test (significance level 5 %) is performed between impedance variation for 1000 V/cm and 1400

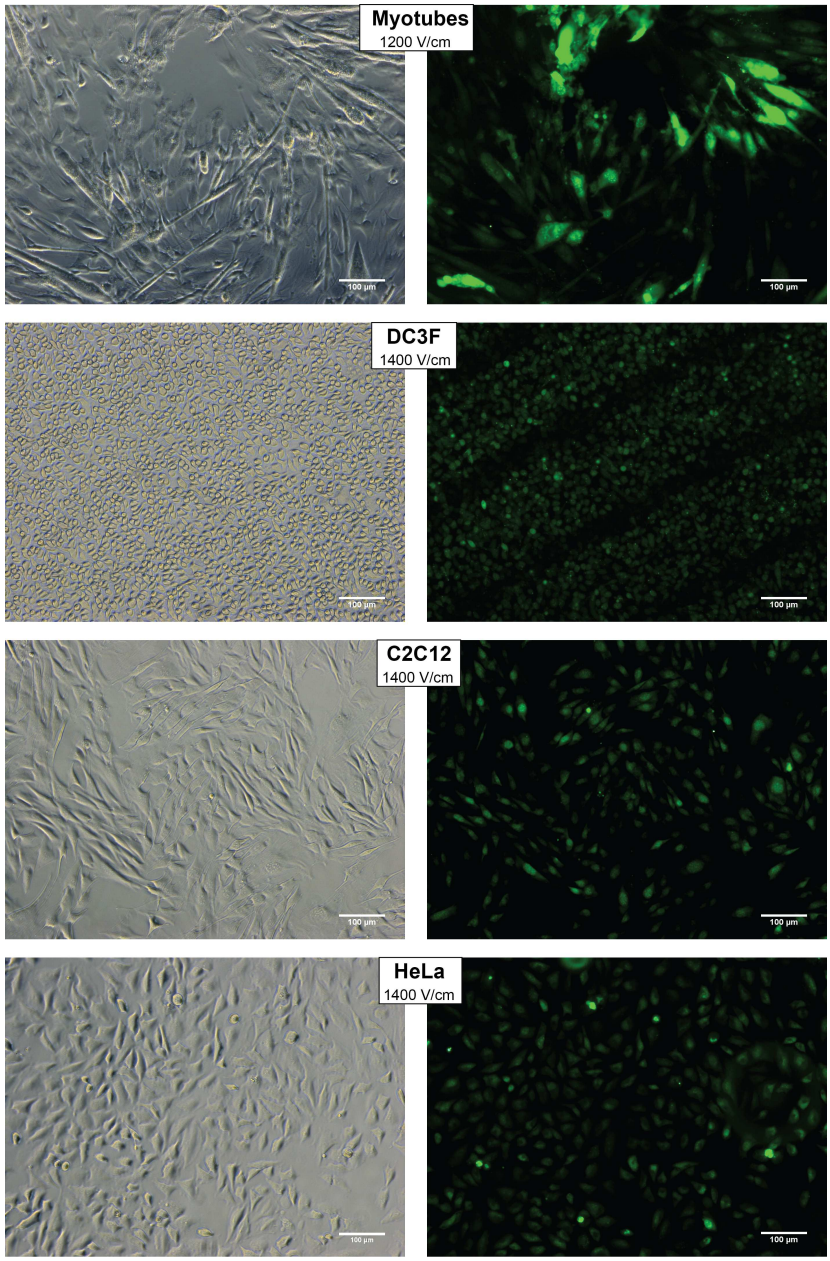

Fig. 6.21 Example of micrographs (phase contrast and fluorescent images) for each cell line. The successful permeabilization assessed by Yo-Pro uptake is shown for an example corresponding to the highest electric field applied in each case.

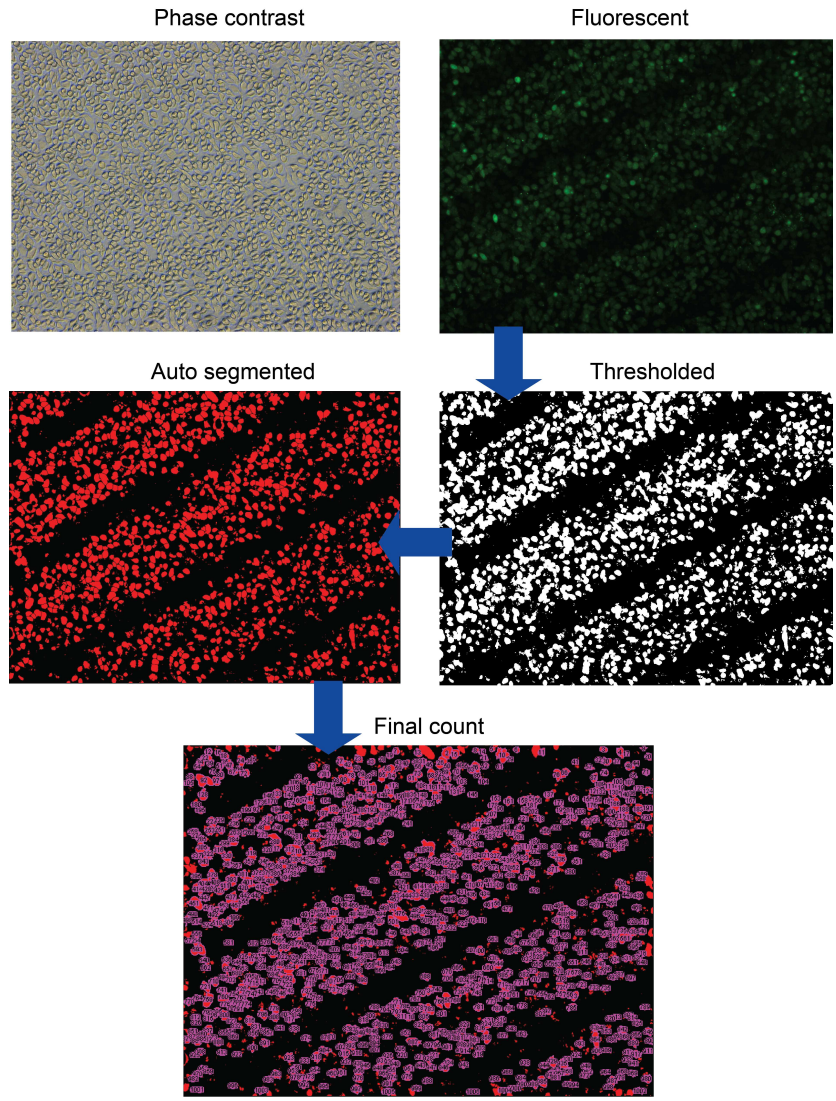

Fig. 6.22 Schematic representation of the image processing procedure performed to quantify the permeabilization rates with ImageJ (MacBiophotonics) software. Example for DC3F cells.

V/cm and also between permeabilization rates for the same field intensities. According to the data shown in Fig. 6.23, in the case of C2C12 and HeLa cells the differences in the permeabilization rates obtained for 1000 V/cm and 1400 V/cm are not significant while, for the same conditions, the average impedance variation differ significantly. This can be explained because the quantification

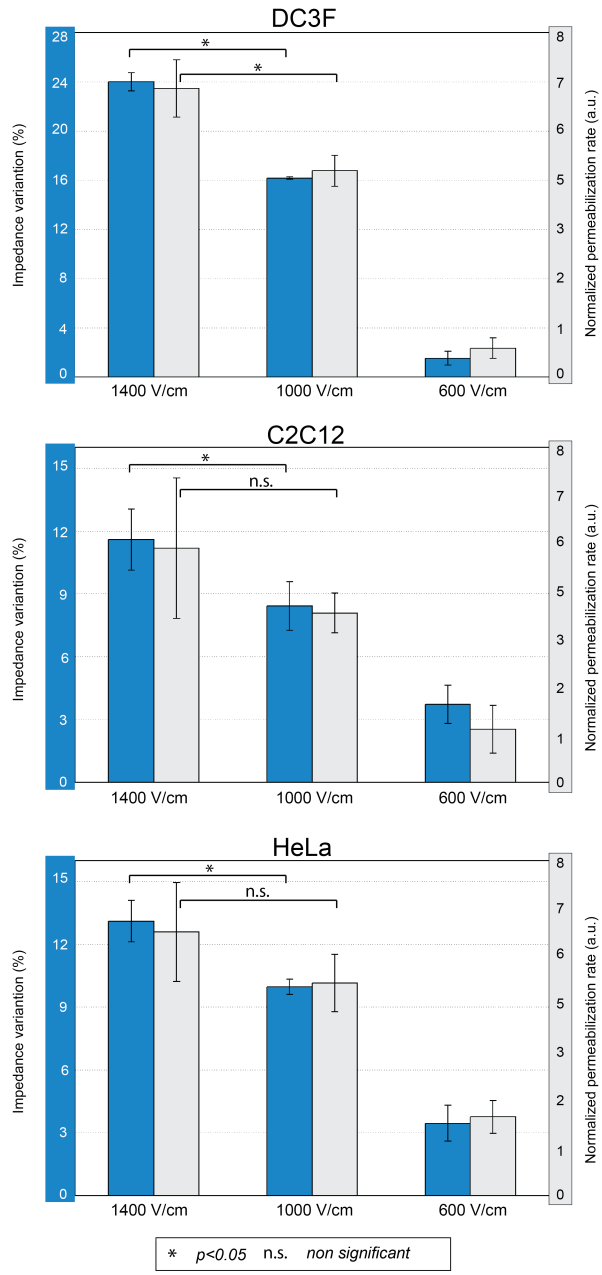

Fig. 6.23 Comparison between the total % of impedance variation extracted from the value at the end of the treatment (t=8 s) with respect to the quantified permeabilization rates. Impedance data correspond to at least three repetition pooled together. In the case of permeabilization rates, three different fields for each repetition were registered and mean values are calculated from at least three repetitions pooled together.

of Yo-Pro uptake is not performed immediately after pulse application. On the contrary, cells are left for 15 min before washing and fluorescence inspection (see section 5.2.4). However, in the case of impedance measurements the information is recorded during pulse application. The application of 1000 V/cm or 1400 V/cm could have permeabilized a similar number and, although the number or size of pores in both cases is not the same, after 15 min the uptake detected could be similar. This observation demonstrates how electrical impedance can quantitatively measure the effects produced in the cell membrane for different electric fields better than traditional permeabilization tests due to the possibility of recording in real time. The information from electrical impedance acquired with the proposed setup can be used to obtain useful information, from the cell monolayer under treatment in this case, by means of a label-free real time method. The technique appears a promising tool that could be used for *in vivo* treatments as a real time method to assess the success tissue electroporation.

The present results show a correlation between permeabilization and impedance variation, however, in the case of macromolecules such as DNA there is no a direct relation between permeabilization and the successful transfer of the macromolecules to the cell cytoplasm. In the future different molecules should be tested in order to study the ability of impedance measurements to detect the success of the treatment in these cases.

6.4 Conclusions

In this study the evolution of the electrical impedance during electroporation of four cell lines is analyzed and compared. First, the impedance of the different cell lines prior to electroporation is analyzed using the Cole model. The results show how the system is able to detect differences between cell lines based on the study of the characteristic frequency parameter f_c. In the present case, the differences observed in this parameter are related to the different sizes of the cells under study. For this reason, C2C12 myoblasts and HeLa cells that show really similar sizes also result in similar values of f_c. Additionally, depending on the organization of the cell monolayer, the impedance spectra can be adjusted to a double arc Cole model reflecting the dispersion in sizes between the long and short axis of cells. In the case of C2C12 cells, it can be clearly observed

the differences detected between the same cells before and after differentiation.

Subsequently, the impedance response during electroporation is analyzed for an illustrative example of each cell line following three different approaches. The first one, based on the analysis of the magnitude and phase angle of impedance, reveals how the magnitude is more affected by the conductivity changes, which occur during electroporation due to ion diffusion, than the phase angle. For this reason, in the case of the phase angle it is possible to observe the fast impedance recovery immediately after pulsing for all cell lines while in the case of the magnitude response, in some cases, the conductivity change masks it. This leads to conclude that the phase angle is more suitable for the observation of the fast impedance variations pulse after pulse.

The second approach to analyze the measurements makes use of the Cole model. The evolution of parameter R_0 agrees with the observed behavior in the magnitude what makes this parameter not suitable for the analysis in all cases. In the present study, it is proposed to combine the information contained in τ_c and α as an equivalent time constant $(\tau_c)^\alpha$ what behaves similar in all cases. As a consequence of the possible inability of the fitting algorithm to assign impedance variations uniquely to one of these two parameters, it is seems more appropriate to use the combined information of both. Additionally, the variations in the τ_c of Cole model suggest the possibility of using an alternative model but once tested, it is shown how this model does not provide better results.

Finally, an electrical equivalent circuit is used. This model represents a good option in order to theoretically study the contribution of the different effects to the system but the need of some a-priori information for the fitting algorithm makes it not suitable as a method to perform a first analysis of the measurements but to confirm some previous results.

The comparative analysis of the time constants τ_1 and τ_2 for the short-term impedance variations for the three proposed methods together with the previous observations help to conclude that phase angle is apparently the most suitable parameter to extract short-term information from the system independently on the cell line analyzed. The only drawback is the need of choosing the frequency where that phase exhibits maximum variations depending on cell line. It is

proposed that the information contained in τ_2 could be and indicator of the long-term resealing ability of cells. Although not demonstrated in the present thesis, it could be used as a marker pf irreversible electroporation.

Lastly, the analysis of the long-term impedance decay observed during the complete treatment is performed studying the evolution of the quotient between low and high frequency impedance magnitude. A similar analysis could be done with the phase or with the Cole model parameters R_0 and R_{infty}. The use of the high frequency information to compensate the collateral effects produced during electroporation represents an advantage in front of using single frequency measurements. Additionally, the impedance change at the end of the treatment is compared to the permeabilization rates quantified with a chemical method. It is demonstrated the good correlation between impedance variation and permeabilization rates what supports the idea that the information extracted from the long-term impedance variation could be useful as an indicator of the success of the treatment. In the analysis it is shown how the measure of electrical impedance in real time is more sensitive to differentiate the effect produced by different electric field intensities than traditional permeabilization tests.

References

[1] D. Miklavčič, G. Serša, E. Brecelj, J. Gehl, D. Soden, G. Bianchi, P. Ruggieri, C. R. Rossi, L. G. Campana, and T. Jarm. Electrochemotherapy: technological advancements for efficient electroporation-based treatment of internal tumors. *Medical & Biological Engineering & Computing*, 50(12):1213–1225, 2012.

[2] Julie Gehl Mir and Lluis M. Determination of optimal parameters for in vivo gene transfer by electroporation, using a rapid in vivo test for cell permeabilization. *Biochemical and Biophysical Research Communications*, 261:377–380, 1999.

[3] D. Cukjati, D. Batiuskaite, F. Andre, D. Miklavcic, and L. M. Mir. Real time electroporation control for accurate and safe in vivo non-viral gene therapy. *Bioelectrochemistry*, 70(2):501–7, 2007.

[4] Michelle Khine, Cristian Ionescu-Zanetti, Andrew Blatz, Lee-Ping Wang, and Luke P. Lee. Single-cell electroporation arrays with real-time monitoring and feedback control. *Lab on a Chip*, 7(4):457–462, 2007.

[5] M. Kranjc, F. Bajd, I. Serša, and D. Miklavčič. Magnetic resonance electrical impedance tomography for measuring electrical conductivity during electroporation. *Physiological Measurement*, 35(6):985, 2014.

[6] R. V. Davalos, D. M. Otten, L. M. Mir, and B. Rubinsky. Electrical impedance tomography for imaging tissue electroporation. *IEEE Trans Biomed Eng*, 51(5):761–7, 2004.

[7] Y. Granot, A. Ivorra, E. Maor, and B. Rubinsky. In vivo imaging of irreversible electroporation by means of electrical impedance tomography. *Phys Med Biol*, 54(16):4927–43, 2009.

[8] B. Blad. Clinical applications of characteristic frequency measurements: preliminaryin vivo study. *Medical and Biological Engineering and Computing*, 34(5):362–365, 1996.

[9] Ivorra Antoni, Genescà Meritxell, Sola Anna, Palacios Luis, Villa Rosa, Hotter Georgina, and Aguiló Jordi. Bioimpedance dispersion width as a parameter to monitor living tissues. *Physiological Measurement*, 26(2):S165, 2005.

[10] R. Bragos, E. Sarro, A. Fontova, A. Soley, J. Cairo, A. Bayes-Genis, and J. Resell. Four versus two-electrode measurement strategies for cell growing and differentiation monitoring using electrical impedance spectroscopy. In *Engineering in Medicine and Biology Society, 2006. EMBS '06. 28th Annual International Conference of the IEEE*, pages 2106–2109, Bragos2006, 2006.

[11] W. D. Gregory, J. J. Marx, C. W. Gregory, W. M. Mikkelson, J. A. Tjoe, and J. Shell. The cole relaxation frequency as a parameter to identify cancer in breast tissue. *Medical Physics*, 39(7):4167–4174, 2012.

[12] E. Sarró, M. Lecina, A. Fontova, C. Solà, F. Gòdia, J. J. Cairó, and R. Bragós. Electrical impedance spectroscopy measurements using a four-electrode configuration improve online monitoring of cell concentration in adherent animal cell cultures. *Biosensors and Bioelectronics*, 31(1):257–263, 2012.

[13] Pierre N. Robillard and Dennis Poussart. Spatial resolution of four electrode array. *Biomedical Engineering, IEEE Transactions on*, BME-26(8):465–470, 1979.

[14] P. Steendijk, Gerrit Mur, E. T. Van Der Velde, and Jan Baan. The four-electrode resistivity technique in anisotropic media: theoretical analysis and application on myocardial tissue in vivo. *Biomedical Engineering, IEEE Transactions on*, 40(11):1138–1148, 1993.

[15] S. Grimnes Martinsen and O. G. *Bioimpedance and Bioelectricity Basics*. Academic Press, San Diego, CA, 2000.

[16] P. N. Goswami, Khan Munna, and Moinuddin. *Bioelectrical Impedance Analysis: Phase Angle - An Independent Predictive Health Marker and its Clinical Applications*, volume 15 of *IFMBE Proceedings*, chapter 82, pages 321–324. Springer Berlin Heidelberg, 2007.

[17] Teresa Malecka-Massalska, Agata Smolen, and Kamal Morshed. Body composition analysis in head and neck squamous cell carcinoma. *European Archives of Oto-Rhino-Laryngology*, 271(10):2775–2779, 2014.

[18] I. Beberashvili, A. Azar, I. Sinuani, G. Shapiro, L. Feldman, K. Stav, J. Sandbank, and Z. Averbukh. Bioimpedance phase angle predicts muscle function, quality of life and clinical outcome in maintenance hemodialysis patients. *Eur J Clin Nutr*, 68(6):683–689, 2014.

[19] A. Navigante, P. Cresta Morgado, O. Casbarien, N. López Delgado, R. Giglio, and M. Perman. Relationship between weakness and phase angle in advanced cancer patients with fatigue. *Supportive Care in Cancer*, 21(6):1685–1690, 2013.

[20] S. Grimnes and O. G. Martinsen. Cole electrical impedance model-a critique and an alternative. *Biomedical Engineering, IEEE Transactions on*, 52(1):132–135, 2005.

[21] A. Silve, A. Guimera Brunet, B. Al-Sakere, A. Ivorra, and L. M. Mir. Comparison of the effects of the repetition rate between microsecond and nanosecond pulses: Electropermeabilization-induced electro-desensitization? *Biochimica et Biophysica Acta (BBA) - General Subjects*, 1840(7):2139–2151, 2014.

[22] Mojca Pavlin and Damijan Miklavcic. Theoretical and experimental analysis of conductivity, ion diffusion and molecular transport during cell electroporation - relation between short-lived and long-lived pores. *Bioelectrochemistry*, 74(1):38–46, 2008.

[23] D. A. Zaharoff, J. W. Henshaw, B. Mossop, and F. Yuan. Mechanistic analysis of electroporation-induced cellular uptake of macromolecules. *Exp Biol Med (Maywood)*, 233(1):94–105, 2008.

[24] K. C. Smith, R. S. Son, T. R. Gowrishankar, and J. C. Weaver. Emergence of a large pore subpopulation during electroporating pulses. *Bioelectrochemistry*, 100:3–10, 2014.

[25] T. J. Collins. Imagej for microscopy. *Biotechniques*, 43(1 Suppl):25–30, 2007.

Chapter 7

Conclusions

Abstract

In this final chapter the most important findings and contributions of the present PhD dissertation are summarized, from the concept of the devices used in this research to the application and possible uses of the fast impedance measurements performed. In addition, several guidelines for further work in the topic are proposed.

7.1 Conclusions

Concept

Regarding the first objective of this work, which consisted in the development of a microelectrode system capable of performing electroporation to adherent cells in standard multiwell plates, it has been shown along this thesis the suitability of the proposed system to accomplish this goal. The microelectrode assemblies and their application concept represent a novel method to use microelectrodes structures with adherent cells. The main novelty of these devices resides in the position of the microelectrodes with respect to the cell monolayer. The design principle consisting in the momentary placement of the microelectrodes above the cell monolayer avoiding physical contact with the cells by means of microseparators has been demonstrated.

The studied system allows the use of microelectrodes in standard multiwell plates what implies a significant advantage with respect to previous systems where cells are grown on the surface of microelectrodes. First, the final user can use this device in the same conditions as the standard chemical methods are applied; there is no need for additional procedures different than those employed in regular protocols what is translated in reducing cell stress. Additionally, the use of standard surfaces to grow cells improves the user's trust and significantly reduces the costs of the electroporation treatment. These advantages are added to the fact that performing *in situ* electroporation to adherent cells is desirable or even necessary in many cases and that few commercial systems are designed to this application.

Microelectrodes

Attending to the technology used in the fabrication of the microelectrodes, standard printed circuit board (PCB) techniques have been applied to produce the prototypes. PCB enables to easily construct bi-layer designs, what was mandatory given the characteristics of the top-positioning concept. One side for the microelectrode structure and microseparators and the opposite side for the connectors. It allows fabricating microelectrode assemblies with dimensions in the order of tens of microns and non-cytotoxic materials can be used as coating. Additionally, the fabrication costs of this technology enable to produce

disposable devices at very low price.

During the course of the study and supported by theoretical electric field simulations, different improvements have been performed to obtain better results. Thanks to the simulations, it was observed that as a consequence of the high thickness of the metal substrate where the electrodes are patterned in PCB technology, if compared to thin film technologies, most of current flow occurred in the lateral space between microelectrodes. For this reason, the first improvement, and the one implying the biggest novelty, consisted in the modification of the fabrication procedure with the aim of forcing the current density to concentrate in the region occupied by the cells and not in the volume space between adjacent lines.

The mentioned improvement consisted in filling the gap between adjacent microelectrodes with a non-conductive material, in the present case, an epoxy resin was used. Once accomplished, this modification led to a reduction in the total electric current necessary to produce cell electropermeabilization, what avoided the apparition of undesired electrolytic reactions, specially when long pulses (1ms) were applied. In order to implement this concept, the basic standard fabrication steps were maintained what allowed keeping the low costs of this fabrication process.

The next modification that was performed with respect the initial prototype relates to the geometry of the microelectrodes. The new spiral topology allows improving the electric field uniformity in the cell monolayer and, more important, using the same microelectrode assembly as an electrical bioimpedance sensor during electroporation. The spiral arrangement is specially conceived to perform measurements with a four-electrode method what is more suitable to avoid the effect of the electrode-electrolyte interface and thus having a more realistic impedance recording.

Electroporation Results

Regarding the experimental results performed to study the ability of the prototypes to produce cell permeabilization, different tests were done. In chapter 3 the concept of the system is validated with two cell lines and a small labeled FITC-dextran molecule. The results confirm the effectiveness of the system in cell electropermeabilization and report permeabilization rates comparable to

other systems. Additionally, it is also observed that the device could be used in cell electrofusion in confluent cell monolayers. This second characteristic is not investigated in detail in the present work.

In chapter 4 the tests are extended to a higher number of cell lines and active molecules. The results indicate that despite the good permeabilization rates assessed with a small molecule, the plasmid transfection results show low expression rates. This supports the concept that first, permeabilization is necessary but not sufficient to obtain transfection and second, the results obtained in adherent cells are lower than those obtained in suspended cells for the same conditions. It is important to state that the goal in this part of the thesis was to demonstrate the suitability of the system to insert different active molecules by electroporation but not to find the optimal conditions that maximize these results. Further effort should be put to improve the low transfection rates obtained.

Impedance measurements

Subsequently, the second part of this dissertation is focused in the application of the presented system in the electrical characterization of cell monolayers during electroporation by means of fast electrical impedance spectroscopy measurements. First, the suitability of the system to detect impedance changes during electroporation is confirmed in chapter 4 with a basic measuring setup. These first results indicate a relation between electric field intensity and impedance decrease. It is shown that the evolution of impedance is not linear with pulse number, suggesting that the level of cell permeabilization saturates with increasing pulse number. The different behavior at different measuring frequencies reinforces the advantage of using impedance spectroscopy to obtain more complete information from the measured system.

Next, a system capable of continuously acquiring impedance spectra at a time resolution of 1 spectrum/ms was developed in order to study the fast changes produced in the cell membrane immediately after each pulse (interpulse measurements). The system is based on a fast EIS measuring technique using multisine excitations. For the first time, with the present setup it is possible to perform continuous multifrequency measurements with such a high time resolution during an electroporation treatment.

In chapter 5 the measurements are shown for differentiated myotubes. This is a clear example where it is necessary a system applicable to adherent cells. In chapter 6 the measurements are extended to other three additional cell lines.

The initial observation of the impedance measurements during electroporation (magnitude and phase) reveals the existence of two different dynamics at low frequency. First, a fast impedance recovery immediately after each pulse, called short-term evolution. This process agrees with the kinetics of short-lived pores that start to reseal immediately after pulse application. This fast resealing process follows a double exponential function with two time constants: a fast time constant in the order of hundreds of milliseconds and a slow time constant in the order of seconds. A second impedance decrease maintained during the complete treatment is also observed (long-term evolution).

At high frequency, where the impedance should not be directly affected by membrane changes, only a slow impedance decrease is observed. This change is attributed to conductivity variation that occurs during electroporation due to ions diffusion from the more conductive cell cytoplasm to the low conductive extracellular buffer.

Fast impedance variations (Short-term)

The comparison of the magnitude and phase angle response obtained from all cell lines reveals that phase angle is more suitable for the detection of the fast impedance variations pulse after pulse. This is explained because, depending on the cell line, the mentioned medium conductivity change affect more to the impedance magnitude than to its phase, thus hiding the fast membrane recovery. The drawback of the direct observation of phase is that only the information at one single frequency can be analyzed at the same time. Additionally the frequency showing the higher phase variations at low frequency differs from one cell line to the other what implies that for the study of the fast membrane changes this frequency needs to be manually selected for each cell line.

Following, in order to extract the most from the multifrequency measurements, we used impedance models to analyze the complete spectral information. First, the widely known Cole model is applied. The detailed analysis and comparison of its parameters reveals that depending on the cell line the fast membrane variations (short-term evolution) could not always be assigned

to the same parameter. From our initial analysis, these should be shown in the parameter R_0 that represents the changes at low frequency. However, depending on the cell line, this parameter does not behave according to the already describe dual dynamics. Similar to the impedance magnitude, R_0 seems to be affected by a second process that hides the fast membrane changes immediately after each pulse.

In this study it is proposed to combine the information contained in τ_c and α as an equivalent time constant $(\tau_c)^\alpha$ that behaves similarly in all cases. The cell membrane represents a pseudo RC network whose time constant variations can provide useful information about membrane permeabilization dynamics.

Finally, R_∞ from the Cole model is useful to obtain information about the collateral variation in the extracellular conductivity.

The advantage of using Cole model is the simplicity of its formulation (only with four parameters) and the cost efficient algorithms that can be used to fit the measurements on real-time. However, the drawback of this model is the lack of a unique physical interpretation of its parameters. Also, during the fitting procedure, an impedance variation can be reflected in different ways in Cole model parameters what makes difficult to provide a general description for the interpretation of this model.

Finally, an alternative electrical equivalent circuit was used in the analysis. The advantage of this type of models is that they enable to identify each process with a different circuit element facilitating the correct interpretation of the results. However, in the present case, different solutions existed for the same set of parameters what implied the need for previous information from the system. For this reason, some restrictions were imposed to the fitting algorithm following the expected behavior of the circuit parameters. In the present case these predictions were extracted from the observed behavior in the Cole model. Using this equivalent circuit, fast membrane dynamics were modeled as an additional parallel resistor in the membrane. With the imposed restrictions, the results were satisfactory and considerably uniform for all cell lines.

Summarizing, this study reveals that more than one method should be used to confirm the analysis of impedance measurements when the goal is the confirmation of a given theoretical explanation, each one having its advantages

and drawbacks. If the goal is, on the contrary, to give a simple description of the dynamical impedance changes in an hypothetical control system any of the present methods would be enough. For the application of this kind of measurements to real-time systems, it is desirable a fast method without the need of previous information. This makes Cole model the best candidate. Direct phase measurements could also be used by taking advantage from the information contained in the pre-electroporation measurements of the sample to decide which frequency should be analyzed. The equivalent circuit is not suitable for real-time measurements but should be used complementary to confirm the results off line.

The possible uses of the values of the time constants from the fast membrane dynamics generated from the impedance spectroscopy measurements are explained next. The fast time constant (referred as τ_1 in the text) describes the first and fastest part of the resealing process. The similarity of the values obtained suggests that this mechanism is similar for all cell lines. However, as shown in chapter 5, the τ_1 values differ between low electric field intensities, near the electroporation threshold, and higher intensities, where clear permeabilization occurs. This suggests that different mechanisms could be activated for the cell membrane recovery when the membrane is massively permeabilizated. The values of τ_1 could be used for the detection of the effective permeabilization threshold in the initial permeabilization tests of a particular cell line. Also this information is interesting to improve the basic knowledge of the membrane resealing mechanisms.

The second time constant τ_2 provides information about the slower resealing process that follows the fast part described above. The values of this time constant are around one second what agrees with observations made in previous studies. However, it has been observed that for high electric field intensities the values increase with increasing pulse number. This could be related with the loose of resealing ability of the cell membrane in these cases. This explanation suggests that the value of τ_2 could be used to detect the initiation of irreversible electroporation. Nonetheless, further studies should be done in the future to demonstrate this fact.

Slow impedance variations (Long-term)

Regarding the slow impedance decrease observed during the complete electroporation treatment, it is related with the creation of long-lasting permeable structures (long-lived pores). Also, the change in conductivity produced by leakage of ions contributes to this decrease. The advantage of performing multifrequency measurements is the ability to compensate the effect of the conductivity variation using the high frequency impedance information. The resulting increase in membrane permeability due to long-lived pores is not linear with pulse number and shows an asymptotic behavior suggesting a limit for permeabilization with pulse number.

The comparison of the impedance change at the end of the treatment with respect to the permeabilization rates quantified with a chemical method demonstrates that the information extracted from the long-term impedance variation could be useful as an indicator of the success of the treatment. Additionally, it has been shown how the impedance measurements are more sensitive in order to differentiate the effect produced by different electric field intensities than traditional permeabilization tests.

The information obtained from the present multifrequency measurements supports the fact that when acquiring complete spectra instead of single frequency measurements, more information about the system can be extracted. The present results demonstrate how fast EIS measurements during an electroporation procedure represent a reliable and alternative method for online monitoring the changes produced in the sample under treatment.

7.2 Future work

Research is a continuous process where improving is always a must. In the present case further effort should be focused on different aspects. First, increasing the DNA transfection rates to obtain results comparable to other systems and extending the experiments to more cell lines and molecules should be addressed. Due to our lack of previous experience, once familiarized with the electroporation technique, the optimal conditions for each experiment should be found by playing with many different variables such as electric field parameters (pulse duration, frequency, number of pulses, polarity, etc.), different buffer compositions, cell density and so on.

Regarding the application of impedance measurements, many questions should also be addressed in the future. First, further work could be oriented in exploiting the advantages of the microelectrode assembly to characterize non-invasively cell monolayers. The system could be used to monitor cell differentiation, cell reprogramming in induced pluripotent stem cells (IPSc), etc.

Attending to measurements during electroporation, the impedance analysis presented in this thesis has been performed in the time lapse between consecutive pulses to reveal fast membrane dynamics. Obviously, the same system could be used to follow the impedance of cell monolayers in a longer time scale to monitor the complete membrane resealing process after electroporation. Also, in-pulse measurements could be performed with the present setup; either measuring current and voltage signals of the applied pulses; or superposing a multifrequency signal such a multisine to the square electroporation pulses and subsequently analyzing the spectral response.

The improvement in the complete understanding of the impedance results obtained should be continued proposing new models that could be applied for a general case. The aim of this models would be enabling the complete separation of the crossed effects in the different parameters even being capable of introducing the electrodes effects. Also varying experimental conditions such as buffer conductivity, time between pulses, pulse duration, etc. could help in the deep understanding of the contribution of different phenomena to the measurements. Additionally, finding a clear relation between the obtained time constants and

the physiological mechanisms of cell resealing should also be studied in depth.

Finally, the extension of the *in vitro* results to measurements in living tissues should be performed in the future. The final goal would imply demonstrating the ability of the fast electrical impedance measurements as an optimal method for online monitoring tissue electroporation either in electrochemotherapy, gene electrotransfer or tissue ablation treatments. The combined use of this measurements with efficient feedback control strategies would enable to develop tools for an optimal and safe electric field treatment dosage.

Complete list of publications

Journal

1. Tomás García-Sánchez, Beatriz Sánchez-Ortiz, Ingrid Vila,María Guitart, Javier Rosell,Anna M. Gómez-Foix and Ramon Bragós. **Design and implementation of a microelectrode assembly for use on non-contact in situ electroporation of adherent cells**. Journal of Membrane Biology 245 (10),617-624. (2012). DOI 10.1007/s00232-012-9474-y.

2. Tomás García-Sánchez, María Guitart, Javier Rosell, Anna M. Gómez-Foix and Ramon Bragós. **A new spiral microelectrode assembly for electroporation and impedance measurements of adherent cell monolayers**. Biomedical Microdevices 16, 575-90. (2014). DOI 10.1007/s10544-014-9860-6.

3. Tomás García-Sánchez, Antoine Azan, Isabelle Leray, Javier Rosell-Ferrer, Ramon Bragós, LLuis M. Mir. **Interpulse multifrequency electrical impedance measurements during electroporation of adherent differentiated myotubes.** Bioelectrochemistry. *Submmited*, December 2014.

Conferences

1. Tomás García-Sánchez, María Guitart, Javier Rosell-Ferrer, Anna M. Gómez-Foix and Ramon Bragós. Automatic system for electroporation of adherent cells growing in standard multi-well plates. 34th Annual Conference of the IEEE EMBS. San Diego, CA. August 2012. Presented (oral presentation).

2. Tomás García-Sánchez, Benjamin Sánchez, Javier Rosell-Ferrer, Ramon Bragós. Inter pulse fast electrical bioimpedance spectroscopy during in vitro electroporation of adherent cell monolayers. XVth International Conference on Electrical Bio-Impedance (ICEBI) and the XIVth Conference on Electrical Impedance Tomography 2013 (EIT). Poster presentation. Presented (poster).

3. Jesús Martínez-Teruel, Tomás García-Sánchez, Andreu Fontova, Ramon Bragós. Electrical Impedance Spectroscopy cell monitoring in a miniaturized bioreactor. 19th IMEKO TC 4 Symposium and 17th IWADC Workshop Advances in Instrumentation and Sensors Interoperability July 18-19, 2013, Barcelona, Spain. Presented (poster).

4. Tomás García-Sánchez, María Guitart, Benjamin Sánchez, Javier Rosell-Ferrer, Anna M. Gómez-Foix and Ramon Bragós. Monitoring cell monolayers during electroporation: Electrical impedance spectroscopy measurements. 19th IMEKO TC 4 Symposium and 17th IWADC Workshop Advances in Instrumentation and Sensors Interoperability July 18-19, 2013, Barcelona, Spain. Presented (oral presentation).

5. Tomás García-Sánchez, María Guitart, Javier Rosell, Anna M. Gómez-Foix and Ramon Bragós. Gene transfer to adherent cells by in situ electroporation with a spiral microelectrode assembly. XIII Mediterranean Conference on Medical and Biological Engineering and Computing (MEDICON 2013). 25-28 September, Seville.Presented (oral presentation).

6. Tomás García-Sánchez, Benjamin Sánchez, Anna M. Gómez-Foix and Ramon Bragós. Electrical impedance measurements on electropermeabilized cells attached to microelectrodes. 6th European Conference of the IFMBE

(MBEC), Dubrovnik (Croacia) 7-11 September 2014. Presented (oral presentation).

Patents

1. PCT Application. PCT/EP2012/058587. "Electrode assembly for generating electric field pulses to perform electroporation to a biological sample". Presented in the European Patent Office (EPO), priority date May 9 2012.

Appendix A

Paper in *The Journal of Membrane Biology*

T. García-Sánchez, B. Sánchez-Ortiz; I. Vila, M. Guitart, J. Rosell, A.M. Gómez-Foix, R. Bragós

Design and Implementation of a Microelectrode Assembly for Use on Noncontact In Situ Electroporation of Adherent Cells

The Journal of Membrane Biology October 2012, Vol.245, #10, p.617–624

Pages 202 to 211 of the thesis, containing the article are available at the editor's web http://link.springer.com/article/10.1007/s00232-012-9474-y

Appendix B

Paper in the *Proceedings of IEEE EMBS 2012*

T. García-Sánchez , M. Guitart, J. Rosell, A.Ma Gomez-Foix, R. Bragós

Automatic system for electroporation of adherent cells growing in standard multi-well plates. 34th Annual International Conference of the IEEE EMBS : San Diego, California USA, 28 August -1 September, 2012 P.2571-2574

Pages 212 to 216 of the thesis, containing the article are available at the editor's web
http://ieeexplore.ieee.org/document/6346489/

Appendix C

Paper in *Biomedical Microdevices*

T. García-Sánchez, M. Guitart, J. Rosell, A.M. Gómez-Foix , R. Bragós

A new spiral microelectrode assembly for electroporation and impedance measurements of adherent cell monolayers.
Biomedical Microdevices August 2014, Vol.16, Issue 4, pp 575–590

Pages 218 to 233 of the thesis, containing the article are available at the editor's web http://link.springer.com/article/10.1007/s10544-014-9860-6